frontiers | Research Topics

Canine lymphoma pathogenesis, diagnosis, prognosis and treatment: Current and future perspectives

Edited by
Vittoria Castiglioni, Sabina Soldati, Jorge Del Pozo and Monica Sforna

Coordinated by
Cynthia De Vries

Published in
Frontiers in Veterinary Science

ISSN 1664-8714
ISBN 978-2-8325-5226-1
DOI 10.3389/978-2-8325-5226-1

About Frontiers

Frontiers is more than just an open access publisher of scholarly articles: it is a pioneering approach to the world of academia, radically improving the way scholarly research is managed. The grand vision of Frontiers is a world where all people have an equal opportunity to seek, share and generate knowledge. Frontiers provides immediate and permanent online open access to all its publications, but this alone is not enough to realize our grand goals.

Frontiers journal series

The Frontiers journal series is a multi-tier and interdisciplinary set of open-access, online journals, promising a paradigm shift from the current review, selection and dissemination processes in academic publishing. All Frontiers journals are driven by researchers for researchers; therefore, they constitute a service to the scholarly community. At the same time, the *Frontiers journal series* operates on a revolutionary invention, the tiered publishing system, initially addressing specific communities of scholars, and gradually climbing up to broader public understanding, thus serving the interests of the lay society, too.

Dedication to quality

Each Frontiers article is a landmark of the highest quality, thanks to genuinely collaborative interactions between authors and review editors, who include some of the world's best academicians. Research must be certified by peers before entering a stream of knowledge that may eventually reach the public - and shape society; therefore, Frontiers only applies the most rigorous and unbiased reviews. Frontiers revolutionizes research publishing by freely delivering the most outstanding research, evaluated with no bias from both the academic and social point of view. By applying the most advanced information technologies, Frontiers is catapulting scholarly publishing into a new generation.

What are Frontiers Research Topics?

Frontiers Research Topics are very popular trademarks of the *Frontiers journals series*: they are collections of at least ten articles, all centered on a particular subject. With their unique mix of varied contributions from Original Research to Review Articles, Frontiers Research Topics unify the most influential researchers, the latest key findings and historical advances in a hot research area.

Find out more on how to host your own Frontiers Research Topic or contribute to one as an author by contacting the Frontiers editorial office: frontiersin.org/about/contact

Canine lymphoma pathogenesis, diagnosis, prognosis and treatment: Current and future perspectives

Topic editors
Vittoria Castiglioni — IDEXX Laboratories, Germany
Sabina Soldati — Pathology Experts, Switzerland
Jorge Del Pozo — University of Edinburgh, United Kingdom
Monica Sforna — University of Perugia, Italy

Topic coordinator
Cynthia De Vries — Laboklin GmbH & Co. KG, Germany

Citation
Castiglioni, V., Soldati, S., Del Pozo, J., Sforna, M., De Vries, C., eds. (2024). *Canine lymphoma pathogenesis, diagnosis, prognosis and treatment: Current and future perspectives*. Lausanne: Frontiers Media SA. doi: 10.3389/978-2-8325-5226-1

Vittoria Castiglioni is an employee for IDEXX Laboratories (Germany) and Sabina Soldati is an Associate in Pathology Experts GmbH.

Table of contents

frontiers | Frontiers in Veterinary Science

TYPE Editorial
PUBLISHED 16 July 2024
DOI 10.3389/fvets.2024.1442964

OPEN ACCESS

EDITED AND REVIEWED BY
Felisbina Luisa Queiroga,
University of Trás-os-Montes and Alto Douro, Portugal

*CORRESPONDENCE
Vittoria Castiglioni
✉ vittoria-castiglioni@idexx.com

RECEIVED 03 June 2024
ACCEPTED 26 June 2024
PUBLISHED 16 July 2024

CITATION
Castiglioni V, Sforna M and de Vries C (2024) Editorial: Canine lymphoma pathogenesis, diagnosis, prognosis and treatment: current and future perspectives.
Front. Vet. Sci. 11:1442964.
doi: 10.3389/fvets.2024.1442964

Editorial: Canine lymphoma pathogenesis, diagnosis, prognosis and treatment: current and future perspectives

Vittoria Castiglioni[1]*, Monica Sforna[2] and Cynthia de Vries[3]

[1]IDEXX Laboratories Italia Srl, Milano, Italy, [2]Dipartimento di Medicina Veterinaria, Patologia Generale e Anatomia Patologica Veterinaria, University of Perugia, Perugia, Italy, [3]Laboklin GmbH & Co. KG, Kissingen, Germany

KEYWORDS

canine lymphoma, pathogenesis, diagnostic tools, therapy, artificial intelligence

Editorial on the Research Topic
Canine lymphoma pathogenesis, diagnosis, prognosis, and treatment: current and future perspectives

Tumors of the hemolymphatic system are divided into lymphoid (lymphoma and leukemia) and myeloid leukemias, with lymphomas arising in lymphoid tissues outside the bone marrow and leukemias arising in the bone marrow or spleen (1). Canine lymphoma itself encompasses a heterogeneous group of malignancies, with different underlying molecular landscapes, clinical presentations, histologic distribution, morphology of cells, immunophenotype, prognosis, therapies, and outcomes. The Kiel and WHO/REAL classifications use multiple parameters to subdivide lymphomas into many categories and there is compelling evidence of the effectiveness of molecular techniques, which are gaining a primary role and complementing these morphologic classifications. There have been significant changes in the diagnosis, staging, classification, and treatment of canine lymphoma over the past few years. These improvements are due in large part to advances in basic understanding of the disease and novel therapies, particularly those used to treat the most aggressive subtypes.

In light of these considerations, lymphoma might be regarded as a fertile starting point for different experts, including internal medicine specialists, clinical and anatomic pathologists, oncologists, diagnostic imaging experts, and surgeons, to profitably discuss, confront, and provide their insights and perspectives. Furthermore, the increasing understanding of the biology of lymphomas developing in nonhuman species has created enthusiasm around the use of animal models that might recapitulate the human disease in more biologically pertinent ways. The development of lymphoma in companion pets, namely dogs, for example, displays many similarities with the human disease, so pets could serve as a meaningful model to improve translational drug development while concomitantly creating new treatment opportunities (2).

We include in the following paragraphs a brief summary of the main findings reported by different authors in their nine manuscripts that form this Research Topic.

Unfortunately, many types of cancer are detected at an advanced stage, when treatment options are limited and prognosis is poor. Early detection is an essential key point in the diagnosis of cancer, substantially increasing survival rates. Addressing this compelling need for cost-effective, simple, rapid, and non-invasive tests and novel diagnostic tools to be

validated, up to five reviews of this Research Topic focus on early diagnostic biomarkers for canine lymphomas.

Sharif et al. validated an ELISA test intendent to measure a canine serum, Thymidine Kinase 1 (TK1), a protein involved in the pathogenesis of lymphoma, and compare its levels among dogs harboring lymphoma and healthy dogs. A statistically significant difference was found between these two groups, placing the canine TK1 ELISA test as an efficient screening tool. On this track, Olayinka et al. identified novel RNA biomarkers as an attempt to have repeatable tools to distinguish early-stage cutaneous T-cell lymphoma (CTCL) from interface dermatitis, with interesting parallelisms with the human counterpart. These are promising instruments to develop targeted therapies and treatment responses for both veterinary and human cutaneous T cell lymphomas.

Hammer et al. focused on MicroRNAs (miRNA, small non-coding RNAs), physiologically occurring small non-coding RNA molecules amounting to ∼18–25 nucleotides that are not able to code for proteins but are involved in regulating gene expressions in the post-transcription process. Dysregulated miRNAs in canine lymphomas were evaluated, exploiting their diagnostic utility and highlighting different expression profiles not only between healthy vs. lymphoma-bearing patients but also among different canine lymphoma subtypes.

Next-generation sequencing (NGS) technology was explored by Fibi-Smetana et al. as a promising molecular tool for characterizing and stratifying canine lymphoma patients. NGS has numerous applications, ranging from whole-genome (re)sequencing to targeted sequencing for variant identification or confirmation. In contrast to whole-genome sequencing, targeted NGS focuses on a specific set of genomic loci that are likely to be involved in the phenotype of interest, delivering higher coverage levels at a more affordable cost, and making it amenable to samples containing small DNA amounts. In detail, the authors developed a targeted sequencing panel for canine lymphoma (TiHoCL), comprising ∼100 canine loci, with encouraging results.

Moving away from molecular biology, Robertson et al. validated a screening test to be performed on canine urine samples, which was able to provide a fingerprint of urine of dogs harboring malignancies, one of which was lymphoma, different from that observed in healthy individuals. This test, known as Raman spectroscopy, has a 94% sensitivity and 90.5% specificity in evaluating metabolomes in urine in a simple, non-invasive, and rapid way.

An *in vitro* assay was presented by Hernández-Suárez et al., detailing changes in components of DNA Damage Response (DDR) in lymphoma cell lines. DDR is one of the pathways whose dysfunction can lead to cancer and resistance to genotoxic stress but might also present an opportunity to be used as a target for anticancer therapies.

An overview on new therapeutical protocols is offered by Lai et al., evaluating the efficacy of two treatments (L-LOP and L-LOPP) for the treatment of canine gastrointestinal (GI) and hepatosplenic (HS) high-grade lymphomas, traditionally associated with a very poor response to chemotherapy and, consequently, poor prognosis. These new suggested protocols turned out to be well tolerated with mild and transient adverse events and longer median survival time and progression-free survival. Moving to B-cell lymphomas, André et al. investigated a promising targeted drug delivery system through liposomes in the treatment of canine B-cell lymphomas, an immunophenotype that accounts for ∼80% of canine lymphomas (3, 4).

Finally, Hubbard-Perez et al. looked to the (close) future, with the application of artificial intelligence (AI) to digital pathology. Deep learning (DL) through convolutional neural networks (CNNs) was applied to distinguish between normal, hyperplastic, and lymphoma-bearing lymph nodes and to discriminate among three common WHO subtypes of canine lymphoma, providing promising results.

Collectively, this Research Topic highlighted current research activities and trends in canine lymphoma, providing a state of art of the tools currently available in diagnosis, prognosis, and treatment and giving insights into the new advances for canine lymphoma in comparative oncology.

Author contributions

VC: Conceptualization, Writing – original draft. MS: Writing – review & editing. CV: Writing – review & editing.

Funding

The author(s) declare that no financial support was received for the research, authorship, and/or publication of this article.

Acknowledgments

We thank the editors, authors, and reviewers that contributed to this Research Topic.

Conflict of interest

CV was employed by Laboklin GmbH & Co. KG. VC was employed by IDEXX Laboratories Italia Srl.

The remaining author declares that the research was conducted in the absence of any commercial or financial relationships that could be construed as a potential conflict of interest.

Publisher's note

References

1. Meuten DJ, Meuten TLK. Tumors of the hemolymphatic system. In: Meuten DJ, editor. *Tumors in Domestic Animals*, 5th edition. Hoboken, NJ: John Wiley & Sons, Inc (2016), p. 632–88.

2. Richards KL, Suter SE. Man's best friend: what can pet dogs teach us about non-Hodgkin's lymphoma? *Immunol Rev.* (2015) 263:173–91. doi: 10.1111/imr.12238

3. Ito D, Frantz AM, Modiano JF. Canine lymphoma as a comparative model for human non-Hodgkin lymphoma: recent progress and applications. *Vet Immunol Immunopathol.* (2014) 159:192–201. doi: 10.1016/j.vetimm.2014.02.016

4. Zandvliet M. Canine lymphoma: a review. *Vet Q.* (2016) 36:76–104. doi: 10.1080/01652176.2016.1152633

frontiers | Frontiers in Veterinary Science

TYPE Original Research
PUBLISHED 16 August 2023
DOI 10.3389/fvets.2023.1227683

OPEN ACCESS

EDITED BY
Monica Sforna,
University of Perugia, Italy

REVIEWED BY
Joy Archer,
University of Cambridge, United Kingdom
Maurice Zandvliet,
Utrecht University, Netherlands

*CORRESPONDENCE
Beatriz Hernández-Suárez
✉ beatriz.hernandez-suarez@upwr.edu.pl

RECEIVED 23 May 2023
ACCEPTED 31 July 2023
PUBLISHED 16 August 2023

CITATION
Hernández-Suárez B, Gillespie DA, Dejnaka E, Kupczyk P, Obmińska-Mrukowicz B and Pawlak A (2023) Studying the DNA damage response pathway in hematopoietic canine cancer cell lines, a necessary step for finding targets to generate new therapies to treat cancer in dogs.
Front. Vet. Sci. 10:1227683.
doi: 10.3389/fvets.2023.1227683

Studying the DNA damage response pathway in hematopoietic canine cancer cell lines, a necessary step for finding targets to generate new therapies to treat cancer in dogs

Beatriz Hernández-Suárez[1]*, David A. Gillespie[2], Ewa Dejnaka[1], Piotr Kupczyk[3], Bożena Obmińska-Mrukowicz[1] and Aleksandra Pawlak[1]

[1]Department of Pharmacology and Toxicology, Faculty of Veterinary Medicine, Wroclaw University of Environmental and Life Sciences, Wrocław, Poland, [2]Facultad de Medicina, Instituto de Tecnologías Biomédicas, Universidad de La Laguna, Tenerife, Spain, [3]Division of General and Experimental Pathology, Department of Clinical and Experimental Pathology, Faculty of Medicine, Wroclaw Medical University, Wroclaw, Poland

Background: Dogs present a significant opportunity for studies in comparative oncology. However, the study of cancer biology phenomena in canine cells is currently limited by restricted availability of validated antibody reagents and techniques. Here, we provide an initial characterization of the expression and activity of key components of the DNA Damage Response (DDR) in a panel of hematopoietic canine cancer cell lines, with the use of commercially available antibody reagents.

Materials and methods: The techniques used for this validation analysis were western blot, qPCR, and DNA combing assay.

Results: Substantial variations in both the basal expression (ATR, Claspin, Chk1, and Rad51) and agonist-induced activation (p-Chk1) of DDR components were observed in canine cancer cell lines. The expression was stronger in the CLBL-1 (B-cell lymphoma) and CLB70 (B-cell chronic lymphocytic leukemia) cell lines than in the GL-1 (B-cell leukemia) cell line, but the biological significance of these differences requires further investigation. We also validated methodologies for quantifying DNA replication dynamics in hematopoietic canine cancer cell lines, and found that the GL-1 cell line presented a higher replication fork speed than the CLBL-1 cell line, but that both showed a tendency to replication fork asymmetry.

Conclusion: These findings will inform future studies on cancer biology, which will facilitate progress in developing novel anticancer therapies for canine patients. They can also provide new knowledge in human oncology.

KEYWORDS

Chk1, Rad51, ATR, Claspin, lymphoma, leukemia

1. Introduction

Comparative oncology studies cancer across a range of animal species. Thanks to that, it can provide new insights into cancer development and risk factors that may also affect humans. According to the American Veterinary Medical Association, about half of the dogs aged over 10 years will suffer from cancer (1) and in the United States, around 4.2 million dogs are diagnosed with cancer each year (2). With this huge number of patients and a shorter life span than humans, the possibility of completing a clinical trial testing new therapies in canine patients is really promising. Due to biological similarities between cancers in humans and dogs, the results of such trials could potentially be extended to human medicine (3).

Several fundamental regulatory cellular processes are frequently altered in cancer. Disturbances in the functioning of the DNA Damage Response (DDR) pathway are often connected with carcinogenesis (4–11) and resistance to genotoxic stress (12–15), but they also present an opportunity to be used as target for anticancer therapies. Such a therapeutic approach includes the use of DDR inhibitors to overcome cell resistance to genotoxic therapies, or documenting variations in the expression of DDR proteins as potential markers of sensitivity to specific therapies in oncological patients (7, 16–18). Thus, there is a need to validate reagents and molecular techniques for use in canine cells, which will facilitate comparative oncology research.

The DDR is one of the pathways whose dysfunction can lead to cancer. ATR and Chk1 comprise the principal DDR pathway available to most cancer cells that lack functional p53, which is found altered in almost 50% of human cancers and has also been reported in a variety of canine cancers (19, 20). The ATR-Chk1-Claspin pathway has been found to be upregulated in cancer cells, as compared with non-cancerous cells in humans (6), therefore its inhibition presents an attractive target for new-generation cancer therapies (18, 21). In normal circumstances, the DDR plays a fundamental role in the regulation of cell cycle progression and DNA replication regulation (Figure 1) (22). For example, after DNA damage or during replication stress, thanks to the activation of various DDR components, it is possible to prevent defective cells from dividing by inducing cell cycle arrest. To this end, ataxia telangiectasia mutated and Rad3-related (ATR) kinase phosphorylates and activates checkpoint kinase 1 (Chk1), which induces cell cycle arrest (23). During this complex process, an important mediator protein called Claspin helps to activate Chk1 (13, 24). While the cell cycle arrest continues, the DDR system cooperates to recruit the repair machinery, including proteins involved in homologous recombination (HR), to repair any DNA damage that has occurred. An important component here is the BRCA1-PALB2-BRCA2 complex, which recruits the recombinase Rad51 to form filaments and bind damaged DNA to form a D-loop structure (two strands of a double strand DNA that are separated by a third strand) (25–27). Rad51 responds to replication stress in three ways: (1) by helping promote fork reversal when DNA polymerase progression on a single-stranded DNA (ssDNA) template is blocked (e.g., by DNA breaks), (2) by protecting the ssDNA ends from being degraded by endonucleases, and (3) by promoting restart of replication fork progression (28).

To facilitate research into the significance of DDR pathway disturbances in cancer, as well as to inform studies on the development of new therapies targeting the DDR in dogs, we conducted a series of experiments on canine lymphoma/leukemia cell lines to assess (1): the expression of transcripts of DDR components by RNA sequencing in two selected canine cancer cell lines (2), the basal expression levels of key proteins involved in the DDR (ATR, Claspin, Chk1, Rad51), together with checking the feasibility of using commercially available antibodies, and (3) the functionality of the DDR pathway in canine model cells by assessing the DDR pathway activation after DNA damage, using the DNA damaging agent etoposide (detection of γH2AX and p-Chk1). Finally, we performed DNA combing assays to assess DNA replication dynamics in canine lymphoma/leukemia cells by directly visualizing replication fork progression rates and replication origin firing.

2. Materials and methods

2.1. Cells and cell culture

A panel of canine lymphoma/leukemia cell lines: CLBL-1 (B-cell lymphoma), CLB70 (B-cell chronic lymphocytic leukemia), and GL-1 (B-cell leukemia) was used in this study. The CLBL-1 cell line was a gift from Barbara Rütgen from the Institute of Immunology, Department of Pathobiology from the University of Vienna (29), the GL-1 cell line was received from Yasuhito Fujino and Hajime Tsujimoto from the Department of Veterinary Internal Medicine at the University of Tokyo (30), and the CLB70 cell line (31) was established with the participation of researchers from our laboratory; the studies involving animals participants were reviewed and approved by the New York Academy of Sciences *Ad Hoc* Committee on Animal Research and were approved by the First Local Committee for Experiments with the Use of Laboratory Animals, Wroclaw, Poland (approval no. 24/2014).

The culture medium RPMI 1640 (Institute of Immunology and Experimental Therapy, Polish Academy of Science, Wrocław, Poland) was used for the CLBL-1 and GL-1 cell lines, and Advanced RPMI (Gibco, Grand Island, NY, United States) for the CLB70 cell line. The culture media were supplemented with 2 mM L-glutamine (Sigma Aldrich, Steinheim, Germany), 100 U/mL of penicillin, 100 µg/mL of streptomycin (Sigma Aldrich, Steinheim, Germany), and 10–20% heat-inactivated fetal bovine serum (FBS; Gibco, Grand Island, NY, United States). The cells were cultured in an atmosphere of 5% CO_2 and 95% humidified air, at 37°C in 25 cm^2 cell culture flasks (Corning, New York).

2.2. RNA sequencing

RNA was obtained from cultures of the selected cell lines CLBL-1 and GL-1 during unperturbed growth and sequenced by Novogene (United Kingdom). The expected number of Fragments Per Kilobase of transcript sequence per Millions of base pairs sequenced (FPKM) was used to calculate relative gene expression (32). The DDR related GO lists used for the intersection analysis were those presented in Table 1, the gene set information was obtained from the GSEA database (33, 34).

2.3. Treatments

DNA damage was induced by treatment with etoposide (Sigma Aldrich, United States) (a topoisomerase II inhibitor), at 20 µM for 2 h.

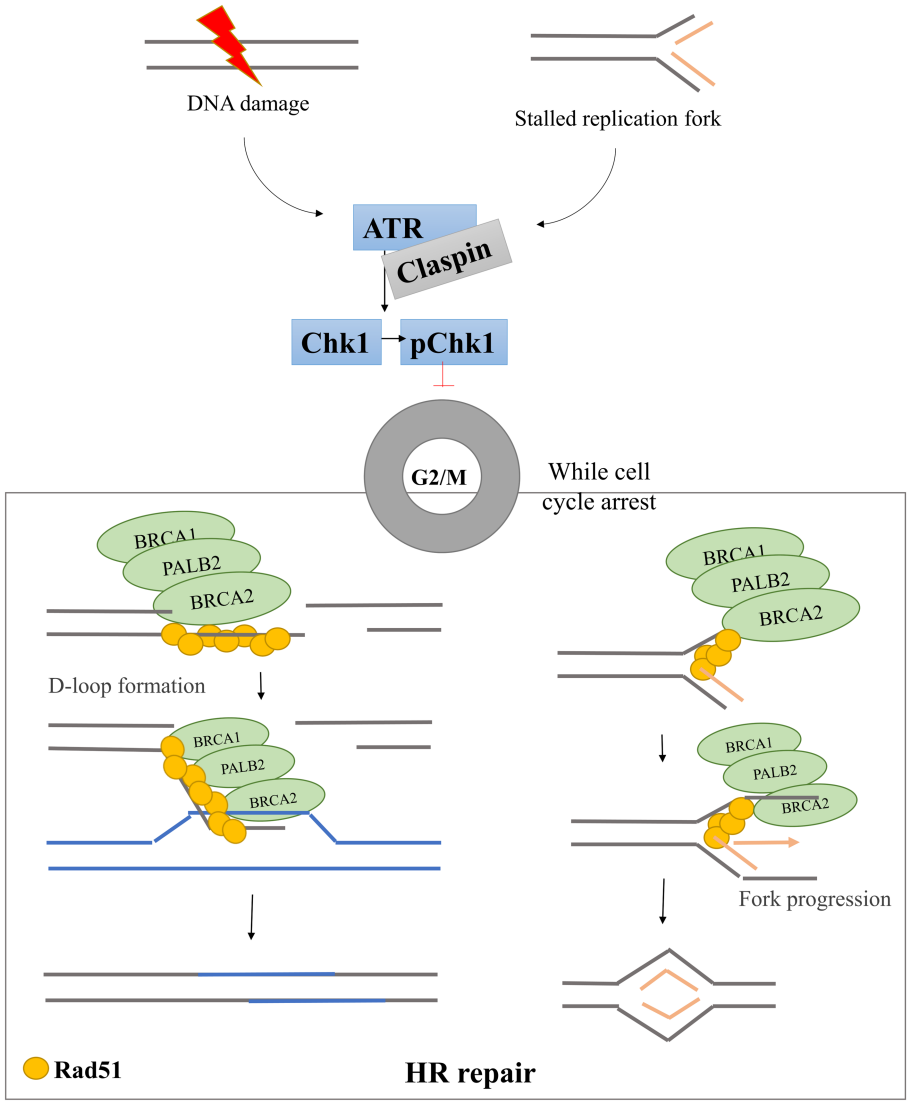

FIGURE 1
DNA damage response pathway scheme. After DNA damage and/or replication fork stalling, the DDR pathway is activated. ATR is phosphorylated and activates Chk1 through phosphorylation. Activated Chk1 induces cell cycle arrest in G2/M phases allowing the BRCA1-PALB2-BRCA2 triad to recruit Rad51 to the damage site. Rad51 forms filaments that bind DNA and promote D-loop formation allowing the HR repair pathways to start.

Treatment conditions were selected based on literature (35) and previous preliminary (Supplementary Figure S5) analysis.

2.4. Western blot

3 x 10^5cells/mL were cultured in 10 mL of media in a 25 cm^2 culture flask per condition. After 48 h of incubation, the samples were lysed in urea/ SDS buffer (composed of 900 µL of 7 M urea, 25 µL of 5 M NaCl, 25 µL 2 M Tris–HCl (pH = 8), 50 µL 20% SDS), and run in 8–12% bis-tris acrylamide gels prepared using a BioRad Mini-PROTEAN Tetra Vertical Electrophoresis Cell system. The samples were transferred to nitrocellulose membrane using BioRad Mini Trans-Blot® Cell for wet transfer and BioRad Trans-Blot® Turbo™ Transfer System device for semi-dry transfer.

The antibodies used in the study were selected based either on available literature data on reactivity with canine cells (Table 2) or comparison of protein sequence homology, and preliminary test results involving a comparison of the observed bands with the predicted molecular mass (kDa) of the protein of interest. Goat Anti-Mouse Immunoglobulins/HRP (#P0447 at 1:20000 concentration in TBS-T solution) and Goat Anti-Rabbit Immunoglobulins/HRP (#P0448 at 1:10000 concentration in TBS-T solution) were used as secondary antibodies. Both secondary antibodies were from Dako, now part of Agilent (United States, Santa Clara).

2.5. qPCR

2.5.1. Bioinformatic sequence analysis and primer design

The *Canis lupus familiaris* nucleotide accession number sequences for mRNA of the target genes (TGs): Atr, Claspin, and six housekeeping genes (HKGs): Actb, Ppia, and Rplp0 were taken from

TABLE 1 DDR related GO lists.

Gene set	Species
AMUNDSON_DNA_DAMAGE_RESPONSE_TP53	Human
GOBP_DNA_DAMAGE_RESPONSE_SIGNAL_TRANSDUCTION_BY_P53_CLASS_MEDIATOR	Human
GOBP_DNA_DAMAGE_RESPONSE_SIGNAL_TRANSDUCTION_BY_P53_CLASS_MEDIATOR	Mouse
GOBP_DNA_DAMAGE_RESPONSE_SIGNAL_TRANSDUCTION_BY_P53_CLASS_MEDIATOR_RESULTING_IN_CELL_CYCLE_ARREST	Human
GOBP_DNA_DAMAGE_RESPONSE_SIGNAL_TRANSDUCTION_BY_P53_CLASS_MEDIATOR_RESULTING_IN_CELL_CYCLE_ARREST	Mouse
GOBP_DNA_DAMAGE_RESPONSE_SIGNAL_TRANSDUCTION_RESULTING_IN_TRANSCRIPTION	Human
GOBP_DNA_DAMAGE_RESPONSE_SIGNAL_TRANSDUCTION_RESULTING_IN_TRANSCRIPTION	Mouse
GOBP_NEGATIVE_REGULATION_OF_DNA_DAMAGE_RESPONSE_SIGNAL_TRANSDUCTION_BY_P53_CLASS_MEDIATOR	Human
GOBP_NEGATIVE_REGULATION_OF_DNA_DAMAGE_RESPONSE_SIGNAL_TRANSDUCTION_BY_P53_CLASS_MEDIATOR	Mouse
GOBP_POSITIVE_REGULATION_OF_DNA_DAMAGE_RESPONSE_SIGNAL_TRANSDUCTION_BY_P53_CLASS_MEDIATOR	Human
GOBP_POSITIVE_REGULATION_OF_DNA_DAMAGE_RESPONSE_SIGNAL_TRANSDUCTION_BY_P53_CLASS_MEDIATOR	Mouse
GOBP_POSITIVE_REGULATION_OF_DNA_DAMAGE_RESPONSE_SIGNAL_TRANSDUCTION_BY_P53_CLASS_MEDIATOR_RESULTING_IN_TRANSCRIPTION_OF_P21_CLASS_MEDIATOR	Human
GOBP_REGULATION_OF_DNA_DAMAGE_RESPONSE_SIGNAL_TRANSDUCTION_BY_P53_CLASS_MEDIATOR	Human
GOBP_REGULATION_OF_DNA_DAMAGE_RESPONSE_SIGNAL_TRANSDUCTION_BY_P53_CLASS_MEDIATOR	Mouse
GOBP_REGULATION_OF_DNA_DAMAGE_RESPONSE_SIGNAL_TRANSDUCTION_BY_P53_CLASS_MEDIATOR_RESULTING_IN_TRANSCRIPTION_OF_P21_CLASS_MEDIATOR	Human
GOBP_REGULATION_OF_DNA_DAMAGE_RESPONSE_SIGNAL_TRANSDUCTION_BY_P53_CLASS_MEDIATOR_RESULTING_IN_TRANSCRIPTION_OF_P21_CLASS_MEDIATOR	Mouse
REACTOME_P53_DEPENDENT_G1_DNA_DAMAGE_RESPONSE	Human
REACTOME_SUMOYLATION_OF_DNA_DAMAGE_RESPONSE_AND_REPAIR_PROTEINS	Human
WP_DNA_DAMAGE_RESPONSE	Human
WP_DNA_DAMAGE_RESPONSE_ONLY_ATM_DEPENDENT	Human
WP_MIRNA_REGULATION_OF_DNA_DAMAGE_RESPONSE	Human
WP_MIRNAS_INVOLVED_IN_DNA_DAMAGE_RESPONSE	Human

the Nucleotide Center for Biotechnology Information (NCBI) database (NCBI, United States). The sequences were transferred into the Universal Probe Library. The designed primers and their amplified sequences were additionally verified for their specificity in the Nucleotide Basic Local Alignment Search Tool - Nucleotide-BLAST (NCBI, USA). Gene names, primer sequences for TGs and HKGs, amplicon size, as well their respective gene accession numbers are summarized in Table 3.

2.5.2. RNA isolation and reverse transcription

A total of 1×10^7 cells cultured in 10 mL from the CLBL-1, CLB70, and GL-1 lymphoma cell lines were centrifuged at 300 g, 4° C, and resuspended in 500 µL of TRIzol reagent (Invitrogen, United States). The cells were immediately transferred to a low-temperature freezer and stored in Eppendorf tubes at −80° C for further analysis. Total RNA isolation was performed using Total RNA Zol-Out™ D (A&A Biotechnology, Poland) according to the protocol provided in the isolation kit. Briefly, the cells were removed from the low-temperature freezer and thawed on ice for 30 min. After that, 167 µL of ultra pure molecular biology water (A&A Biotechnology, Poland) were added, and the sample was mixed by inversion. Next, the cells were spun for 10 min at 10000 rpm. The supernatant was mixed with 1 volume of 96–100% ethanol (Stanlab, Poland) and gently agitated until a homogenous solution was obtained. The supernatants from each tube were transferred into new tubes with an RNA membrane binding column and were centrifuged through the column for 1 min at 10000 rpm and 4° C. The columns were rinsed with 700 µL washing A2W buffer for 2 min at 10000 rpm. DNA digestion for 15 min at 37° C in a thermoblock was performed using DNAse according to the manufacturer's protocol. The enzymatic activity of the digestive buffer was inhibited by adding 700 µL of R81 buffer and centrifugation [1 min at 10000 rpm at room temperature (RT)]. The filtrate was collected and loaded again onto the column. The membranes were rinsed twice with 700 µL and 200 µL of A2W buffer, centrifuged as described above, and transferred into new Eppendorf tubes. Then, 40 µL of sterile water were added, and after 3-min incubation at RT the tubes with the membranes were centrifuged as above. RNA quality and quantity were estimated using Implen NanoPhotometer (Eppendorf, Germany), and only the samples with a 260/280 nm absorbance coefficient between 1.8 and 2.1 were used for the final experiments. The TranScriba noGenome Kit (A&A Biotechnology, Poland) was used to perform reverse transcription, according to the manufacturer's recommendations in the MJ Research PTC-100 thermocycler (Marshall Scientific, United States). First, 1 µg of total RNA was mixed with the noGenome master mix. After a 10-min incubation at 42° C, 7 µL of the mentioned mix were added to the RT master

mix. The RT master mix included 4 µL of TranScriba buffer, 0.5 µL of RNAse inhibitor, 2 µL of dNTP, 1 µL of starter oligo (dT), 4 µL of TranScriba reverse transcriptase and 1.5 µL of sterile water for one reaction. The reverse transcription protocol was as follows: the first step of 60 min at 42°C, the second step of 5 min at 70°C, and the final step of 5 min at 4°C. The obtained cDNA was stored at −20°C.

2.5.3. Gene expression analysis using real-time PCR

The real-time PCR gene expression analyzes were performed in triplicate from three independent cell cultures. The reaction mix (per well) included 5 µL of RT PCR Mix SYBR® (A&A Biotechnology, Poland), 0.5 µM of forward and reverse primers (Eurofins Genomics AT GmbH, Poland), and 1 µL of cDNA diluted with molecular biology water (16.65 ng cDNA per well). Real-time PCR was performed using the LightCycler 480 II (Roche Molecular Systems Inc., United States) instrument under the following conditions: pre-incubation at 95°C for 10 min, 50 cycles of amplification: 10 s at 95°C for denaturation, 30 s at 60°C for annealing, and 15 s at 72°C for elongation. The gene detection analyzes and primer specificity were further improved by melting curve analysis. The gene expression was categorized using the following scale:

"0" lack of gene expression, Ct values above 35.
"1" very low gene expression, Ct values between 30 and 35.
"2" low gene expression, Ct values between 28 and 30.
"3" regular gene expression, Ct values between 22 and 28.
"4" high gene expression, Ct values between 15 and 22.
"5" very high gene expression, Ct values below 15.

2.6. DNA combing assay

A total of 1.6×10^6 cells were cultured in 10 mL of media, then pulse-labeled with 5-iodo-2′-deoxyuridine (IdU) at 25 µM, followed by 5-chloro-2′-deoxyuridine (CldU) at 200 µM, for 15 min each. The cells were recovered by centrifugation at 300 g after each pulse, and the media were refreshed with each analog. Next, the cells were resuspended in cold PBS and warmed to 42°C, using 5×10^5 cells per agarose plug. The cells were gently mixed with 1% agarose in PBS and divided into the casting mold to generate the plugs. After treatment with proteinase K (in a buffer made of 1% Sarkosyl, 10 mM Tris pH 7.5, 50 mM EDTA) at 50°C overnight, the DNA was stained with YOYO-1 (5 µM in TE solution for 2–5 min) to check the quality of the fibers. After melting the agarose, the extracted DNA was poured into a reservoir, where a coverslip was inserted, and the DNA fibers were stretched. The resulting fibers were visualized by immunofluorescence detecting the IdU and CldU analogs with red and green antibodies. The coverslips were incubated for 45 min with murine anti-BrdU (IdU, ref. 34,780 Becton Dickinson, United States), and rat anti-BrdU (CIdU, Eurobio ref. ABC117-7513, France), as primary antibodies for the analogs, and for 30 min with goat anti-mouse IgG1 Alexa 564 (ref. A21123 Molecular Probes, Thermo Fisher Scientifics, United States) and chicken anti-rat Alexa 488 (ref. A21470 Molecular Probes, Thermo Fisher Scientifics, United States) as secondary antibodies for the analogs. The coverslips were incubated for 30 min with autoanti-ssDNA DSHB by Voss, E.W. (Hybridoma Product autoanti-ssDNA) autoanti-ssDNA DSHB by Voss, E.W. (DSHB, United States) to detect whole DNA fibers, and then for 30 min with a secondary antibody goat anti-mouse IgG2a Alexa 647 (ref. A21241 Molecular Probes, Thermo Fisher Scientifics, United States). Image acquisition was performed with a 40x objective using a confocal microscope (DM6000; Leica). The fork velocity (FV) was calculated by multiplying the length of the green track of the fiber in micrometers by 2 to obtain Kb, and dividing it by 15 min (time of pulse). Fork asymmetry (FA) was calculated by dividing the long track by the short track. For this analysis, only the first analog incorporation tracks (green tracks) were considered.

2.7. Statistical analysis

For the combing assay analysis, the Mann–Whitney test was performed to compare the cell lines and analyze potential differences. Scatterplots were prepared to visually represent the differences between the two cell lines.

Statistical analysis was performed using TIBCO Software Inc. (2017) Statistica (data analysis software system), version 13 http://statistica.io.

TABLE 2 Antibody list showing percentage protein identity between human and dog DDR components.

Protein	Clone	Ref. catalog	Dilution used in the study	% homology*		Literature
				Total protein	Epitope region	
Chk1	G-4	sc-8,408	1:1000 in 3% BSA in TBS-T	96.2		(36–39)
Phospho-Chk1 (SER345)	133D3	#2348	1:1000 in 3% BSA in TBS-T	96.2	100	(36, 38–41)
β-Actin	C4	sc-47,778	1:1000 in 3% milk in TBS-T	97.22	100	(42–47)
ATR	C-1	sc-515,173	1:800 in 3% BSA in TBS-T	94.75	100	(39, 40, 48)
Rad51	G-9	sc-377,467	1:600 in 3% BSA in TBS-T	99.12	100	(41, 49, 50)
Claspin	B-6	sc-376,773	1:800 in 3% BSA in TBS-T	84.47	88	(40)
Anti-gamma H2AX	9F3	ab26350	1:1000 in 3% BSA in TBS-T	99.17	100	(43, 44, 48, 51, 52)

Basic Local Alignment Search Tool (BLAST) of protein sequences. Antibodies immunogen sequences were analyzed in BLAST from National Center for Biotechnology Information (NCBI) (www2) (53).
Values are given for both total protein and, where known, for the specific polypeptide region used as immunogen to generate each antibody.

TABLE 3 Gene names, forward (F) and reverse (R) primer sequences, amplicon nucleotide (nt) sizes with their respective gene accession numbers.

Gene name	Forward (F) and Reverse (R) primer sequences	Amplicon size (nt)	Gene accesion number
Target Genes (TGs):			
ATR	F: ACCAGACAGCCTACAATGCT R: CCACTTTGCCCTCTCCACAT	77	XM_038432561.1
CLSPN	F: CGCACAAAGCCAGGTGAAAA R: CGTTCCTCATGCCTACGGAG	80	XM_539598.6
Housekeeping genes (HKGs):			
ACTB	F: CGCAAGGACCTCTATGCCAA R: CTTCTGCATCCTGTCAGCGA	78	NM_001195845.3
PPIA	F: TTTGGCAAGGTCAAGGAGGG R: TGGTCTTGCCATTCCTGGAC	73	XM_038689274.1
RPLP0	F: ACATGCTGAACATCTCCCCC R: CAGGGTTGTAGATGCTGCCA	80	XM_038436104.1

3. Results

3.1. RNA-sequencing analysis revealed the presence of principal components of the DDR pathway in canine cell lines

The canine lymphoma cell line CLBL-1 and the canine leukemia cell line GL-1 expressed a total of 16,220 genes, from which 271 (~2%) are DDR pathway members. Specifically, the CLBL-1 cell line expressed 260 DDR genes, and the GL-1 cell line 266, with 255 genes in common (Figure 2A). The relative expression of the most important genes with a role in the ATR- and HR-repair pathways was analyzed for both cell lines. Higher expression of all the genes was found in the CLBL-1 than in the GL-1 cell line, except for RAD51 which showed slightly higher expression in the GL-1 cell line (Figure 2B).

3.2. Expression and activation of the DDR pathway components in canine cancer cells

Considering that ATR, Claspin, Chk1, and Rad51 are among the most important proteins of the DDR pathway, they are still quite uncharacterized in dogs. Thanks to the progress made in recent years in veterinary medicine, and in particular in veterinary oncology, currently there are some tools available for their study in dogs (for example antibodies and siRNAs).Our initial aim was to identify commercial antibodies against key components (ATR, Claspin, Chk1, Rad51) of the DDR that would be suitable for use in canine cells. Western blot screening was performed to analyze the basal protein expression levels, and to determine whether the pathway activation in response to DNA damage occurs in canine cells (detection of γH2AX and p-Chk1; Figure 3A; Supplementary Figure S4). All the antibodies used in the study were monoclonal antibodies generated using human epitopes as immunogens. The BLAST alignment comparing human and canine protein sequences demonstrated high homology overall and, where known, within the polypeptide region used as immunogen (Table 2; alignments in Supplementary material).

As detecting high-molecular-weight proteins by means of a western blot can be technically challenging (54), a qPCR was performed for the genes encoding ATR and Claspin, in order to obtain more information about the expression of these DDR components in the panel of the analyzed cell lines.

3.2.1. ATR

BLAST alignment demonstrated 94.75% identity between the human and canine ATR protein sequences, which justified the assumption that an antibody directed against a human protein would cross-react with the canine protein. Indeed, the band detected with the antibody ATR C-1 (Santa Cruz sc-515,173) corresponded with the ~220 kDa molecular mass expected for this protein. ATR was readily detected in only two of the three cell lines analyzed, with expression of ATR being higher in CLB70 cells than CLBL-1 and undetectable in GL-1 cells (Figure 3A). As ATR is considered essential for cell proliferation/ survival, and ATR mRNA expression was readily detected in the GL-1 cell line (see below), we assume that the level of ATR protein expression in this cell line is below the limit of detection using this particular method of cell extraction/ WB.

qPCR analysis confirmed that ATR mRNA is expressed in the three cell lines tested, with mean threshold cycle (Ct) values of 25.21 ± 0.27 for the CLBL-1 cell line, 28.15 ± 3.29 for the CLB70 cell line, and 25.72 ± 0.61 for the GL-1 cell line. Although the expression of ATR was substantially lower than the expression of the HKGs (Figure 3B), Ct values below 29 indicate that ATR mRNA is relatively abundant in these cells.

3.2.2. Claspin

In the case of Claspin, BLAST alignment demonstrated 84.47% identity between the human and canine proteins, again supporting the possibility of cross-reactivity of human antibodies with canine proteins. The expression of Claspin was detectable using the Claspin B-6 (Santa Cruz sc-376,773) antibody. The antibody recognized a protein of the expected molecular mass of ~180 kD, thus confirming cross-reactivity with canine Claspin. Claspin expression was observed in all three cell lines, although the expression levels varied. Claspin expression levels were substantially higher in the CLBL-1 and CLB70 cell lines than in the GL-1 cell line, similar to the expression of ATR (Figure 3A).

qPCR analysis showed that the Claspin mRNA was also expressed in the three cell lines, with Ct values of 24.95 ± 0.17 for the CLBL-1 cell

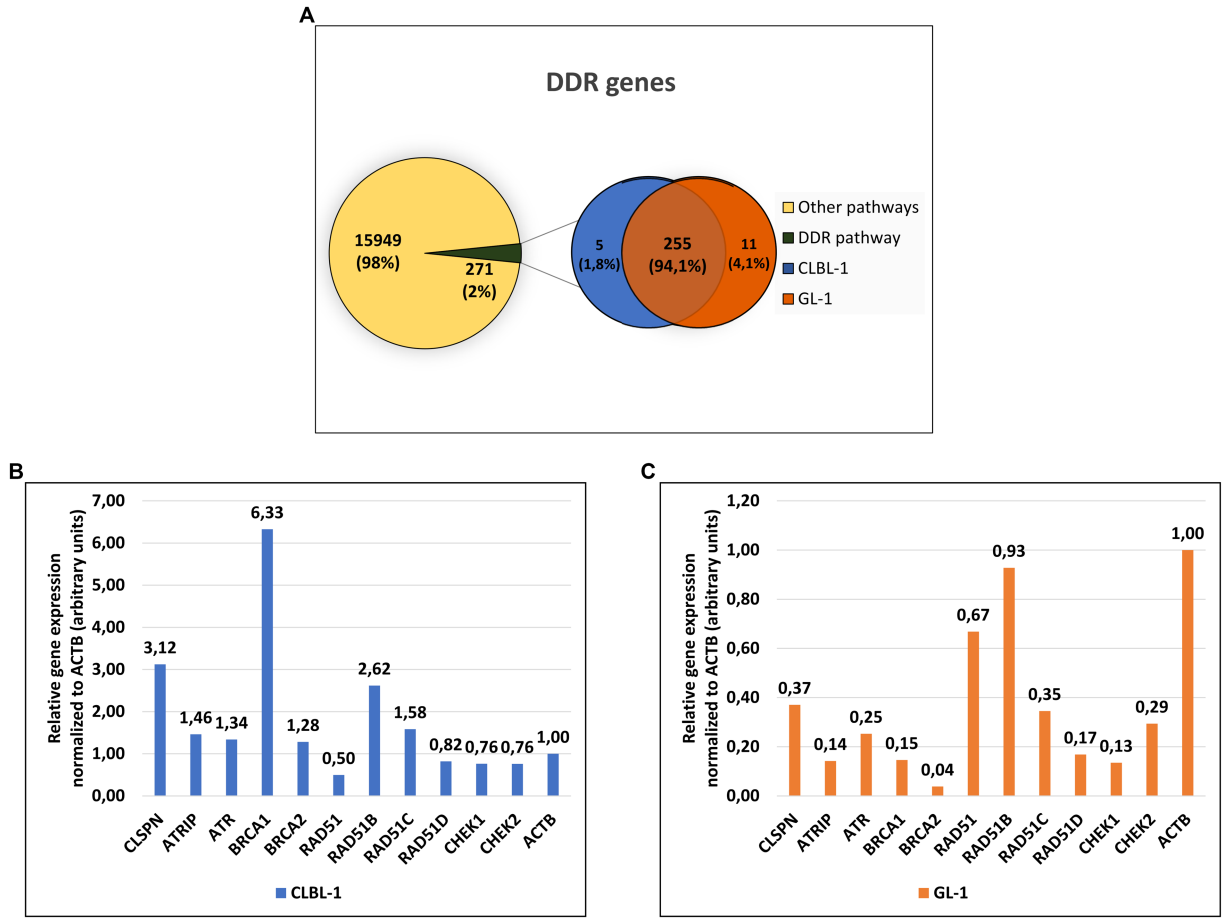

FIGURE 2
Approximately 2 % of the genes expressed in the lymphoma and leukemia canine cells encode components of the DDR pathway. **(A)** From the 16,220 genes expressed in the CLBL-1 and GL-1 cell lines, only 271 genes are from DDR pathway. **(B,C)** The relative gene expression (calculated by FPKM method) of the ATR-pathway and HR repair components were compared after being normalized to the expression of ACTB gene in CLBL-1 and GL-1, respectively.

line, 27.63 ± 2.70 for the CLB70 cell line, and 26.19 ± 0.74 for the GL-1 cell line. Similar to ATR, the expression of the Claspin mRNA in each case was substantially lower than that of the HKGs (Figure 3B).

3.2.3. Chk1 and p-Chk1

BLAST alignment for Chk1 protein sequences between humans and dogs showed a high 96.2% identity. This analysis also confirmed that canine Chk1 contains the key regulatory site, serine 345 (S345), that is phosphorylated by ATR to activate Chk1 in response to genotoxic stress. This means that with the use of the tested antibodies Chk1 G-4 (Santa Cruz sc-8,408) and Phospho-Chk1 (SER345) 133D3 (Cell Signaling #2348) directed against human epitopes, both the basal level expression of Chk1 kinase and its activation after DNA damage can be tested in canine cells. Indeed, both antibodies detected proteins of the expected molecular mass (~56 KD) in all three cell lines (Figure 3A). Interestingly, however, the two cell lines with the highest basal expression of Chk1 were again CLBL-1 and CLB70, which also exhibited the highest expression of both ATR and Claspin. Basal levels of active, phospho-S345 Chk1 were also detected in all three cell lines, being highly expressed in CLB70 as compared with the other cell lines (Figure 4). The ability to monitor the level of Chk1 kinase, as well as its activation, will facilitate the development of new molecularly targeted therapies in canine oncology.

3.2.4. Rad51

BLAST alignment comparing Rad51 protein sequences demonstrated 99.12% identity between human and canine protein, indicating a high probability that an antibody directed at the human protein will detect the canine homolog. As expected, using Rad51 G-9 (Santa Cruz sc-377,467) antibody, we detected a band of ~37 kDa corresponding to the expected molecular mass of Rad51. Basal Rad51 recombinase expression was detected in all three cell lines with the highest level of expression in the CLBL-1 cell line (Figure 3A).

3.3. Activation of the DDR pathway after etoposide treatment observed as an increase in Chk1 kinase S345 phosphorylation

Next, we analyzed the expression levels and possible regulatory modifications of the canine DDR proteins after inducing activation of the DDR pathway by treating the cells with

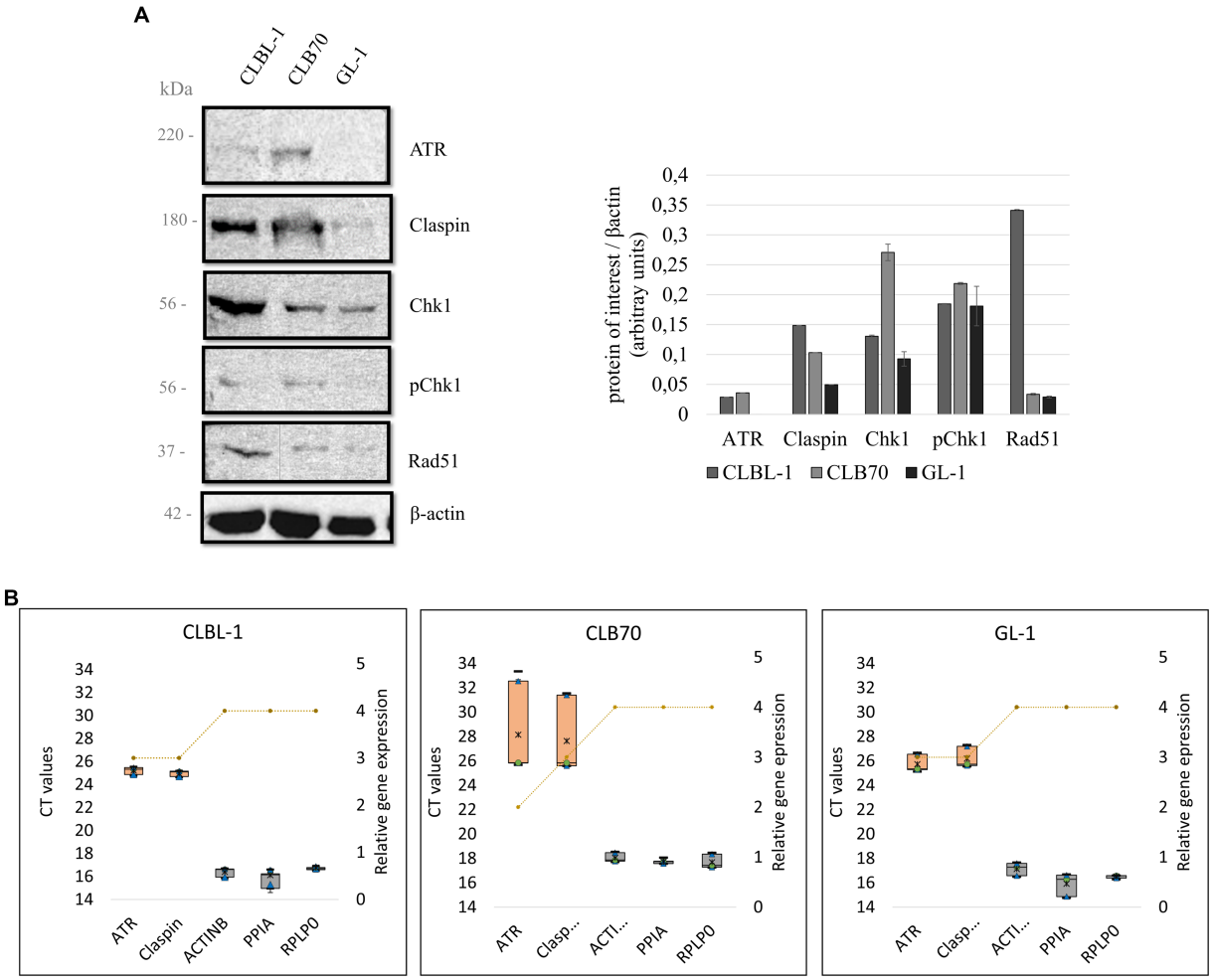

FIGURE 3
(A) Basal expression levels of key DDR proteins in canine lymphoma/leukemia cell lines. Selected proteins of the DDR were analyzed to verify their basal expression level in different canine cell lines. Quantification was performed by normalizing the expression level of the protein of interest to the expression level of the loading control, β-actin. Mean and standard deviations were calculated based on three repetitions from independent experiments. **(B)** Relative gene expression of ATR and Claspin in different cell lines. A box and whiskers plots present raw Ct values obtained with the qPCR for ATR, Claspin, and three selected HKGs: ACTB, PPIA, and RPLP0 (left Y axis). The orange boxes represent the target genes, and the gray ones the HKGs. Minimum and maximum Ct values are represented as black lines, the 25 and 75% quartiles are represented as blue triangles, the median is represented with a green dot, and the mean with a black asterisk. The relative gene expression (right Y axis) of ATR, Claspin and the HKGs for different cell lines is represented by a yellow striped line. The rank for the gene expression is 0 = no expression (Ct above 35), 1 = very low expression (30–35), 2 = low expression (28–30), 3 = regular expression (22–28), 4 = high expression (15–22), and 5 = very high expression (10–15).

a classic DNA damaging agent, etoposide. Several studies have reported DDR activation through phosphorylation of Chk1 and an increase of Rad51 expression after treatment with the DNA damaging agent etoposide (55, 56). This information, together with the fact that etoposide is a chemotherapeutic drug used as a treatment for several cancers (57, 58), are the reasons why we decided to select it for our study to induce DNA damage. There were no major changes in the expression levels of total Chk1 after the treatment with etoposide, but the level of Chk1 phosphorylated at S345 varied considerably after exposure to this toxic agent (20 µM for 2 h). The CLBL-1 and CLB70 cell lines, which showed S345 phosphorylation of Chk1 in basal conditions, were also found to present a considerable increase in the phosphorylation levels after the treatment with the DNA damaging agent, while in the GL-1 cell line, this increase was more modest (Figure 4).

3.4. DNA combing assay in the canine cells

Advanced techniques, such as DNA combing, can provide much greater insight into DNA replication dynamics by directly visualizing replication fork progression rates and replication origin firing. Due to the important role of ATR-Chk1 in replication, we wished to evaluate the feasibility of performing DNA combing in canine cells.

The selected cell lines for this study were GL-1 and CLBL-1, since both present high expression level of Rad51 (Figure 3A; Supplementary Figures S1, S2), which may be related to replication stress. The protocol had to be slightly modified for use with suspension cells. Following the modified protocol, the cells were treated with proteinase K at 0.4 mg/mL. In the first experiment, many fibers were seen to be broken, so subsequently the cells were treated with a lower concentration of proteinase K (0.2 mg/mL), and the quality of the fiber integrity improved (Figure 5).

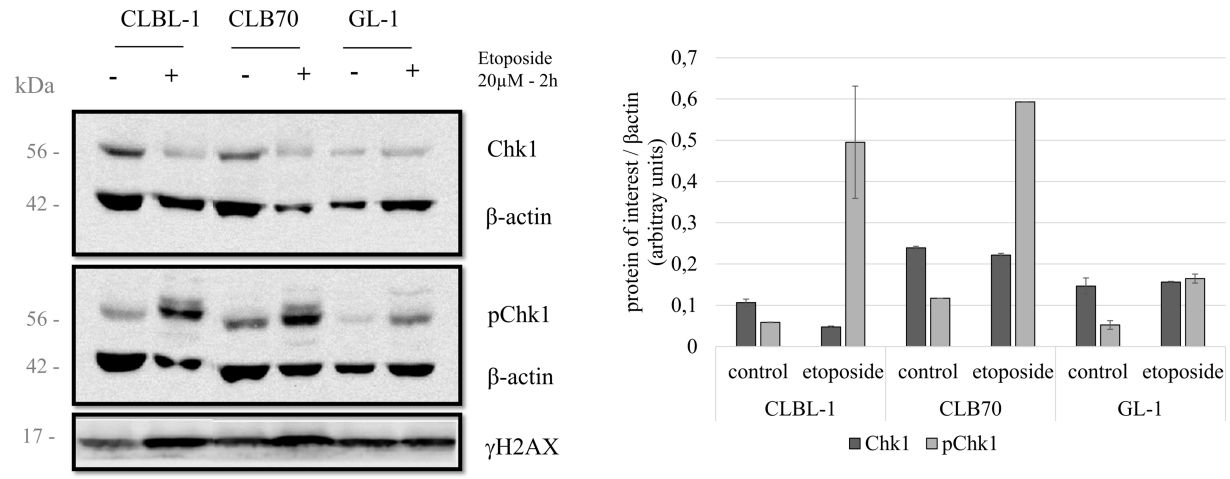

FIGURE 4
Chk1 protein levels and regulatory phosphorylation after etoposide treatment. Three cell lines were treated with 20 μM of the DNA damaging agent etoposide for 2 h in order to study the changes in the activation of Chk1. Expression levels for total Chk1 and S345-phosphorylated Chk1 were analyzed. Expression levels of γH2AX were also determined as a control for DNA damage. Quantification compares the basal condition against the expression after treatment, normalized to β-actin. Mean and standard deviations were calculated based on three independent replicate experiments.

We then used the DNA combing assay to examine replication dynamics in two selected cell lines, CLBL-1 and GL-1. The data are summarized in Table 4 and Figure 6. The replication fork speed was significantly ($p = 8.86^{-21}$) faster in the GL-1 line (1.5 Kb/min) than in the CLBL-1 line (0.86 Kb/min; Figure 6A). When replication fork asymmetry was analyzed, both cell lines had similar means for the calculated ratios, 1.27 for the CLBL-1 and 1.32 for the GL-1 line (Figure 6B), indicating that both exhibited similar levels of replication fork asymmetry.

4. Discussion

4.1. RNA-sequencing analysis revealed the presence of principal components of the DDR pathway in canine cell lines

Due to the important role of the DDR in cancer and the paucity of information about it in canine cancer cells, an RNA-Seq analysis was initially performed in the selected cell lines, CLBL-1 and GL-1, under normal growth conditions. CLBL-1 and GL-1 cell lines were selected for this analysis as representative of common hematopoietic cancers - lymphoma (CLBL-1) and leukemia (GL-1). After sorting the genes by Gene Ontology terms (GO) related to the DDR (Table 1), we found that approximately 2% of expressed genes encode components of the DDR pathway (Figure 2A). Interestingly, the relative expression of most DDR genes in the CLBL-1 line was higher than in the GL-1 cell line, but the expression patterns changed as well. For the CLBL-1 cell line, the most highly expressed genes were *BRCA1*, *CLSPN*, and paralogue B of *RAD51* (*RAD51B*), while *RAD51* exhibited the lowest relative expression (Figure 2B, in blue). In the case of the GL-1 line, the pattern was different, the highest expression was detected for *RAD51B* and *RAD51*, and the lowest for *BRCA2* (Figure 2C, in orange).

Thus, this RNA-Seq analysis revealed that the canine lymphoma and leukemia cells shared expression of a majority of DDR genes, but that the expression of certain key components differed substantially between the tumor types.

4.2. Expression and activation of the DDR pathway components in canine cancer cells

The first screening for the basal expression of DDR proteins (Supplementary Figure S1) indicated significant variations in the protein expression levels for different cancer cell lines. Based on these findings, together with the results of the RNA-Seq analysis (Figure 2), several lymphoma and leukemia cell lines were selected for further experiments. Validation of antibodies that recognize DDR proteins in dogs is needed, and selected commercial antibodies were tested in this study. The BLAST alignment analyzes were performed to check the homology between the human and canine protein sequences. With confirmed high homology, it was assumed that if an antibody detects a single band of correct molecular mass, there is a high probability that this corresponds to the protein of interest, particularly as all the tested antibodies were monoclonal (59, 60).

4.2.1. ATR

ATR was detected in all the cell lines at the mRNA level (Figure 3B). The obtained melting curves showed only one amplicon, which validated the identity of this qPCR product (Supplementary Figure S3). Ct values of 25.21 ± 0.27 for the CLBL-1 cell line, 28.15 ± 3.29 for the CLB70 cell line, and 25.72 ± 0.61 for the GL-1 cell line were observed, indicating robust ATR mRNA expression in all tested cell lines (61).

The BLAST alignment for ATR protein showed a 94.75% protein identity in humans and dogs, meaning that the probability of an

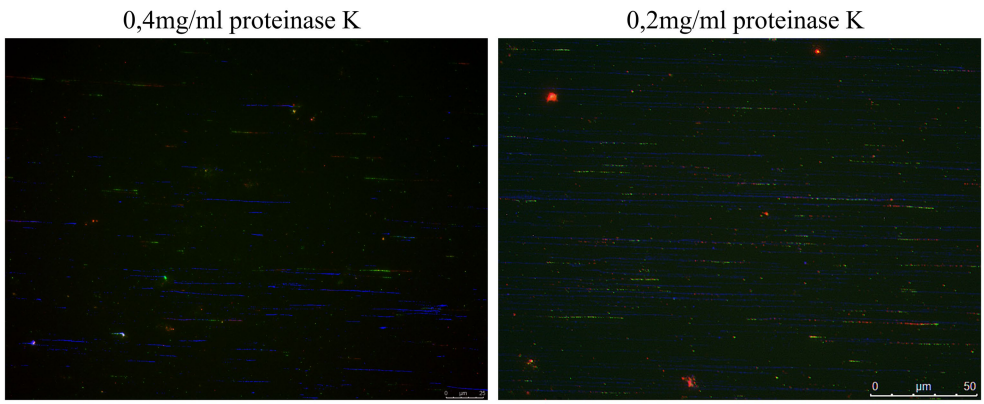

FIGURE 5
Comparison of fiber integrity after treatment with proteinase K. DNA fibers obtained after treatment with proteinase K at 0.4 mg/mL were frequently broken into relatively short tracts. Lowering the concentration of proteinase K to 0.2 mg/mL improved the quality of the fibers (DNA fibers in blue).

TABLE 4 Fiber patterns found in the analyzed cells.

Cell line	Progressing fiber	Initiation during the first pulse	Initiation before the first pulse	Termination	Cluster
CLBL-1	128	8	2	24	1
GL-1	124	14	5	21	10

antibody designed to recognize the human protein cross-reacting with the dog protein is high. As presented in Figure 3A, the tested ATR antibody recognized the canine protein. To our knowledge, no previous studies on ATR at the protein level have been performed in dogs. Curiously, we found that ATR protein at the basal level was only detected in the CLBL-1 and CLB70 cell lines and not in GL-1, despite clear evidence for ATR mRNA expression in the latter. It is well known however that protein and mRNA levels do not always correlate; several studies demonstrated that the correlation can vary in adenocarcinoma samples (62), can be modulated after treatments with drugs such as rapamycin (63), and may vary during the cell cycle in synchronized cultures (64). What we can conclude from the presented results is that the *ATR* gene is widely expressed in the canine lymphoma/leukemia cell lines. However, as ATR has a high molecular weight of 220 kDa, and high-molecular-weight proteins are difficulted to transfer (54), it is likely that its expression was below the threshold of detection in the GL-1 cell line for unknown reasons. Nuclear extraction and/ or immunoprecipitation are options that could be used to increase the sensitivity of ATR protein detection in GL-1 cells and other canine cancers.

Variations in ATR expression are considered a marker of sensitivity and/or resistance to certain anticancer drugs. High expression of ATR protein has been proposed as a marker of cisplatin sensitivity in patients with bladder cancer (7). Also, in the case of a doxorubicin-resistant canine hemangiosarcoma cell line established to study drug resistance, it was found that the DDR pathway was attenuated, as the mRNAs for ATM, ATR, and Chk1 were significantly decreased, suggesting a possible role for ATR in doxorubicin resistance (15). Another study reported that ATR inhibitors in combination with pyrrolobenzodiazepine (PBD) increased the cytotoxicity of PBD as compared with the drug alone, and helped to overcome the resistance to PBD (65). In other work, human multiple myeloma (MM) cells were treated with MEDI2228, a ligand of the B-cell maturation antigens that induces ATM/ATR-Chk1/2 pathway activation, in combination with different inhibitors of the principal kinases of the DDR (ATM, ATR, and WEE1) (66). The results of that study showed an increase in the toxicity of this ligand when combined with the inhibitor, an interesting example of the use of ATR as a target to induce cell death in MM cells and to abrogate resistance to MEDI2228.

To our knowledge, this is the first time that ATR has been detected in canine lymphoma/leukemia cells providing a new opportunity to study this protein in veterinary oncology.

4.2.2. Claspin

A high percentage of protein identity between the human and canine Claspin proteins was confirmed by BLAST alignment (84.47%). Indeed, Claspin protein expression was detected in all the cell lines of our panel as a single band with a molecular mass of 180 kDa as seen in human cell lines (40). Claspin was highly expressed in the CLBL-1 cells compared to the other cell lines (Figure 3A). Interestingly, the mRNA of the Claspin gene was detected in all three cell lines although at a somewhat lower level in CLB70 cells (Ct value of 27) than in the other lines (Figure 3B). The melting curves showed only one peak, meaning that the primers designed for Claspin specifically amplify a single amplicon (Supplementary Figure S3). Contrary to what we observed in the CLB70 cell line for ATR, Claspin protein expression and its mRNA level in the CLBL-1 cell line were higher than in the other cell lines of the panel. This corresponded with the observation from RNA-Seq that the *CLSPN* gene was among the most highly expressed genes in the CLBL-1 cell line (Figure 2B). This could be an

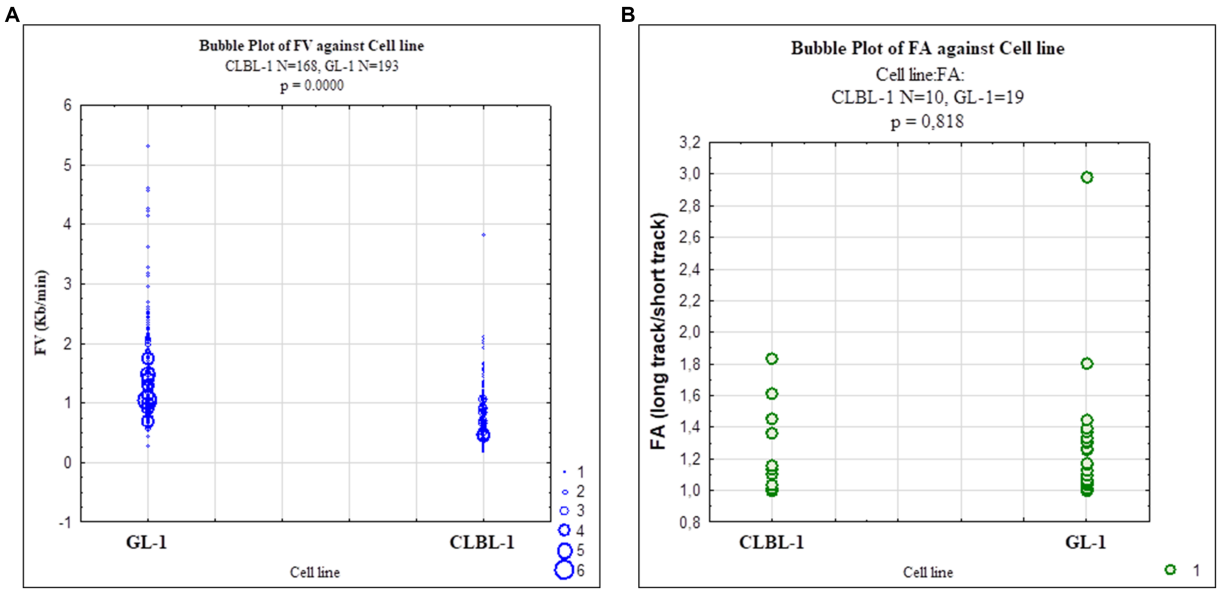

FIGURE 6
Scatterplots representing replication fork dynamics in CLBL-1 and GL-1 cells The replication fork speed and fork asymmetry were measured in the CLBL-1 and GL-1 cell lines. **(A)** Fork velocity of the GL-1 line was higher than in the CLBL-1 line. **(B)** Fork asymmetry did not differ significantly between the two cell lines.

example of a regulated correlation between protein and mRNA expression, which is not as common as one might expect (64).

Claspin has been described to be highly expressed in prostate cancer cells in comparison with non-cancerous prostate cells (6). Many cancer cells present higher expression of the components of the ATR-Claspin-Chk1 pathway, as compared with non-cancerous cells, which can be related to resistance to radiotherapy (13, 14). To our knowledge, only one other study has analyzed Claspin in canine cells (67). In that experiment, a polyclonal antibody included in an apoptosis antibody array kit (Catalog # ARY009) was used. In our study, a monoclonal antibody for Claspin was validated in three different canine cell lines. This indicates the potential utility of this antibody in future veterinary research to test the effects of inhibiting Claspin, or to detect the protein expression level in different tumor samples.

4.2.3. Chk1 and p-Chk1

Chk1 showed a 96.7% identity between the human and canine protein sequences in the BLAST alignment (Supplementary Figure S1). Consistent with this, Chk1 protein was detected in all the cell lines at various levels, with the CLB70 and CLBL-1 lines showing higher expression than the GL-1 line (Figure 3). We also detected high Chk1 mRNA level in the CLBL-1 line (Figure 2B). Interestingly, Chk1 was found to be highly expressed in several tumors, as compared with non-malignant tissues (4, 5). It was described to be overexpressed in human leukemia cells, B-cell lymphomas, and highly expressed in hematopoietic cancers as compared with solid tumors (8, 9, 68), which is consistent with the results obtained in our canine lymphoma/leukemia cell lines. Interestingly, in the CLBL-1 and CLB70 cell lines, the basal level of kinase phosphorylation was much higher than in the GL-1 cell line, suggesting that the response to DNA damage in these two cell lines might be faster and stronger than in the latter.

Upregulation of Chk1 has been proposed as a target for anticancer therapies. Different studies have confirmed Chk1 inhibitors acting as apoptosis inducers in various human and canine tumor cells, indicating, for example, proliferation decrease in human neoplastic B-cells and mast tumor cell (MTC) canine cell lines (68, 69). Currently, there are several Chk1 inhibitors in phase II of clinical trials and the results in human cancers seem promising (8, 70). Knowing that Chk1 is overexpressed in human B-cell lymphomas, and that the antibodies have been validated in our canine cells, we propose the use of canine B-cell lymphoma/leukemia cell lines as a model to study the role of Chk1 in canine B-cell malignancies.

4.2.4. Rad51

The last protein we examined was Rad51. BLAST alignment showed 99.12% Rad51 sequence identity between humans and dogs. This suggests that antibodies designed to recognize human Rad51 will also recognize the canine homolog. In our study, the antibody employed recognized Rad51 protein in all the canine cell lines tested. Its expression was the highest in the CLBL-1 line, both at the protein and gene level (Figures 2B, 3). In the literature, high expression of Rad51 protein is related to genome instability (10, 11), which is a hallmark of cancer. Rad51 is overexpressed in mammary carcinomas, and this is related to metastases in lymph nodes in both humans and dogs (71–74). Rad51 is a protein which has been studied in canine tumors due to its connection with BRCA2, and several studies have documented Rad51 mutations in tumor canine cells (75–77) Bortezomib, a proteasome inhibitor that impairs HR and thus decreases the expression of Rad51, has been used to potentiate the effect of other drugs, such as inhibitors of poly (ADP-ribose) polymerase (iPARP) or MEDI2228. Such combinations can also downregulate Rad51 protein expression, increase cell death, and even help to eradicate tumors in *in vivo* mice models (66, 78). The effects of these drugs on Rad51 function and expression in dogs have not been studied yet. However, as bortezomib is a drug that can be safely administered in dogs (79), treatment with a combination of

bortezomib and other DNA damaging agents in canine cell lines could yield useful information to be potentially implemented in the veterinary clinic. Here, a new Rad51 antibody, clone G-9, has been validated in canine cells, and it was also recently validated in other hematopoietic human cell lines (49).

4.3. DNA replication dynamics in canine lymphoma/leukemia cell lines

Replication stress arises in cells with DDR defects during the replication of damaged DNA. Replication stress may cause fork asymmetry and consequently, fork stalling and collapse that promotes genetic instability (80). Cancer cells often seem to experience replication stress under conditions where normal cells do not, even when they replicate rapidly (18, 81). A reduction in fork speed has been described under conditions of replication or oxidative stress in cancer cells (82), while pronounced asymmetry of replication forks has been detected in medulloblastoma stem cells (83). Thus, measurement of fork speed and fork asymmetry could help to better understand and describe the phenotype of a cancer cell type, which may later be used in order to choose therapeutic approaches. The ATR-Chk1 pathway is a critical regulator of the replication stress, as its role is to regulate the replication fork progression and stability, presenting potential targets for combination therapies (84) Thus, the analysis of cellular replication in canine cancer cells could bring new opportunities to find targets for therapies. Here we presented for the first time the use of the DNA combing assay in canine cells.

The analysis was performed in two of the canine lymphoma/leukemia cell lines, CLBL-1 and GL-1. The CLBL-1 cell line presented a high basal level of Rad51, and the GL-1 cell line showed the highest expression of Rad51 after etoposide treatment. Both situations may indicate cell replication stress (Figure 2A; Supplementary Figure S2). The replication fork speed in human cells is approximately 2–3 Kb/min (85). In our study, the replication fork speed in the canine cells seemed to be lower, around 1.5 Kb/min for the GL-1 cell line, and 0.86 Kb/min for the CLBL-1 cell line (Figure 6; Supplementary Table S1). It can be concluded that GL-1 cells have a higher replication speed than CLBL-1, which is interesting as the GL-1 cell line's doubling time is 27.3 h, and for the CLBL-1 it is 19 h (30, 86). The mean values of fork asymmetry were higher than 1 in both cell lines (Supplementary Table S1), indicating a significant number of replication forks terminate asymmetrically in both cell lines (87).

Advanced and novel biomolecular techniques need to be applied in veterinary science in order to improve the quality of the research and stimulate progress in therapy and clinical discoveries. Basic research analysis studying the role of proteins and cellular responses to different treatments is a first step needed to generate a new therapy to treat cancer or any other disease. The structural and functional properties of the principal components of the DDR system are conserved in mammals, but little is known about them specifically in dogs (88, 89). This cellular pathway is under intense investigation in human medicine due to its effects on the clinical aspects of cancer and its potential use in new therapies (90–93). Even where there are effective therapies based on targeting DDR proteins, such as PARP inhibitors (94–96), further investigation is needed due to the fact that cancer cells develop resistance (97). The knowledge about the functioning of the proteins involved in tumor-related pathways, and specifically their behavior in cancer cells is fundamental to finding new targets to be used in therapies.

4.4. Importance of validation of techniques and reagents to improve veterinary medicine research

Comparative clinical trials showed analogous results in human and canine patients treated with iniparib and F14512 (topoisomerase II inhibitor), highlighting the similarity of both species in the way naturally occurring cancer and lymphoma respond to therapies (98, 99). Cell lines represent a predictive tool for developing therapies in both human and veterinary medicine (100–102), which means that canine cancer cells represent a tractable model to study cancer that can generate valuable information also for human medicine. We have presented here a set of techniques and reagents validated in selected canine lymphoma/leukemia cell lines, which will facilitate further research in this field. All the data obtained in this work make the selected canine cell lines attractive models to study molecular aspects of lymphoma and leukemia. Experiments on combinations of the tested drugs with inhibitors of the principal components of the studied pathways are planned in the near future.

5. Conclusion

To conclude, we propose the use of canine lymphoma/leukemia cells as a model to study DDR in cancer, with ATR, Claspin, Chk1, and Rad51 as promising targets for further analysis. Our results will facilitate further investigation on DDR in canine cancer by identifying validated antibodies for ATR, Claspin, Chk1, p-Chk1, and Rad51, and primers for ATR and Chk1, and bringing numerous opportunities to develop new targeted-anticancer therapies which later may be also implemented in human medicine.

Data availability statement

The datasets presented in this study can be found in online repositories. The names of the repository/repositories and accession number(s) can be found in the article/Supplementary material.

Author contributions

AP: conceptualization and project administration. BH-S and AP: methodology. BH-S: software, validation, formal analysis, data curation, writing–original draft preparation, visualization, and funding acquisition. BH-S, AP, PK, and ED: investigation. BO-M: resources. AP and DG: writing–review and editing. AP, DG, and BO-M: supervision. All authors have read and agreed to the published version of the manuscript.

Funding

The publication was financed by the project "UPWR 2.0:international and interdisciplinary program of development of

Wrocław University of Environmental and Life Sciences," co-financed by the European Social Fund under the Operational Program Knowledge Education Development, under contract No. POWR.03.05.00-00-Z062/18 of June 4, 2019 and by the Polish National Agency for Academic Exchange under Grant No. PPI/APM/2019/1/00044/U/00001. DG was an Agustín de Betancourt Investigador of the Universidad de La Laguna.

Conflict of interest

The authors declare that the research was conducted in the absence of any commercial or financial relationships that could be construed as a potential conflict of interest.

Publisher's note

Supplementary material

The Supplementary material for this article can be found online at: https://www.frontiersin.org/articles/10.3389/fvets.2023.1227683/full#supplementary-material.

References

1. American Veterinary Medical Association. (n.d.). Available at: https://www.avma.org/resources/pet-owners/petcare/cancer-pets.

2. Schiffman JD, Breen M. Comparative oncology: what dogs and other species can teach us about humans with cancer. *Philos Trans R Soc B Biol Sci*. (2015) 370:20140231. doi: 10.1098/rstb.2014.0231

3. Thamm DH, Vail DM. Veterinary oncology clinical trials: design and implementation. *Vet J*. (2015) 205:226–32. doi: 10.1016/j.tvjl.2014.12.013

4. Khanna A, Thoms JAI, Stringer BW, Chung SA, Ensbey KS, Jue TR, et al. Constitutive CHK1 expression drives a pSTAT3–CIP2A circuit that promotes glioblastoma cell survival and growth. *Mol Cancer Res*. (2020) 18:709–22. doi: 10.1158/1541-7786.MCR-19-0934

5. Zhang Y, Hunter T. Roles of Chk1 in cell biology and cancer therapy. *Int J Cancer*. (2014) 134:1013–23. doi: 10.1002/ijc.28226

6. Cai C, Luo J, Liu Q, Liu Z, Zhao Y, Wu X, et al. Claspin overexpression promotes tumor progression and predicts poor clinical outcome in prostate Cancer. *Genet Test Mol Biomarkers*. (2021) 25:131–9. doi: 10.1089/gtmb.2020.0226

7. Li CC, Yang JC, Lu MC, Lee CL, Peng CY, Hsu WY, et al. ATR-Chk1 signaling inhibition as a therapeutic strategy to enhance cisplatin chemosensitivity in urothelial bladder cancer. *Oncotarget*. (2016) 7:1947–59. doi: 10.18632/oncotarget.6482

8. Boudny M, Trbusek M. ATR-CHK1 pathway as a therapeutic target for acute and chronic leukemias. *Cancer Treat Rev*. (2020) 88:102026. doi: 10.1016/j.ctrv.2020.102026

9. Sarmento LM, Póvoa V, Nascimento R, Real G, Antunes I, Martins LR, et al. CHK1 overexpression in T-cell acute lymphoblastic leukemia is essential for proliferation and survival by preventing excessive replication stress. *Oncogene*. (2015) 34:2978–90. doi: 10.1038/onc.2014.248

10. Richardson C. RAD51, genomic stability, and tumorigenesis. *Cancer Lett*. (2005) 218:127–39. doi: 10.1016/j.canlet.2004.08.009

11. Parplys AC, Seelbach JI, Becker S, Behr M, Wrona A, Jend C, et al. High levels of RAD51 perturb DNA replication elongation and cause unscheduled origin firing due to impaired CHK1 activation. *Cell Cycle*. (2015) 14:3190–202. doi: 10.1080/15384101.2015.1055996

12. Bargiela-Iparraguirre J, Prado-Marchal L, Fernandez-Fuente M, Gutierrez-González A, Moreno-Rubio J, Muñoz-Fernandez M, et al. CHK1 expression in gastric Cancer is modulated by p53 and RB1/E2F1: implications in chemo/radiotherapy response. *Sci Rep*. (2016) 6:21519. doi: 10.1038/srep21519

13. Hsiao HW, Yang CC, Masai H. Roles of Claspin in regulation of DNA replication, replication stress responses and oncogenesis in human cells. *Genome Instab Dis*. (2021) 2:263–80. doi: 10.1007/s42764-021-00049-8

14. Choi SH, Yang H, Lee SH, Ki JH, Nam DH, Yoo HY. TopBP1 and Claspin contribute to the radioresistance of lung cancer brain metastases. *Mol Cancer*. (2014) 13:211. doi: 10.1186/1476-4598-13-211

15. Morita A, Aoshima K, Gulay KCM, Onishi S, Shibata Y, Yasui H, et al. High drug efflux pump capacity and low DNA damage response induce doxorubicin resistance in canine hemangiosarcoma cell lines. *Res Vet Sci*. (2019) 127:1–10. doi: 10.1016/j.rvsc.2019.09.011

16. Burgess BT, Anderson AM, McCorkle JR, Wu J, Ueland FR, Kolesar JM. Olaparib combined with an ATR or Chk1 inhibitor as a treatment strategy for acquired Olaparib-resistant BRCA1 mutant ovarian cells. *Diagnostics*. (2020) 10:121. doi: 10.3390/diagnostics10020121

17. Kim H, Xu H, George E, Hallberg D, Kumar S, Jagannathan V, et al. Combining PARP with ATR inhibition overcomes PARP inhibitor and platinum resistance in ovarian cancer models. *Nat Commun [Internet]*. (2020) 11:3726. doi: 10.1038/s41467-020-17127-2

18. Forment JV, O'Connor MJ. Targeting the replication stress response in cancer. *Pharmacol Ther*. (2018) 188:155–67. doi: 10.1016/j.pharmthera.2018.03.005

19. Loukopoulos P, Thornton JR, Robinson WF. Clinical and pathologic relevance of p53 index in canine osseous tumors. *Vet Pathol*. (2003) 40:237–48. doi: 10.1354/vp.40-3-237

20. Broustas CG, Lieberman HB. DNA damage response genes and the development of Cancer metastasis. *Radiat Res*. (2014) 181:111–30. doi: 10.1667/RR13515.1

21. Smith J, Mun Tho L, Xu NA, Gillespie D. The ATM–Chk2 and ATR–Chk1 pathways in DNA damage signaling and Cancer. *Adv Cancer Res*. (2010) 108:73–112. doi: 10.1016/B978-0-12-380888-2.00003-0

22. Tian H, Gao Z, Li HZ, Zhang BF, Wang G, Zhang Q, et al. DNA damage response - a double-edged sword in cancer prevention and cancer therapy. *Cancer Lett*. (2015) 358:8–16. doi: 10.1016/j.canlet.2014.12.038

23. Smits VAJ, Gillespie DA. DNA damage control: regulation and functions of checkpoint kinase 1. *FEBS J*. (2015) 282:3681–92. doi: 10.1111/febs.13387

24. Smits VAJ, Cabrera E, Freire R, Gillespie DA. Claspin–checkpoint adaptor and DNA replication factor. *FEBS J*. (2019) 286:441–55. doi: 10.1111/febs.14594

25. Simhadri S, Vincelli G, Huo Y, Misenko S, Foo TK, Ahlskog J, et al. PALB2 connects BRCA1 and BRCA2 in the G2/M checkpoint response. *Oncogene*. (2019) 38:1585–96. doi: 10.1038/s41388-018-0535-2

26. Laurini E, Marson D, Fermeglia A, Aulic S, Fermeglia M, Pricl S. Role of Rad51 and DNA repair in cancer: a molecular perspective. *Pharmacol Ther*. (2020) 208, 208:107492. doi: 10.1016/j.pharmthera.2020.107492

27. Morrical SW. DNA-pairing and annealing processes in homologous recombination and homology-directed repair. *Cold Spring Harb Perspect Biol*. (2015) 7:a016444. doi: 10.1101/cshperspect.a016444

28. Grundy MK, Buckanovich RJ, Bernstein KA. Regulation and pharmacological targeting of RAD51 in cancer. *NAR Cancer*. (2020) 2:zcaa024. doi: 10.1093/narcan/zcaa024

29. Rütgen BC, Hammer SE, Gerner W, Christian M, de Arespacochaga AG, Willmann M, et al. Establishment and characterization of a novel canine B-cell line derived from a spontaneously occurring diffuse large cell lymphoma. *Leuk Res*. (2010) 34:932–8. doi: 10.1016/j.leukres.2010.01.021

30. Nakaichi M, Taura Y, Kanki M, Mamba K, Momoi Y, Tsujimoto H, et al. Establishment and characterization of a new canine B-cell leukemia cell line. *J Vet Med Sci*. (1996) 58:469–71. doi: 10.1292/jvms.58.469

31. Pawlak A, Ziolo E, Kutkowska J, Blazejczyk A, Wietrzyk J, Krupa A, et al. A novel canine B-cell leukaemia cell line. Establishment, characterisation and sensitivity to chemotherapeutics. *Vet Comp Oncol*. (2017) 15:1218–31. doi: 10.1111/vco.12257

32. Mortazavi A, Williams BA, McCue K, Schaeffer L, Wold B. Mapping and quantifying mammalian transcriptomes by RNA-Seq. *Nat Methods*. (2008) 5:621–8. doi: 10.1038/nmeth.1226

33. Subramanian A, Tamayo P, Mootha VK, Mukherjee S, Ebert BL, Gillette MA, et al. Gene set enrichment analysis: a knowledge-based approach for interpreting genome-wide expression profiles. *Proc Natl Acad Sci*. (2005) 102:15545–50. doi: 10.1073/pnas.0506580102

34. Mootha VK, Lindgren CM, Eriksson KF, Subramanian A, Sihag S, Lehar J, et al. PGC-1α-responsive genes involved in oxidative phosphorylation are coordinately downregulated in human diabetes. *Nat Genet*. (2003) 34:267–73. doi: 10.1038/ng1180

35. Yang M, Tian X, Fan Z, Yu W, Li Z, Zhou J, et al. Targeting RAD51 enhances chemosensitivity of adult Tcell leukemialymphoma cells by reducing DNA doublestrand break repair. *Oncol Rep*. (2019) 42:2426–34. doi: 10.3892/or.2019.7384

36. Mehta KPM, Thada V, Zhao R, Krishnamoorthy A, Leser M, Lindsey Rose K, et al. CHK1 phosphorylates PRIMPOL to promote replication stress tolerance. *Sci Adv*. (2022) 8:eabm0314. doi: 10.1126/sciadv.abm0314

37. Gong EY, Hernández B, Nielsen JH, Smits VAJ, Freire R, Gillespie DA. Chk1 KA1 domain auto-phosphorylation stimulates biological activity and is linked to rapid proteasomal degradation. *Sci Rep*. (2018) 8:17536. doi: 10.1038/s41598-018-35616-9

38. Zhang J, Wang Y, Yin C, Gong P, Zhang Z, Zhao L, et al. Artesunate improves venetoclax plus cytarabine AML cell targeting by regulating the Noxa/Bim/Mcl-1/p-Chk1 axis. *Cell Death Dis*. (2022) 13:379. doi: 10.1038/s41419-022-04810-z

39. Saha S, Rundle S, Kotsopoulos IC, Begbie J, Howarth R, Pappworth IY, et al. Determining the potential of DNA damage response (DDR) inhibitors in cervical Cancer therapy. *Cancers (Basel)*. (2022) 14:4288. doi: 10.3390/cancers14174288

40. Guerra B, Doktor TK, Frederiksen SB, Somyajit K, Andresen BS. Essential role of CK2α for the interaction and stability of replication fork factors during DNA synthesis and activation of the S-phase checkpoint. *Cell Mol Life Sci*. (2022) 79:339. doi: 10.1007/s00018-022-04374-3

41. Ha DH, Min A, Kim S, Jang H, Kim SH, Kim HJ, et al. Antitumor effect of a WEE1 inhibitor and potentiation of olaparib sensitivity by DNA damage response modulation in triple-negative breast cancer. *Sci Rep*. (2020) 10:9930. doi: 10.1038/s41598-020-66018-5

42. Pawlak A, Henklewska M, Hernández-Suárez B, Siepka M, Gładkowski W, Wawrzeńczyk C, et al. Methoxy-substituted γ-Oxa-ε-lactones derived from flavanones–comparison of their anti-tumor activity in vitro. *Molecules*. (2021) 26:6295. doi: 10.3390/molecules26206295

43. Pawlak A, Bajzert J, Bugiel K, Hernández Suárez B, Kutkowska J, Rapak A, et al. Ubiquitin-specific protease 7 as a potential therapeutic target in dogs with hematopoietic malignancies. *J Vet Intern Med*. (2021) 35:1041–51. doi: 10.1111/jvim.16082

44. Pawlak A, Henklewska M, Suárez BH, Łużny M, Kozłowska E, Obmińska-Mrukowicz B, et al. Chalcone Methoxy derivatives exhibit Antiproliferative and Proapoptotic activity on canine lymphoma and leukemia cells. *Molecules*. (2020) 25:4362. doi: 10.3390/molecules25194362

45. Gundu C, Arruri VK, Sherkhane B, Khatri DK, Singh SB. GSK2606414 attenuates PERK/p-eIF2α/ATF4/CHOP axis and augments mitochondrial function to mitigate high glucose induced neurotoxicity in N2A cells. *Curr Res Pharmacol Drug Discov*. (2022) 3:100087. doi: 10.1016/j.crphar.2022.100087

46. Kim TW, Hong DW, Hong SH. PB01 suppresses radio-resistance by regulating ATR signaling in human non-small-cell lung cancer cells. *Sci Rep*. (2021) 11:12093. doi: 10.1038/s41598-021-91716-z

47. Li X, Zhou D, Cai Y, Yu X, Zheng X, Chen B, et al. Endoplasmic reticulum stress inhibits AR expression via the PERK/eIF2α/ATF4 pathway in luminal androgen receptor triple-negative breast cancer and prostate cancer. *NPJ Breast Cancer*. (2022) 8:2. doi: 10.1038/s41523-021-00370-1

48. Zhang Y, Li P, Rong J, Ge Y, Hu C, Bai X, et al. Small molecule CDS-3078 induces G2/M phase arrest and mitochondria-mediated apoptosis in HeLa cells. *Exp Ther Med*. (2020) 20:284–1. doi: 10.3892/etm.2020.9414

49. Arena A, Romeo MA, Benedetti R, Gilardini Montani MS, Cirone M. Targeting c-Myc unbalances UPR towards cell death and impairs DDR in lymphoma and multiple myeloma cells. *Biomedicines*. (2022) 10:731. doi: 10.3390/biomedicines10040731

50. Benedetti R, Arena A, Romeo MA, Gilardini Montani MS, Gonnella R, Santarelli R, et al. Concomitant inhibition of IRE1α/XBP1 Axis of UPR and PARP: a promising therapeutic approach against c-Myc and Gammaherpesvirus-driven B-cell lymphomas. *Int J Mol Sci*. (2022) 23:9113. doi: 10.3390/ijms23169113

51. Gareau A, Rico C, Boerboom D, Nadeau ME. In vitro efficacy of a first-generation valosin-containing protein inhibitor (CB-5083) against canine lymphoma. *Vet Comp Oncol*. (2018) 16:311–7. doi: 10.1111/vco.12380

52. Nadeau MÈ, Rico C, Tsoi M, Vivancos M, Filimon S, Paquet M, et al. Pharmacological targeting of valosin containing protein (VCP) induces DNA damage and selectively kills canine lymphoma cells. *BMC Cancer*. (2015) 15:479–14. doi: 10.1186/s12885-015-1489-1

53. Altschul S. Gapped BLAST and PSI-BLAST: a new generation of protein database search programs. *Nucleic Acids Res*. (1997) 25:3389–402. doi: 10.1093/nar/25.17.3389

54. Heda GD, Shrestha L, Thapa S, Ghimire S, Raut D. Optimization of western blotting for the detection of proteins of different molecular weight. *BioTechniques*. (2020) 68:318–24. doi: 10.2144/btn-2019-0124

55. Fan Z, Luo H, Zhou J, Wang F, Zhang W, Wang J, et al. Checkpoint kinase1 inhibition and etoposide exhibit a strong synergistic anticancer effect on chronic myeloid leukemia cell line K562 by impairing homologous recombination DNA damage repair. *Oncol Rep*. (2020) 44:2152–64. doi: 10.3892/or.2020.7757

56. Yao Q, Weigel B, Kersey J. Synergism between etoposide and 17-AAG in leukemia cells: critical roles for Hsp90, FLT3, topoisomerase II, Chk1, and Rad51. *Clin Cancer Res*. (2007) 13:1591–600. doi: 10.1158/1078-0432.CCR-06-1750

57. Ohmoto A, Fuji S. Clinical feasibility of oral low-dose etoposide and sobuzoxane for conventional chemotherapy–intolerant lymphoma patients. *Expert Rev Anticancer Ther*. (2021) 21:715–22. doi: 10.1080/14737140.2021.1898376

58. Tariq S, Kim SY, de Oliveira M, Novaes J, Cheng H. Update 2021: management of Small Cell Lung Cancer. *Lung*. (2021) 199:579–87. doi: 10.1007/s00408-021-00486-y

59. Bordeaux J, Welsh AW, Agarwal S, Killiam E, Baquero MT, Hanna JA, et al. Antibody validation. *Biotechniques*. (2010) 48:197–209. doi: 10.2144/000113382

60. Pillai-Kastoori L, Heaton S, Shiflett SD, Roberts AC, Solache A, Schutz-Geschwender AR. Antibody validation for Western blot: by the user, for the user. *J Biol Chem*. (2020) 295:926–39. doi: 10.1074/jbc.RA119.010472

61. Chong G, Kuo FW, Tsai S, Lin C. Validation of reference genes for cryopreservation studies with the gorgonian coral endosymbiont Symbiodinium. *Sci Rep*. (2017) 7:39396. doi: 10.1038/srep39396

62. Chen G, Gharib TG, Huang CC, Taylor JMG, Misek DE, Kardia SLR, et al. Discordant protein and mRNA expression in lung adenocarcinomas. *Mol Cell Proteomics*. (2002) 1:304–13. doi: 10.1074/mcp.M200008-MCP200

63. Fournier ML, Paulson A, Pavelka N, Mosley AL, Gaudenz K, Bradford WD, et al. Delayed correlation of mRNA and protein expression in rapamycin-treated cells and a role for Ggc1 in cellular sensitivity to rapamycin. *Mol Cell Proteomics*. (2010) 9:271–84. doi: 10.1074/mcp.M900415-MCP200

64. Ly T, Ahmad Y, Shlien A, Soroka D, Mills A, Emanuele MJ, et al. A proteomic chronology of gene expression through the cell cycle in human myeloid leukemia cells. *Elife*. (2014) 3:e01630. doi: 10.7554/eLife.01630

65. Mao S, Chaerkady R, Yu W, D'Angelo G, Garcia A, Chen H, et al. Resistance to pyrrolobenzodiazepine dimers is associated with SLFN11 downregulation and can be reversed through inhibition of ATR. *Mol Cancer Ther*. (2021) 20:541–52. doi: 10.1158/1535-7163.MCT-20-0351

66. Xing L, Lin L, Yu T, Li Y, Cho SF, Liu J, et al. A novel BCMA PBD-ADC with ATM/ATR/WEE1 inhibitors or bortezomib induce synergistic lethality in multiple myeloma. *Leukemia*. (2020) 34:2150–62. doi: 10.1038/s41375-020-0745-9

67. Graner AN, Hellwinkel JE, Lencioni AM, Madsen HJ, Harland TA, Marchando P, et al. HSP90 inhibitors in the context of heat shock and the unfolded protein response: effects on a primary canine pulmonary adenocarcinoma cell line*. *Int J Hyperthermia*. (2017) 33:303–17. doi: 10.1080/02656736.2016.1256503

68. Derenzini E, Agostinelli C, Imbrogno E, Iacobucci I, Casadei B, Brighenti E, et al. Constitutive activation of the DNA damage response pathway as a novel therapeutic target in diffuse large B-cell lymphoma. *Oncotarget*. (2015) 6:6553–69. doi: 10.18632/oncotarget.2720

69. Takeuchi Y, Fujino Y, Watanabe M, Nakagawa T, Ohno K, Sasaki N, et al. Screening of therapeutic targets for canine mast cell tumors from a variety of kinase molecules. *J Vet Med Sci*. (2011) 73:1295–302. doi: 10.1292/jvms.11-0093

70. Daud AI, Ashworth MT, Strosberg J, Goldman JW, Mendelson D, Springett G, et al. Phase I dose-escalation trial of checkpoint kinase 1 inhibitor MK-8776 as monotherapy and in combination with gemcitabine in patients with advanced solid tumors. *J Clin Oncol*. (2015) 33:1060–6. doi: 10.1200/JCO.2014.57.5027

71. Klopfleisch R, Gruber AD. Increased expression of BRCA2 and RAD51 in lymph node metastases of canine mammary adenocarcinomas. *Vet Pathol*. (2009) 46:416–22. doi: 10.1354/vp.08-VP-0212-K-FL

72. Klopfleisch R, Schütze M, Gruber AD. RAD51 protein expression is increased in canine mammary carcinomas. *Vet Pathol*. (2010) 47:98–101. doi: 10.1177/0300985809353310

73. Nakanoko T, Saeki H, Morita M, Nakashima Y, Ando K, Oki E, et al. Rad51 expression is a useful predictive factor for the efficacy of neoadjuvant Chemoradiotherapy in squamous cell carcinoma of the esophagus. *Ann Surg Oncol*. (2014) 21:597–604. doi: 10.1245/s10434-013-3220-2

74. Abdelmegeed S, Mohammed S. Canine mammary tumors as a model for human disease (review). *Oncol Lett*. (2018) 15:8195–205. doi: 10.3892/ol.2018.8411

75. Ozmen O, Kul S, Risvanli A, Ozalp G, Sabuncu A, Kul O. Single nucleotide variations of the canine RAD51 domains, which directly binds PALB2 and BRCA2. *Jpn J Vet Res*. (2017) 65:75–82. doi: 10.14943/jjvr.65.2.75

76. Uemura M, Ochiai K, Morimatsu M, Michishita M, Onozawa E, Azakami D, et al. The canine RAD51 mutation leads to the attenuation of interaction with PALB2. *Vet Comp Oncol*. (2019) 18:247–55. doi: 10.1111/vco.12542

77. Ochiai K, Morimatsu M, Tomizawa N, Syuto B. Cloning and sequencing full length of canine Brca2 and Rad51 cDNA. *J Vet Med Sci*. (2001) 63:1103–8. doi: 10.1292/jvms.63.1103

78. Neri P, Ren L, Gratton K, Stebner E, Johnson J, Klimowicz A, et al. Bortezomib-induced "BRCAness" sensitizes multiple myeloma cells to PARP inhibitors. *Blood*. (2011) 118:6368–79. doi: 10.1182/blood-2011-06-363911

79. Araujo KPC, Bonuccelli G, Duarte CN, Gaiad TP, Moreira DF, Feder D, et al. Bortezomib (PS-341) treatment decreases inflammation and partially rescues the expression of the dystrophin-glycoprotein complex in GRMD dogs. *PLoS One*. (2013) 8:e61367. doi: 10.1371/journal.pone.0061367

80. Haradhvala NJ, Polak P, Stojanov P, Covington KR, Shinbrot E, Hess JM, et al. Mutational Strand asymmetries in Cancer genomes reveal mechanisms of DNA damage and repair. *Cells*. (2016) 164:538–49. doi: 10.1016/j.cell.2015.12.050

81. Zhang J, Dai Q, Park D, Deng X. Targeting DNA replication stress for Cancer therapy. *Genes (Basel)*. (2016) 7:51. doi: 10.3390/genes7080051

82. Técher H, Pasero P. The replication stress response on a narrow path between genomic instability and inflammation. *Front Cell Dev Biol*. (2021) 9:702584. doi: 10.3389/fcell.2021.702584

83. Bartek J, Merchut-Maya JM, Maya-Mendoza A, Fornara O, Rahbar A, Bröchner CB, et al. Cancer cell stemness, responses to experimental genotoxic treatments, cytomegalovirus protein expression and DNA replication stress in pediatric medulloblastomas. *Cell Cycle*. (2020) 19:727–41. doi: 10.1080/15384101.2020.1728025

84. Zhu H, Swami U, Preet R, Zhang J. Harnessing DNA replication stress for novel Cancer therapy. *Genes (Basel)*. (2020) 11:990. doi: 10.3390/genes11090990

85. Méchali M. Eukaryotic DNA replication origins: many choices for appropriate answers. *Nat Rev Mol Cell Biol*. (2010) 11:728–38. doi: 10.1038/nrm2976

86. Maeda J, Froning CE, Brents CA, Rose BJ, Thamm DH, Kato TA. Intrinsic radiosensitivity and cellular characterization of 27 canine cancer cell lines. *PLoS One*. (2016) 11:1–18. doi: 10.1371/journal.pone.0156689

87. Stanojcic S, Kuk N, Ullah I, Sterkers Y, Merrick CJ. Single-molecule analysis reveals that DNA replication dynamics vary across the course of schizogony in the malaria parasite plasmodium falciparum. *Sci Rep*. (2017) 7:4003. doi: 10.1038/s41598-017-04407-z

88. Grosse N, Van Loon B, Rohrer BC. DNA damage response and DNA repair–dog as a model? *BMC Cancer*. (2014) 14:1–8. doi: 10.1186/1471-2407-14-203

89. Hernández-Suárez B, Gillespie DA, Pawlak A. DNA damage response proteins in canine cancer as potential research targets in comparative oncology. *Vet Comp Oncol*. (2022) 20:347–61. doi: 10.1111/vco.12795

90. Rozpedek W, Pytel D, Mucha B, Leszczynska H, Diehl JA, Majsterek I. The role of the PERK/eIF2α/ATF4/CHOP signaling pathway in tumor progression during endoplasmic reticulum stress. *Curr Mol Med*. (2016) 16:533–44. doi: 10.2174/1566524016666160523143937

91. Toledo LI, Murga M, Fernandez-Capetillo O. Targeting ATR and Chk1 kinases for cancer treatment: a new model for new (and old) drugs. *Mol Oncol*. (2011) 5:368–73. doi: 10.1016/j.molonc.2011.07.002

92. Brandsma I, Fleuren EDG, Williamson CT, Lord CJ. Directing the use of DDR kinase inhibitors in cancer treatment. *Expert Opin Investig Drugs*. (2017) 26:1341–55. doi: 10.1080/13543784.2017.1389895

93. Marciniak SJ, Chambers JE, Ron D. Pharmacological targeting of endoplasmic reticulum stress in disease. *Nat Rev Drug Discov*. (2022) 21:115–40. doi: 10.1038/s41573-021-00320-3

94. Faraoni I, Compagnone M, Lavorgna S, Angelini DF, Cencioni MT, Piras E, et al. BRCA1, PARP1 and γH2AX in acute myeloid leukemia: role as biomarkers of response to the PARP inhibitor olaparib. *Biochim Biophys Acta*. (2015) 1852:462–72. doi: 10.1016/j.bbadis.2014.12.001

95. Gadducci A, Guerrieri ME. PARP inhibitors alone and in combination with other biological agents in homologous recombination deficient epithelial ovarian cancer: from the basic research to the clinic. *Crit Rev Oncol Hematol*. (2017) 114:153–65. doi: 10.1016/j.critrevonc.2017.04.006

96. Park HJ, Bae JS, Kim KM, Moon YJ, Park SH, Ha SH, et al. The PARP inhibitor olaparib potentiates the effect of the DNA damaging agent doxorubicin in osteosarcoma. *J Exp Clin Cancer Res*. (2018) 37:107. doi: 10.1186/s13046-018-0772-9

97. D'Andrea AD. Mechanisms of PARP inhibitor sensitivity and resistance. *DNA Repair (Amst)*. (2018) 71:172–6. doi: 10.1016/j.dnarep.2018.08.021

98. Tierny D, Serres F, Segaoula Z, Bemelmans I, Bouchaert E, Pétain A, et al. Phase i clinical pharmacology study of F14512, a new polyamine-Vectorized anticancer drug, in naturally occurring canine lymphoma. *Clin Cancer Res*. (2015) 21:5314–23. doi: 10.1158/1078-0432.CCR-14-3174

99. Saba C, Paoloni M, Mazcko C, Kisseberth W, Burton JH, Smith A, et al. A comparative oncology study of Iniparib defines its pharmacokinetic profile and biological activity in a naturally-occurring canine Cancer model. *PLoS One*. (2016) 11:e0149194. doi: 10.1371/journal.pone.0149194

100. Boonstra JJ, Tilanus HW, Dinjens WNM. Translational research on esophageal adenocarcinoma: from cell line to clinic. *Dis Esophagus*. (2015) 28:90–6. doi: 10.1111/dote.12095

101. Pawlak A, Rapak A, Zbyryt I, Obmińska-Mrukowicz B. The effect of common antineoplastic agents on induction of apoptosis in canine lymphoma and leukemia cell lines. *In Vivo*. 28:843–50.

102. Seiser EL, Thomas R, Richards KL, Kathryn Kelley M, Moore P, Suter SE, et al. Reading between the lines: molecular characterization of five widely used canine lymphoid tumour cell lines. *Vet Comp Oncol*. (2013) 11:30–50. doi: 10.1111/j.1476-5829.2011.00299.x

frontiers | Frontiers in Veterinary Science

TYPE Original Research
PUBLISHED 30 August 2023
DOI 10.3389/fvets.2023.1236136

OPEN ACCESS

EDITED BY
Monica Sforna,
University of Perugia, Italy

REVIEWED BY
Vittoria Castiglioni,
IDEXX Laboratories, Germany
Andrzej Rapak,
Polish Academy of Sciences, Poland

*CORRESPONDENCE
Frederico Aires-da-Silva
✉ fasilva@fmv.ulisboa.pt

RECEIVED 07 June 2023
ACCEPTED 07 August 2023
PUBLISHED 30 August 2023

CITATION
André AS, Dias JNR, Aguiar SI, Leonardo A, Nogueira S, Amaral JD, Fernandes C, Gano L, Correia JDG, Cavaco M, Neves V, Correia J, Castanho M, Rodrigues CMP, Gaspar MM, Tavares L and Aires-da-Silva F (2023) Panobinostat-loaded folate targeted liposomes as a promising drug delivery system for treatment of canine B-cell lymphoma. *Front. Vet. Sci.* 10:1236136. doi: 10.3389/fvets.2023.1236136

Panobinostat-loaded folate targeted liposomes as a promising drug delivery system for treatment of canine B-cell lymphoma

Ana S. André[1,2], Joana N. R. Dias[1,2], Sandra I. Aguiar[1,2], Ana Leonardo[1,2], Sara Nogueira[1,2], Joana D. Amaral[3], Célia Fernandes[4], Lurdes Gano[4], João D. G. Correia[4], Marco Cavaco[5], Vera Neves[5], Jorge Correia[1,2], Miguel Castanho[5], Cecília M. P. Rodrigues[3], Maria Manuela Gaspar[3], Luís Tavares[1,2] and Frederico Aires-da-Silva[1,2]*

[1]Faculty of Veterinary Medicine, CIISA-Centre for Interdisciplinary Research in Animal Health, University of Lisbon, Avenida da Universidade Técnica, Lisbon, Portugal, [2]Associate Laboratory for Animal and Veterinary Sciences (AL4AnimalS), Lisbon, Portugal, [3]Research Institute for Medicines (iMed.ULisboa), Faculty of Pharmacy, Universidade de Lisboa, Lisbon, Portugal, [4]Departamento de Engenharia e Ciências Nucleares, Centro de Ciências e Tecnologias Nucleares, Instituto Superior Técnico, Universidade de Lisboa, CTN, Bobadela, Portugal, [5]Faculdade de Medicina, Instituto de Medicina Molecular-João Lobo Antunes, Universidade de Lisboa, Lisbon, Portugal

Introduction: Cancer is a major public health problem with over 19 million cases reported in 2020. Similarly to humans, dogs are also largely affected by cancer, with non-Hodgkin's lymphoma (NHL) among the most common cancers in both species. Comparative medicine has the potential to accelerate the development of new therapeutic options in oncology by leveraging commonalities between diseases affecting both humans and animals. Within this context, in the present study, we investigated the potential of panobinostat (Pan)-loaded folate-targeted PEGylated liposomes (FA-PEG-Pan-Lip) for the treatment of canine B-cell lymphoma, while contributing to new perspectives in comparative oncology.

Methods and results: Two formulations were developed, namely: PEG-Pan-Lip and FA-PEG-Pan-Lip. Firstly, folate receptor expression in the CLBL-1 canine B-cell lymphoma cell line was assessed. After confirming receptor expression, both Pan-loaded formulations (PEG-Pan-Lip, FA-PEG-Pan-Lip) demonstrated dose-dependent inhibitory effects on CLBL-1 cell proliferation. The FA-PEG-Pan-Lip formulation (IC_{50} = 10.9 ± 0.03 nM) showed higher cytotoxicity than the non-targeted PEG-Pan-Lip formulation (IC_{50} = 12.9 ± 0.03 nM) and the free panobinostat (Pan) compound (IC_{50} = 18.32±0.03 nM). Moreover, mechanistically, both Pan-containing formulations induced acetylation of H3 histone and apoptosis. Flow cytometry and immunofluorescence analysis of intracellular uptake of rhodamine-labeled liposome formulations in CLBL-1 cells confirmed cellular internalization of PEG-Lip and FA-PEG-Lip formulations and higher uptake profile for the latter. Biodistribution studies of both radiolabeled formulations in CD1 and SCID mice revealed a rapid clearance from the major organs and a 1.6-fold enhancement of tumor uptake at 24 h for ^{111}In-FA-PEG-Pan-Lip (2.2 ± 0.1 %ID/g of tumor) compared to ^{111}In-PEG-Pan-Lip formulation (1.2±0.2 %ID/g of tumor).

Discussion: In summary, our results provide new data validating Pan-loaded folate liposomes as a promising targeted drug delivery system for the treatment of canine B-cell lymphoma and open innovative perspectives for comparative oncology.

KEYWORDS

non-Hodgkin lymphoma, canine B-cell lymphoma, liposome, folate, panobinostat, drug delivery

Introduction

Cancer is a major public health and economic issue, and its burden continues to increase worldwide. With over 19 million cases in 2020, it is expected that there will be 29 million cases by 2040 due to aging and growing population (1). The past few decades have seen unprecedented advances in the development of new cancer treatments, particularly with the major advances in immunotherapy and the approval of emerging therapeutics, such as immune-checkpoint inhibitors, antibody-drug conjugates, bispecific antibodies, and CAR-T cells. Nevertheless, although the landscape of cancer treatment has changed dramatically in recent years, new approaches to fight cancer need to be explored rapidly and effectively. Comparative medicine has the potential to accelerate the development of new therapeutic options in the field of oncology by leveraging commonalities between diseases that are common to humans and animals. In particular, the canine model provides a powerful resource for developing models of naturally occurring tumors, that share many clinical and pathophysiological features with their human counterparts (2, 3). Domestic dogs are highly affected by cancer and approximately 4 million dogs die from cancer each year, making it the leading cause of death (2). Thus, efforts are also being made in comparative research to provide quality cancer treatment options for dogs as caregivers are becoming increasingly demanding.

Non-Hodgkin's lymphoma (NHL) is one of the most common cancers in both species (2–5). NHL is a malignancy that originates from cells of the immune system, the vast majority of which are B lymphocytes (5). In humans, NHL is among the 15 most prevalent and deadly malignancies worldwide (1). The incidence in dogs is similar to that in humans, affecting 15–30 per 100 000 dogs (2). Owing to the great similarity in pathologic presentation shared between canine and human NHL, the World Health Organization (WHO) classification criteria is also used for canine tumors (3, 6). Although NHL encompasses several subtypes, diffuse large B-cell lymphoma (DLBCL) accounts for one third of all NHL, making it the most common aggressive form in both humans and dogs (2, 6, 7). Veterinary therapies have evolved with human therapies, and similar to humans, CHOP (cyclophosphamide, doxorubicin, vincristine, and prednisolone)-based chemotherapy is the standard treatment for canine lymphoma. Although treatment response and resistance also present (8–11) clinical patterns comparable to human NHL, the low-dose chemotherapeutic protocol used in dogs significantly reduces cure rates in veterinary medicine. In most cases disease relapse occurs after remission and the 2-year survival rate is only 20%, demonstrating the urgent need for novel treatment strategies (5, 7, 12). Moreover, the toxicity of conventional chemotherapy often limits its efficacy. Therefore, interest in designing and developing more targeted and specific molecules has increased over recent years.

Cancer is highly associated with genetic alterations, with epigenetic processes playing a key role in carcinogenesis, namely influencing gene transcription, regulating anti-oncogenes and DNA repair genes. Therefore, new research and discoveries have been directed toward the development of agents that can regulate these epigenetic mechanisms. Among the compounds targeting epigenetic regulators, histone deacetylase inhibitors (HDACis) have emerged as a promising new class of anticancer therapeutics (13). Histone deacetylases are important naturally occurring enzymes that promote deacetylation of histones and alter gene transcription. HDACis act on a variety of proteins mainly involved in the control of cell growth, differentiation, and apoptosis. On the other hand, by inducing acetylation of histone and non-histone proteins, HDACis promote cell differentiation, cell cycle arrest, angiogenesis inhibition and apoptosis induction (13–15). The activity of HDACis has been demonstrated in a number of hematological malignancies, including lymphoblastic leukemia, cutaneous T-cell lymphoma, DLBCL, Hodgkin lymphoma and Burkitt lymphoma (16). Currently, three HDACis are approved by the U.S. Food and Drug Administration (FDA) for clinical use in human cancer therapy: vorinostat, romidepsin, and belinostat. Only belinostat and panobinostat (Pan) have been approved by the European Medicines Agency (EMA) (17–20). Considering the high efficacy of HDACis in human targeted cancer therapy, we recently conducted the first investigation on their antitumor properties using a canine B-cell lymphoma model. For this purpose, a panel of seven HDACis (CI-994, Pan, SBHA, SAHA, scriptaid, trichostatin A and tubacin) were initially tested on the well-characterized CLBL-1 canine B-cell lymphoma cell line, and Pan was identified as the most promising compound with strong *in vitro* and *in vivo* antitumor properties (21). Our results have validated HDACis, and in particular, Pan as a novel anticancer therapy for veterinary medicine, while contributing to comparative oncology. Nevertheless, owing to their potent and broad-spectrum inhibition, HDACis have been associated with significant dose-limiting toxicities, which might lead to some limitations, clinical utility, and safety as a single/adjuvant agent. There are many ways to mitigate the toxicity presented by HDACi, such as the synthesis of more efficient and safer molecules, modification of existing molecules and exploration of drug delivery systems to specifically deliver the HADCi into cancer cells, such as liposomes.

Nanomedicine and drug delivery systems play a prominent role in modern medicine and can help to circumvent the current pitfalls of several anticancer drugs, including non-targeted HDACis. Lipid-based nanosystems, particularly liposomes, represent an attractive nanocarrier for drug delivery for cancer treatment (22–25).

Liposomes are lipid vesicles composed of one or more bilayers enclosing one or various internal aqueous compartments that are able to incorporate both hydrophilic and hydrophobic compounds. Liposomes have many advantages such as biodegradability, biocompatibility, improvement of pharmacokinetic profiles, low cytotoxicity and the ability to be modified to allow pH and temperature sensitive release (23, 26, 27). Moreover, due to their unique properties, liposomes can be designed to deliver active drugs to specific sites, through surface modification. In recent years, several ligands, such as monoclonal antibodies, antibody fragments, proteins, peptides, vitamins, carbohydrates, and glycoproteins, have been attached to the surface of liposomes to selectively target tumor cells overexpressing a specific cell surface receptor (8–11). The folate receptor (FR) has been identified as a promising target because it is highly overexpressed on the surface of a variety of tumor types, while its distribution in normal tissues and organs is limited. Some studies have shown that conjugation of folic acid (FA) is a promising approach for active targeting of liposomes to increase the amount of drug delivered to the target cell compared to free drugs or passively targeted liposomes (9, 10, 28). Within this context, in the present study we aimed to develop Pan-loaded folate targeted PEGylated liposomes with improved therapeutic outcomes for the treatment of canine B-cell lymphoma. For this purpose, non-targeted Pan-loaded and folate-targeted PEGylated liposomal formulations were prepared and their cytotoxic and targeting properties were thoroughly investigated.

Materials and methods

Materials

Dipalmitoyl phosphatidyl choline (DPPC), poly(ethylene glycol) (PEG-2000) covalently linked to distearoyl phosphatidyl ethanolamine (DSPE-PEG), rhodamine covalently linked to phosphatidyl ethanolamine (Rho-PE) and the functionalized DSPE-PEG phospholipids with folate (DSPE-PEG-FA) were purchased from Avanti Polar Lipids (Alabaster, AL, USA). Cholesterol (Chol), and phosphate buffered saline (PBS) were obtained from Sigma-Aldrich (St. Louis, MO, USA). Pan was purchased from Selleckchem (Houston, TX USA, Cat # S1030). All other reagents were of analytical grade.

Liposomes preparation

Encapsulation of Pan in liposomes was achieved by an active loading method with an ammonium sulfate gradient as previously described by us (10). Briefly, the relevant lipids, DPPC: Chol: DSPE-PEG in a molar ratio of 1.85: 1: 0.15 for non-targeted liposomes and DPPC: Chol: DSPE-PEG: DSPE-PEG-FA in a molar ratio of 1.85: 1: 0.12: 0.03 for targeted liposomes were dissolved in chloroform and the organic solvent was removed by rotary evaporation. The homogeneous lipid film formed was hydrated with water and the resulting suspension was frozen (-70°C) and lyophilized (Edwards, CO, USA) overnight. Rehydration of the lyophilized powder was performed with ammonium sulfate (135 mM, pH 5.4) at 45°C for 30 min. To produce a homogeneous liposome suspension, the unloaded liposomes were filtered under nitrogen pressure (10–500 lb/in2), through polycarbonate membranes of proper pore size (at 45°C), using a Lipex thermo-barrel extruder (Lipex: Biomembranes Inc., Vancouver, BC, Canada) until the liposomes reached a mean size of 0.1 μm. An ammonium sulfate gradient was established by replacing the extraliposomal medium with PBS buffer (pH 7.4) using a desalting column (Econo-Pac 10 DG, Bio-Rad, Hercules, CA, USA). Pan was incubated with unloaded liposomes at a molar ratio of 1:16 μmol of lipid, previously diluted in PBS (from a stock solution at 67 mg/mL) for 1 h at 45°C. To separate the unencapsulated Pan an ultracentrifugation was performed at 250,000 g for 2 h at 15°C in a Beckman LM-80 ultracentrifuge (Beckman Instruments, Fullerton, CA, USA). The pellet was suspended in PBS (pH 7.4). Four different formulations were prepared: folate-targeted unloaded liposomes (FA-PEG-Lip), non-targeted unloaded liposomes (PEG-Lip), folate-targeted loaded with Pan liposomes (FA-PEG-Pan-Lip) and non-targeted loaded with Pan liposomes (PEG-Pan-Lip).

For flow cytometry studies unloaded liposomes and Pan liposomes were prepared as above described. The only difference was the inclusion in the lipid composition of Rho-PE at 0.2 mol% of total lipid.

For biodistribution studies, selected Pan liposomes were labeled with Indium-111 (^{111}In). For that, the chelating agent diethylenetriamine pentaacetic acid (DTPA) at a concentration of 6 μM was encapsulated during liposome preparation after achievement of the lipid film and before lyophilization (29). Then liposomes were prepared as above described. Pan liposomes co-loaded with DTPA were then labeled with ^{111}In using the lipophilic complex ^{111}In-oxine as precursor, as describe below.

Characterization of panobinostat liposomal formulations

After disruption of liposomes with ethanol, Pan was quantified by spectrophotometry with the aid of a calibration curve (standards ranged from 2.5 to 20 μg/mL). The absorbance of all samples were read at 282 nm. The lipid content of liposomal formulation under study was determined using an enzyme-linked colorimetric method, Phospholipids Choline Oxidase-Peroxidase (Spinreact, Spain) (30). Liposomes were characterized in terms of lipid composition and by the following encapsulation parameters: the initial and final Pan to lipid ratios [(Pan/Lip)i and (Pan/lip)f, respectively]; and encapsulation efficiency defined as the percentage of [(Pan/Lip)f]/[(Pan/Lip)i]. Pan liposomes mean size was determined by dynamic light scattering in a Zetasizer Nano S (Malvern Instruments Inc., Malvern, UK). As a measure of particle size distribution of the dispersion, the system reports the polydispersity index ranging from 0.0 for a completely monodisperse sample up to 1.0 for a polydisperse suspension. The zeta potential was determined by laser Doppler electrophoresis in a Zetasizer Nano Z (Malvern Instruments Inc, Malvern, UK).

Cell line and culture

The canine CLBL-1 B-cell lymphoma cell line (provided by Dr. Barbara Rütgen, Department of Pathobiology, University of

Veterinary Medicine, Vienna, Austria) (31, 32) was cultured in Roswell Park Memorial Institute-1640 (RPMI 1640) medium (Gibco, Thermo Fisher Scientifics, Waltham, MA, USA) supplemented with 10% heat inactivated fetal calf serum (FCS, Gibco) and penicillin 100 U/ml/streptomycin 0.1 mg/ml (Gibco) at 37°C in a humidified atmosphere of 5% CO_2 (T75-tissue culture flasks, Greiner Bio-One, Kremsmünster, Austria).

Immunoblotting

Cells were harvested, washed twice with PBS and lysed with RIPA lysis Buffer (25 mM TrisHCL pH 7.6, 150 mM NaCl, 1% NP-40, 1% sodiumdeoxycholate, 0.1% SDS) supplemented with protease inhibitor cocktail (Roche, Basel, Switzerland). An increasing amount of total protein cell extract was loaded onto 15% SDS—polyacrylamide gel electrophoresis (SDS-PAGE) and transferred to nitrocellulose membranes. The membranes were blocked in 5% non-fat milk in PBS containing 0.2% Tween-20. After blocking, the membranes were incubated with primary antibodies. To evaluate folate expression, membranes were incubated with folate receptor alpha antibody (1:500 dilution, 0.5 mg/ml, Invitrogen, Thermo Fisher scientific, Carlsbad, CA, USA) or anti-α-tubulin antibody (monoclonal, mouse, 1:1,250 dilution, Sigma-Aldrich). To assess acetylation of H3 histone, membranes were incubated with anti-acetylhistone H3 (Lys9, Lys14) antibody (polyclonal, rabbit, 1:2,500 dilution, Thermo Fisher Scientific, Rockford, IL, USA) or anti-histone H3 (polyclonal, rabbit, 1:1,000 dilution, Thermo Fisher Scientific). Membranes were then incubated with secondary antibody: Peroxidase-AffiniPure anti-rabbit IgG antibody (polyclonal, goat, 1:10,000 dilution, Jackson ImmunoResearch, PA, USA) or anti-mouse IgG HRP antibody (polyclonal, sheep, 1:7,500 dilution, Jackson ImmunoResearch) to assess folate expression and Peroxidase-AffiniPure anti-rabbit IgG antibody (polyclonal, goat, 1:10,000 dilution, Jackson ImmunoResearch, PA, USA), to evaluate H3 acetylation. Proteins were detected using Luminata Forte Western HRP (Merck Millipore, Billerica, MA, USA) and acquired using the ChemiDoc XRS+ imaging system (Bio-Rad, Hercules, CA, USA).

Cytotoxic assay

To determine the effect of Pan loaded in non-targeted and FA-targeted liposomal formulations on CLBL-1 cell proliferation, a cell viability assay was performed using the Alamar blue cell viability (Invitrogen). Briefly, 6×10^5 of cells were seeded in 96-well plates in 200 µl of culture medium and subjected to increasing doses (0.4–2,000 nM) of each PEG-Pan-Lip and FA-PEG-Pan-Lip formulations. Free Pan was used as a control. After 24 h treatment, cell viability was determined using Alamar Blue reagent, according to the manufacturer's instructions. Absorbance at 570 nm and 600 nm was measured using the iMark microplate Reader (Bio-Rad). Cell viability was calculated using the formula provided by the manufacturer. Two replicate wells were used to determine each data point and two independent experiments were carried out in different days. Best-fit EC_{50} values of each formulation were calculated using GraphPad Prism software (version 9.2.0, San Diego, CA, USA) using response vs. log (inhibitor) function with variable slope.

Evaluation of apoptotic cell death

The percentage of apoptotic cells after treatment with each liposomal formulation was determined by flow cytometry using the Guava Nexin Assay. Cells were seeded and treated with increasing concentrations (1–20 nM) of liposome formulations loaded with Pan for 24 h. After treatment, cells were recovered, centrifuged at 500 g for 5 min and resuspended in PBS containing 2% FBS. Then, an equal volume of Guava Nexin reagent was added to 50 µl of the cell suspension and incubated for 20 min, at room temperature, protected from light. Guava easyCyte 5HT flow cytometer using the Nexin software module was used for sample acquisition and analysis.

Caspase-3 and 7 activities were measured using Caspase Glo 3/7 Assay (Promega, Madison, WI, USA). For this purpose, CLBL-1 cells were seeded and treated with 1–20 nM of each liposomal formulation loaded with Pan for 24 h. After treatment, 100 µl of each cell suspension was transferred into a white 96-well plate and 75 µl of caspase-Glo 3/7 reagent was added. The mixture was mixed by orbital shaking for 30 s and then incubated at room temperature for 30 min. Incubation allowed complete cell lysis, stabilization of cleavage of the proluminescent substrate mediated by caspases and an increase in the luminescent signal. Luminescence was measured using the GloMax-Multi+ Detection System (Promega).

Cellular uptake by immunofluorescence and flow cytometry

To perform the qualitative analysis, 1.5×10^5 of CLBL-1 cells were plated on ibidi µ-Slide 8 Well Glass Bottom (Ibidi, Fitchburg, WI, USA) and incubated for 24 h at 37°C in a humidified atmosphere of 5% CO_2. Then, the rhodamine-labeled PEG-Lip and FA-PEG-Lip was added to the cells and incubated at 37°C for 3 and 6 h, respectively. After incubation, cells were washed twice with PBS, fixed with PFA 4% for 15 min at room temperature and washed twice. After washing, DAPI Vectashield (Vector Labs, Burlingame, CA, USA) was added to the cells. Image acquisition was performed on a confocal point-scanning Zeiss LSM 880 microscope (Carl Zeiss, Germany) equipped with a Plan-Apochromat DIC X63 oil objective (1.40 numerical aperture). Diode 405-30 laser was used to excite DAPI, and DPSS 561-20 laser to excite Rhodamine. In the Airyscan acquisition mode, ×1.80 zoom images were recorded at 1,024 × 1,024 resolution. ZEN software was used for image acquisition and Fiji software was used for image processing.

To determine the quantitative cellular uptake of PEG-Lip and FA-PEG-Lip formulations, flow cytometry was performed. Briefly, 1×10^6 of CLBL-1 cells were incubated with 5 µmol/ml or 7.5 µmol/ml of the rhodamine-labeled PEG-Lip and FA-PEG-Lip in a complete medium without phenol red for 90 min, 3 h and 6 h at 37°C. The cells were centrifuged and washed twice with PBS to remove unbound liposomes. Data were collected and analyzed using the Attune NxT flow cytometer (Thermo Scientific).

Animals

All animal-handling procedures were performed in accordance to EU recommendations for good practices and animal welfare and were approved by the Animal Care and Ethical Committee of the Faculty of Veterinary Medicine (Protocol_0050132016). All methods were performed in accordance with the relevant guidelines and regulations. Female 6–8-week-old SOPF/SHO SCID mice or CD1 mice were purchased from Charles River. Immunodeficient mice were maintained in microisolation cages under pathogen-free conditions. CD1 mice were maintained under standard conditions. Room conditions included a room temperature of 24–26°C and a cycle of 12 h light and 12 h of darkness. Food and water were sterilized and provided *ad libitum*.

Preparation of ^{111}In-liposomes

The diethylenetriaminepentaacetic acid(DTPA)-containing liposomes were labeled with Indium-111 (^{111}In) upon incubation of the respective liposome with ^{111}In-8-hydroxyquinoline (oxine) following a modified procedure of the literature (33). The radiolabeling of oxine involved, firstly, the preparation of an ethanolic solution of oxine (250 μL, 13.8 mM), which was diluted with 0.4 M acetate buffer pH 5.5 (1,000 μL). The resulting oxine solution was added to indium (^{111}In) chloride (290 μL, 370 MBq/mL, Mallinckrodt/Curium, The Netherlands) and then incubated at room temperature for 15 min. The lipophilic components were extracted with dichloromethane (3×) and then evaporated to dryness under a gentle stream of nitrogen. The radiochemical yield was generally >95 % ^{111}In-oxine as determined by instant thin-layer chromatography using glass microfiber chromatography paper impregnated with silica gel (iTLC-SG, Agilent Technologies) and ethanol as eluent. The obtained dry residue containing ^{111}In-oxine was firstly dissolved in ethanol (30 μL) and phosphate-buffered saline (PBS) pH 7.4 (80 μL) was added. The resulting mixture was incubated with the DTPA-containing liposomes (300–1.5 mL) for 45 min at 37°C. The ^{111}In-liposomes were purified by ultrafiltration using a centrifugal concentrator—Amicon Ultra-0.5 Centrifugal Filter Unit (100 kDa MWCO, 0.5 mL sample volume, Merck) following the manufacturer's instructions. The labeling efficiency, which varied between 51% and 80% depending on the type of liposome, was determined by dividing the radioactivity from the concentrate that corresponds to ^{111}In-liposome by the total amount loaded onto the Amicon filter.

Biodistribution studies in CD1 mice

To evaluate the biodistribution in healthy mice, targeted and non-targeted ^{111}In-labeled liposomes diluted in PBS (100 μL) were injected intravenously via the tail vein into CD1 mice. At 1 h, 3 h and 24 h post-injection (p.i.), mice were sacrificed by cervical dislocation. The injected radioactivity dose and the radioactivity in the sacrificed animal were measured using a dose calibrator (Carpintec CRC-15W, Ramsey, USA). The difference between the radioactivity in the injected dose and the sacrificed animals was accepted to be due to excretion. After sacrificed, tissue samples were collected, rinsed with PBS, weighed, and counted in a gamma counter (Hidex AMG, Hidex, Turku, Finland). Results are expressed as the mean percentage of the injected dose (ID) per gram of tissue (%ID/g tissue) (mean ± SD) ($n = 3$ per liposomal formulation).

Tumor induction, biodistribution, and tumor targeting in SCID mice

For tumor induction, 1×10^6 CLBL-1 cells diluted in PBS and matrigel (1:1) (Corning, NY, USA, Cat) were subcutaneously injected into the dorsal interscapular region of SCID mice as previously described (34). Tumor volume was calculated using the formula $(\text{width})^2$ x length. When the tumor reached a minimum volume of 150 mm^3, the mice were randomized and divided into two distinct groups (targeted and non-targeted ^{111}In-labeled liposomal formulations). Subsequently, the radiolabeled liposomes were intravenous injected into SCID mice. After sacrifice, the tissues were dissected and counted in a gamma counter, at different time points (24 h and 48 h p.i.). Tumor and tissue uptake were expressed as percentage of the injected dose per gram of tissue (%ID/g).

Histopathological analysis

Tumors were fixed in 10% buffered formalin and embedded in paraffin utilizing a Leica tissue processor. Sections were cut from paraffin blocks and stained with hematoxylin and eosin (H&E). sections were mounted onto superfrost ultra plus slides (Menzel-Glaser, Braunschweig, DE) for immunohistochemistry.

Immunohistochemistry analysis

A representative area of each tumor was selected and tissue sections of 3 μm thickness were mounted on glass slides (Superfrost glass slides, Thermo Scientific, Braunschweig, Germany), deparaffinized with xylene and hydrated in a graded ethanol series of distilled water. The Novolink Polymer Detection System (Noocastra, Leica Biosystems, Newcastle, UK) was used according to the manufacturer's instructions. The antigen retrieval treatment was achieved by microwave treatment (5 min at 900 watts plus 15 min at 650 watts) in Tris-EDTA buffer (pH 9.0). To block endogenous peroxidase and to prevent unspecific labeling, the system's Peroxidase Block Solution and Protein Block Solution were used sequentially. Sections were incubated 30 min at room temperature with polyclonal rabbit anti-human CD20 (Thermo Fisher Scientific), diluted 1:200 and rabbit polyclonal anti-human CD3 (Dako, Glostrup, Denmark), diluted 1:400. Labeling was developed by incubating the slides with system's chromogen, diaminobenzidine (DAB), and hydrogen peroxide as substrate. Nuclear background staining was performed with Gill's hematoxylin (30 s). Labeling without the primary antibody was used as negative control, while dog lymph node sections were used as positive control.

TABLE 1 Characterization of target and non-targeted liposomes unloaded and loaded with Pan.

Lipid composition (molar ratio)	(Pan/Lip)i (μg/μmol)	(PAN/Lip)f (μg/μmol)	E.E. (%)	Mean size (nm) (P.I.)	Zeta pot (mV)
PEG-Pan-Lip; DPPC:Chol:DSPE-PEG (1.85:1.0.15)	39 ± 1	21 ± 1	56 ± 2	130 (<0.050)	−2 ± 1
FA-PEG-Pan-Lip; DPPC:Chol:DSPE-PEG: DSPE-PEG-FA (1.85:1.0.12:0.03)	35 ± 1	33 ± 1	94 ± 2	130 (<0.050)	−2 ± 1
PEG- Lip; DPPC:Chol:DSPE-PEG (1.85:1.0.15)	na	na	na	130 (<0.070)	−3 ± 1
FA-PEG-Lip; DPPC:Chol:DSPE-PEG: DSPE-PEG-FA (1.85:1.0.12:0.03)	na	na	na	130 (<0.070)	−3 ± 1

FA, Folate; (PAN/Lip)i, initial Pan to lipid ratio; (PAN/Lip)f, final Pan to lipid ratio; E.E., encapsulation efficiency; na, not applicable; P.I., polydispersity index.

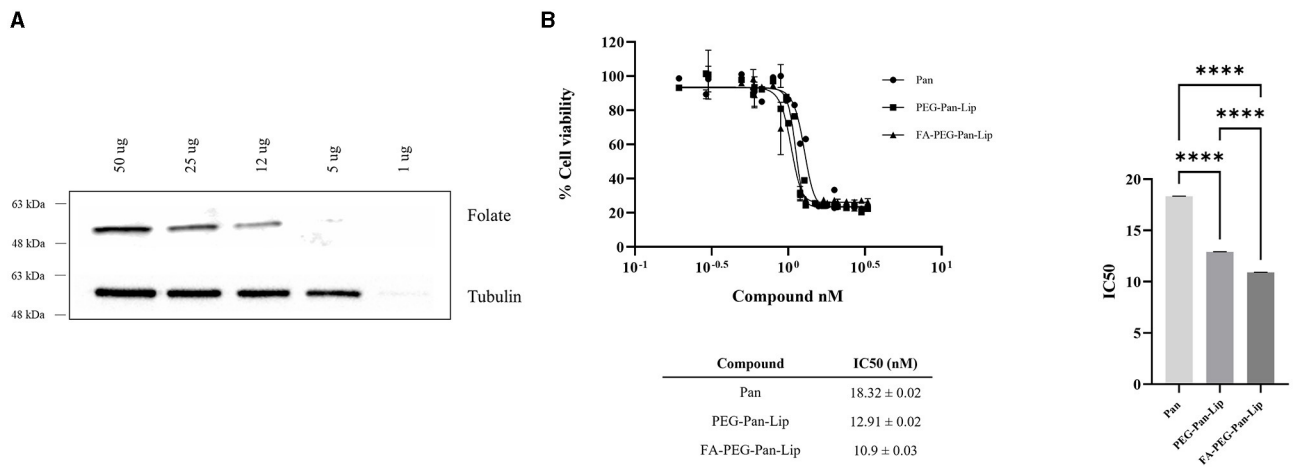

Compound	IC50 (nM)
Pan	18.32 ± 0.02
PEG-Pan-Lip	12.91 ± 0.02
FA-PEG-Pan-Lip	10.9 ± 0.03

FIGURE 1
Evaluation of folate receptor expression and cytotoxic activity of folate-targeted and nontargeted liposomes loaded with panobinostat was evaluated in CLBL-1 cells. **(A)** Folate receptor expression was evaluated in total cell extracts from CLBL-1 cells using an anti-folate receptor antibody. Loading was controlled with an anti-tubulin antibody. Representative blots are shown. **(B)** Cells were treated with increasing concentrations of liposomes. After 24 h treatment, cell viability was measured using Alamar Blue reagent. Two replicate wells were utilized to determine each data point and three independent experiments were carried out in different days. Best-fit IC50 values of each formulation were calculated using the log (inhibitor) vs response (variable slope) function. Statistical significance was determined with one-way ANOVA followed by a Tukey's test. Values of $p < 0.05$ were considered significant. $^{****}p < 0.0001$.

Statistical analysis

Results are expressed as mean ± standard deviation (SD) or mean ± standard error mean (SEM). Statistical analysis was performed using one-way ANOVA and two-tailed Student's *t*-test using GraphPad Prism® 9 (GraphPad Software, CA, USA). $P < 0.05$ was considered statistically significant.

Results

Physicochemical properties of panobinostat loaded liposomes are suitable for drug delivery

Owing to the potent anticancer activity of Pan on canine B-cell lymphoma demonstrated previously by our group (21, 34), this HDACi was selected for the study described herein. Although Pan exhibited promising cytotoxicity and antitumor properties *in vitro* and *in vivo*, it has been associated with significant dose-limiting toxicities, which might lead to some limitations for its clinical translation and safety as a single/adjuvant agent. Therefore, there is an urgent need to mitigate the high toxicity of Pan, as well as other HDACis. One of the best strategies to overcome this issue is to explore drug delivery systems. Within this context, in the present study we aimed to develop a Pan loaded PEGylated liposome drug delivery system with improved therapeutic outcomes. For this purpose, unloaded and loaded folate-targeted (FA-PEG-Lip and FA-PEG-Pan-Lip) and non-targeted liposomal formulations (PEG-Lip and PEG-Pan-Lip) were prepared, characterized and their biological activity tested. All liposomal formulations were prepared using the dehydration-rehydration method followed by an extrusion step to reduce and homogenize the mean size of the liposomes. The physicochemical properties of the liposomes,

10.3389/fvets.2023.1236136

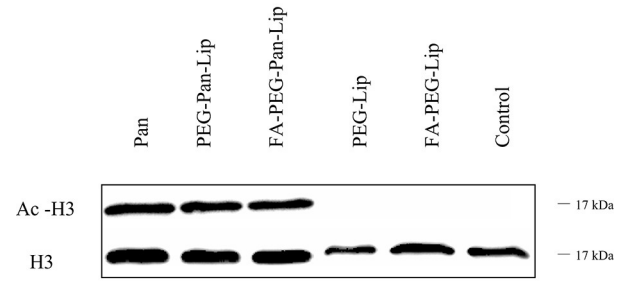

FIGURE 2
Assessment of H3 Histone Acetylation. H3 histone acetylation was assessed in total cell extracts from CLBL-1 cells after 24 h treatment with 20 uM of folate-targeted liposomes and nontargeted liposomes loaded with Panobinostat. Acetylation of H3 histones was evaluated by western blotting with an anti-acetyl-histone H3 polyclonal antibody. As loading control, H3 histone was assessed using anti-histone H3 polyclonal antibody. Representative blots are presented.

namely particle size, zeta potential, and incorporation parameters, such as encapsulation efficiency and loading capacity, are listed in Table 1. All liposome formulations presented a mean size of 130 nm and a PI < 0.2, demonstrating the high homogeneity of the so developed liposomes. The Zeta potential revealed a neutral surface charge under all the conditions being in accordance with the presence of DSPE-PEG at liposomal surface. Regarding Pan incorporation parameters, liposomes loaded with folate presented a higher encapsulation efficiency (94%), with a final loading capacity of 33 μg/μmoL than non-targeted liposomes (21 μg/μmoL). Nevertheless, all formulations were selected to study their cytotoxic and targeting properties against canine B-cell lymphoma.

Folate receptor is expressed in canine lymphoma cells

The folate receptor is overexpressed in cancer cells, making it a suitable molecular target for specific drug delivery (9). Therefore, to assess the feasibility of using the folate receptor as a target for canine B-cell lymphoma, we evaluated its expression by western blot analysis in the well-characterized CLBL-1 canine lymphoma cell line (31, 32). Immunoblotting analysis (Figure 1A) confirmed folate receptor expression in the canine DLBCL cell line and demonstrated an increasing presence of the receptor, in agreement with the increasing amount of cellular extract. These results confirmed the presence of the folate receptor in CLBL-1, allowing us to explore it as a promising target and to evaluate the cytotoxic and targeting properties of the different liposome formulations prepared.

Panobinostat-loaded liposomes present cytotoxicity in canine B-cell lymphoma

To evaluate the potential cytotoxic activity of the different liposome formulations in canine B-cell lymphoma, we conducted a cell viability assay in the CLBL-1 cell line. Cell viability of lymphoma cells subjected to a 24 h treatment with non-targeted and folate-targeted liposomes loaded with Pan was evaluated using Alamar Blue reagent, as described in the Materials and Methods section. PEG-Lip, FA-PEG-Lip and free Pan were used as controls. As shown in Figure 1B, Pan liposome formulations (PEG-Pan-Lip and FA-PEG-Pan-Lip) exhibited a dose-dependent inhibitory effect on CLBL-1 cell proliferation. In contrast, no cytotoxicity was observed for the PEG-Lip and FA-PEG-Lip formulations (data not shown). The differences between the IC_{50} values for each liposomal formulation and Pan-free were statistically significant. Moreover, the cytotoxicity of Pan was potentiated after incorporation in liposomes, probably due to a higher internalization in tumor cells. Importantly, the obtained data have shown that the IC_{50} values were in the nM range and that the Pan folate-targeted liposomal formulation seems to exhibit a slightly higher cytotoxic effect than the non-target liposomal formulation and Pan-free (FA-PEG-Pan-Lip, $IC_{50} = 10.9 \pm 0.03$ nM, PEG-Pan-Lip, $IC_{50} = 12.91 \pm 0.02$ nM and Pan-free, $IC_{50} = 18.32 \pm 0.024$ nM).

Panobinostat-loaded liposomes induce H3 histone acetylation and apoptosis

Pan alters gene expression by inducing the acetylation of histones at an early stage, causing several effects on the cell cycle and resulting in cell death. Thus, to validate the mechanism of action of Pan-loaded liposomes in CLBL-1 cells, we evaluated the acetylation status of H3 histones by western blot. The acetylation status of cells treated with liposomes loaded with Pan were compared to unloaded liposome formulations. Immunoblotting analysis (Figure 2) demonstrated that CLBL-1 cells presented a hyperacetylation status, after 24 h of treatment with PEG-Pan-Lip, FA-PEG-Pan-Lip formulations, when compared with PEG-Lip and FA-PEG-Lip formulations and vehicle-/control-treated cells. Cell death occorred by apoptosis (Figures 3A, B). These results are in agreement with the cell viability and proliferation data upon Pan treatment, indicating that the cytotoxic activity of Pan in the CLBL-1 cell line is consistent with the induction of apoptosis. To confirm that apoptosis is a central mechanism of Pan-loaded liposome-induced cell death, the caspase 3/7 activity levels and the percentage of apoptotic cells after 24 h of treatment were determined. The results shown in Figure 3C indicate that caspase 3/7 activity was promoted in a dose-dependent manner by the PEG-Pan-Lip and FA-PEG-Pan-Lip formulations and the maximum caspase-3/7 activity was seen at 20 nM.

Uptake of liposome formulations in CLBL-1 cells

Intracellular uptake of rhodamine-labeled liposome formulation in CLBL-1 cells was evaluated by flow cytometry and immunofluorescence. For flow cytometry, labeled liposomes were incubated with CLBL-1 cells at different time points (90 min, 3 h and 6 h). The uptake of both formulations (FA-PEG-Pan-Lip and PEG-Pan-Lip) differed significantly, as shown in Figure 4A.

10.3389/fvets.2023.1236136

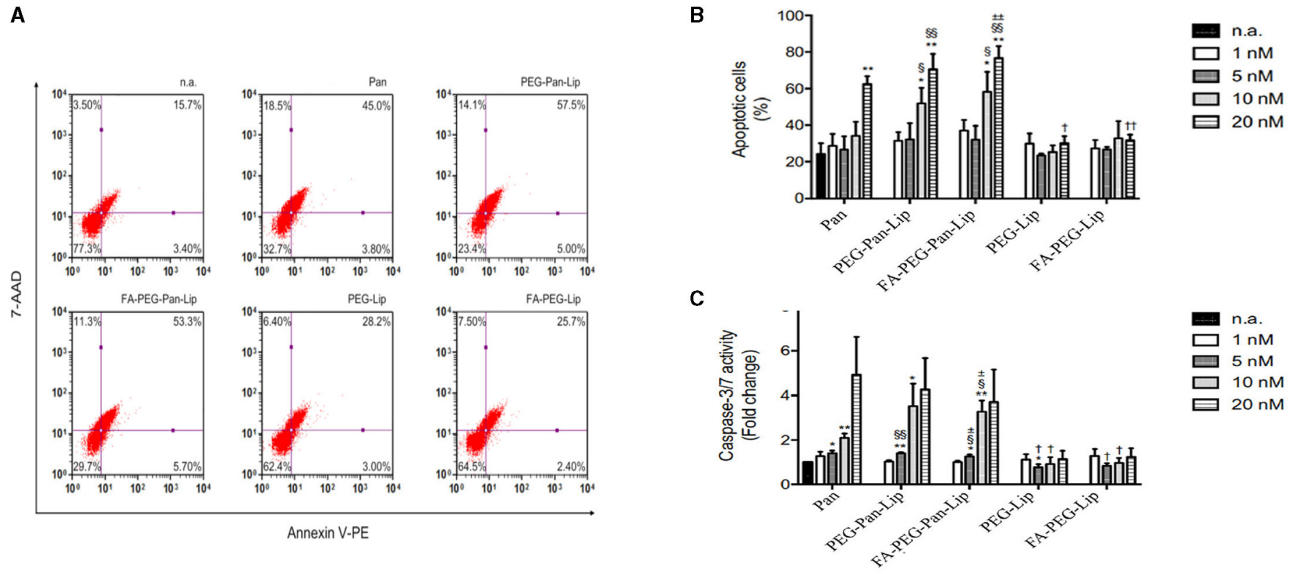

FIGURE 3
Evaluation of apoptotic cell death. **(A)** CLBL-1 cells were treated with 20 nM folate-targeted and nontargeted liposomes loaded with panobinostat for 24 h and representative flow cytometry plots using Annexin V/7-AAD staining are shown. **(B)** The percentage of apoptotic cells was determined in CLBL-1 cells subjected to a range of concentrations of folate-targeted and nontargeted liposomes loaded with panobinostat. After 24 h treatment, apoptotic cells were determined by flow cytometry using the Guava Nexin Assay. **(C)** Caspase 3/7 activity was evaluated in CLBL-1 cells subjected to increasing concentrations of folate-targeted and nontargeted liposomes loaded with panobinostat. After 24 h treatment, activity was determined using the Caspase-Glo 3/7 assay. Results are expressed as means ± SEM fold change to control cells. $*p < 0.05$ and $**p < 0.01$ from n.a.; $^{\dagger}p < 0.05$ and $^{\dagger\dagger}p < 0.005$ from Pan; $^{\S}p < 0.05$ and $^{\S\S}p < 0.01$ from PEG-Lip; $^{\pm}p < 0.05$ and $^{\pm\pm}p < 0.001$ from FA-PEG-Lip. Statistical analysis was performed using Student's t-test. Values of $p < 0.05$ were considered significant. n.a., no addition.

The uptake was higher in the formulation containing folate at all time-points tested, demonstrating the importance of folate in facilitating cellular uptake. Additionally, the cellular uptake seemed to be time-dependent, since the amount of liposomes increased with time, reaching the highest value after 6 h incubation. Live/dead reagent was used to exclude dead cells, and background noise was evaluated in the control with the secondary antibody (data not shown). To better characterize the uptake efficiency of all liposomal formulations in CLBL-1 cells, we further evaluated the cellular internalization properties of the liposomes using confocal point-scanning microscopy after staining the nucleus with DAPI. As shown in Figure 4B, liposomes accumulated in the perinuclear area, confirming the internalization of both formulations. Moreover, FA-PEG-Pan-Lip significantly increased the fluorescent signal in the perinuclear region, in comparison with the PEG-Pan-Lip.

Biodistribution studies in CD1 mice and xenograft mice model of canine B-cell lymphoma

To assess the *in vivo* stability, pharmacokinetic and tumor uptake profile of non-targeted and folate-targeted liposome formulations, we performed a biodistribution study in CD1 mice and in SCID xenograft mouse model of CLBL-1, respectively. For that purpose, FA-PEG-Pan-Lip and PEG-Pan-Lip formulations were radiolabeled with ^{111}In, according to a previously reported procedure (29, 35). Both ^{111}In-lipossomes were intravenously administrated to CD1 or to SCID mice and the biodistribution was evaluated at different time points. The biodistribution data of ^{111}In-labeled PEG-Pan-Lip and FA-PEG-Pan-Lip, expressed as %ID/g of the main tissues and tumors, are presented in Tables 2, 3. Analysis of the data, in the CD1 mouse model, revealed that both ^{111}In-liposomal preparations presented a similar tissue distribution profile with a moderate blood clearance (12.7 ± 3.8, 3.5 ± 0.6, 0.67 ± 0.08 %ID/g for ^{111}In-PEG-Pan-Lip and 12.8 ± 0.7, 5.4 ± 0.7, 1.2 ± 0.6 %ID/g for ^{111}In-FA-PEG-Pan-Lip, at 1 h, 24 h and 48 h p.i., respectively). Moderate hepatic uptake was found (1.1 ± 0.6, 5.9 ± 0.5/g of liver for ^{111}In-PEG-Pan-Lip and 2.19 ± 0.05, 6.8 ± 1.4 %ID/g for ^{111}In-FA-PEG-Pan-Lip, at 1 h, 24 h, respectively) that slightly decreased at 48 h indicating the hepatobiliar path as the main elimination route. However, the involvement of the urinary excretory pathway is also evident in the kidney uptake and in the whole-body radioactivity excretion rate. In fact, the untargeted formulation (^{111}In-PEG-Pan-Lip) had a low kidney uptake (< 2.7 ± 0.3 %ID/g of kidney) associated to a rapid total excretion (59.7 ± 6.6, 68.3 ± 0.4, 82.3 ± 4.2 %ID, at 1 h, 24 h and 48 h p.i., respectively). The kidney uptake of the targeted formulation (^{111}In-FA-PEG-Pan-Lip) increased over time (1.7 ± 0.9, 5.6 ± 0.3, 4.1 ± 2.7 %ID/g of kidney, at 1 h, 24 h and 48 h p.i., respectively) probably due to the presence of the folate moiety in the liposomes since the high expression of folate receptors

10.3389/fvets.2023.1236136

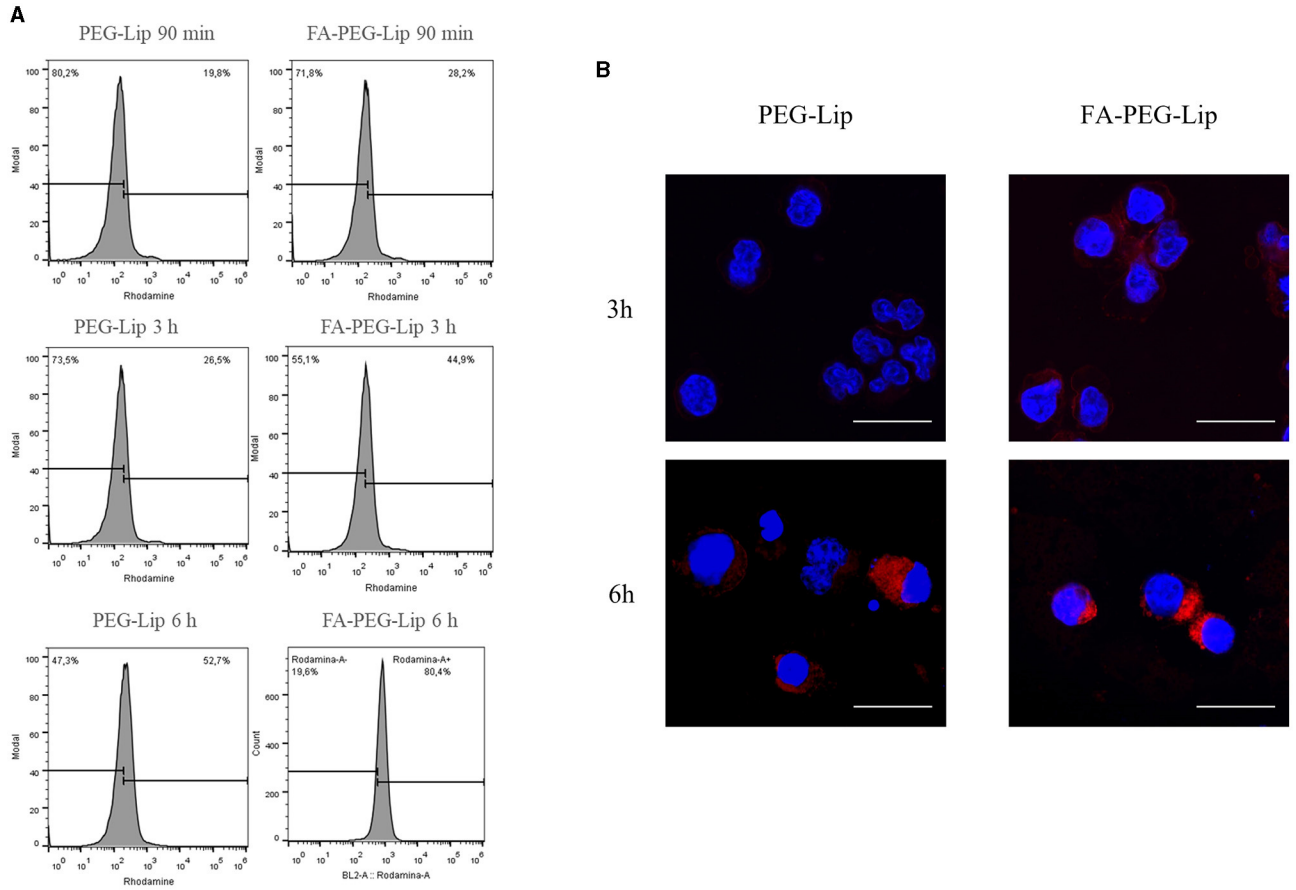

FIGURE 4
Evaluation of cellular uptake by flow cytometry and immunofluorescence. **(A)** To evaluate the quantitative cellular uptake of the liposomes, flow cytometry was performed. 1×10^6 of CLBL-1 cells were incubated with 5 μmol/ml of PEG and PEG Folate labeled with phosphatidyl ethanolamine covalently linked to rhodamine for 90 min, 3 h and 6 h. Cellular uptake seems to be time dependent, achieving a high value after 6 h of incubation. Moreover, the percentage of uptake was higher in the formulation containing folate. **(B)** To determine the qualitative analysis, immunofluorescence was performed. 1×10^5 of CLBL-1 cells were incubated for 3 h and 6 h with liposomes labeled with rhodamine. An accumulation of liposomes in the perinuclear area, confirmed the internalization of both formulations.

in the renal proximal tubules is known. Consequently, the rate of total excretion is lower, ∼30%, at 1 h p.i. The washout from major organs, except spleen was also rapid in both formulations. Liposomes were promptly eliminated from the heart, intestine, lungs, intestines and stomach. Radioactivity accumulation of radiolabeled liposomes was observed in the spleen (1.7 ± 0.4, 12.5 ± 4.2, 11.2 ± 3.9 %ID/g for ^{111}In-PEG-Pan-Lip and 2.6 ± 1.1, 7.8 ± 1.5, 8.2 ± 1.6 %ID/g for ^{111}In-FA-PEG-Pan-Lip, at 1 h, 24 h and 48 h p.i., respectively) reflecting the expected uptake from the mononuclear phagocyte system. Regarding the biodistribution and tumor uptake in the SCID xenograft mouse model of CLBL-1, the trend of the biodistribution profile is similar. Moderate blood clearance associated to hepatic and splenic uptake. Higher kidney uptake and lower rate of total excretion of ^{111}In-FA-PEG-Pan-Lip than ^{111}In-PEG-Pan-Lip. Moreover, and importantly, this preliminary biodistribution study demonstrated the ability of the targeted formulation (^{111}In-FA-PEG-Pan-Lip) to accumulate in FR-expressing tumors. Indeed, the tumor uptake was 1.6-fold higher at 24h p.i (2.2 ± 0.9 %ID/g of tumor) than the ^{111}In-PEG-Pan-Lip formulation (1.32 ± 0.2 %ID/g of tumor), as shown in Table 3.

Moreover, it is important to mention that histological and immunohistochemical analysis demonstrated that xenograft tumors maintained histological features and expression of B-cell markers were positive and expression of T-cell markers were negative, reflecting those of the original CLBL-1 cell line xenografts (Figure 5).

Discussion

Lymphoma and NHL, in particular, are responsible for millions of deaths worldwide, representing a disturbing global health problem. The similarities between human NHL and canine lymphoma make NHL a transversal disease for both species, opening new opportunities to explore the advantages of translational research. In the present study, we explored a novel liposome-based drug delivery system to enhance the therapeutic benefits of Pan, a validated anticancer drug in comparative medicine (34). Pan is a cytotoxic compound belonging to the HDACi class that has shown great promise in relapsed DLBCL patients, inducing long-lasting durable responses in a phase 2

10.3389/fvets.2023.1236136

TABLE 2 Biodistribution profiles of radiolabeled FA-PEG-Pan-Lip and PEG-Pan-Lip in healthy mice.

Organ	^{111}In-PEG-Pan-Lip			^{111}In-FA-PEG-Pan-Lip		
	1 h	24 h	48 h	1 h	24 h	48 h
Blood	12.7 ± 3.8	3.5 ± 0.6	0.67 ± 0.08	12.8 ± 0.7	5.4 ± 0.7	1.2 ± 0.6
Liver	1.1 ± 0.6	5.9 ± 0.5	4.5 ± 1.4	2.19 ± 0.05	6.8 ± 1.4	6.3 ± 1.6
Intestine	0.55 ± 0.06	0.98 ± 0.07	0.6 ± 0.2	1.0 ± 0.4	1.2 ± 0.2	1.1 ± 0.2
Spleen	1.7 ± 0.4	12.5 ± 4.2	11.2 ± 3.9	2.6 ± 1.1	7.8 ± 1.5	8.2 ± 1.6
Heart	0.7 ± 0.2	1.3 ± 0.3	0.7 ± 0.2	0.7 ± 0.4	1.9 ± 0.7	0.9 ± 0.2
Lung	1.0 ± 0.5	1.6 ± 0.6	0.6 ± 0.2	1.4 ± 0.6	2.2 ± 0.4	0.5 ± 0.3
Kidney	1.3 ± 0.6	2.7 ± 0.3	2.2 ± 0.0	1.7 ± 0.9	5.6 ± 0.3	4.1 ± 2.7
Muscle	0.4 ± 0.1	1.3 ± 0.9	0.26 ± 0.02	1.5 ± 0.1	0.7 ± 0.5	0.6 ± 0.1
Bone	0.6 ± 0.3	0.7 ± 0.3	0.6 ± 0.1	0.8 ± 0.2	1.0 ± 0.2	0.63 ± 0.02
Stomach	1.7 ± 0.9	1.1 ± 0.2	0.7 ± 0.3	1.2 ± 0.8	1.3 ± 0.7	0.8 ± 0.4
Brain	0.13 ± 0.03	0.16 ± 0.07	0.07 ± 0.05	0.17 ± 0.01	0.13 ± 0.03	0.04 ± 0.01
Carcass (%ID)	18.0 ± 0.9	26.0 ± 2.3	13.4 ± 0.7	37.2 ± 5.6	33.5 ± 3.9	28.8 ± 3.9
Excretion (%ID)	59.7 ± 6.6	68.3 ± 0.4	82.3 ± 4.2	25.7 ± 3.9	54.3 ± 1.4	63.5 ± 0.4

Radiolabeled liposomes were intravenous injected into CD1 mice. After sacrifice, the tissues were dissected and counted in a gamma counter, at different time points (1 h, 24 h and 48 h p.i.). Results are expressed as the mean percentage of the injected dose (ID) per gram of tissue (%ID/g tissue) (mean ± SD) (n = 3 per liposomal formulation).

TABLE 3 Biodistribution of radiolabeled folate-targeted and non-targeted liposomes in xenograft mice.

Organ	^{111}In-PEG-Pan-Lip		^{111}In-FA-PEG-Pan-Lip	
	24 h	48 h	24 h	48 h
Blood	1.8 ± 0.5	1.0 ± 0.3	4.6 ± 0.7	2.4 ± 0.4
Liver	5.0 ± 0.6	5.8 ± 1.6	11.9 ± 2.1	8.5 ± 2.0
Intestine	0.8 ± 0.2	0.73 ± 0.08	1.7 ± 0.1	1.6 ± 0.2
Spleen	20.6 ± 2.4	25.8 ± 0.5	16.8 ± 4.1	12.4 ± 4.4
Heart	0.32 ± 0.07	0.40 ± 0.02	1.2 ± 0.3	0.9 ± 0.2
Lung	0.68 ± 0.07	0.7 ± 0.2	2.3 ± 0.7	1.1 ± 0.6
Kidney	2.5 ± 0.3	1.9 ± 0.5	4.6 ± 0.9	4.4 ± 1.6
Muscle	0.12 ± 0.06	0.3 ± 0.2	0.7 ± 0.4	0.6 ± 0.4
Bone	0.3 ± 0.2	0.29 ± 0.07	0.8 ± 0.1	0.6 ± 0.1
Stomach	0.5 ± 0.2	0.40 ± 0.07	1.5 ± 0.7	1.0 ± 0.2
Brain	0.05 ± 0.02	0.04 ± 0.01	0.2 ± 0.1	0.05 ± 0.02
Tumor	1.3 ± 0.2	2.08 ± 0.09	2.2 ± 0.9	2.5 ± 0.8
Carcass (%ID)	14.5 ± 1.3	12.1 ± 1.2	34.4 ± 4.9	31.8 ± 3.5
Excretion (%ID)	69.8 ± 0.2	73.0 ± 1.1	27.8 ± 6.2	39.0 ± 9.1

Radiolabeled liposomes were intravenous injected into CD1 mice. After sacrifice, the tissues were dissected and counted in a gamma counter, at different time points (1 h, 24 h and 48 h p.i.). Results are expressed as the mean percentage of the injected dose (ID) per gram of tissue (%ID/g tissue) (mean ± SD) (n = 3 per liposomal formulation).model of cNHL. Radiolabeled liposomes were intravenous injected into SCID mice. After sacrifice, the tissues were dissected and counted in a gamma counter, at different time points (24 h and 48 h p.i.). Results are expressed as the mean percentage of the injected dose (ID) per gram of tissue (%ID/g tissue) (mean ± SD) (n = 3 per liposomal formulation).

clinical study (36). Recently, we demonstrated its anticancer activity against canine B-cell lymphoma (34). However, this study revealed some *in vivo* toxic effects that can limit its clinical progression as a treatment option for canine lymphoma. The primary goal of anticancer therapy in veterinary medicine is to provide the best quality of life for as long as possible, as such dogs are not good candidates for aggressive regimens independent of their curability potential. This is also a concern in human medicine, considering that the potential of these molecules as anticancer therapeutics has been hampered by toxicity- and specificity-related issues. Although a multitude of drugs acting via HDAC inhibition are currently in clinical trials or in the market, only HDACis, such as vorinostat, romidepsin, and belinostat have been approved for some T-cell lymphomas and Pan for multiple myeloma. In addition to its non-specificity, HDACis, including valproic acid, trichostatin A, sodium butyrate, and vorinostat, are associated with clinical toxic effects, such as thrombocytopenia, nausea, and fatigue. Furthermore, vorinostat and romidepsin, two FDA-approved HDACis, are reported to have no partial or complete response in solid tumors and are linked to severe cardiac toxicity. Thus, in the present study, we hypothesized that the encapsulation of Pan into liposome nanocarriers could improve their therapeutic index and further reduce associated systemic toxicity effects, extending their use in both human and veterinary clinical settings.

Due to their biological and technological advantages, liposomes have been considered in the past few years as promising drug delivery systems for cancer applications. Remarkable advances have been made and multiple biomedical applications of liposomes have been tested in clinical trials or have already been approved (37, 38). The first liposomal formulation used in human medicine was Doxil, a doxorubicin liposomal formulation, approved for the treatment of ovarian cancer, multiple myeloma, and HIV-associated Kaposi's sarcoma (39). Over the years, other formulations have been approved for cancer therapy, such as Myocet, Marqibo and Vyxeos (40). Many studies in veterinary medicine have reported the use of drugs encapsulated in liposomes. Doxorubicin liposomes have been tested in canine models to evaluate their pharmacokinetics, biodistribution, and safety profiles (41–43). These studies confirmed that Doxil did not induce cardiotoxicity or myelosuppression in dogs, one of the most

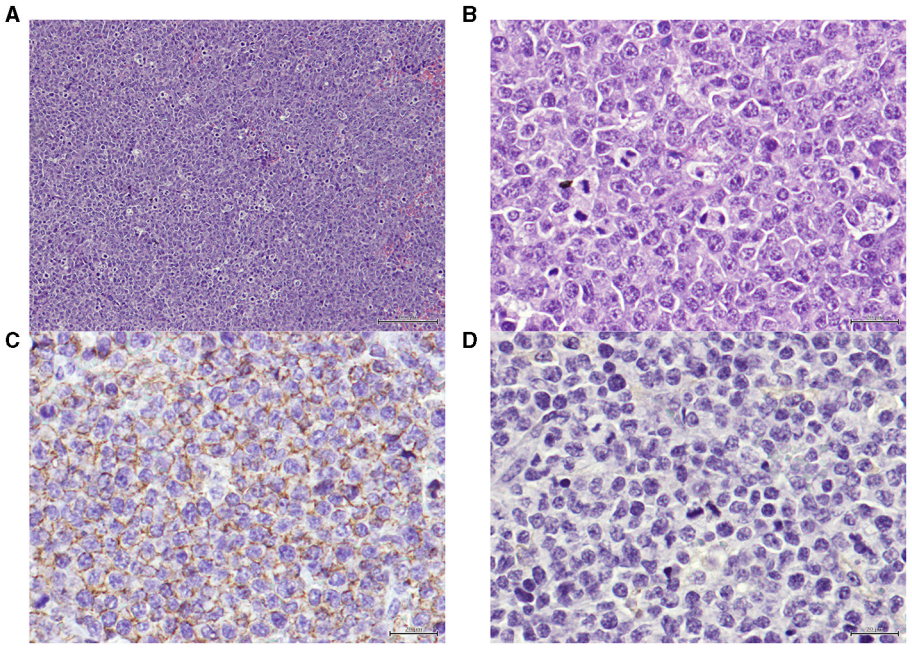

FIGURE 5
(A) Xenograft tumor section presenting a neoplasia, classified as high grade centroblastic diffuse malignant lymphoma. The neoplasia consists of monomorphic large cells with a high cell density and a starry-sky pattern. Hematoxylin and eosin (H&E) stained. Magnification = 100×, scale bar = 100 μm. **(B)** Xenograft tumor section presenting a lymphoma. The neoplastic is composed by monomorphic round cells, with several marginal and small nucleoli per cell and high mitotic index. Hematoxylin and eosin (H&E) stained. Magnification = 400×, scale bar = 20 μm. **(C)** Xenograft tumor section presenting the immunohistochemistry technique for B-cells, exhibiting positive staining on the cellular membrane level in virtually 100% of the tumor. Anti-CD20 antibody, Gill's hematoxylin. Magnification = 400×, scale bar = 20 μm. **(D)** Xenograft tumor section presenting the immunohistochemistry technique for T-cells, showing that the tumor cells are negative for this marker (anti-CD3, Gill's hematoxylin, 100x). Anti-CD3 antibody, Gill's hematoxylin. Magnification = 400×, scale bar = 20 μm.

important side effects of free doxorubicin, making it a viable therapeutic option (41, 42). Another pilot study conducted by Hauck et al. reported results from a phase I clinical trial in dogs with spontaneous tumors, namely sarcomas and carcinomas, using low-temperature doxorubicin-loaded liposomes. Of the 21 patients enrolled in the study, 12 presented with stable disease and six had a partial response to the treatment. This study showed favorable clinical responses, validating a novel approach of a liposome-based delivery system for veterinary use (44).

Within this context, in the present study we aimed to develop Pan-loaded folate-targeted PEGylated liposomes with improved therapeutic outcomes for the treatment of canine B-cell lymphoma. For this purpose, non-targeted and folate-targeted PEGylated liposomal formulations were prepared and their cytotoxic and targeting properties against canine diffuse large B-cell lymphoma were thoroughly investigated. While non-targeted liposomes rely on enhanced permeability and retention to deliver the therapeutic agent to the tumor site, targeted liposomes are functionalized with surface ligands to improve selective tumor targeting and facilitate intracellular uptake. Due to its overexpression in a wide range of tumors, folate receptor targeting has shown great potential in mediating the tumor uptake of a variety of drugs (45). Several studies by Gabizon et al. demonstrated significant differences between non-targeted and folate-targeted liposomes in folate receptor-overexpressing tumors, including lymphoma (46, 47). This study compared the *in vivo* distribution of folate-targeted and non-targeted liposomes and found that folate-targeted liposomes were more effective than non-targeted liposomes in a lymphoma tumor model (47). The conclusions of this study were further reinforced by Shmeeda et al., who demonstrated intracellular uptake of folate-targeted liposomes in lymphoma cells (48). In another study, Gabizon et al. proved that folate-targeted liposomes loaded with doxorubicin were more effective than the non-targeted liposomes in a lymphoma model (46). More recently, Qiu et al. demonstrated the application of this drug delivery system in NHL by using vincristine-loaded lipid-polymer hybrid liposomes (VCR-loaded LPNs). This study reported a targeted effect in the delivery of FA-VCR-loaded LPNs toward B-cell lymphoma cells, with an outstanding therapeutic effect in the treatment of lymphoma, reducing systemic toxicity (49). Considering the high efficacy of drug-loaded folate-targeted liposomes in human lymphoma, we evaluated the folate receptor expression in canine diffuse large B-cell lymphoma and confirmed its overexpression in the CLBL-1 canine lymphoma B-cell line.

Pan liposomes were prepared using an active loading method and both formulations exhibited high incorporation parameters, particularly the one containing FA (PEG-Pan-Lip EE = 56± 2 % and FA-PEG-Pan-Lip EE = 94 ± 2 %). The methodology used in the present work, active loading, means that Pan was incorporated in pre-formed unloaded liposomes (10) in opposition to a passive loading where the compound is incorporated during

liposome preparation (50). The active loading method presents several advantages over the passive methods namely stability and higher incorporation parameters as widely demonstrated in literature (51, 52). The pH or salt gradient differences between intra and extraliposomal membrane are the most known underlying mechanisms dictating the active drug loading. Moreover, active loading is based on the fact that uncharged drugs will cross the liposomal membrane and become protonated and entrapped inside the aqueous compartment of liposomes thus contributing to achieve high loadings and high stable liposomal formulations (53).

Liposomal formulations were further investigated *in vitro* to assess the suitability of their drug delivery properties. Firstly, cytotoxicity assays were performed to assess the effect of the liposomal formulations on the viability of canine diffuse large B-cell lymphoma cells. The data demonstrated that encapsulated Pan in both formulations (FA-PEG-Pan-Lip and PEG-Pan-Lip) maintained its cytotoxicity in CLBL-1 cells, when compared with Pan-free. The IC_{50} values determined for liposomal formulations were lower in comparison with Pan-free data, indicating that cytotoxic properties of the compound were not only preserved after incorporation in liposomes but potentiated. In addition, our data demonstrated that the cytotoxicity activity of the FA-PEG-Pan-Lip formulation was slightly higher than PEG-Pan-Lip formulation (FA-PEG-Pan-Lip $IC_{50} = 10.9 \pm 0.03$ nM vs. PEG-Pan-Lip $IC_{50} = 12.91 \pm 0.02$ nM). These data are in accordance with those reported in the literature, where folate is expected to enhance tumor uptake (45). Moreover, our data demonstrated that FA-PEG-Pan-Lip and PEG-Pan-Lip formulations were able to induce histone H3 acetylation in the CLBL-1 canine lymphoma cell line, the key molecular mechanism of HDACis.

HDAC inhibitors can induce multiple antitumor pathways. One of the main mechanisms of transformed cell death is the activation of apoptosis via intrinsic and extrinsic pathways (54). Activation of caspase-3 and 7 is an essential step during apoptosis and is used as a reliable marker for cells undergoing apoptosis (55). All liposomal formulations loaded with Pan at 20 nM demonstrated a high percentage of apoptotic cells and high levels of caspase-3 and 7 activation, similar to the data for the Pan-free formulation. Finally, to assess the *in vivo* stability and pharmacokinetic profile of each liposomal formulation, we performed biodistribution studies in CD1 mice and in a xenograft SCID mouse model of canine B-cell lymphoma. Biodistribution data demonstrated that FA-PEG-Pan-Lip formulation remained in circulation for a longer time, suggesting extended drug retention. In FA-PEG-Pan-Lip and PEG-Pan-Lip formulations, fast clearance from the major organs was observed, which is crucial to prevent systemic toxicity. However, a high accumulation of liposomal formulations was noted in the liver and spleen. Liposomes have specific clearance mechanisms from the bloodstream. The main mechanism is via recognition and uptake by macrophages of the reticuloendothelial system; consequently, the two main organs that present a major capacity for liposomal accumulation are the liver and the spleen (56). Thus, accumulation in the spleen and liver could be related to the elimination of liposomes. Importantly, the biodistribution data in the xenograft SCID mouse model of CLBL-1 have shown that the tumor uptake was higher with the targeted formulation (^{111}In-FA-PEG-Pan-Lip) with a percentage of 2.2% and 2.5% ID/g of tumor at 24 h and 48 h, respectively. To the best of our knowledge, this is the first study to report the use of a liposome-based drug delivery system loaded with Pan in the treatment of canine B-cell lymphoma. Overall, these results validated that folate-targeted liposomes encapsulated with Pan can be a promising drug delivery system to be explored for a more effective and safer cancer treatment modality. Although this target-liposome-based drug delivery system showed strong cytotoxicity in canine lymphoma cells, additional preclinical studies in canine B-cell lymphoma xenograft murine models are needed to evaluate its *in vivo* efficacy and safety, to then allow its further progression to clinical studies in canine patients. In conclusion, this study contributes to the development of Pan nanocarriers for the treatment of canine B-cell lymphoma as a predictive preclinical surrogate for human NHL, mutually benefiting both species and opening up perspectives in comparative oncology.

Data availability statement

The original contributions presented in the study are included in the article/supplementary material, further inquiries can be directed to the corresponding author.

Ethics statement

The animal study was approved by Animal Care and Ethical Committee of the Faculty of Veterinary Medicine. The study was conducted in accordance with the local legislation and institutional requirements.

Author contributions

AA and JD performed and analyzed the majority of the experiments and wrote the manuscript. SIA assisted with the cytotoxic assays, biodistribution studies, and reviewed the manuscript. AL and SN performed the flow cytometry experiments. JA and CR performed the apoptosis assays. MCav, VN, and MCas performed the immunofluorescence microscopy. CF, LG, and JDGC radiolabeled the liposomes and performed the biodistribution studies and reviewed the manuscript. JC performed the histopathological and immunohistochemistry analysis. MMG prepared and characterized liposomal formulations and reviewed the manuscript. LT supervised the work and reviewed the manuscript. FA-d-S was responsible for the research concept, experimental work supervision, and manuscript revision. All authors read and approved the final manuscript.

Funding

This study was funded by the Portuguese Funding Agency, Fundação para a Ciência e Tecnologia, FCT IP (SAICT/2017/32085, PTDC/QUI-OUT/3989/2021, PTDC/BTM-MAT/2472/2021, 2121.00895.CEECIND, UIDB/04138/2020, UIDP/04138/2020, and Ph.D. fellowship SFRH/BD/131468/2017 to AA) and Gilead GÉNESE PGG-050-2019. CIISA has provided

support through Project UIDB/00276/2020, funded by FCT and LA/P/0059/2020-AL4AnimalS.

Conflict of interest

The authors declare that the research was conducted in the absence of any commercial or financial relationships that could be construed as a potential conflict of interest.

Publisher's note

References

1. Sung H, Ferlay J, Siegel RL, Laversanne M, Soerjomataram I, Jemal A, et al. Global cancer statistics 2020: GLOBOCAN estimates of incidence and mortality worldwide for 36 cancers in 185 countries. *CA Cancer J Clin.* (2021) 71:209–49. doi: 10.3322/caac.21660

2. Gardner HL, Fenger JM, London CA. Dogs as a model for cancer. *Annu Rev Anim Biosci.* (2016) 4:199–222. doi: 10.1146/annurev-animal-022114-110911

3. Schiffman JD, Breen M. Comparative oncology: what dogs and other species can teach us about humans with cancer. *Philos Trans R Soc Lond, B, Biol Sci.* (2015) 370:20140231. doi: 10.1098/rstb.2014.0231

4. Bray F, Ferlay J, Soerjomataram I, Siegel RL, Torre LA, Jemal A. Global cancer statistics 2018: GLOBOCAN estimates of incidence and mortality worldwide for 36 cancers in 185 countries. *CA Cancer J Clin.* (2018) 68:394–424. doi: 10.3322/caac.21492

5. Bowzyk Al-Naeeb A, Ajithkumar T, Behan S, Hodson DJ. Non-Hodgkin lymphoma. *BMJ.* (2018) 362:k3204. doi: 10.1136/bmj.k3204

6. Ito D, Frantz AM, Modiano JF. Canine lymphoma as a comparative model for human non-Hodgkin lymphoma: recent progress and applications. *Vet Immunol and Immunopathol.* (2014) 159:192–201. doi: 10.1016/j.vetimm.2014.02.016

7. Ansell SM. Non-Hodgkin lymphoma: diagnosis and treatment. *Mayo Clin Proc.* (2015) 90:1152–63. doi: 10.1016/j.mayocp.2015.04.025

8. Aguiar SI, Dias JNR, André AS, Silva ML, Martins D, Carrapiço B, et al. Highly specific blood-brain barrier transmigrating single-domain antibodies selected by an *in vivo* phage display screening. *Pharmaceutics.* (2021) 13:1598. doi: 10.3390/pharmaceutics13101598

9. Chaudhury A, Das S. Folate receptor targeted liposomes encapsulating anti-cancer drugs. *Curr Pharm Biotechnol.* (2015) 16:333–43. doi: 10.2174/1389201016666150118135107

10. Gaspar MM, Radomska A, Gobbo OL, Bakowsky U, Radomski MW, Ehrhardt C. Targeted delivery of transferrin-conjugated liposomes to an orthotopic model of lung cancer in nude rats. *J Aerosol Med Pulm Drug Deliv.* (2012) 25:310–8. doi: 10.1089/jamp.2011.0928

11. Torchilin VP. Passive and active drug targeting: drug delivery to tumors as an example. *Handb Exp Pharmacol.* (2010) 2010:3–53. doi: 10.1007/978-3-642-00477-3_1

12. Paoloni M, Khanna C. Translation of new cancer treatments from pet dogs to humans. *Nat Rev Cancer.* (2008) 8:147–56. doi: 10.1038/nrc2273

13. Eckschlager T, Plch J, Stiborova M, Hrabeta J. Histone deacetylase inhibitors as anticancer drugs. *Int J Mol Sci.* (2017) 18:1414. doi: 10.3390/ijms18071414

14. Glozak MA, Seto E. Histone deacetylases and cancer. *Oncogene.* (2007) 26:5420–32. doi: 10.1038/sj.onc.1210610

15. Chun P. Histone deacetylase inhibitors in hematological malignancies and solid tumors. *Arch Pharm Res.* (2015) 38:933–49. doi: 10.1007/s12272-015-0571-1

16. Sermer D, Pasqualucci L, Wendel H-G, Melnick A, Younes A. Emerging epigenetic-modulating therapies in lymphoma. *Nat Rev Clin Oncol.* (2019) 16:494–507. doi: 10.1038/s41571-019-0190-8

17. Bertino EM, Otterson GA. Romidepsin: a novel histone deacetylase inhibitor for cancer. *Expert Opin Investig Drugs.* (2011) 20:1151–8. doi: 10.1517/13543784.2011.594437

18. Lee H-Z, Kwitkowski VE, Del Valle PL, Ricci MS, Saber H, Habtemariam BA, et al. FDA approval: belinostat for the treatment of patients with relapsed or refractory peripheral T-cell lymphoma. *Clin Cancer Res.* (2015) 21:2666–70. doi: 10.1158/1078-0432.CCR-14-3119

19. Mann BS, Johnson JR, Cohen MH, Justice R, Pazdur R. FDA approval summary: vorinostat for treatment of advanced primary cutaneous T-cell lymphoma. *Oncologist.* (2007) 12:1247–52. doi: 10.1634/theoncologist.12-10-1247

20. Shah RR. Safety and tolerability of histone deacetylase (HDAC) inhibitors in oncology. *Drug Saf.* (2019) 42:235–45. doi: 10.1007/s40264-018-0773-9

21. Dias JNR, Aguiar SI, Pereira DM, André AS, Gano L, Correia JDG, et al. The histone deacetylase inhibitor panobinostat is a potent antitumor agent in canine diffuse large B-cell lymphoma. *Oncotarget.* (2018) 9:28586–98. doi: 10.18632/oncotarget.25580

22. Co S, Jo P, Jm L, Aj A, Mm G, C R. Current trends in cancer nanotheranostics: metallic, polymeric, and lipid-based systems. *Pharmaceutics.* (2019) 11:22. doi: 10.3390/pharmaceutics11010022

23. De Souza C, Ma Z, Lindstrom AR, Chatterji BP. Nanomaterials as potential transporters of HDAC inhibitors. *Med Drug Discov.* (2020) 6:100040. doi: 10.1016/j.medidd.2020.100040

24. Ferreira M, Ogren M, Dias JNR, Silva M, Gil S, Tavares L, et al. Liposomes as antibiotic delivery systems: a promising nanotechnological strategy against antimicrobial resistance. *Molecules.* (2021) 26:2047. doi: 10.3390/molecules26072047

25. Luiz H, Oliveira Pinho J, Gaspar MM. Advancing medicine with lipid-based nanosystems-the successful case of liposomes. *Biomedicines.* (2023) 11:435. doi: 10.3390/biomedicines11020435

26. Bulbake U, Doppalapudi S, Kommineni N, Khan W. Liposomal formulations in clinical use: an updated review. *Pharmaceutics.* (2017) 9:12. doi: 10.3390/pharmaceutics9020012

27. Sercombe L, Veerati T, Moheimani F, Wu SY, Sood AK, Hua S. Advances and challenges of liposome assisted drug delivery. *Front Pharmacol.* (2015) 6:286. doi: 10.3389/fphar.2015.00286

28. Chaudhury A, Das S, Bunte RM, Chiu GNC. Potent therapeutic activity of folate receptor-targeted liposomal carboplatin in the localized treatment of intraperitoneally grown human ovarian tumor xenograft. *Int J Nanomedicine.* (2012) 7:739–51. doi: 10.2147/IJN.S26172

29. Gaspar MM, Boerman OC, Laverman P, Corvo ML, Storm G, Cruz MEM. Enzymosomes with surface-exposed superoxide dismutase: *in vivo* behaviour and therapeutic activity in a model of adjuvant arthritis. *J Control Rel.* (2007) 117:186–95. doi: 10.1016/j.jconrel.2006.10.018

30. Pinho JO, Amaral JD, Castro RE, Rodrigues CM, Casini A, Soveral G, et al. Copper complex nanoformulations featuring highly promising therapeutic potential in murine melanoma models. *Nanomedicine.* (2019) 14:835–50. doi: 10.2217/nnm-2018-0388

31. Rütgen BC, Hammer SE, Gerner W, Christian M, de Arespacochaga AG, Willmann M, et al. Establishment and characterization of a novel canine B-cell line derived from a spontaneously occurring diffuse large cell lymphoma. *Leuk Res.* (2010) 34:932–8. doi: 10.1016/j.leukres.2010.01.021

32. Rütgen BC, Willenbrock S, Reimann-Berg N, Walter I, Fuchs-Baumgartinger A, Wagner S, et al. Authentication of primordial characteristics of the CLBL-1 cell line prove the integrity of a canine b-cell lymphoma in a murine *in vivo* model. *PLoS ONE.* (2012) 7:e40078. doi: 10.1371/journal.pone.0040078

33. Yang F-Y, Wang H-E, Liu R-S, Teng M-C, Li J-J, Lu M, et al. Pharmacokinetic analysis of 111In-labeled liposomal doxorubicin in murine glioblastoma after blood-brain barrier disruption by focused ultrasound. *PLoS ONE.* (2012) 7:e45468. doi: 10.1371/journal.pone.0045468

34. Dias JNR, André AS, Aguiar SI, Ministro J, Oliveira J, Peleteiro MC, et al. Establishment of a bioluminescent canine B-cell lymphoma xenograft model for monitoring tumor progression and treatment response in preclinical studies. *PLoS ONE.* (2018) 13:e0208147. doi: 10.1371/journal.pone.0208147

35. Pinho JO, Matias M, Marques V, Eleutério C, Fernandes C, Gano L, et al. Preclinical validation of a new hybrid molecule loaded in liposomes for melanoma management. *Biomed Pharmacother.* (2023) 157:114021. doi: 10.1016/j.biopha.2022.114021

36. Assouline SE, Nielsen TH Yu S, Alcaide M, Chong L, MacDonald D, Tosikyan A, et al. Phase 2 study of panobinostat with or without rituximab in relapsed diffuse large B-cell lymphoma. *Blood.* (2016) 128:185–94. doi: 10.1182/blood-2016-02-699520

37. Beltrán-Gracia E, López-Camacho A, Higuera-Ciapara I, Velázquez-Fernández JB, Vallejo-Cardona AA. Nanomedicine review: clinical developments in liposomal applications. *Cancer Nanotechnol.* (2019) 10:11. doi: 10.1186/s12645-019-0055-y

38. Bozzuto G, Molinari A. Liposomes as nanomedical devices. *Int J Nanomedicine.* (2015) 10:975–99. doi: 10.2147/IJN.S68861

39. Barenholz Y. Doxil®-the first FDA-approved nano-drug: lessons learned. *J Control Release.* (2012) 160:117–34. doi: 10.1016/j.jconrel.2012.03.020

40. Liu P, Chen G, Zhang J, A. Review of liposomes as a drug delivery system: current status of approved products, regulatory environments, and future perspectives. *Molecules.* (2022) 27:1372. doi: 10.3390/molecules27041372

41. Sorenmo K, Samluk M, Clifford C, Baez J, Barrett JS, Poppenga R, et al. Clinical and pharmacokinetic characteristics of intracavitary administration of pegylated liposomal encapsulated doxorubicin in dogs with splenic hemangiosarcoma. *J Vet Intern Med.* (2007) 21:1347–54.

42. Teske E, Rutteman GR, Kirpenstein J, Hirschberger J. A randomized controlled study into the efficacy and toxicity of pegylated liposome encapsulated doxorubicin as an adjuvant therapy in dogs with splenic haemangiosarcoma. *Vet Comp Oncol.* (2011) 9:283–9. doi: 10.1111/j.1476-5829.2011.00266.x

43. Vail DM, Kravis LD, Cooley AJ, Chun R, MacEwen EG. Preclinical trial of doxorubicin entrapped in sterically stabilized liposomes in dogs with spontaneously arising malignant tumors. *Cancer Chemother Pharmacol.* (1997) 39:410–6. doi: 10.1007/s002800050591

44. Hauck ML. Phase I trial of doxorubicin-containing low temperature sensitive liposomes in spontaneous canine tumors. *Clin Cancer Res.* (2006) 12:4004–10. doi: 10.1158/1078-0432.CCR-06-0226

45. Kumar P, Huo P, Liu B. Formulation strategies for folate-targeted liposomes and their biomedical applications. *Pharmaceutics.* (2019) 11:381. doi: 10.3390/pharmaceutics11080381

46. Gabizon A, Tzemach D, Gorin J, Mak L, Amitay Y, Shmeeda H, et al. Improved therapeutic activity of folate-targeted liposomal doxorubicin in folate receptor-expressing tumor models. *Cancer Chemother Pharmacol.* (2010) 66:43–52. doi: 10.1007/s00280-009-1132-4

47. Gabizon A, Horowitz AT, Goren D, Tzemach D, Shmeeda H, Zalipsky S. *In vivo* fate of folate-targeted polyethylene-glycol liposomes in tumor-bearing mice. *Clin Cancer Res.* (2003) 9:6551–9.

48. Shmeeda H. Intracellular uptake and intracavitary targeting of folate-conjugated liposomes in a mouse lymphoma model with up-regulated folate receptors. *Mol Cancer Ther.* (2006) 5:818–24. doi: 10.1158/1535-7163.MCT-05-0543

49. Qiu L, Dong C, Kan X. Lymphoma-targeted treatment using a folic acid-decorated vincristine-loaded drug delivery system. *Drug Des Devel Ther.* (2018) 12:863–72. doi: 10.2147/DDDT.S152420

50. Gaspar MM, Calado S, Pereira J, Ferronha H, Correia I, Castro H, et al. Targeted delivery of paromomycin in murine infectious diseases through association to nano lipid systems. *Nanomedicine.* (2015) 11:1851–60. doi: 10.1016/j.nano.2015.06.008

51. Barenholz Y. (Chezy) "Doxil®–the first FDA-approved nano-drug: from an idea to a product. In: *Handbook of Harnessing Biomaterials in Nanomedicine*. Dubai: Jenny Stanford Publishing (2021)

52. Nakhaei P, Margiana R, Bokov D, Abdelbasset WK, Kouhbanani M, Varma RS, et al. Liposomes: structure, biomedical applications, and stability parameters with emphasis on cholesterol. *Front Bioeng Biotechnol.* (2021) 9:705886. doi: 10.3389/fbioe.2021.705886

53. Sur S, Fries AC, Kinzler W, Zhou S, Vogelstein B. Remote loading of preencapsulated drugs into stealth liposomes. *Proc Natl Acad Sci U S A.* (2014) 111:2283–8. doi: 10.1073/pnas.1324135111

54. Xu WS, Parmigiani RB, Marks PA. Histone deacetylase inhibitors: molecular mechanisms of action. *Oncogene.* (2007) 26:5541–52. doi: 10.1038/sj.onc.1210620

55. Shim MK, Yoon HY, Lee S, Jo MK, Park J, Kim J-H, et al. Caspase-3/-7-specific metabolic precursor for bioorthogonal tracking of tumor apoptosis. *Sci Rep.* (2017) 7:16635. doi: 10.1038/s41598-017-16653-2

56. Ait-Oudhia S, Mager D, Straubinger R. Application of pharmacokinetic and pharmacodynamic analysis to the development of liposomal formulations for oncology. *Pharmaceutics.* (2014) 6:137–74. doi: 10.3390/pharmaceutics6010137

frontiers | Frontiers in Veterinary Science

TYPE Original Research
PUBLISHED 22 September 2023
DOI 10.3389/fvets.2023.1243853

OPEN ACCESS

EDITED BY
Monica Sforna,
University of Perugia, Italy

REVIEWED BY
Aleksandra Pawlak,
Wroclaw University of Environmental and Life Sciences, Poland
Ellen Sparger,
University of California, Davis, United States

*CORRESPONDENCE
Henrik Rönnberg
✉ Henrik.Ronnberg@slu.se

†PRESENT ADDRESS
Kiran Kumar Jagarlamudi,
AroCell AB,
Stockholm, Sweden

‡These authors have contributed equally to this work

§These authors share last authorship

RECEIVED 21 June 2023
ACCEPTED 25 August 2023
PUBLISHED 22 September 2023

CITATION
Sharif H, Saellström S, Kolli B, Jagarlamudi KK, Wang L, Rönnberg H and Eriksson S (2023) A monoclonal antibody-based sandwich ELISA for measuring canine Thymidine kinase 1 protein and its role as biomarker in canine lymphoma.
Front. Vet. Sci. 10:1243853.
doi: 10.3389/fvets.2023.1243853

A monoclonal antibody-based sandwich ELISA for measuring canine Thymidine kinase 1 protein and its role as biomarker in canine lymphoma

Hanan Sharif[1,2‡], Sara Saellström[3‡], Bhavya Kolli[1], Kiran Kumar Jagarlamudi[1†], Liya Wang[2], Henrik Rönnberg[3,4*§] and Staffan Eriksson[1,2§]

[1]Alertix Veterinary Diagnostics AB, Stockholm, Sweden, [2]Department of Anatomy, Physiology, and Biochemistry, Swedish University of Agricultural Sciences, Biomedical Center, Uppsala, Sweden, [3]University Animal Hospital, Swedish University of Agricultural Sciences, Uppsala, Sweden, [4]Center of Clinical Comparative Oncology (C3O), Department of Clinical Sciences, Swedish University of Agricultural Sciences, Uppsala, Sweden

Introduction: Dogs play an important role in society, which increased during the covid epidemics. This has led to a much higher workload for the veterinarians. Therefore, there is a need for efficient diagnostic tools to identify risk of malignant diseases. Here the development of a new test that can solve some of these problems is presented. It is based on serum Thymidine Kinase 1 (TK1), which is a biomarker for cell proliferation and cell lysis.

Methods: Anti-TK1 monoclonal antibodies were produced against two different epitopes, the active site of the TK1 protein and the C-terminal region of canine TK1. The antibodies were developed with hybridoma technology and validated using dot blot, Quartz Crystal Microbalance (QCM) technology, western blots, immunoprecipitation (IP), and enzyme-linked immunosorbent assay (ELISA). Clinical evaluation of Canine TK1 ELISA was done by using sera from 131 healthy dogs and 93 dogs with lymphoma. The two selected Anti-TK1 monoclonal antibodies have Kd values in the range of 10^{-9} M and further analysis with dot and western blots confirmed the high affinity binding of these antibodies. A sandwich Canine TK1 ELISA was developed using the anti-TK1 antibodies, and TK1 concentrations in serum samples were determined using dog recombinant TK1 as a standard.

Results: Serum TK1 protein levels were significantly higher in dogs with lymphoma compared to those in healthy dogs ($p < 0.0001$). Receiver operating curve analysis showed that the canine TK1-ELISA obtain a sensitivity of 0.80, at a specificity of 0.95. Moreover, the Canine TK1 ELISA has a positive predictive value (PPV) of 97%, and the negative predictive value (NPV) of 83%, reflecting the proportion of test results that are truly positive and negative. Furthermore, Canine TK1 ELISA had significantly higher capacity to differentiate dogs with T-cell lymphoma from those with B-cell lymphoma compared to earlier used TK1 activity assays.

Discussion: These results demonstrate that the Canine TK1 ELISA can serve as an efficient tool in the diagnosis and management of dogs with lymphomas.

KEYWORDS

canine TK1 ELISA, monoclonal antibody, immunoassay, serum TK1 activity, serum TK1 concentration, canine lymphoma, blood biomarker, tumor marker

1. Introduction

The typical canine malignant lymphoma patient presents with generalized lymphadenopathy with or without other clinical signs, but far from always this is the situation in the clinic. Malignant lymphoma can be found in many anatomical locations and with varying nonspecific symptoms. Therefore, dogs are usually tested with several additional clinical diagnostic tools, including blood sampling, imaging, cytology, and several biopsies Sometimes exploratory surgery and/or endoscopy to obtain a final diagnosis is necessary. Furthermore, some of the dogs with lymphoma are generally depressed and thus not amenable for many advanced procedures. Thus, a serum biomarker can significantly help in the diagnosis as a routine procedure for canine lymphoma, and both add value in terms of increased animal welfare and avoid several often-costly diagnostic procedures. Moreover, a serum biomarker is well suited as a monitoring tool during medical therapy, where a decrease in the biomarker serum concentration reflects a positive response, and stable or increased level may lead to a change in the protocols or initiation of rescue therapy. The aim of this study was to develop a canine specific Thymidine kinase 1-ELISA, to contribute to the diagnosis of malignant lymphomas in dogs.

Thymidine kinase 1 (TK1) is a pyrimidine salvage pathway enzyme involved in DNA precursors synthesis. TK1 catalyzes the conversion of thymidine-to-thymidine monophosphate (dTMP), that undergoes further phosphorylation's and finally incorporated into DNA (1). TK1 is upregulated in the late G1 and S phases of the cell cycle and dramatically decreases at the M-phase as a result of a specific degradation pathway (2). However, TK1 activity remains elevated in the G2 and M phases in highly proliferating cells, such as in tumor cells (3). This leads to the release of TK1 protein into the blood stream originating from disrupted tumor cells (4).

TK1 activity-based assays have been used as biomarker for diagnosis and therapy monitoring of different malignancies from many decades in human medicine (5–7). Studies in dogs with hematological malignancies have demonstrated that increased serum TK1 (STK1) activity can be used to detect and monitor these types of diseases in veterinary medicine (8–12). Although the STK1 activity assays are efficient tools for prediction and therapy monitoring of canine hematologic malignancies, difficulties involved in using radio-labeled substrates and need of special equipment have so far led to a limited the use of STK1 activity-based assays.

However, design and development of peptide-based antibodies against human TK1 provided a different approach for TK1 determinations which can overcome the limitations of the activity assays (12–14). Recently, a polyclonal prototype canine TK1 ELISA was developed that could extend the clinical application of TK1 in canine oncology (14, 15). The assay could discriminate between healthy subjects and dogs with different malignancies. Critical issues associated with polyclonal antibodies such as batch-to-batch variation and long-term stability limited further extended use of this biomarker. Therefore, a monoclonal antibody-based Canine TK1 ELISA may significantly improve the clinical applications of TK1.

Here we describe the selection and characterization of monoclonal antibodies (Mabs) that show high affinity for the dog TK1 protein. Furthermore, a Canine sandwich TK1 ELISA was developed using two selected and molecularly defined anti-TK1 antibodies for the determination of canine serum TK1 protein levels. The performance of Canine TK1 ELISA was assessed by using 93 serum samples from dogs with lymphoma. In addition, the assay performance was compared with the established [^{3}H] - dThd phosphorylation assay.

2. Materials and methods

2.1. Canine anti-TK1 antibodies

The two anti-TK1 antibodies were raised against peptides from different regions of the TK1 sequence; The first antibody (Mab-1) was produced against the active site of the human enzyme, which is a conserved part of the protein in both the human and dog TK1 protein. The other antibody (Mab-2) is directed against the C-terminal of the canine TK1 sequence which has several differences in amino acid sequence as compared to human TK1 as shown in Figure 1. The mouse monoclonal antibodies were produced by GenScript (Piscataway, NJ, United States) using the selected amino acid sequence as previously described (14, 15).

2.2. Dog recombinant TK1

Different concentrations of recombinant dog TK1 were used as a standard. The recombinant dog TK1 cDNA was cloned and expressed in *E.coli* and the protein was purified by Ni-Sepharose affinity chromatography as described previously (16).

2.3. Electrochemiluminescent dot blot and western blot analysis

2.3.1. Dot blot assay

The ECL dot blot assay was carried out as described previously (12). In brief, 3 µL of recombinant TK1 from different species at varying concentrations, ranging from 20 to 1.25 ng were applied to nitrocellulose membranes (Thermo Fisher Scientific, Sweden). Membranes were blocked with non-fat dry milk 10% (AH diagnostics AB, Sweden) for 1 h and then incubated initially with the hybridoma supernatants, and subsequently with purified monoclonal antibodies overnight at 4°C. Membranes were washed and incubated with the biotinylated second antibody conjugated with horseradish peroxidase directed against mouse IgG (GE healthcare, United Kingdom) for 1 h at room temperature, followed by addition of the ECL reagent. Finally, the signal was detected and quantified by the BIORAD ChemiDoc Imaging System.

2.3.2. Western blot assay

Recombinant dog and human TK1 (10, 5 and 0.5 ng) as well as cytosolic extract from human CEM cells positive and negative for TK1 (12), containing 25 µg of protein, were diluted in the denaturing sample buffer, boiled, and loaded onto a 12% polyacrylamide gel. The gel was run in the SDS running buffer and proteins transferred to PVDF membranes (Millipore, UnitedSA) using a semi-dry slot device. The immunoblotting was carried out as described previously (12).

2.3.3. Immunoprecipitation with Dynabeads

Recombinant dog TK1 (5 ng and 2.5 ng) and diluted 10x serum samples from dogs with different malignancies were separately

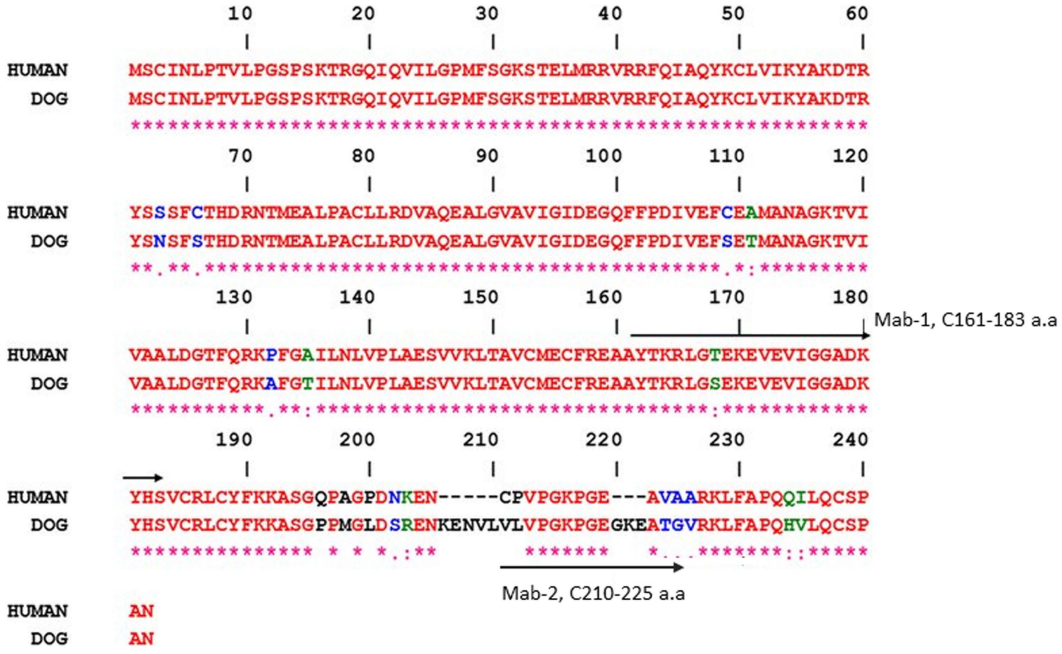

FIGURE 1
Residues that differ between the two sequences are shown in different colors. The peptide sequences that were used to produce the monoclonal antibodies are indicated by arrows, i.e., mouse monoclonal antibodies Mab-1 (161–183 a.a) and Mab-2 (210–225 a.a). Gene Bank accession numbers are XM_540461 (dog) and KO_2582 (human). The alignments were done using the ESPript program.

incubated with the supernatants from hybridoma cultures diluted 10x in the initial screening procedure and subsequently with the purified monoclonal antibodies (4 µg/mL) for 1 h at 4°C and 15 min at 23°C. Dynabeads M-280 (Dynal® sheep anti-mouse IgG, Invitrogen) was prepared according to the manufacturer's description and incubated with the antigen–antibody complexes for 1 h at 4°C. The beads and the complexes were transferred to a magnetic rack and the supernatants were then analyzed for TK1 activity. The results are presented as % of TK1 activity that bound to the magnetic beads coated with Mab-1 or Mab-2.

2.4. Determination of Ka and Kd values

The binding properties of monoclonal TK1 antibodies to recombinant dog TK1 were tested on a QCM biosensor Attana A 200 (Attana AB, Stockholm, Sweden). Recombinant dog TK1 (10, 5 and 2.5 µg/mL) was immobilized onto a LNB carboxyl chip by amine coupling using EDC and S-NHS (17). Assays were performed with a flow rate of 10 µL/mL during amine coupling and 25 µL/mL during binding measurements at 22°C, using HBS-T (10 mM HEPES, 150 mM NaCl, 0.005% Tween 20, pH = 7.4) as a running buffer. Two-fold dilutions of recombinant dog TK1 in HBS-T, were injected over the surface at 10 µL/min and the association and dissociation was monitored for 84 s and 120 s, respectively. HBS-T injection was used as a blank. Sample injections were performed by the C-Fast auto sampler (Attana AB). The binding surface was regenerated after injection by applying 100 mM HCl for 60s and 20 mM NaOH for 30s. Data was processed in the Attana attached software and curve fitting was performed using the TraceDrawer software (Ridgeview instruments). The kinetic parameters including association rate (Ka), dissociation rate (Kd) and the maximum binding capacity (Bmax) were calculated.

2.5. Serum sample and specimen handling

The study includes 93 serum samples from dogs diagnosed with lymphoma that were collected from two sources, i.e., 51 samples were purchased from the Flint Animal Cancer Center (Colorado State University) and 42 samples of lymphoma and 131 samples from healthy dogs were collected at the University Animal Hospital, at the Swedish University of Agricultural Sciences (SLU), Uppsala, Sweden, and stored at −20°C until analysis. Information about the clinical staging, grading, and typing of the lymphomas was available for subgroup identification. Data on age, breed, immunophenotype is provided in Supplementary Table 1. The data covering blood count, biochemistry panel, and urinalysis were gathered for all dogs. The dogs with tumors were naive and have not received any prior treatment for cancer.

The group of control dogs were considered healthy based on their medical history, physical examination, hematology, and a basic biochemistry analysis. Most of these subjects were recruited from voluntary blood donor dogs at the University Animal Hospital, SLU, Uppsala, Sweden. Serum samples from dogs with naive lymphoma and from healthy dogs were collected over a 4-year period (2018–2022). At least 1 mL of blood was drawn from each dog and centrifuged within 1 h of collection. The serum samples were stored at −20°C until analysis.

2.5.1. Ethics statement

This project was approved by the Swedish Animal Ethics Committee (ref. no. C12/15) and samples were used only with the owners' signed consent.

2.6. Canine TK1 ELISA

The canine TK1 ELISA was developed by using two selected monoclonal antibodies in a sandwich format. The ELISA procedure is similar to those described previously (11, 12) with slight modifications. Briefly, Mab-1 was immobilized on microtiter plates by Mercodia AB (Uppsala, Sweden) as described (14). Dog sera (60 µL) and different concentrations of recombinant TK1 ranging from 0.120 ng/mL to 2.0 ng/mL were diluted 1:1 with sample dilution buffer (SDB, Alertix AB, Sweden) with recombinant TKI dilutions serving to generate a standard curve. Both serum samples and calibrators were pre-incubated for 1 h at RT and 100 µL of these samples were added to the Mab-1 coated plates and incubated for 2 h. The plates were washed and incubated with biotin labeled Mab-2 (3 µg/mL) for 1 h at RT. The plates were then washed as described above and incubated with 100 µL streptavidin-HRP solution for 30 min (Thermo fisher Scientific, Sweden). After a final wash, the wells were incubated with 100 µL of 1-Step Ultra TMB (Thermo fisher Scientific, Sweden) and the reactions were stopped by adding 100 µL of 1 N, HCL. The absorbance was measured at 450 nm (Tecan M-200+, Switzerland) and samples were analyzed in duplicates. The TK1 protein levels in sera from lymphoma dogs and healthy dogs were determined by using the absorbance of calibrators as a standard in the 4-parameter logistic model provided by SoftMax Pro 7.1.

TK1 protein levels in serum samples were expressed as ng/mL. The canine TK1 ELISA has a limit of blank value (LOB) of 0.02 ng/mL, a limit of detection (LOD) of 0.10 ng/mL and the limit of quantification (LOQ) was 0.15 ng/mL. The cut-off value was set as 2xSD above the mean of TK1 protein levels in healthy dogs. Intra assay CVs with all non-zero calibration points were $\leq$ 10% and between-run imprecision was $\leq$15% at concentrations down to 0.12 ng/mL.

2.7. The [^{3}H]-dThd phosphorylation assay

Serum TK1 activity in all clinical samples were measured by a radiochemical assay using the DEAE filter technique as described previously (PerkinElmer, Waltham-United States) (10). In brief, the reaction mixture contained Tris–HCl pH 7.6, 10 mM; Dithiotreitol, 2 mM; $MgCl_2$, 5 mM; NaF, 5 mM; ATP, 5 mM; 5 µM [^{3}H]-dThd and 10 µL of serum sample were incubated at 37°C for 1 h. Three aliquots of the reaction mixture were applied to DEAE filter papers which were dried at ambient temperatures. Filters were then washed twice with 1 mM Ammonium Formate for 5 min and the reaction products were eluted for 45 min in 0.1 M HCl and 0.2 M KCl. Finally, the radioactivity was measured by β-scintillation liquid counting and the TK1 activity was expressed as pmol/min/mL. The cut-off value was determined as 2xSD above the mean based on TK1 activity levels in healthy dogs. The TK1 activity assay had an LOD of 0.34 pmol/min/mL and LOQ of 0.9 pmol/min/mL.

2.8. Statistical analysis

The distributions of TK1 protein and activity levels in the healthy and lymphoma groups were evaluated for normality using the D'Agostino and Pearson omnibus normality test. The Mann–Whitney U test was used to evaluate the difference between the groups. The Spearman correlation coefficient (r_s) was used to determine the correlation between TK1 protein and other TK1 determination assays. The Receiver operating characteristic (ROC) curves were constructed to evaluate the performance of the TK1 assays. All statistical analysis were performed using Graph Pad Prism 5.0.4 (Graph Pad Software, La Jolla, CA, United States) and MedCalc 17.6 (Seoul, Republic of Korea). The level of statistical significance was set $p \leq 0.05$.

3. Results

3.1. Selection and characterization of anti-dog TK1 monoclonal antibodies

The reactivity of the hybridoma supernatants and the purified monoclonal antibodies with recombinant TK1 proteins from canine, feline, equine, and human sources at varying concentrations were determined using a dot blot assay (12). Mab-1 raised against the active site of the TK1 showed binding with recombinant TK1 from all species. (Figure 2A). In contrast, Mab-2 produced against the canine C-terminal peptide sequence was only bound to dog recombinant TK1 (Figure 2B).

SDS-PAGE analysis with recombinant TK1 (canine and human) as well as human cell extracts showed a strong binding single band with Mab-1 (Figure 2C). Membrane stained with Mab-2 (2 µg/mL) showed bands with recombinant canine TK1 at varying concentrations, but no bands were observed with human TK1 in agreement with the results using the dot blot assay (Figure 2D). These results demonstrate that the two monoclonal antibodies showed strong reactivity with recombinant dog TK1.

In addition, immunoprecipitation (IP) was performed to determine the reactivity of the antibodies with serum TK1. The IP results with Mab-1 showed that approximately 95% of the recombinant canine TK1 was able to bind to the beads at varying concentrations and experimental conditions (Figure 2E). Moreover, the Mab-1 antibody showed high reactivity with the serum TK1, and 70–85% of serum TK1 was bound to the beads (Figure 2E). The IP results with Mab-2 showed that 90% of the recombinant canine TK1 was able to bind to the beads at 4°C and 23°C (Figure 2F), while 40–60% of TK1 were bound to the beads when serum samples from dogs with leukemia, lymphoma and histiocytic sarcoma were analyzed (Figure 2F). These results demonstrated that the selected monoclonal antibodies have reactivity with both recombinant and serum TK1, but to a different extent, with Mab-1 being somewhat more efficient than Mab-2. However, the detector Mab-2 provided the high specificity for dog TK1 in the sandwich ELISA.

3.2. Kinetic characterization of the monoclonal antibodies using the Attana QCM binding technique

The binding constants for the interactions between Mab-1 and Mab-2 with recombinant Canine TK1 were determined as described

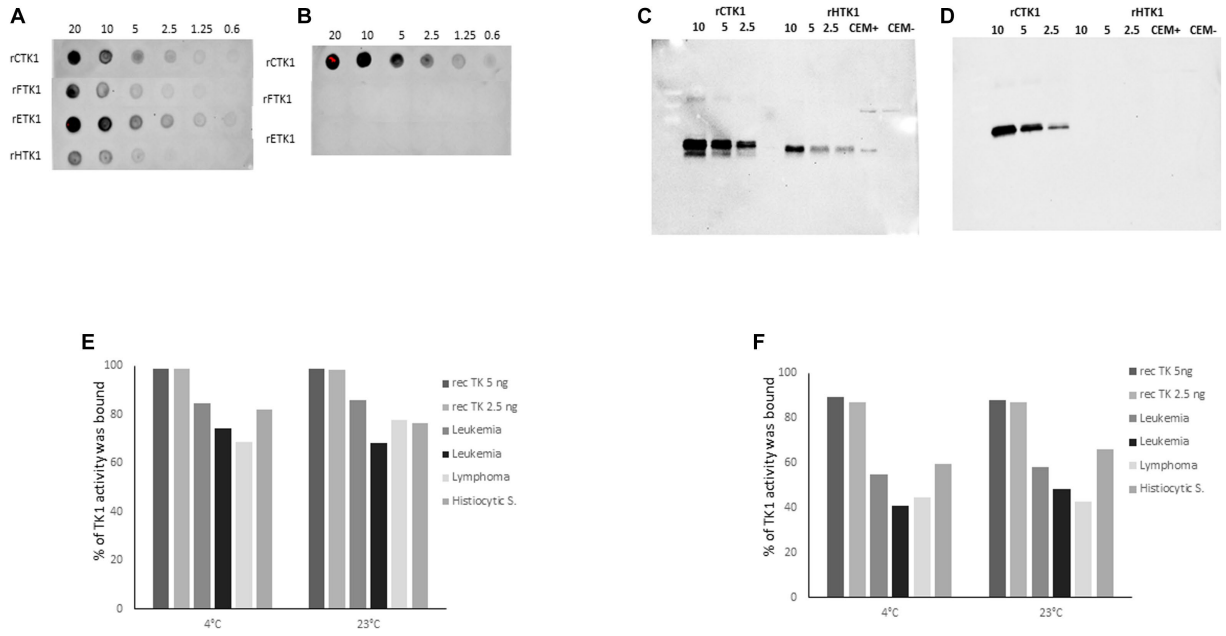

FIGURE 2
Dot blot results using recombinant enzymes from canine (rCTK1), feline (rFTK1), equine (rETK1) and human (rHTK1) at concentration ranging from 0.6–20 ng. The membranes were developed with **(A)** the monoclonal antibody produced against the active site: Mab-1 (3 µg/mL) and **(B)** the monoclonal antibody produced against the C terminal region: Mab-2 (3 µg/mL). **(C)** Western blot experiments result with 2 µg/mL of Mab-1. **(D)** Western blot results with 2 µg/mL of Mab-2. Immunoprecipitation results with recombinant canine TK1 5 and 2.5 ng and sera from dogs with different malignancies diluted 10x and incubated at 4°C and room temperature in **(E)** with 4 µg/mL of Mab-1, in **(F)** with 4 µg/mL of Mab- 2. The results are presented as the percentage of TK1 protein bound to the magnetic beads coated with anti-mouse IgG.

TABLE 1 **Results from the kinetic analysis of Mab-1 and Mab-2 using the Attana QCM binding technique.**

Monoclonal antibody	K_a (M^{-1S-1})	K_d (S^{-1})	K_D (nM)	B_{max}
Mab-1	$2.4–3.0*10^{5}$	$6.1*10^{-5}–2.3*10^{-4}$	0.3–0.75	34–50
Mab-2	$5.0–5.4*10^{5}$	$1.1–1.9*10^{-4}$	0.2–0.4	12–16

The kinetic analysis was performed individually for three replicates for canine TK1 and in this table the range between the values are presented. K_a, association rate constant; K_d, dissociation rate constant; K_D, dissociation equilibrium constant; B_{max}, binding capacity.

in the Material and Method section. The analysis showed that the association rate (Ka) of Mab-2 was about two times higher than the Mab 1 (5.1×10^5 and 2.4×10^5, respectively). However, the dissociation rate (Kd) was faster for Mab-1 than that of Mab-2. Consequently, clear interactions in the nanomolar range were observed for canine recombinant TK1 with both Mab-1 (0.5 nM) and Mab-2 (0.3 nM) (Table 1). Thus, Mab-1 and Mab-2 had sufficient binding affinities to detect canine TK1 protein in the nM range, which is clinically relevant for ELISA applications. A similar analysis with serum TK1 was not possible because of the structural complexity of serum TK1 (13).

3.3. Age distribution in dogs

The age distribution of dogs in the lymphoma group (n = 93) was 2–15 years, with a median age of 8 years, comprising 27 males, 14 females, 31 neutered males, and 21 spayed females. Whereas the age distribution in healthy dogs (n = 131) were between 1–9 years with a median of 3 years, comprising 62 males, 32 females, 19 neutered males, and 2 spayed females. Thus, the dogs in the lymphoma group were about 5 years older than the healthy subjects ($p \leq 0.0001$).

3.4. TK1 protein and TK1 activity levels in healthy dogs and dogs with lymphoma

Healthy dogs: The serum TK1 protein levels in healthy dogs were in the range of 0.10 to 0.56 ng/mL. However, 7/131 healthy were identified as outliers using the Grubbs test and these sera were excluded from the statistical analysis. After excluding the 7 dogs, the median TK1 protein of the 124 healthy dogs was 0.13 ng/mL, and the cut off value was 0.22 ng/mL.

The STK1 activity levels in healthy dogs (n = 124) were in the range of 0.4 to 3.2 pmol/min/mL (median = 1.3 pmol/min/mL) and the cut off was 2.3 pmol/min/mL.

To investigate the effect of age on the level of STK1, the healthy group was divided into two subgroups (below and above 4 years). No significant difference was observed regarding both the TK1 activity and TK1 protein levels (Supplementary Figures 1A,B). However, the dogs younger than 4 years showed slightly higher level of TK1 protein compared to dogs above 4 years, Supplementary Figure 1B. The median age of neutered male dogs was significantly higher compared to the intact males and females (Supplementary Figure 1C). Furthermore, the neutered male group showed a significantly lower

TK1 protein concentration in comparison to the intact male. Similarly, the female dogs appeared to have a higher median TK1 protein level compared to the neutered dogs, even though this did not reach statistically significance (Supplementary Figure 1D).

Dogs with lymphoma: The TK1 concentrations in the lymphoma group were in the range from 0.10 to 10.6 ng/mL (median 0.47 ng/mL), thus significantly higher compared to healthy dogs (Figure 3A). The TK1 activity levels in the healthy group were in the range of 0.50 to 62 pmol/min/mL (median was 2.8 pmol/min/mL, Figure 3B), and there was a significant difference between the healthy and lymphoma groups. ROC curve analysis showed that the Canine TK1 ELISA had an area under the curve (AUC) of 0.88, $p < 0.0001$ (95% confidence interval (CI) 0.82–0.93), with a sensitivity of 0.80 at a specificity of 0.95 (Figure 3C). Further analysis showed an expected positive predictive value (PPV) for Canine TK1 ELISA of 94% and a negative predictive value (NPV) of 80%. In comparison, the dThd phosphorylation assay had an AUC of 0.77 ($p < 0.0001$, 95% CI 0.70–0.84) with a sensitivity of 0.56 at a specificity of 0.95. The PPV for the TK1 activity assay was 96% and NPV was 74%. In addition, there was a significant difference in the AUC between Canine TK1 ELISA and dThd phosphorylation assay as shown in Figure 3C ($p = 0.0002$).

Interestingly, the Canine TK1 ELISA could differentiate T-cell and B-cell lymphoma subgroups from healthy dogs (Figure 4A). The median value of TK1 protein in T-cell lymphoma was 0.23 ng/mL, while the median value in B-cell lymphoma was 1.8 ng/mL. In contrast, the dThd phosphorylation assay could not differentiate T-cell lymphoma from healthy dogs ($p > 0.05$, Figure 4B). The median TK1 activity value in T-cell was 1.3 pmol/min/mL and in B-cell was 3.9 pmol/min/mL. The ROC curve analysis with the canine TK1 ELISA showed a significantly higher AUC compared to the dThd phosphorylation assay in the differentiation of T-cell lymphoma from B-cell lymphomas ($p = 0.028$; Figure 4C). In case of healthy dogs, a weak correlation was found between canine TK1 ELISA and dThd phosphorylation assay ($r_s = 0.34$, Figure 5A), while the correlation was significantly higher between the assays in the lymphoma group (rs = 0.9) (Figure 5B).

3.5. Comparison with the DiviTum TK1® and AroCell TK 210 ELISA® assays

A subset of serum samples from dogs with lymphoma ($n = 25$) and healthy dogs ($n = 20$) were evaluated with four different TK1 assays, two of which were based on TK1 activity measurements (DiviTum assay Biovica, Uppsala, Sweden and dThd phosphorylation assay) and two immunoassays (Canine TK1 ELISA and AroCell TK 210 ELISA, Arocell, Bromma, Sweden). Both the TK1 activity determined with DiviTum assay as well as dThd phosphorylation assay showed significantly higher levels compared to healthy controls and similar results were observed with Canine TK1 ELISA also (Supplementary Figures 2A–C). However, the ROC curve analysis demonstrates that Canine TK1 ELISA had higher

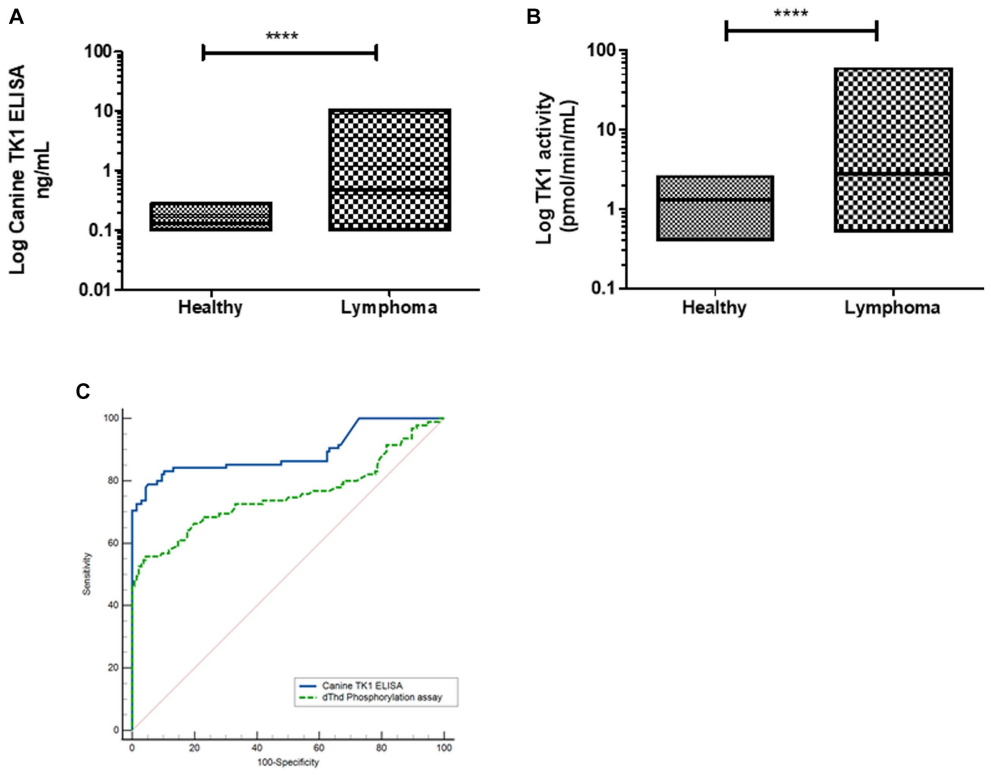

FIGURE 3
(A) Log STK1 protein concentrations measured in sera from healthy dogs ($n = 124$) and dogs with lymphoma ($n = 93$), the lines represent the median values **(B)**. The distribution of Log STK1 activity values in sera from healthy dogs ($n = 124$) and in sera from dogs with lymphoma ($n = 93$), error bars represent the median values. **(C)** Receiver operating characteristic (ROC) curves of the STK1 protein concentrations (blue line) and TK1 activity values (green line) in sera from dogs with tumors and healthy dogs.

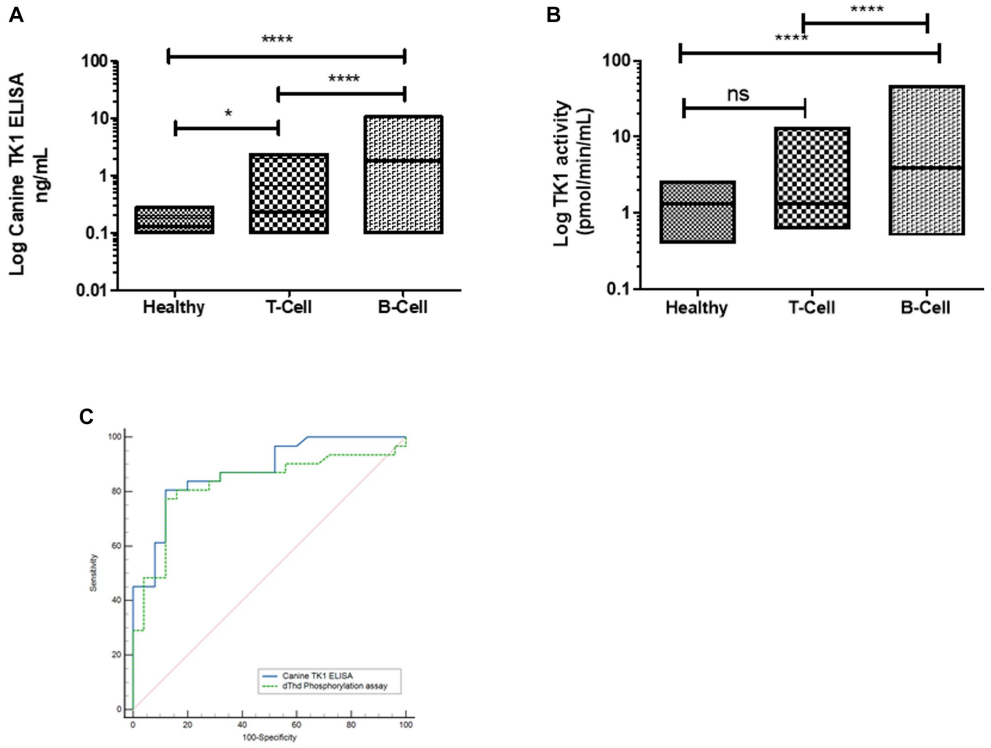

FIGURE 4
(A) Log STK1 protein concentration in sera from healthy dogs ($n = 124$), dogs with T-cell lymphoma ($n = 25$) and B-cell lymphoma ($n = 32$). **(B)** Log STK1 activity levels in healthy dogs, dogs with T-cell lymphoma and B-cell lymphoma. **(C)** ROC curves of STK1 protein values (blue line) and TK1 activity values (green line) to differentiate between dogs with T-cell lymphoma and B-cell lymphoma. * $p < 0.05$; ** $p < 0.01$; *** $p < 0.001$.

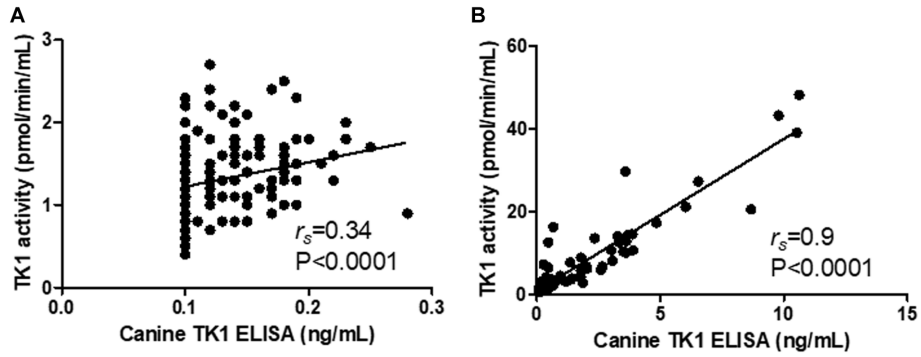

FIGURE 5
Correlation between the results with the Canine TK ELISA versus the dThd phosphorylation assay in the healthy group **(A)** the lymphoma group **(B)**.

sensitivity compared to the two activity assays in differentiating lymphoma from the healthy dog subgroups (Supplementary Figures 2D–F). The AroCell TK 210 ELISA could not detect any TK1 protein in extracts from the lymphoma or the healthy dogs. The Divitum and Arocell assays were used per manufacturers' instructions.

Furthermore, significant correlations were observed between the Canine TK1 ELISA and the DiviTum assay results ($r_s = 0.63$, $p < 0.0001$; Supplementary Figure 3A), and between the Canine TK1 ELISA and the dThd phosphorylation assay results ($r_s = 0.81$, $p = 0.0001$; Supplementary Figure 3B). This was also observed with the dThd phosphorylation assay and the DiviTum assay ($r_s = 0.7$, $p < 0.0001$; Supplementary Figure 3C) when assaying the lymphoma subgroups ($N = 25$).

4. Discussion

The gold standard of canine lymphoma diagnosis is cytology and/or biopsy of suspicious lesions. All diagnostics have a risk of false positive and false negative results and often the clinical appearance of canine lymphoma is not obvious at first presentation. Adding a serum

biomarker with high sensitivity and specificity for canine lymphoma would add significant value to the diagnostic standard procedure. Moreover, since blood sampling almost always is part of the examination of dogs with symptoms TK1-ELISA determinations may lead to less need for additional testing.

Immunophenotyping to distinguish between B- or T-cell lymphomas usually include multiple biopsies and immunohistochemistry, flow-cytometry, as well as the PARR PCR test, targeting the CDR3 region of T-cell receptor. All of these tests have different challenges and (can) vary in availability. Thus, having the possibility to discriminate between a B- versus T-cell phenotype with TK1-ELISA adds value in the clinical situation.

This is the first report of the development and application of a sandwich monoclonal TK1 ELISA with sera from healthy dogs and dogs with lymphoma. Earlier studies with a poly/monoclonal antibody-based dog TK1ELISA demonstrated similar sensitivity as the activity assay for prognosing and therapy monitoring of hematological malignancies (14). However, there were problems with the reactivity of polyclonal antibodies such as batch-to batch variation and stability. To avoid this, a monoclonal antibody-based ELISA that could improve the production and clinical applicability of a TK1 assay in routine diagnostics was designed and validated. In the present study we described the development and initial clinical evaluation of monoclonal antibody-based sandwich canine TK1 ELISA. This assay uses antibodies that recognize different epitopes on the TK1 protein which increase its sensitivity as well as specificity. Furthermore, it allows adaptation to clinically used automated platforms. The antibody characterization showed that antibodies raised against the C-terminal of TK1 leads to canine specificity with no cross reactivity with TK1 from other species.

Serum TK1 is a biomarker that reflects accelerated cell proliferation and cell lysis both in normal and tumor cells. The STK1 activity levels have been found to be up regulated in dogs with different malignancies but are often very low or undetectable in healthy dogs (9–11). In the present study, about 20% of healthy dogs showed TK1 protein concentration lower than the detection limit.

Development of a specific routine assay for TK1 ELISA may improve health screening tests for older dogs and lead to early detection of malignant diseases (11). However, a transient increase of STK1 have been detected in several infectious and inflammatory diseases (8, 18). Therefore, when evaluating elevated levels of TK1 as a risk factor for malignancies, markers specific for inflammatory conditions could increase the diagnostic accuracy (15, 19, 20).

This study also showed that the Canine TK1 ELISA was able to aid in the differentiation between the T-cell and B-cell within the lymphoma group, which is of large clinical importance for the type of treatment and prognosis of dogs with malignant lymphoma. Furthermore, the capacity of this assay in monitoring treatments in most lymphoma cases is a major advantage since it may ensure that the side effects and costs are motivated. This as, high grade T-cell lymphomas normally imply a worse prognosis and moreover often suggest using other drugs and protocol complimentary to the standard CHOP mostly used in B-cell lymphoma (21). Finally, the T-cell phenotype are often associated with a larger degree of drug resistance (21). Yet to be proven is if the magnitude of serum TK1 concentration determined by this Canine TK1 ELISA upon initial presentation of the patient can be prognostic. This has been reported in humans for TK1 in both breast cancer and NHL and would add value for the individual dog (owner) as well as the treating veterinarian (22, 23).

Future other possible applications of TK1 could be to address level of tissue trauma or amount of hypoxia in intensive care cases, then reflecting TK1 leakages from normal cells.

The results specifically presented here demonstrate that the monoclonal canine TK1 ELISA may serve as an efficient tool to estimate the increased cell proliferation responsible for the aggressiveness and type of canine lymphoma, which can aid cancer management in veterinary medicine.

Data availability statement

The original contributions presented in the study are included in the article/supplementary material, further inquiries can be directed to the corresponding author.

Ethics statement

The animal studies were approved by the Swedish Animal Ethics Committee (ref. no. C12/15) and samples were used only with the owners' signed consent. The studies were conducted in accordance with the local legislation and institutional requirements. Written informed consent was obtained from the owners for the participation of their animals in this study.

Author contributions

HR, HS, SS, BK, KJ, LW, and SE substantially contributed to the design of the work as well as interpretation of data for the work, revising it critically for important intellectual content, provided approval for publication of the content and agreed to be accountable for all aspects of the work in ensuring that questions related to the accuracy or integrity of any part of the work are appropriately investigated and resolved. HS drafted the manuscript. SS sampled, provided, clinically phenotyped, and treated the majority of the included samples in the study. All authors contributed to the article and approved the submitted version.

Funding

This study was supported by funds from the Swedish Research Council (SE), the Swedish University of Agricultural Sciences future platform SLU Future animals, nature, and health (SS and HR) and the Johansson Family Swedish Boxer Club Cancer Donation (SS and HR). Some minor funding from Alertix Veterinary Diagnostic AB to support the completion of the experiments has been obtained. The funders were not involved in the study design, collection, analysis, interpretation of data, the writing of this article or the decision to submit it for publication.

Acknowledgments

The authors would like to thank our collaborators who provided the samples from dogs with different tumors, The SLU biobank coordinator Susanne Gustafsson (Uppsala, Sweden) and Flint Animal Cancer Center Biobank (Colorado State University, United States). The human rTK1 (rHTK1), feline rTK1 (rFTK1), and equine rTK1 (rETK1) proteins were cloned and provided according to (16) by the co-author of this article LW.

Conflict of interest

HS, BK, and SE, were employed by Alertix Veterinary Diagnostics AB. KJ was employed by AroCell AB. SE is a co-inventor of a TK1 activity patent licensed to DiaSorin Inc. (and several patents owned by AroCell AB). He is a co-founder, shareholder, and consultant to the company AroCell AB, Uppsala. There is a U.S. patent pending for the antibodies and assay procedures described in this manuscript: Determination of Non-Human Mammal TK1 protein levels, with KJ, HR, and SE as inventors. HR is member of the scientific advisory board and shareholder of Alertix. This does not alter the authors' adherence to all the Frontiers Journal's policies on sharing data and materials.

The remaining authors declare that the research was conducted in the absence of any commercial or financial relationships that could be construed as a potential conflict of interest.

Publisher's note

All claims expressed in this article are solely those of the authors and do not necessarily represent those of their affiliated organizations, or those of the publisher, the editors and the reviewers. Any product that may be evaluated in this article, or claim that may be made by its manufacturer, is not guaranteed or endorsed by the publisher.

Supplementary material

The Supplementary material for this article can be found online at: https://www.frontiersin.org/articles/10.3389/fvets.2023.1243853/full#supplementary-material

References

1. Eriksson S, Munch-Petersen B, Johansson K, Eklund H. Structure and function of cellular deoxyribonucleoside kinases. *Cell Mol Life Sci*. (2002) 59:1327–46. doi: 10.1007/s00018-002-8511-x

2. Ke PY, Chang ZF. Mitotic degradation of human thymidine kinase 1 is dependent on the anaphase-promoting complex/cyclosome-Cdh1-mediated pathway. *Mol Cell Biol*. (2004) 24:514–6. doi: 10.1128/MCB.24.2.514-526.2004

3. Chang ZF, Huang DY. The regulation of thymidine kinase in HL-60 human promyeloleukemia cells. *J Biol Chem*. (1993) 268:1266–71. doi: 10.1016/S0021-9258(18)54069-2

4. Jagarlamudi KK, Shaw M. Thymidine kinase 1 as a tumor biomarker: technical advances offer new potential to an old biomarker. *Biomark Med*. (2018) 12:1035–48. doi: 10.2217/bmm-2018-0157

5. Ohrvik A, Lindh M, Einarsson R, Grassi J, Eriksson S. Sensitive nonradiometric method for determining thymidine kinase 1 activity. *Clin Chem*. (2004) 50:1597–06. doi: 10.1373/clinchem.2003.030379

6. Gronowitz JS, Kallander FR, Diderholm H, Hagberg H, Pettersson U. Application of an in vitro assay for serum thymidine kinase: results on viral disease and malignancies in humans. *Int J Cancer*. (1984) 33:5–12. doi: 10.1002/ijc.2910330103

7. Nisman B, Allweis T, Kadouri L, Mali B, Hamburger T, Baras M, et al. Comparison of diagnostic and prognostic performance of two assays measuring thymidine kinase 1 activity in serum of breast cancer patients. *Clin Chem Lab Med*. (2013) 51:439–7. doi: 10.1515/cclm-2012-0162

8. Nakamura N, Momoi Y, Watari T, Yoshino T, Tsujimoto H, Hasegawa A. Plasma thymidine kinase activity in dogs with lymphoma and leukemia. *J Vet Med Sci*. (1997) 59:957–0. doi: 10.1292/jvms.59.957

9. von Euler H, Einarsson R, Olsson U, Lagerstedt AS, Eriksson S. Serum thymidine kinase activity in dogs with malignant lymphoma: a potent marker for prognosis and monitoring the disease. *J Vet Intern Med*. (2004) 18:696–2. doi: 10.1111/j.1939-1676.2004.tb02608.x

10. Sharif H, von Euler H, Westberg S, He E, Wang L, Eriksson S. A sensitive and kinetically defined radiochemical assay for canine and human serum thymidine kinase 1 (TK1) to monitor canine malignant lymphoma. *Vet J*. (2012) 194:40–7. doi: 10.1016/j.tvjl.2012.03.006

11. von Euler HP, Ohrvik AB, Eriksson SK. A non-radiometric method for measuring serum thymidine kinase activity in malignant lymphoma in dogs. *Res Vet Sci*. (2006) 80:17–24. doi: 10.1016/j.rvsc.2005.05.001

12. Wu C, Yang R, Zhou J, Bao S, Zou L, Zhang P, et al. Production and characterisation of a novel chicken IgY antibody raised against C-terminal peptide from human thymidine kinase 1. *J Immunol Methods*. (2003) 277:157–9. doi: 10.1016/S0022-1759(03)00062-0

13. Jagarlamudi KK, Westberg S, Ronnberg H, Eriksson S. Properties of cellular and serum forms of thymidine kinase 1 (TK1) in dogs with acute lymphocytic leukemia (ALL) and canine mammary tumors (CMTs): implications for TK1 as a proliferation biomarker. Bmc. *Vet Res*. (2014) 10:10. doi: 10.1186/s12917-014-0228-1

14. Jagarlamudi KK, Moreau L, Westberg S, Ronnberg H, Eriksson S. A new Sandwich ELISA for quantification of thymidine kinase 1 protein levels in sera from dogs with different malignancies can aid in disease management. *PLoS One*. (2015) 10:e0137871. doi: 10.1371/journal.pone.0137871

15. Saellstrom S, Sharif H, Jagarlamudi KK, Ronnberg H, Wang L, Eriksson S. Serum TK1 protein and C-reactive protein correlate to treatment response and predict survival in dogs with hematologic malignancies. *Res Vet Sci*. (2022) 145:213–1. doi: 10.1016/j.rvsc.2022.02.019

16. Wang L, Munch-Petersen B, Herrstrom Sjoberg A, Hellman U, Bergman T, Jornvall H, et al. Human thymidine kinase 2: molecular cloning and characterisation of the enzyme activity with antiviral and cytostatic nucleoside substrates. *FEBS Lett*. (1999) 443:170–4. doi: 10.1016/S0014-5793(98)01711-6

17. Peiris D, Spector AF, Lomax-Browne H, Azimi T, Ramesh B, Loizidou M, et al. Cellular glycosylation affects Herceptin binding and sensitivity of breast cancer cells to doxorubicin and growth factors. *Sci Rep*. (2017) 7:43006. doi: 10.1038/srep43006

18. Sharif H, Hagman R, Wang L, Eriksson S. Elevation of serum thymidine kinase 1 in a bacterial infection: canine pyometra. *Theriogenology*. (2013) 79:17–23. doi: 10.1016/j.theriogenology.2012.09.002

19. Selting KA, Sharp CR, Ringold R, Knouse J. Serum thymidine kinase 1 and C-reactive protein as biomarkers for screening clinically healthy dogs for occult disease. *Vet Comp Oncol*. (2015) 13:373–4. doi: 10.1111/vco.12052

20. Selting KA, Ringold R, Husbands B, Pithua PO. Thymidine kinase type 1 and C-reactive protein concentrations in dogs with spontaneously occurring Cancer. *J Vet Intern Med*. (2016) 30:1159–66. doi: 10.1111/jvim.13954

21. Zandvliet M. Canine lymphoma: a review. *Vet Q*. (2016) 36:76–4. doi: 10.1080/01652176.2016.1152633

22. Gatt ME, Goldschmidt N, Friedman M, Kalichman I, Anne Charlotte A, Barak V. Thymidine kinase levels correlate with prognosis in high grade lymphoma, and can discriminate patients with a clinical suspicion of low grade to high grade transformation. *Anticancer Res*. (2015) 35:3019–26.

23. Matikas A, Wang K, Lagoudaki E, Acs B, Zerdes I, et al. Prognostic role of serum thymidine kinase 1 kinetics during neoadjuvant chemotherapy for early breast cancer. *ESMO Open*. (2021) 6:100076–9. doi: 10.1016/j.esmoop.2021.100076

frontiers | Frontiers in Veterinary Science

TYPE Original Research
PUBLISHED 03 November 2023
DOI 10.3389/fvets.2023.1225764

OPEN ACCESS

EDITED BY
Jorge Del Pozo,
University of Edinburgh, United Kingdom

REVIEWED BY
Carlos Eduardo Fonseca-Alves,
Paulista University, Brazil
Vittoria Castiglioni,
IDEXX Laboratories (Germany), Germany

*CORRESPONDENCE
Jillian M. Richmond
✉ jillian.richmond@umassmed.edu
Ramón M. Almela
✉ ramon.almela@tufts.edu

†PRESENT ADDRESSES
Jadesola Temitope Olayinka,
NYU Department of Dermatology,
New York, NY, United States
Nicholas A. Robinson,
Alnylam, Cambridge, MA, United States

RECEIVED 19 May 2023
ACCEPTED 18 October 2023
PUBLISHED 03 November 2023

CITATION
Olayinka JT, Nagarkar A, Ma DJ, Wong NB, Romasco A, Piedra-Mora C, Wrijil L, David CN, Gardner HL, Robinson NA, Hughes KL, Barton B, London CA, Almela RM and Richmond JM (2023) Cathepsin W, T-cell receptor-associated transmembrane adapter 1, lymphotactin and killer cell lectin like receptor K1 are sensitive and specific RNA biomarkers of canine epitheliotropic lymphoma. *Front. Vet. Sci.* 10:1225764. doi: 10.3389/fvets.2023.1225764

Cathepsin W, T-cell receptor-associated transmembrane adapter 1, lymphotactin and killer cell lectin like receptor K1 are sensitive and specific RNA biomarkers of canine epitheliotropic lymphoma

Jadesola Temitope Olayinka[1,2†], Akanksha Nagarkar[1], Diana Junyue Ma[1], Neil B. Wong[1], Andrew Romasco[1], Cesar Piedra-Mora[3], Linda Wrijil[3], Clement N. David[4], Heather L. Gardner[5], Nicholas A. Robinson[3†], Kelly L. Hughes[6], Bruce Barton[7], Cheryl A. London[5], Ramón M. Almela[5*] and Jillian M. Richmond[1*]

[1]Department of Dermatology, UMass Chan Medical School, Worcester, MA, United States, [2]SUNY Downstate School of Medicine, New York, NY, United States, [3]Pathology Department, Tufts Cummings School of Veterinary Medicine, North Grafton, MA, United States, [4]Nanostring Technologies, Seattle, WA, United States, [5]Department of Clinical Sciences, Tufts Cummings School of Veterinary Medicine, North Grafton, MA, United States, [6]Department of Microbiology, Immunology and Pathology, Colorado State University Veterinary Diagnostic Laboratory, Fort Collins, CO, United States, [7]Department of Population and Quantitative Health Sciences, UMass Chan Medical School, Worcester, MA, United States

Cutaneous T-cell lymphoma (CTCL) is an uncommon type of lymphoma involving malignant skin-resident or skin-homing T cells. Canine epitheliotropic lymphoma (EL) is the most common form of CTCL in dogs, and it also spontaneously arises from T lymphocytes in the mucosa and skin. Clinically, it can be difficult to distinguish early-stage CTCLs apart from other forms of benign interface dermatitis (ID) in both dogs and people. Our objective was to identify novel biomarkers that can distinguish EL from other forms of ID, and perform comparative transcriptomics of human CTCL and canine EL. Here, we present a retrospective gene expression study that employed archival tissue from biorepositories. We analyzed a discovery cohort of 6 canines and a validation cohort of 8 canines with EL which occurred spontaneously in client-owned companion dogs. We performed comparative targeted transcriptomics studies using NanoString to assess 160 genes from lesional skin biopsies from the discovery cohort and 800 genes from the validation cohort to identify any significant differences that may reflect oncogenesis and immunopathogenesis. We further sought to determine if gene expression in EL and CTCL are conserved across humans and canines by comparing our data to previously published human datasets. Similar chemokine profiles were observed in dog EL and human CTCL, and analyses were performed to validate potential biomarkers and drivers of disease. In dogs, we found enrichment of T cell gene signatures, with upregulation of *IFNG*, *TNF*, *PRF1*, *IL15*, *CD244*, *CXCL10*, and *CCL5* in EL in dogs compared to healthy controls. Importantly, *CTSW*, *TRAT1* and *KLRK1* distinguished EL from all other forms of interface dermatitis we studied, providing much-needed biomarkers for the veterinary field. *XCL1*/*XCL2* were also highly

specific of EL in our validation cohort. Future studies exploring the oncogenesis of spontaneous lymphomas in companion animals will expand our understanding of these disorders. Biomarkers may be useful for predicting disease prognosis and treatment responses. We plan to use our data to inform future development of targeted therapies, as well as for repurposing drugs for both veterinary and human medicine.

KEYWORDS

cutaneous T cell lymphoma (CTCL), epitheliotropic lymphoma (EL), interface dermatitis (ID), dog (canine), cathepsin W (CTSW), T cell receptor associated transmembrane adaptor 1 (TRAT1), killer cell lectin like receptor K1 (KLRK1), lymphotactin/XCL1/XCL2

Background

Cutaneous T cell lymphomas (CTCL) are a heterogenous group of non-Hodgkin's lymphomas characterized by the proliferation of neoplastic T-lymphocytes in the skin (1). The most common subtype in humans is mycosis fungoides (MF), which is known for its progression of three stages: patches, plaques, and tumors of which their mushroom-like appearance inspires the name (2). CTCLs often present with patches, plaques, ulcerations, or other skin rashes, and can evolve into cutaneous tumors and/or progress to visceral involvement. In the United States, the overall annual age-adjusted incidence of CTCL was 6.4 per million persons over the time period of 1973 to 2002, with an annual incidence increase of 2.9×10^{-6} (3). The incidence is greater in males than in females, and in Black people than in White people (3).

Dogs also develop cutaneous lymphomas, including T and B cell lymphomas (4–6). In canine cutaneous epitheliotropic lymphoma (EL), neoplastic lymphocytes infiltrate the skin and mucosa (7). Canine epitheliotropic T cell lymphoma (T-EL) has different subtypes when described with the same standards as humans, including MF, Sézary syndrome, and pagetoid reticulosis (8). The disease progression in both human CTCL and canine T-EL are very similar, and usually involve progression from patch stage to plaque stage to tumor stage. Clinical presentations of both diseases involve exfoliative erythroderma, ulceration, depigmentation, plaques, and nodules, and both diseases are difficult to diagnose in earlier stages due to similar clinical presentation to inflammatory or benign processes (6). While $CD4^+$ helper T-cells predominantly drive disease in human CTCL, canine T-EL is predominantly a disease of $CD8^+$ cytotoxic T-cells (8).

One challenge in the veterinary field that remains is distinguishing early-stage EL in dogs from other immune-mediated interface dermatitis conditions (6). Both clinical and histopathological features of early-stage EL can be mistaken for atopy or other immune-mediated processes (7, 9). A reliable biomarker to differentiate EL from other interface diseases would enable initiation of treatment at earlier stages of disease. A recently published study examined transcriptional differences between canine EL and immune-mediated dermatoses using RNA sequencing (10). Here, we employ microarray technology and demonstrate that *CTSW*, *TRAT1*, *KLRK1* and *XCL1/2* probes may be used to distinguish EL from other forms of interface dermatitis in dogs. Further, comparative immunology approaches to assess the gene expression patterns of canine EL to human CTCL revealed shared signatures, indicating that these may also serve as biomarkers of some forms of human CTCL. This may be particularly important to distinguish CTCL from clinical mimickers, thereby preventing misdiagnosis in both veterinary and human patients.

Abbreviations: CTCL, Cutaneous T cell lymphoma; DEGs, Differentially expressed genes; EL, Epitheliotropic lymphoma; FFPE, Formalin fixed paraffin embedded; ID, Interface dermatitis; MF, Mycosis fungoides.

Methods

Study design

The goals of this study were to: (1) define the transcriptome of EL using RNA isolated from diagnostic archival tissue biopsies using NanoString and (2) determine whether gene biomarkers can be used to distinguish EL from ID.

Clinical samples

Skin biopsies from the biorepository at Tufts Cummings School were selected based on pathology reports. H&E sections were reexamined by a board-certified veterinary pathologist to confirm diagnoses and absence of obvious infectious disease, and clinical notes were reexamined by a board-certified veterinary dermatologist. Healthy control skin samples were obtained from leg margin biopsies from amputations. For the discovery cohort, six epitheliotropic lymphoma samples were obtained from shave and/or punch biopsies of dogs as noted in the case presentation section. Samples were obtained as part of routine medical care under the guidance of a veterinarian at the Foster Hospital for Small Animals at Cummings School of Veterinary Medicine, spanning the years 2011–2019. For the validation cohort, eight EL samples were obtained from the Colorado State University Veterinary Diagnostic Laboratory, seven of which yielded enough RNA for downstream analyses. Cases were reviewed by a board-certified veterinary pathologist to confirm diagnosis.

Isolation of RNA from FFPE blocks

Thirty μm curls were cut from FFPE blocks and stored in Eppendorf tubes at ambient temperature. RNA was isolated using the

Qiagen FFPE RNeasy kit per the manufacturer directions. Briefly, razor blades were treated with RNase, excess paraffin was removed, and tissues were sliced into thin strips (5 µm) to create more surface area prior to incubation with deparaffinization solution (Qiagen). The manufacturer protocol was followed and RNA was quantified using a Nanodrop spectrophotometer (Fisher Scientific).

Nanostring cartridge and processing

A custom designed Nanostring canine gene panel of 160 genes including cytokine, chemokine, and immune genes, as well as skin and immune cell specific transcripts was created as previously described (11). We used *B2M*, *RPL13A*, *CCZ1* and *HPRT* as housekeeping genes for this study. For the validation cohort, the NanoString canine immune-oncology (IO) panel was used. RNA (150 ng/assay) was hybridized for 18 h using a BioRad C1000 touch thermal cycler, and samples were loaded into Nanostring cartridges and analyzed with a Sprint machine according to manufacturer's instructions. Gene expression data are deposited on GEO under Accession # GSE213087.

nSolver analysis

NanoString's software, nSolver was used for all NanoString analysis. Raw counts were plotted with GraphPad Prism. Advanced analysis was used for the "cell type score," which is a summary statistic of the expression of the marker genes for each cell type. It is the geometric mean of the log2-transformed normalized counts for each set of marker genes. NanoString validated these cell Type Scores against FACS and IHC (12).

IHC

IHC was performed on 5 µm sections using rabbit-anti-human/mouse/rat CD244 (catalog #521141; US Biological), rabbit-anti-canine/human CTSK/CTSO/CTSX/CTSO2 (catalog # 139662; US Biological) or isotype control (Biolegend catalog # 910801) at 1:100 dilution using a Dako automated slide staining machine. Briefly, antigen retrieval was performed using Retrievagen A (pH 6.0; BD Pharmingen) in the microwave set to high setting twice for 10 min. Primary antibodies were incubated at room temperature for 60 min. The DAKO Duel link system (code K4065) was used for secondary antibody staining for 45 min at room temperature per the manufacturer's protocol. All sections were counterstained with hematoxylin. H&E images were taken using an Olympus BX51 microscope with Nikon NIS Elements software version 3.10, and IHC images were taken using an Olympus BX40 microscope with cellSens Entry software version 1.14.

qPCR

cDNA synthesis was performed on RNA extracted from FFPE or frozen lymphoma samples using BioRad iScript cDNA synthesis kit per manufacturer instructions. qPCR for *CTSW* or *GAPDH* housekeeping gene was performed with technical duplicates on 3 biologic samples per condition using iTaq universal SYBR green supermix per the manufacturer's protocols on either a QuantStudio (Applied Biosystems) or BioRad CFX96 machine. Relative copy numbers were calculated using the formula in Excel "=(10^((Ct value $_{CTSW}$ − 40)/−3.32)))/(10^((Ct value $_{\text{Average GAPDH}}$ − 40)/−3.32)))."

Comparison to human CTCL

The human CTCL dataset from Nielsen et al. (13) (GSE143382; https://www.ncbi.nlm.nih.gov/geo/query/acc.cgi?acc=GSE143382) was analyzed using Geo2R. Gene lists were truncated in Microsoft Excel using the formula "=IF(ISERROR(VLOOKUP(cell,reference,1, FALSE)),FALSE,TRUE)" and shared DEGs between human and canine were analyzed with BioVenn (14).

Statistics

Differentially expressed genes (DEGs) were analyzed using Rosalind software and/or nSolver software. We also analyzed raw and/or normalized counts between groups using nSolver and GraphPad Prism software version 9 to examine potential differences in previously identified genes pertinent to EL and CTCL pathogenesis. Normality tests were performed in GraphPad Prism. Normally distributed data were analyzed using student's *t*-test and non-normally distributed data were analyzed using Mann–Whitney *U* test. Receiver operator characteristic (ROC) curves were calculated in GraphPad Prism. Multi-ROC curves were calculated by a biostatistician in SPSS. A statistically significant difference was considered as $p < 0.05$.

Results

Canine EL exhibits differentially expressed immune and skin genes compared to healthy controls

Canine EL can present with different features including depigmentation, crusting, erythema, ulceration and/or alopecia (Figure 1). We analyzed residual tissue blocks from diagnostic biopsies to assess gene expression (Figure 2A; Table 1). Using the NanoString nCounter platform, which is optimized for FFPE RNA analysis, we performed targeted transcriptomics studies on 160 custom curated genes from lesional skin biopsies from 6 canine EL cases and 5 healthy canine cases. Our NanoString probeset targets included cytokine, chemokine, and immune related genes, as well as skin associated genes and neuroendocrine genes. Advanced cell type analysis revealed cytotoxic T cells were significantly abundant ($p = 0.0001$; not shown). Comparing the EL samples to healthy margins revealed 32 upregulated DEGs and 7 down regulated differentially expressed genes (DEGs) with $p_{adj} < 0.01$ (Figures 2B,C). An array of genes involved in cytotoxic processes were all upregulated, including *GZMA*, *KLRB1*, *KLRD1*, *KLRK1*, and *PRF1*. *CPA3*, which is involved in proteolysis and degradation of endogenous proteins, was upregulated in EL lesions. Principal component analysis revealed that EL cases could be readily distinguished from healthy controls in 95% confidence intervals, with the exception of one early relapse case which fell in between the EL and healthy skin gene signatures (Figure 2D).

FIGURE 1
Clinical presentations of epitheliotropic lymphoma in dogs. **(A)** Widely disseminated lesions with hair loss associated with severe scale-crusting. **(B)** Erythematous alopecia patch and hyperkeratotic plaque lesions on the dorsum. **(C)** Mild crusting with depigmentation, loss of nose cobblestone appearance and erythema on the muzzle. (**D**) Alopecia, erythema and crusting on the nasal planum and **(E)** hind legs. **(F)** Depigmentation, loss of nose cobblestone appearance and erythema on the muzzle, which can be mistaken for other immune-mediated processes. **(G)** Footpad involvement with crusting and ulcerations. **(H)** Multifocal lesions with erythema and crusting and without notable hair loss. Please note that breed is not associated with a particular presentation of the disease.

Gene biomarkers can distinguish EL from other interface dermatitis conditions

Next, we compared EL gene expression to other forms of interface dermatitis (ID) including lupus erythematosus, pemphigus subtypes, and erythema multiforme spectrum conditions. Seventeen genes were significantly downregulated and 14 were significantly upregulated with p_{adj} <0.05 (Figures 3A,B). To evaluate whether any of these DEGs could serve as potential diagnostic biomarkers for EL, we analyzed RNA counts of the highest DEGs singly (Figure 3C). Of these, *CTSW* exhibited no overlap between cases and cleanly distinguished EL from other potential clinical mimickers. Receiver operator characteristic (ROC) curves of *CTSW* was 100% sensitive and specific for counts >1,092 (Figure 3D). *TRAT1* and *KLRK1* were also highly significant ($p < 0.0001$), and ROC analysis revealed 83.3% sensitivity and 96.77% specificity for *TRAT1* counts >213, and 100% sensitivity and 96.77% specificity for *KLRK1* counts >292.5.

To confirm this finding, we performed analysis on a validation cohort of 6 EL and 9 interface dermatitis (ID) samples using the NanoString canine IO panel (Figures 4A,B; Supplementary Table S1). *CTSW* exhibited 100% sensitivity and 88.9% specificity to distinguish the two conditions at a count >121.8 (Figures 4C,D). *TRAT1* exhibited 88.89% sensitivity and 83.33% specificity to distinguish EL from ID at a count >59.7. *KLRK1* was 100% sensitive and specific at counts >346.9. The difference in absolute counts between the discovery cohort and the validation cohort is likely due to the 2 different gene panels used (160 custom gene codeset versus canine IO ~800 gene codeset). We noted that an additional biomarker was identified by the canine IO panel: lymphotactin also called *XCL1*/*XCL2*, though we were unable to verify this gene in our discovery cohort because it was not included in the 160 gene codeset. Last, we examined whether combining biomarkers could more accurately identify EL compared to each gene alone. Multi-biomarker ROC analysis revealed that combining *CTSW*, *TRAT1* and *KLRK1* is highly sensitive and specific for identifying EL as compared to other forms of ID (Figure 4E).

Comparative analysis of canine EL and human CTCL reveals shared inflammatory and immunoregulatory gene expression signatures

We also compared our EL findings to a previously published human CTCL dataset [Human Dataset GSE143382 (13)]. We focused on the DEGs between early MF and ID (Figure 5A). First, we truncated the datasets to a common denominator gene list of 327 based on the NanoString panels (canine IO and human Myeloid v2). Next, we compared which of these genes were significantly differentially expressed ($p < 0.05$), identifying 87 overlapping DEGs (Figure 5B). We examined specific genes identified in our DEG overlap as well as other published genes of interest and found similar expression trends in human and canine datasets (Figure 5C). We examined whether the

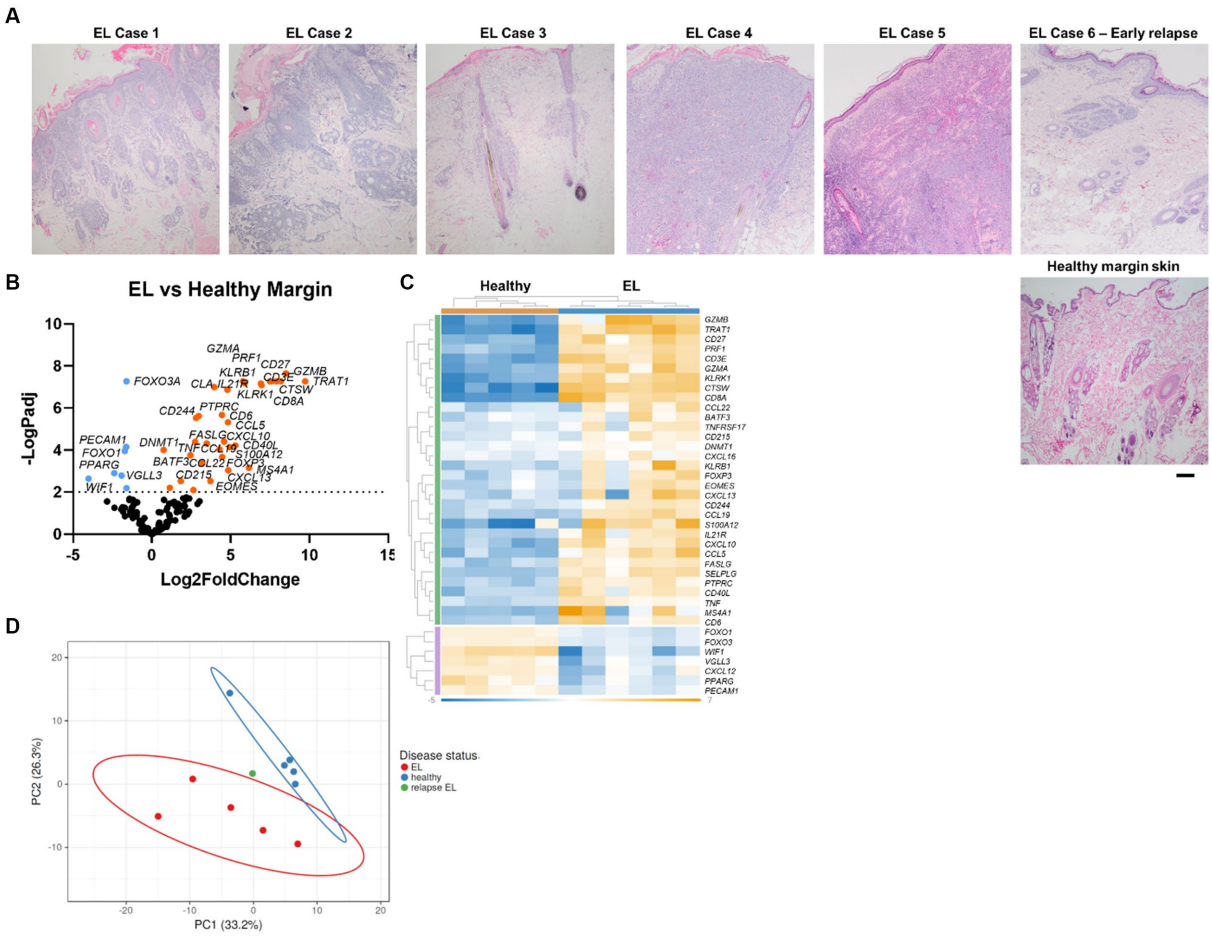

FIGURE 2
Gene expression in EL versus healthy margin controls reveals CD8⁺ cytotoxic T cell signatures. **(A)** Sample H&E photomicrographs of healthy and EL tissue (scale bar 200 µm). **(B)** Volcano plot of differentially expressed genes (DEGs) between healthy and EL. **(C)** Heatmap of DEGs generated with Rosalind software. **(D)** Principal component analysis (PCA) of cases versus healthy margins generated with ClusVis software (n = 6 EL and 5 healthy controls, p_{adj} <0.05 considered significant).

two-gene classifier identified in human MF by Nielsen et al. (13) would also distinguish canine EL from ID, and found that while *TOX* and *TRAF1* could separate the cases (green) from controls (black), better separation is achieved with *CTSW* and *TRAT1* (Figure 5D).

Cathepsins and CD244 are expressed at the protein level in canine EL and ID lesions, but RNA probe is superior to antibody for distinguishing the conditions

To confirm protein level expression of key genes, we performed IHC for CTSK/CTSO/CTSX/CTSO2 cathepsin family members using an antibody reactive to dog/human, and CD244 using antibodies that react to human/mouse/rat proteins with predicted homology to canine amino acid sequences, as no canine specific antibodies for CTSW or CD244 are commercially available. IHC staining did not differentiate EL from ID lesions, indicating possible cross-reactivity of the antibodies to other epitopes and/or discordance between RNA transcripts and protein level expression in the different conditions (Supplementary Figures S1, S2). Similarly, qPCR for *CTSW* was not effective at distinguishing EL from ID in FFPE samples, which may be due to the highly fragmented RNA (Supplementary Figure S3; Supplementary Table S2). To this end, we developed a truncated microarray diagnostic tool with our 4 biomarkers and 5 housekeeping genes, which was able to sensitively and specifically distinguish EL from ID in FFPE samples (Supplementary Figure S4).

Discussion

Here, we identified biomarkers that can sensitively and specifically detect EL to distinguish it from other forms of ID. These biomarkers may have biological relevance to tumor biology, as we will delineate below.

CTSW is a member of the cathepsin S family that is a papain-like protease. Cathepsins have been reported to regulate cancer progression and therapeutic responses (15). Cathepsin S is upregulated in follicular lymphoma, and an activating mutation Y132D drives lymphomagenesis through alterations in antigen presentation (16) and a pro-tumorigenic microenvironment (17). Cathepsin W is known to be expressed in human CD8⁺ T cells (18) and natural killer (NK) cells

TABLE 1 Discovery cohort signalments.

Case and diagnosis	Signalment[a]	Breed	Relevant clinical and histopathological findings
EL case 1	11 yo, MN	Dachshund	Patch/plaque stage
EL case 2	13 yo, MN	Labrador Cross	Multifocal ulceration with moderate neutrophilic inflammation
EL case 3	11 yo, FS	Labrador Retriever	Significant eosinophilic infiltrate accompanying the neoplastic population; multifocal ulceration, serocellular crusts and intracorneal neutrophilic pustules
EL case 4	9 yo, FS	Bloodhound	Significant dermal neoplastic involvement
EL case 5	11 yo, FS	Olde English Bulldogge	Significant dermal neoplastic involvement with epitheliotropism restricted to the adnexa with relative sparing of the epidermis
EL case 6	13 yo, MN	Golden Retriever	Early stage epitheliotropic lymphoma with minimal to absent dermal involvement. This is a recurrence from epitheliotropic lymphoma that had undergone remission
Healthy 1	8 yo, FS	Labrador Retriever	NA
Healthy 2	11 yo, FS	Siberian Husky Cross	NA
Healthy 3	11 yo, MN	Golden Retriever	NA
Healthy 4	12 yo, MN	German Shepherd Cross	NA
Healthy 5	6 yo, FS	Alaskan Malamute	NA

FS, female spayed; MN, male neutered.[a]Age at time of biopsy.

(19, 20). Similarly, family member cathepsin G is 2-fold upregulated in early disease stages (IA/IB) (21). In breast cancer, increased expression of cathepsin B and cathepsin L is associated with poorer prognosis, greater mortality, and greater disease metastases (15). In colorectal cancer, elevated cathepsin B and cathepsin L are associated with increased disease metastasis and poorer prognosis (22), while elevated cathepsin S predicts both decreased survival when treated with surgery alone, with potential benefit from adjuvant 5-fluorouracil and folinic acid treatment. High cathepsin B expression in lung, ovarian, pancreatic neuroendocrine cancers and pancreatic adenocarcinomas, is negatively correlated with survival and positively associated with recurrence, invasion, and/or tumor grade. Upregulation of cathepsin K in osteosarcomas predicts poor prognosis and disease metastasis. Generally, it seems that the tumor microenvironment helps activate cathepsins, which in turn activate oncogenesis: mutant HRAS in mammary epithelial cells upregulates *CTSB* and *CTSL*; the *HER2* oncogene drives expression of *CTSB* through the transcription factor myeloid zinc finger 1 (MZF1), and *CTSB* is a functional driver of the invasive phenotype.

TRAT1 is a 30 Kd type III transmembrane protein expressed by human T lymphocytes and natural killer (NK) cells. *TRAT1* regulates T-cell receptor expression (23). It consists of an extracellular domain, transmembrane region, and cytosolic tail. TRAT1 facilitates CTLA-4 shuttling from the trans Golgi network to the T-cell surface where it stabilizes the T-cell antigen receptor and CD3 complex. TRAT1 knockdown experiments demonstrated reduced CTLA-4 mediated cytokine release as well as CTLA-4 cell surface expression and subcellular distribution. When TRAT1 is overexpressed in Jurkat T cells, there is an increase in T-cell receptor expression, however this is not the case in regular T cells (24). By contributing to the structural integrity of the TCR/CD3 complex, TRAT1 has a significant role in TCR functions, which include triggering antigen-specific T-cell responses (25). In non-blood cancers (solid tumors), *TRAT1* expression is important for a good prognosis. However, in T cell lymphomas, *TRAT1* can be highly expressed in tumor cells. It remains unknown how this relates to prognosis.

KLRK1 is also known as NKG2D. It is a killer type lectin receptor expressed on NK cells and cytotoxic T cells (26). *KLRK1* is upregulated in human peripheral T cell lymphomas (27). A recent study demonstrated that benign T cells drive inflammation in MF tumors in humans (28): an influx of $CD8^+$ T cells following immunotherapy in CD4-driven tumors was protective. Therefore, caution should be exercised in fully characterizing the tumor (e.g., CD4 or CD8; does the tumor itself bear *KLRK1,* or is it expressed by the infiltrating T cells (29)) to ascertain whether *KLRK1* both as a biomarker and a potential treatment target is beneficial or detrimental (28).

LOC490356 was a top DEG in our validation cohort. This locus encodes *lymphotactin*, also known as *XCL1*/*XCL2*. This chemokine is homeostatically expressed by NK cells and has antimicrobial activity (30). *XCL1* is downregulated in human Sezary syndrome (31, 32), but was expressed by T-3B cells in a case report of a patient with concurrent T and B cell cutaneous lymphomas (33) and by T cells in a patient with lymphoproliferative disorder (34). As with *KLRK1*, it is unclear whether *XCL1* could be protective or pathogenic in the EL setting. In murine tumor models, injection of XCL1-expressing myeloma cells in Balb/c and nude mice resulted in tumor regression (35). An XCL1 fusion peptide improved tumor rejection in a mouse B16 model of melanoma via recruitment of $XCR1^+$ dendritic cells to the tumor (36). This also raises the point that some of the associated biomarkers identified for EL and other forms of CTCL may be expressed by infiltrating immune cells and not the tumor itself. Nevertheless, these seem to serve as sensitive and specific biomarkers for identifying early stage EL apart from other forms of interface dermatitis.

Other biologically relevant genes identified in our datasets correspond to both tumor and immune cell function. *CD6*, *CD86*, and *CD8A* were all upregulated, and are implicated in T-cell activation and regulation. *MS4A1*, a gene that encodes the B-cell marker CD20, was upregulated in EL. *PTPRC* was also upregulated, and is essential for T- and B-cell antigen receptor signaling. Immunoregulatory cytokines and their receptors were upregulated including *IL6* and *IL21R*. *S100A12* regulates inflammatory and

10.3389/fvets.2023.1225764

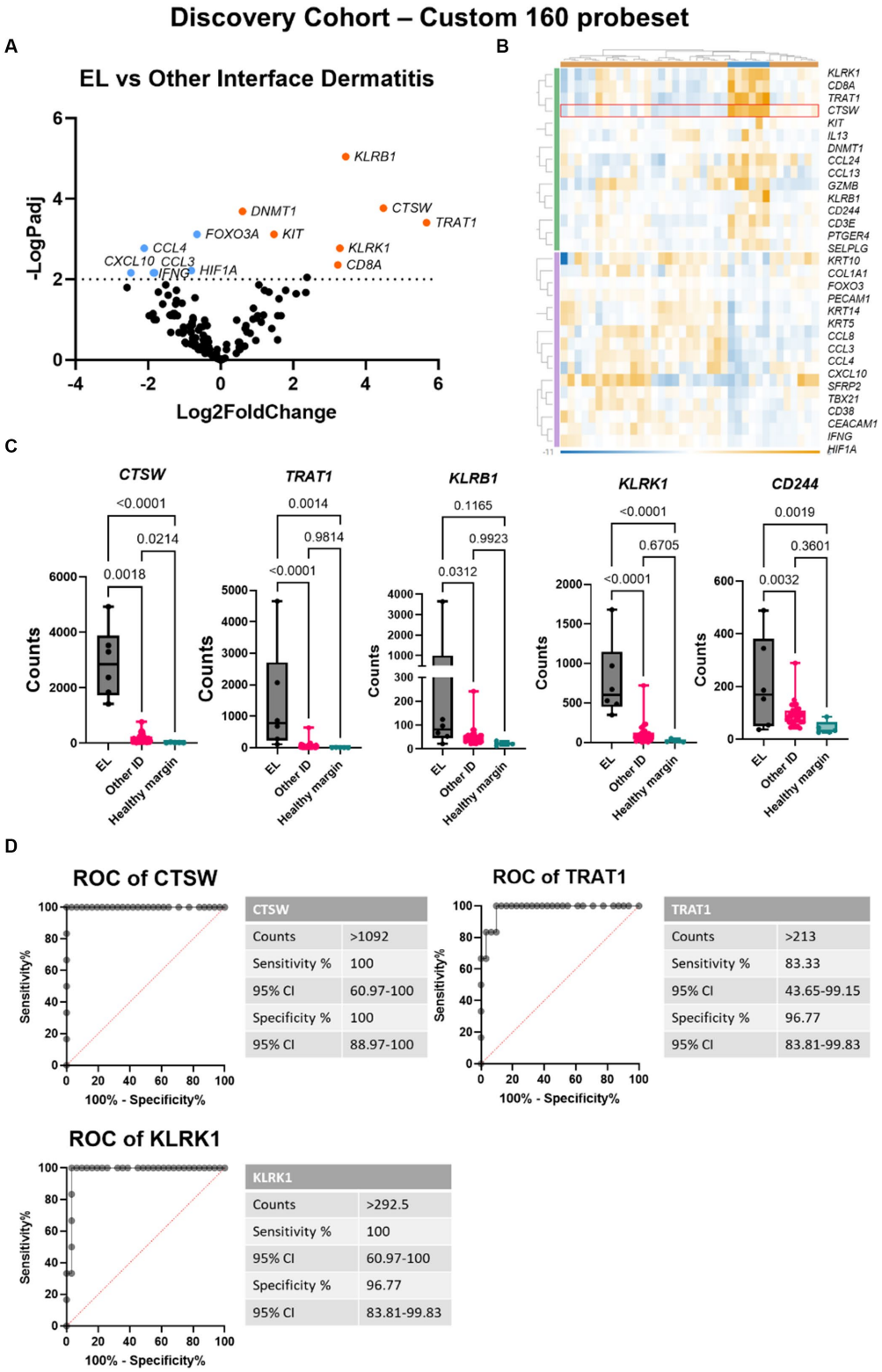

FIGURE 3
Gene expression analysis reveals *CTSW*, *TRAT1* and *KLRK1* distinguish between epitheliotropic lymphoma and interface dermatitis. **(A)** Volcano plot of EL versus other interface dermatitis conditions including cutaneous lupus erythematosus, pemphigus, and erythema multiforme spectrum disorders. **(B)** Heatmap generated in Rosalind software. **(C)** Raw counts of the top DEGs between EL and ID (one-way ANOVA with Tukey's post tests significant as indicated). **(D)** Receiver operator characteristic (ROC) curves of *CTSW*, *TRAT1* and *KLRK1* (n = 6 EL and 31 other interface dermatitis conditions; p_{adj} <0.05 considered significant).

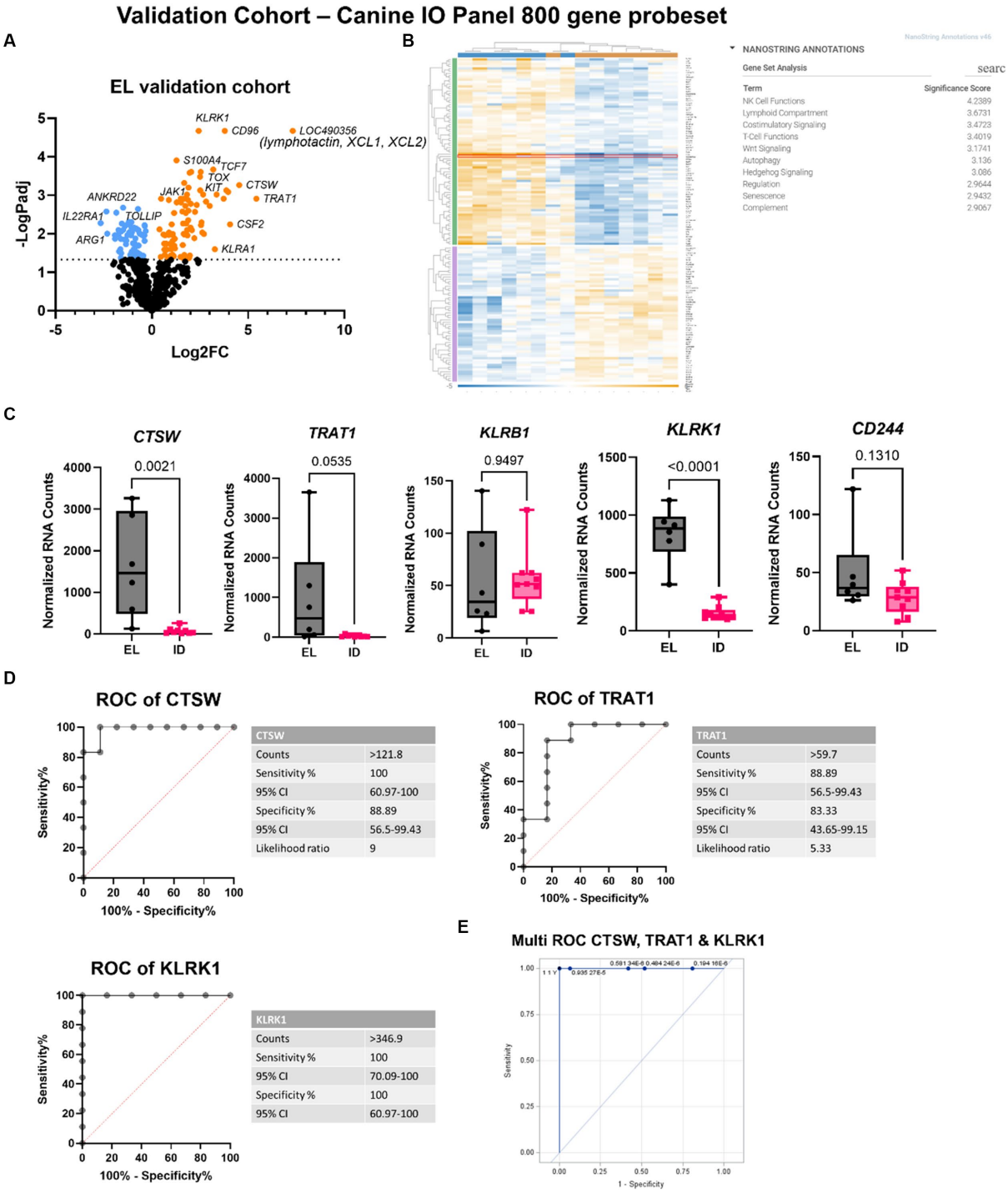

FIGURE 4
Validation cohort confirms *CTSW*, *TRAT1*, *KLRK1* and identifies *XCL1*/*XCL2* as potential biomarkers for EL. **(A)** Volcano plot of EL versus other interface dermatitis conditions. **(B)** Heatmap and gene set analysis generated in Rosalind software. **(C)** Raw counts of the top DEGs between EL and ID (one-way ANOVA with Tukey's post tests significant as indicated). **(D)** Receiver operator characteristic (ROC) curves of *CTSW* and *TRAT1*. **(E)** Multi-ROC curve combining *CTSW*, *TRAT1* and *KLRK1* normalized counts for distinguishing EL from ID in the discovery and validation cohorts (discovery cohort: $n = 6$ EL and 31 other interface dermatitis conditions; validation cohort: $n = 6$ EL and 9 other interface dermatitis conditions; $p_{adj} < 0.05$ considered significant).

immune responses, and was upregulated in EL. Tumor necrosis factor alpha (TNF-alpha) has been implicated in the pathogenesis of CTCL (37). *TNF*, *TNFRSF17*, *CD27*, and *FASLG* were all significantly upregulated in canines with EL. *CD27*, a TNF family member required for the maintenance of T-cell immunity, was significantly upregulated. *FoxP3* has been reported to be variably expressed depending on the stage of disease in CTCL (38). *FoxP3* was not significantly differentiated in the EL canines compared to

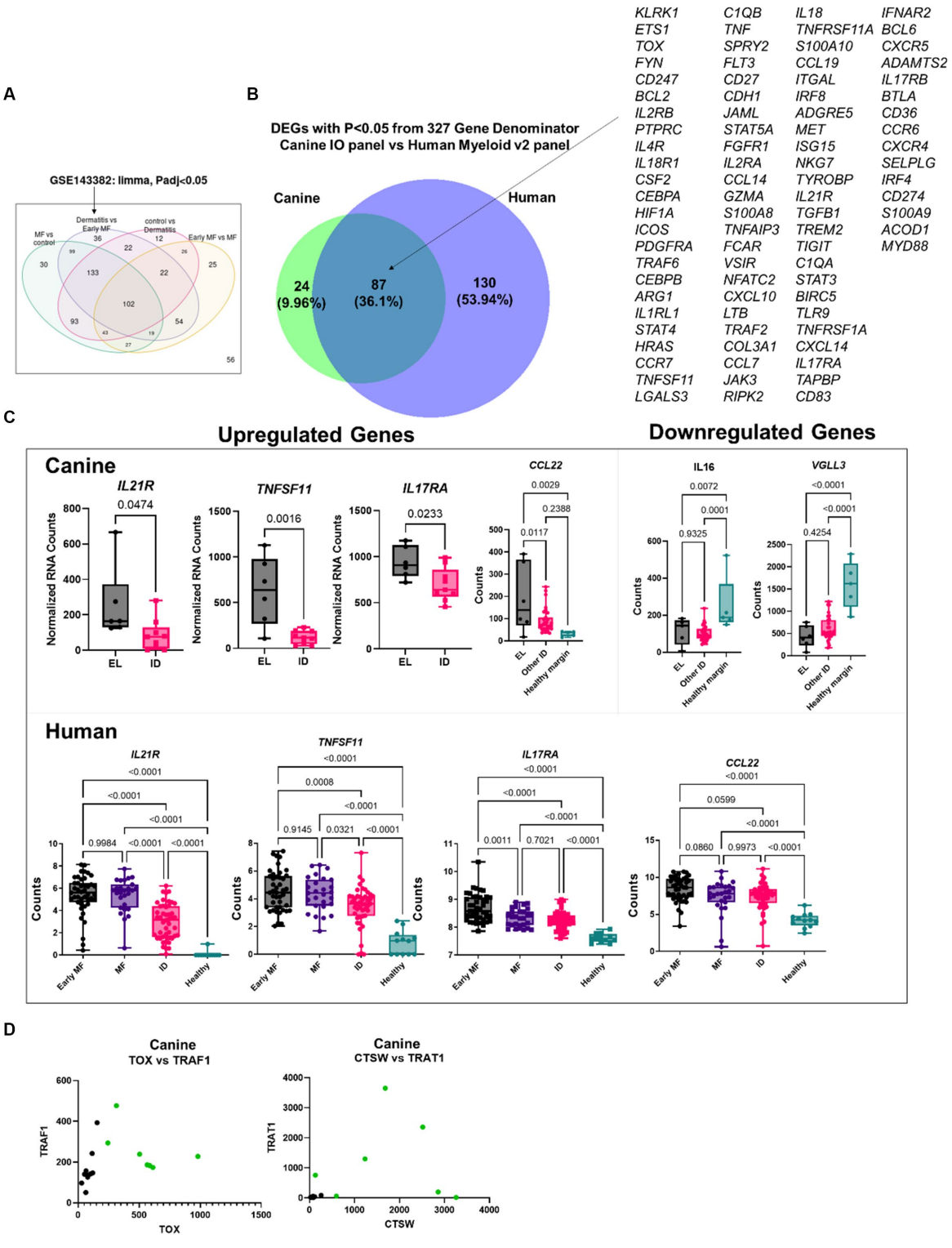

FIGURE 5
Comparative transcriptomics of human MF and canine EL versus ID DEGs. **(A)** Geo2R reanalysis of GSE143382 human MF dataset. DEGs from dermatitis vs. early MF were used as they represent the closest clinical match. **(B)** DEG overlap between the canine validation cohort (canine IO panel) and human dataset (myeloid v2 panel) using the 327 common denominator genes from the respective NanoString probesets. **(C)** Comparison of previously published up-and downregulated genes in canine and human datasets. **(D)** Analysis of *TOX* vs. *TRAF1*, which was used to distinguish human MF from ID, or *CTSW* vs. *TRAT1* in canine samples.

the healthy controls; however two canines, Sample 3 and Sample 4, had relatively greater counts than all other cases. They represent cases with significant dermal neoplastic involvement and patch/plaque stage, respectively. Last, given that *CCL22* was upregulated, *CCR4* depleting antibodies like mogamulizumab may be helpful for treating canine EL.

We also observed downregulated genes that may be biologically significant in EL. *VGLL3* has been recognized as a tumor suppressor gene in serous ovarian carcinomas (39, 40) and stomach adenocarcinoma (41). *VGLL3*, which regulates the Hippo pathway (42), was downregulated in EL skin. *IL16* was also downregulated, reflecting the pattern observed in severe Sézary syndrome (43). Reintroduction of pro-IL16 in MOLT4 tumors can induce regression in nude mice (44). Therefore, adding back tumor suppressor genes may serve as a therapeutic option for EL and should be considered in future veterinary clinical trials.

Forms of CTCL that express $CD8^+$ phenotype in humans have been reported (38): in some rare cases, well-defined types of CTCL (such as MF) express $CD8^+$ and have similar clinical presentation and disease prognosis as the more common $CD4^+$ cases (45). Outside of these, studies suggest separate groups of more aggressive $CD8^+$ cytotoxic CTCLs (46), including an epidermotropic type and a panniculitis-like subcutaneous T cell lymphoma type. Therefore, it is possible that, genetically and/or transcriptionally, canine EL matches human $CD8^+$ lymphomas more closely than MF as a general subtype. Future comparative oncology studies should further characterize these rare $CD8^+$ tumors to better understand which condition is most closely modeled in dogs.

In conclusion, comparative studies investigating the conservation of oncogenic processes and tumor immune landscapes across species are important for identifying biomarkers and treatment targets. Further investigation is warranted to expand our understanding of these disorders and predict disease prognosis and treatment responses. We plan to use our newly identified biomarkers to diagnose and track dogs with EL in veterinary clinical trials, and our long-term goal is to develop targeted therapies for both veterinary and human CTCLs.

Data availability statement

The datasets presented in this study can be found in online repositories. The names of the repository/repositories and accession number(s) can be found at: https://www.ncbi.nlm.nih.gov/geo/, GSE213087.

Ethics statement

Ethical approval was not required for the study involving humans in accordance with the local legislation and institutional requirements. Written informed consent to participate in this study was not required from the participants or the participants' legal guardians/next of kin in accordance with the national legislation and the institutional requirements. The animal studies were approved by Tufts Cummings School of Veterinary Medicine IACUC. The studies were conducted in accordance with the local legislation and institutional requirements. Written informed consent was obtained from the owners for the participation of their animals in this study.

Author contributions

JR: conceptualization and project administration. NR and JR: methodology. CD: software. CP-M, AR, AN, HG, KH, BB, and JR: validation. JO, DM, NW, BB, and JR: formal analysis. C-PM, NR, JR, CD, and LW: investigation. NR, KH, CL, and JR: resources. NR, RA, JO, CP-M, KH, and JR: data curation. JO, AN, and JR: writing—original draft. JO, AN, DM, NW, AR, CP-M, LW, CD, HG, NR, KH, BB, CL, RA, and JR: writing—review & editing. JO, CP-M, NW, DM, and JR: visualization. JR, RA, and NR: supervision. JR and JO: funding acquisition. All authors contributed to the article and approved the submitted version.

Funding

This work was supported by a Diversity Research Supplement Award (JO) and a Women's Health Career Development Award (JR) from the Dermatology Foundation. The funding body did not have any role in the design, analysis and reporting of the study.

Acknowledgments

The authors thank Yu Liu and Colton Garelli from UMass Chan, and Gina Scariglia and Sarah Ducat from Tufts for technical assistance. The authors thank Ginette Okoye for insightful discussions of MF. The authors thank the Finberg lab at UMass Chan for the use of their microscope. Immunohistochemistry studies were performed in collaboration with the UMass Chan Morphology core. The NanoString Sprint machine is maintained by the Silverman lab in the UMass Chan Department of Medicine.

Conflict of interest

JO, RA, and JR are inventors on a use patent filed for "Diagnosis of skin conditions in veterinary and human patients." JR is an inventor on use patents for targeting CXCR3 (0#15/851,651) and IL15 (# 62489191) for the treatment of vitiligo. NR is an employee of Alnylam. CD is an employee of NanoString Technologies.

The remaining authors declare that the research was conducted in the absence of any commercial or financial relationships that could be construed as a potential conflict of interest.

Publisher's note

Supplementary material

The Supplementary material for this article can be found online at: https://www.frontiersin.org/articles/10.3389/fvets.2023.1225764/full#supplementary-material

References

1. Willemze R, Cerroni L, Kempf W, Berti E, Facchetti F, Swerdlow SH, et al. The 2018 update of the WHO-EORTC classification for primary cutaneous lymphomas. *Blood*. (2019) 133:1703–14. doi: 10.1182/blood-2018-11-881268

2. Muñoz-González H, Molina-Ruiz AM, Requena L. Clinicopathologic variants of mycosis fungoides. *Actas Dermosifiliogr*. (2017) 108:192–208. doi: 10.1016/j.ad.2016.08.009

3. Criscione VD, Weinstock MA. Incidence of cutaneous T-cell lymphoma in the United States, 1973–2002. *Arch Dermatol*. (2007) 143:854–9. doi: 10.1001/archderm.143.7.854

4. Brachelente C, Affolter VK, Fondati A, Porcellato I, Sforna M, Lepri E, et al. CD3 and CD20 coexpression in a case of canine cutaneous epitheliotropic T-cell lymphoma (mycosis fungoides). *Vet Pathol*. (2016) 53:563–6. doi: 10.1177/0300985815604724

5. Meuten DJ. *Tumors in domestic animals*. John Wiley & Sons (2016).

6. Gross TL. *Skin diseases of the dog and cat: clinical and histopathologic diagnosis*. Ames: Blackwell Science (2005).

7. Fontaine J, Bovens C, Bettenay S, Mueller RS. Canine cutaneous epitheliotropic T-cell lymphoma: a review. *Vet Comp Oncol*. (2009) 7:1–14. doi: 10.1111/j.1476-5829.2008.00176.x

8. Moore PF, Olivry T, Naydan D. Canine cutaneous epitheliotropic lymphoma (mycosis fungoides) is a proliferative disorder of CD8$^+$ T cells. *Am J Pathol*. (1994) 144:421–9.

9. Rook KA. Canine and feline cutaneous epitheliotropic lymphoma and cutaneous lymphocytosis. *Vet Clin North Am Small Anim Pract*. (2019) 49:67–81. doi: 10.1016/j.cvsm.2018.08.007

10. Gerber N, Brunner MAT, Jagannathan V, Leeb T, Gerhards NM, Welle MM, et al. Transcriptional differences between canine cutaneous epitheliotropic lymphoma and immune-mediated dermatoses. *Genes*. (2021) 12:12. doi: 10.3390/genes12020160

11. Garelli CJ, Wong NB, Piedra-Mora C, Wrijil LM, Scarglia G, David CN, et al. Shared inflammatory and skin-specific gene signatures reveal common drivers of discoid lupus erythematosus in canines, humans and mice. *Curr Res Immunol*. (2021) 2:41–51. doi: 10.1016/j.crimmu.2021.03.003

12. Danaher P, Warren S, Dennis L, D'Amico L, White A, Disis ML, et al. Gene expression markers of tumor infiltrating leukocytes. *J Immunother Cancer*. (2017) 5:18. doi: 10.1186/s40425-017-0215-8

13. Nielsen PR, Eriksen JO, Lindahl LM, Wehkamp U, Bzorek M, Andersen G, et al. Diagnostic two-gene classifier in early-stage mycosis fungoides: a retrospective multicenter study. *J Invest Dermatol*. (2021) 141:213–7.e5. doi: 10.1016/j.jid.2020.04.026

14. Hulsen T, de Vlieg J, Alkema W. BioVenn—a web application for the comparison and visualization of biological lists using area-proportional Venn diagrams. *BMC Genomics*. (2008) 9:488–6. doi: 10.1186/1471-2164-9-488

15. Olson OC, Joyce JA. Cysteine cathepsin proteases: regulators of cancer progression and therapeutic response. *Nat Rev Cancer*. (2015) 15:712–29. doi: 10.1038/nrc4027

16. Dheilly E, Battistello E, Katanayeva N, Sungalee S, Michaux J, Duns G, et al. Cathepsin S regulates antigen processing and T cell activity in non-Hodgkin lymphoma. *Cancer Cell*. (2020) 37:674–89.e12. doi: 10.1016/j.ccell.2020.03.016

17. Bararia D, Hildebrand JA, Stolz S, Haebe S, Alig S, Trevisani CP, et al. Cathepsin S alterations induce a tumor-promoting immune microenvironment in follicular lymphoma. *Cell Rep*. (2020) 31:107522. doi: 10.1016/j.celrep.2020.107522

18. Linnevers C, Smeekens SP, Brömme D. Human cathepsin W, a putative cysteine protease predominantly expressed in CD8$^+$ T-lymphocytes. *FEBS Lett*. (1997) 405:253–9. doi: 10.1016/S0014-5793(97)00118-X

19. Wex T, Bühling F, Wex H, Günther D, Malfertheiner P, Weber E, et al. Human cathepsin W, a cysteine protease predominantly expressed in NK cells, is mainly localized in the endoplasmic reticulum. *J Immunol*. (2001) 167:2172–8. doi: 10.4049/jimmunol.167.4.2172

20. Stoeckle C, Gouttefangeas C, Hammer M, Weber E, Melms A, Tolosa E. Cathepsin W expressed exclusively in CD8$^+$ T cells and NK cells, is secreted during target cell killing but is not essential for cytotoxicity in human CTLs. *Exp Hematol*. (2009) 37:266–75. doi: 10.1016/j.exphem.2008.10.011

21. Shin J, Monti S, Aires DJ, Duvic M, Golub T, Jones DA, et al. Lesional gene expression profiling in cutaneous T-cell lymphoma reveals natural clusters associated with disease outcome. *Blood*. (2007) 110:3015–27. doi: 10.1182/blood-2006-12-061507

22. Kuester D, Lippert H, Roessner A, Krueger S. The cathepsin family and their role in colorectal cancer. *Pathol Res Pract*. (2008) 204:491–500. doi: 10.1016/j.prp.2008.04.010

23. Kirchgessner H, Dietrich J, Scherer J, Isomäki P, Korinek V, Hilgert I, et al. The transmembrane adaptor protein TRIM regulates T cell receptor (TCR) expression and TCR-mediated signaling via an association with the TCR zeta chain. *J Exp Med*. (2001) 193:1269–84. doi: 10.1084/jem.193.11.1269

24. Valk E, Leung R, Kang H, Kaneko K, Rudd CE, Schneider H. T cell receptor-interacting molecule acts as a chaperone to modulate surface expression of the CTLA-4 coreceptor. *Immunity*. (2006) 25:807–21. doi: 10.1016/j.immuni.2006.08.024

25. Boćko D, Bilińska M, Dobosz T, Żołedziewska M, Suwalska K, Tutak A, et al. Lack of association between an exon 1 CTLA-4 gene polymorphism A (49) G and multiple sclerosis in a polish population of the lower Silesia region. *Arch Immunol Ther Exp*. (2003) 51:201–5. https://www.researchgate.net/profile/Tadeusz-Dobosz/publication/10632143_Lack_of_association_between_an_exon_1_CTLA-4_gene_polymorphism_A_49_G_and_multiple_sclerosis_in_a_Polish_population_of_the_Lower_Silesia_region/links/00463516e8cfadcec4000000/Lack-of-association-between-an-exon-1-CTLA-4-gene-polymorphism-A-49-G-and-multiple-sclerosis-in-a-Polish-population-of-the-Lower-Silesia-region.pdf

26. Lanier LL. NKG2D receptor and its ligands in host defense. *Cancer Immunol Res*. (2015) 3:575–82. doi: 10.1158/2326-6066.CIR-15-0098

27. Iqbal J, Weisenburger DD, Greiner TC, Vose JM, McKeithan T, Kucuk C, et al. Molecular signatures to improve diagnosis in peripheral T-cell lymphoma and prognostication in angioimmunoblastic T-cell lymphoma. *Blood*. (2010) 115:1026–36. doi: 10.1182/blood-2009-06-227579

28. Vieyra-Garcia P, Crouch JD, O'Malley JT, Seger EW, Yang CH, Teague JE, et al. Benign T cells drive clinical skin inflammation in cutaneous T cell lymphoma. *JCI Insight*. (2019) 4:4. doi: 10.1172/jci.insight.124233

29. Kamarashev J, Burg G, Mingari MC, Kempf W, Hofbauer G, Dummer R. Differential expression of cytotoxic molecules and killer cell inhibitory receptors in CD8$^+$ and CD56$^+$ cutaneous lymphomas. *Am J Pathol*. (2001) 158:1593–8. doi: 10.1016/S0002-9440(10)64114-4

30. Yang D, Chen Q, Hoover DM, Staley P, Tucker KD, Lubkowski J, et al. Many chemokines including CCL20/MIP-3α display antimicrobial activity. *J Leukoc Biol*. (2003) 74:448–55. doi: 10.1189/jlb.0103024

31. Hahtola S, Tuomela S, Elo L, Häkkinen T, Karenko L, Nedoszytko B, et al. Th1 response and cytotoxicity genes are down-regulated in cutaneous T-cell lymphoma. *Clin Cancer Res*. (2006) 12:4812–21. doi: 10.1158/1078-0432.CCR-06-0532

32. Rindler K, Jonak C, Alkon N, Thaler FM, Kurz H, Shaw LE, et al. Single-cell RNA sequencing reveals markers of disease progression in primary cutaneous T-cell lymphoma. *Mol Cancer*. (2021) 20:124. doi: 10.1186/s12943-021-01419-2

33. Jonak C, Alkon N, Rindler K, Rojahn TB, Shaw LE, Porkert S, et al. Single-cell RNA sequencing profiling in a patient with discordant primary cutaneous B-cell and T-cell lymphoma reveals micromilieu-driven immune skewing. *Br J Dermatol*. (2021) 185:1013–25. doi: 10.1111/bjd.20512

34. Visentini M, Carbonari M, Ghia E, De Propriis S, Guarini A, Girmenia C, et al. A lymphotactin-producing monoclonal T-cell lymphoproliferative disorder with extreme lymphocytopenia and progressive leukoencephalopathy. *Leuk Lymphoma*. (2006) 47:1421–3. doi: 10.1080/10428190600581807

35. Cairns CM, Gordon JR, Li F, Baca-Estrada ME, Moyana T, Xiang J. Lymphotactin expression by engineered myeloma cells drives tumor regression: mediation by CD4$^+$ and CD8$^+$ T cells and neutrophils expressing XCR1 receptor. *J Immunol*. (2001) 167:57–65. doi: 10.4049/jimmunol.167.1.57

36. Mizumoto Y, Hemmi H, Katsuda M, Miyazawa M, Kitahata Y, Miyamoto A, et al. Anticancer effects of chemokine-directed antigen delivery to a cross-presenting dendritic cell subset with immune checkpoint blockade. *Br J Cancer*. (2020) 122:1185–93. doi: 10.1038/s41416-020-0757-2

37. Alpdogan O, Kartan S, Johnson W, Sokol K, Porcu P. Systemic therapy of cutaneous T-cell lymphoma (CTCL). *Chin Clin Oncol*. (2019) 8:20. doi: 10.21037/cco.2019.01.02

38. Berti E, Tomasini D, Vermeer MH, Meijer CJ, Alessi E, Willemze R. Primary cutaneous CD8-positive epidermotropic cytotoxic T cell lymphomas. A distinct clinicopathological entity with an aggressive clinical behavior. *Am J Pathol*. (1999) 155:483–92. doi: 10.1016/S0002-9440(10)65144-9

39. Gambaro K, Quinn MCJ, Wojnarowicz PM, Arcand SL, de Ladurantaye M, Barrès V, et al. VGLL3 expression is associated with a tumor suppressor phenotype in epithelial ovarian cancer. *Mol Oncol*. (2013) 7:513–30. doi: 10.1016/j.molonc.2012.12.006

40. Cody NAL, Shen Z, Ripeau J-S, Provencher DM, Mes-Masson A-M, Chevrette M, et al. Characterization of the 3p12.3-pcen region associated with tumor suppression in a novel ovarian cancer cell line model genetically modified by chromosome 3 fragment transfer. *Mol Carcinog*. (2009) 48:1077–92. doi: 10.1002/mc.20535

41. Zhang L, Li L, Mao Y, Hua D. VGLL3 is a prognostic biomarker and correlated with clinical pathologic features and immune infiltrates in stomach adenocarcinoma. *Sci Rep*. (2020) 10:1355. doi: 10.1038/s41598-020-58493-7

42. Hori N, Okada K, Takakura Y, Takano H, Yamaguchi N, Yamaguchi N. Vestigial-like family member 3 (VGLL3), a cofactor for TEAD transcription factors, promotes cancer cell proliferation by activating the Hippo pathway. *J Biol Chem*. (2020) 295:8798–807. doi: 10.1074/jbc.RA120.012781

43. Richmond J, Tuzova M, Parks A, Adams N, Martin E, Tawa M, et al. Interleukin-16 as a marker of Sezary syndrome onset and stage. *J Clin Immunol*. (2011) 31:39–50. doi: 10.1007/s10875-010-9464-8

44. Richmond J, Finkel M, Studwell A, Little F, Cruikshank W. Introduction of pro-interleukin-16 inhibits T-lymphoblastic leukemia growth in mice. *J Cancer Res Clin Oncol*. (2011) 137:1581–5. doi: 10.1007/s00432-011-1017-x

45. Querfeld C, Guitart J, Kuzel TM, Rosen ST. Primary cutaneous lymphomas: a review with current treatment options. *Blood Rev*. (2003) 17:131–42. doi: 10.1016/S0268-960X(03)00004-3

46. Gormley RH, Hess SD, Anand D, Junkins-Hopkins J, Rook AH, Kim EJ. Primary cutaneous aggressive epidermotropic CD8$^+$ T-cell lymphoma. *J Am Acad Dermatol*. (2010) 62:300–7. doi: 10.1016/j.jaad.2009.02.035

frontiers | Frontiers in Veterinary Science

TYPE Original Research
PUBLISHED 08 December 2023
DOI 10.3389/fvets.2023.1301536

OPEN ACCESS

EDITED BY
Vittoria Castiglioni,
IDEXX Laboratories, Germany

REVIEWED BY
Diana Giannuzzi,
University of Padua, Italy
Jillian M. Richmond,
University of Massachusetts Medical School, United States

*CORRESPONDENCE
Leila Taher
✉ leila.taher@tugraz.at
Hugo Murua Escobar
✉ hugo.murua.escobar@med.uni-rostock.de

RECEIVED 25 September 2023
ACCEPTED 20 November 2023
PUBLISHED 08 December 2023

CITATION
Fibi-Smetana S, Inglis C, Schuster D, Eberle N, Granados-Soler JL, Liu W, Krohn S, Junghanss C, Nolte I, Taher L and Murua Escobar H (2023) The TiHoCL panel for canine lymphoma: a feasibility study integrating functional genomics and network biology approaches for comparative oncology targeted NGS panel design.
Front. Vet. Sci. 10:1301536.
doi: 10.3389/fvets.2023.1301536

The TiHoCL panel for canine lymphoma: a feasibility study integrating functional genomics and network biology approaches for comparative oncology targeted NGS panel design

Silvia Fibi-Smetana[1], Camila Inglis[2,3], Daniela Schuster[4,5], Nina Eberle[2], José Luis Granados-Soler[2,6], Wen Liu[3], Saskia Krohn[3], Christian Junghanss[3], Ingo Nolte[2], Leila Taher[1,3,4,5]* and Hugo Murua Escobar[3]*

[1]Institute of Biomedical Informatics, Graz University of Technology, Graz, Austria, [2]Small Animal Clinic, University of Veterinary Medicine Hannover Foundation, Hannover, Germany, [3]Clinic for Hematology, Oncology and Palliative Care, Rostock University Medical Center, University of Rostock, Rostock, Germany, [4]Division of Bioinformatics, Department of Biology, Friedrich-Alexander-University, Erlangen, Germany, [5]Institute for Biostatistics and Informatics in Medicine and Ageing Research, Rostock University Medical Center, University of Rostock, Rostock, Germany, [6]UQVETS Small Animal Hospital, School of Veterinary Science, The University of Queensland, Gatton, QLD, Australia

Targeted next-generation sequencing (NGS) enables the identification of genomic variants in cancer patients with high sensitivity at relatively low costs, and has thus opened the era to personalized human oncology. Veterinary medicine tends to adopt new technologies at a slower pace compared to human medicine due to lower funding, nonetheless it embraces technological advancements over time. Hence, it is reasonable to assume that targeted NGS will be incorporated into routine veterinary practice in the foreseeable future. Many animal diseases have well-researched human counterparts and hence, insights gained from the latter might, in principle, be harnessed to elucidate the former. Here, we present the TiHoCL targeted NGS panel as a proof of concept, exemplifying how functional genomics and network approaches can be effectively used to leverage the wealth of information available for human diseases in the development of targeted sequencing panels for veterinary medicine. Specifically, the TiHoCL targeted NGS panel is a molecular tool for characterizing and stratifying canine lymphoma (CL) patients designed based on human non-Hodgkin lymphoma (NHL) research outputs. While various single nucleotide polymorphisms (SNPs) have been associated with high risk of developing NHL, poor prognosis and resistance to treatment in NHL patients, little is known about the genetics of CL. Thus, the ~100 SNPs featured in the TiHoCL targeted NGS panel were selected using functional genomics and network approaches following a literature and database search that shielded ~500 SNPs associated with, in nearly all cases, human hematologic malignancies. The TiHoCL targeted NGS panel underwent technical validation and preliminary functional assessment by sequencing DNA samples isolated from blood of 29 lymphoma dogs using an Ion Torrent™ PGM System achieving good sequencing run metrics. Our design framework holds new possibilities for the design of similar molecular tools applied to other diseases for which limited knowledge is available and will improve drug target discovery and patient care.

10.3389/fvets.2023.1301536

KEYWORDS

targeted next-generation sequencing, canine lymphoma, genomic variants, comparative oncology, personalized oncology, patient stratification, comparative genomics, network biology

1 Introduction

Driven by plummeting costs, next-generation sequencing (NGS) has revolutionized biomedical research, playing an instrumental role in advancing our understanding of the molecular basis of various diseases (1). NGS has numerous applications, ranging from whole-genome (re) sequencing to targeted sequencing for variant identification or confirmation. In contrast to whole-genome sequencing, targeted NGS focuses on a specific set of genomic loci that are likely to be involved in the phenotype of interest, delivering higher coverage levels at a more affordable cost, and making it amenable to samples containing small DNA amounts. Furthermore, targeted NGS produces substantially smaller datasets, which are easier to manage and analyze (2). These attributes make targeted NGS particularly well suited to detect and characterize specific tumor cell sub-populations, such as subclones harboring drug resistant variants (3), and hence, very attractive for clinical oncology (4, 5). Indeed, in human medicine, targeted NGS has become a common tool to diagnose and monitor cancer, as well as to select therapeutic agents and quantify treatment resistance.

Due to various factors, including financial considerations and the diversity of animal species and breeds, veterinary medicine tends to adopt technological advances more slowly than human medicine. Nonetheless, there are a number of cases in which the use of targeted NGS has already proved to be cost-effective. For example, targeted NGS panels are routinely used in the clinic to detect ovine and equine pathogens (6, 7). And given the growing significance of the well-being of companion animals in our society, it is inevitable that cutting-edge technologies such as targeted NGS will be progressively adopted to improve their health and quality of life.

Targeted NGS requires a certain knowledge of the genetic basis of the disease of interest, in particular, of the variants or mutations that are associated with it. This can pose challenges for diseases that lack extensive research, as it is generally the case for animal diseases. However, biological processes and genetic mechanisms are frequently conserved across species, making findings in human medicine relevant to veterinary medicine –and vice versa–, and facilitating research and technology transfer between the two fields (8). Consistently, veterinary medicine often resorts to comparative approaches to gain insights into health and disease. Herein, we illustrate how knowledge can be leveraged across species and/or diseases to develop a targeted sequencing panel for canine lymphoma (CL).

CL is a spontaneous disease that closely resembles human Non-Hodgkin lymphoma (NHL), a heterogeneous group of lymphoid malignancies, with different cells of origin and biological behaviors. Specifically, CL and NHL present similar clinical, histological, cytogenetic, and molecular features (9, 10). Furthermore, CL and NHL are classified according to analogous histologic systems and treated with the same chemotherapeutic agents. In particular, the standard backbone treatment for CL and NHL is a chemotherapy combination known as CHOP [cyclophosphamide, hydroxydaunorubicin, oncovin/vincristine, prednisone or prednisolone; (11, 12)]. Groundbreaking CD20 antibody strategies, as used in humans, are unfortunately not available in dogs, thus conventional chemotherapy remains the key strategy for CL. Naturally, although CL and NHL are similar in many regards, they also exhibit important differences. Most notably, while NHL patients often respond well to treatment and over 50% of them are cured after initial therapy (9, 10, 13–17), CL is considered incurable. Indeed, even though over 80% of dogs achieve complete remission upon induction chemotherapy, most of them relapse within 12 months (9, 10, 13–15). Moreover, relapsed patients frequently become refractory to therapy (18) and ultimately die of their disease, with a median overall survival time of only 10–14 months (13).

As in NHL and other canine cancers, increased risk, poor prognosis, and resistance to treatment in CL are very likely related to the genetic background of the host (19–26). Candidate gene, linkage and genome-wide association studies (GWASs) have revealed multiple genetic variants associated with NHL (25, 27–30). Specifically, genetic alterations associated with NHL include both single nucleotide variants and large rearrangements that place genes under the control of promoters and enhancers that are typically only active in the lymphocytes, leading to dysregulation of genes in pathways involving immune function, cell cycle, apoptosis, DNA repair, and carcinogen metabolism (31–33). Although genetic studies are still incipient for CL, evidence suggests that many of the same pathways dysregulated in NHL also exhibit perturbations in CL (31, 32). Nevertheless, how to use this information for patient stratification remains a matter of investigation (34).

Here we present the TiHoCL targeted sequencing panel, which comprises approximately 100 canine loci chosen using a combination of comparative genomics and network-based approaches. Our panel was designed starting from ~600 single nucleotide polymorphisms (SNPs) associated with lymphoma risk and prognosis in humans and only three in dogs, and was successfully technically and functionally assessed on 29 DNA samples extracted from whole blood of CL patients using the Ion Torrent™ Personal Genome Machine (PGM)™ technology. The TiHoCL targeted sequencing panel is a proof of principle to demonstrate how we can use knowledge from human research to develop clinical tools for other species. Facilitated by declining sequencing costs, the broad application of NGS panels like the TiHoCL targeted panel opens the door to the discovery of new drug targets and improved patient care.

2 Materials and methods

2.1 Identification of lymphoma-associated canine and human SNPs

First, we mined the Online Mendelian Inheritance in Man (OMIM) (35), the GWAS catalog (36), and PubMed for single

nucleotide polymorphisms (SNPs). We accessed OMIM through their API; text searches for "lymphoma" were restricted to those containing allelic variants using the search field "av_exists." The GWAS catalog was queried using the web interface; we searched for SNPs using the keyword "lymphoma" and required a *p*-value for the SNP-disease/trait association $<1\times10^{-5}$. Finally, we searched PubMed using the Entrez Programming Utilities (E-Utilities) (37) with the PubMed filters: "lymphoma[Title/Abstract] AND ("allelic variation" OR polymorphism) AND humans[MeSH]" (for human SNPs), and "lymphoma[Title/Abstract] AND ("allelic variation" OR polymorphism) AND dogs[Title/Abstract]" (for canine SNPs). The abstracts resulting from this query were searched for Reference SNP (rs) numbers. Next, we manually searched PubMed for articles published between the years of 2005 and 2015 with the keywords "lymphoma[MeSH]" and "genetic polymorphism[MeSH]" or "single nucleotide polymorphism[MeSH]." Any human or canine SNPs mentioned in the full text of these articles that were significantly associated (p-value $<10^{-5}$) with hematological malignancy risk, prognosis, outcome and resistance to treatment were selected as relevant.

We merged the SNPs resulting from all searches, removing duplicates and excluding those SNPs absent in dbSNP build 147 (38).

2.2 Identification of canine orthologous loci for human SNPs

To identify the canine orthologous locus of each human SNP we first retrieved the orthologous sequences of a 100-bp window centered at the human (GRCh38/hg38) SNP in the dog (CanFam3.1/canFam3), gorilla (gorGor4.1/gorGor4), mouse (GRCm38/mm10), and cat (ICGSCFelis_catus_8.0/felCat8) genomes with the LiftOver tool from the UCSC Genome Browser (39). SNPs in genomic windows for which no orthologous canine sequence was retrieved or for which the orthologous canine sequence exceeded 1,000-bp were excluded from further analyses. Finally, multiple sequence alignments were computed with T-Coffee v11.00.8cbe486 (40) to assess the evolutionary conservation of each SNP and flanking nucleotides. SNPs aligned to a gap in the canine genome were excluded from further analyses.

2.3 Genomic annotation of canine loci

Canine loci were annotated with the "annotatePeaks.pl" command from the HOMER v4.11.1 suite (41) using canFam3 as genome.

2.4 Gene annotation

Gene annotation was obtained from Ensembl [release 90, (42)] in GTF format.[1]

2.5 Identification of canine loci overlapping with UTRs

Gene annotation was filtered for features covering 50 bp or less. Bedtools intersect v2.27.1 (43) was used to identify overlaps with the remaining gene annotation features. Loci overlapping with annotated UTRs that did not overlap with coding exons in any transcript of the same gene or that overlapped with coding exons for less than two thirds of their length were reported as overlapping with UTRs.

2.6 Identification of canine loci for which the nearest upstream or downstream transcription start site is that of a gene annotated as a transcription factor

The nearest upstream and downstream TSS to each locus was identified based on the gene annotation with bedtools closest. The corresponding genes were classified according to the protein class that they encode (if any) using the online web server of the PANTHER Protein Classification System Database v11.0 (44).[2]

2.7 Identification of differentially expressed genes in CL patients

Differential expression analysis was performed on a total of 67 samples from three Gene Expression Omnibus [GEO, (45)] datasets: GSE112474, GSE30881, and GSE41917. GSE112474 is an RNA-seq dataset containing 12 B-cell, one T-cell, three intestinal lymphoma and four healthy lymph node samples. Intestinal lymphoma samples were considered as T-cell lymphoma samples (46). Differential expression analysis of RNA-seq read counts was performed using the R/Bioconductor package DESeq2 (47). B-cell and T-cell lymphoma libraries were compared to healthy lymph nodes separately. Genes with a p-value $\leq 1\times10^{-5}$ were considered differentially expressed. GSE30881 and GSE41917 are gene expression microarray (Affymetrix Canine Genome 2.0) datasets. GSE30881 contains 23 diffuse large b-cell lymphoma lymph node samples and 10 healthy lymph node samples; GSE41917 includes seven B-cell, three T-cell lymphoma and four healthy lymph node samples. CEL files were processed and analyzed with the "simpleaffy" (48) and "affy" (49) R/Bioconductor packages. The robust multi-array average algorithm from the affy package was used for background correction and quantile normalization. Each disease sample group was independently compared to the healthy lymph node sample group. Variance estimators were computed with the empirical Bayes method in the "limma" (50) R/Bioconductor packages. Results were adjusted for multiple testing using the false discovery rate (FDR). Genes with a log_2 fold-change above 2 and an FDR ≤ 0.05 were considered differentially expressed. The two microarray datasets were analyzed independently. Finally, the RNA-seq and microarray DEGs were pooled, removing duplicates. DEGs that could not be assigned to

1 https://ftp.ensembl.org/pub/release-90/gtf/canis_familiaris/Canis_familiaris.CanFam3.1.90.gtf.gz, last accessed July 20, 2023.

2 http://pantherdb.org/, last accessed July 20, 2023.

the chromosomes 1 to 38 or X were filtered out. A total 1,169 DEGs were identified in at least one of the comparisons.

2.8 Key regulators of gene expression in CL patients

The 1,000-bp sequences upstream of the TSS of the aforementioned 1,159 DEGs were searched for a maximum of 10 enriched motifs using MEME v4.11.2 (51) with parameters "-dna -nmotifs 5 -maxsize 500,000." Identified motifs were compared to the JASPAR 2016 CORE vertebrate collection of motifs (52) with TOMTOM v4.11.2 (53) with parameters "-min-overlap 5 -dist pearson -evalue -thresh 10.0" to determine which transcription factor (TF) is likely to bind each motif. The analysis was performed separately for each sample group. A total of 21 TFs were identified as such.

2.9 Network analysis of DEGs in CL patients

The Search Tool for the Retrieval of Interacting Genes/Proteins [STRING, (54)] database v10.0 was used to investigate the interaction partners of the DEGs. Individual canine Ensembl gene identifiers were queried by means of the application programming interface (API). For example, the following URL was used to retrieve the interaction partners of "ENSCAFG00000000068": http://version10.string-db.org/api/psi-mi-tab/interactionsList?identifiers=ENSCAFG00000000068&limit=500&required_score=500&species=9615 (last accessed July 20, 2023). The URL indicates the database, the access type ("api"), the output format ("PSI-MI TAB"), the list of requests (interaction partners for any of the query items), the gene of interest, the maximum number of network nodes (proteins) that are to be returned ("limit"), the threshold of significance to include an interaction ("required_score"), and the species ("9,615," the taxonomy identifier for *Canis lupus familiaris*). After querying, we searched the output for interactions involving the Ensembl protein identifier(s) of the corresponding gene for which the score derived from curated data ("dscore") was greater than 0.5.

2.10 Canine haplotype block map

Genotyping data for 60,968 SNPs in 600 dogs and 10 wolves (55–62) was kindly provided by Adam Boyko (Cornell University). The PLINK tool set v1.90 (63) was used to estimate the canine haplotype block structure. Because of the missing phenotype data, the option "no-phenoreq," which removes the phenotype restriction, was added to the default settings. The coordinates of the haplotype blocks were converted from the assembly version CanFam2 to the assembly version CanFam3.1 using UCSC's LiftOver tool.

2.11 Primer design and synthesis

Primers for generation of amplicons were designed based on sequences with a maximum length of 120 bp centered at the selected SNPs using the Ion AmpliSeq Designer v5.63 (Thermo Fisher Scientific, Waltham, MA, United States).

2.12 Canine lymphoma patient selection

Dogs referred to the Small Animal Clinic of the University of Veterinary Medicine Hannover for diagnostic investigation and treatment for CL between 2008 and 2014 were prospectively considered for enrollment in this study. Diagnosis was conducted based on cytological or histological evaluation of lymph nodes or extranodal lesions such as liver, spleen, and bone marrow. Patients underwent complete staging, consisting of history and physical examination, complete blood cell count, serum biochemistry profile, thoracic radiographs, abdominal ultrasound, cytological evaluation of liver and spleen regardless of their sonographic appearance, and bone marrow aspiration. Clinical staging was based on the World Health Organization (WHO) for canine lymphoma (64). Immunophenotype was determined by flow cytometry. The presence of the CD21 antigen and absence of CD3 antigen was considered diagnostic for B-cell lymphoma. All patients received standard treatment, namely CHOP followed by CCNU (lomustine), with or without L-asparaginase (see (65) for details). Inclusion criteria was a confirmed diagnosis of multicentric B-cell lymphoma. and absence of concomitant diseases that limited study compliance.

2.13 Clinical assessment

Response duration was assessed according to the Veterinary Cooperative Oncology Group (VCOG) consensus document (66). We reported response duration as progression-free survival (PFS), overall survival (OS). PFS was defined as the time from treatment initiation to first relapse; OS was defined as the time from treatment initiation to death from any cause. At the time of sequencing, 22 dogs had died from lymphoma-related causes, and seven were lost to follow-up.

2.14 Sample collection and DNA isolation

Before the first chemotherapeutic administration, blood samples of 29 dogs were collected for routine hematological and biochemical analyses. An aliquot of 200 µL retrieved from residual whole blood of each patient was preserved in EDTA and frozen in −80°C. DNA was extracted using the NucleoSpin Blood Kit (Macherey-Nagel) according to the manufacturer's instructions. DNA quantification was carried out through Qubit 2.0 fluorometry (Thermo Fisher Scientific, Waltham, United States).

2.15 Library preparation and targeted NGS

From each sample, 10 ng of genomic DNA was used to prepare Ion Torrent sequencing libraries. Initial multiplex PCR was carried out at 2 min at 99°C, 18 cycles of 15 s at 99°C, 4 min at 60°C, and held at 10°C. Library quantification was performed via qPCR using Ion Library Quantitation Kit. Library nanosphere coupling and amplification was performed according to standard IonTorrent procedures using Ion OneTouch 2 and Ion OneTouch ES. Single-end sequencing was performed on an Ion Torrent™ Personal Genome Machine™ (PGM™) System using 318 v2 chips and 400 flows (Thermo Fisher Scientific, Waltham, United States).

2.16 Variant calling

The Torrent Suite software v5.4 (Thermo Fisher Scientific, Waltham, United States) was used to demultiplex reads, map the reads to the dog reference genome, and generate run metrics. Specifically, read mapping was performed against the dog reference genome [CanFam3.1[3], (67)] using the Torrent Mapping Alignment Program (TMAP) with default cost values for mismatches (2) and indels (3) and minimum reference similarity (80%). Mapping quality (MAPQ) scores are reported in the Phred-scale.

Reads with mapping quality (MAPQ) below 90 were excluded using SAMtools view v1.10 (68). Duplicate marking was not deemed suitable for amplicon sequencing and thus omitted. Base calling was performed on the remaining reads with Freebayes v0.9.21.7 (69), GATK's Haplotypecaller v4.1.7.0 (70), and BCFtools mpileup and call v1.9 (68). Each sample was processed separately. Reads used as input for Freebayes were realigned with ABRA2 v2.24 (71). Freebayes was run with default parameters; variants called across the entire genome were filtered for those within the amplicon regions with vcftools v0.1.16 (72). BCFtools mpileup was executed with parameters "-d 100,000 -L 100000" to ensure that all available reads were used for variant calling and that regions with high coverage were not skipped during indel calling; in addition, the "-r" parameter was used to restrict variant calling to amplicon regions. The output of mpileup served as input for BCFtools call, which was executed with the multiallelic and rare-variant calling model and parameter "-v" to output variant sites only (i.e., sites at which the sample had a non-reference allele). The reference genome dictionary and index required by GATK Haplotypecaller were generated with picard CreateSequenceDictionary v2.18.29 (73) and GATK IndexFeatureFile, respectively. GATK BaseRecalibrator and ApplyBQSR were used for base quality recalibration; all variants in the Ensembl Variation database[4] were used with the parameter "--known-sites." Finally, GATK Haplotypecaller was run restricting the analysis to the panel amplicons (with the "--intervals" parameter) and with parameter "--max-reads-per-alignment-start" set to 0 to disable read downsampling. The variants called with each of the three variant callers were then filtered with BCFtools view so that only variants with a quality score ≥20 were kept for further analyses and normalized with BCFtools norm to left-align and normalize indels. Finally, BCFtools isec was used with parameters "--collapse both" (to collapse SNPs and indels) and "--nfiles +1"to identify the variants called by 1, 2, and 3 variant callers in each of the samples. Variants called by all three variant callers in at least one sample are subsequently referred to as "pooled." Only sites that were not called variants by any of the three variant callers were considered homozygous for the reference allele.

Pooled variants were annotated with the Variant Effector Predictor (VEP) v109.3 (72, 74).

2.17 Survival analyses

Survival analysis was performed for PFS and OS using the R packages "survminer" v0.4.9 (75), "survival" v3.5–5 (76), and "MASS" v7.3–53 (77). For OS, the seven patients lost to follow-up at the time of sequencing were censored at the latest date of available records.

Univariable Cox regression (78) was performed using the cophx() function of the "survival" package to analyze associations with the covariates "WHO clinical stage," "sex," "neuter status," "chemotherapeutic protocol," and "age at diagnosis." All variables were treated as categorical; "age at diagnosis" was encoded as 1 for "adult" (2–7 years) and 0 for "senior" (8–11 years).

Pooled variants homozygous or heterozygous for the alternate allele in 11 to 18 dogs and homozygous for the reference allele in all other dogs of the study cohort were subjected to survival analysis following the approach from Collett (79). Briefly, we first performed a univariable Cox regression for each variant using the cophx() function of the "survival" package. Next, we included variants with a p-value ≤ 0.5 in a multivariable Cox regression model, and conducted stepwise backward selection with the stepAIC() function of the "MASS" package to select a combination of variants with lowest Akaike Information Criterion (AIC) value. All variants with a p-value ≤ 0.1 in the resulting model were used for multivariable Cox regression with stepwise forward selection of any variables with a p-value ≤ 0.5 in the univariate Cox regression. Variants with a p-value ≤ 0.1 in the resulting model were used for stepwise bidirectional –forward and backward– regression. Variants with a p-value ≤ 0.05 in the final model were considered significant.

3 Results

3.1 Database mining unveiled 482 putative lymphoma-associated canine loci

To identify putative lymphoma-associated loci in the canine genome, we first mined the Online Mendelian Inheritance in Man (OMIM) database (35), the GWAS catalog (36), and PubMed titles and articles for human or canine SNPs (Methods). This Initial search yielded 89, 173, and 228 human SNPs, respectively. Furthermore, we manually reviewed all full text articles about NHL and CL indexed in PubMed, identifying 219 human and three canine SNPs (Methods). In total, this accounted for 592 non-redundant human (Figure 1A) and three canine SNPs. These three canine SNPs were the only SNPs predisposing for canine B-cell lymphoma that could be identified by a GWAS involving 41 cases and 172 controls (80).

To assess the evolutionary conservation of the 592 human SNPs and identify their orthologous canine loci, we computed multiple sequence alignments between 100 bp-long sequences centered at each human SNP and their orthologous sequences in the dog and three additional species' genomes (Methods). Thereby, we found canine orthologs for 524 (89%) human sequences, but discarded one that diverged considerably in length (Methods) and one on pseudo-chromosome "chrUn" (contigs that could not be assigned to any chromosome). From the remaining 522 canine sequences, 43 contained insertions or deletions at the site orthologous to the SNP in the human sequence, and thus were not considered evolutionary conserved. Excluding these 43 sequences yielded 479 putative lymphoma associated canine loci.

Overall, taking into account the three canine SNPs reported in the literature, we discovered 482 putative lymphoma associated canine loci. Of these, 420 (87%) were non-protein-coding.

3 ftp://ftp.ensembl.org/pub/release-90/fasta/canis_familiaris/dna/, last accessed on September 2017.

4 https://ftp.ensembl.org/pub/release-100/variation/vcf/canis_lupus_familiaris/canis_lupus_familiaris.vcf.gz, last accessed on October 25, 2022.

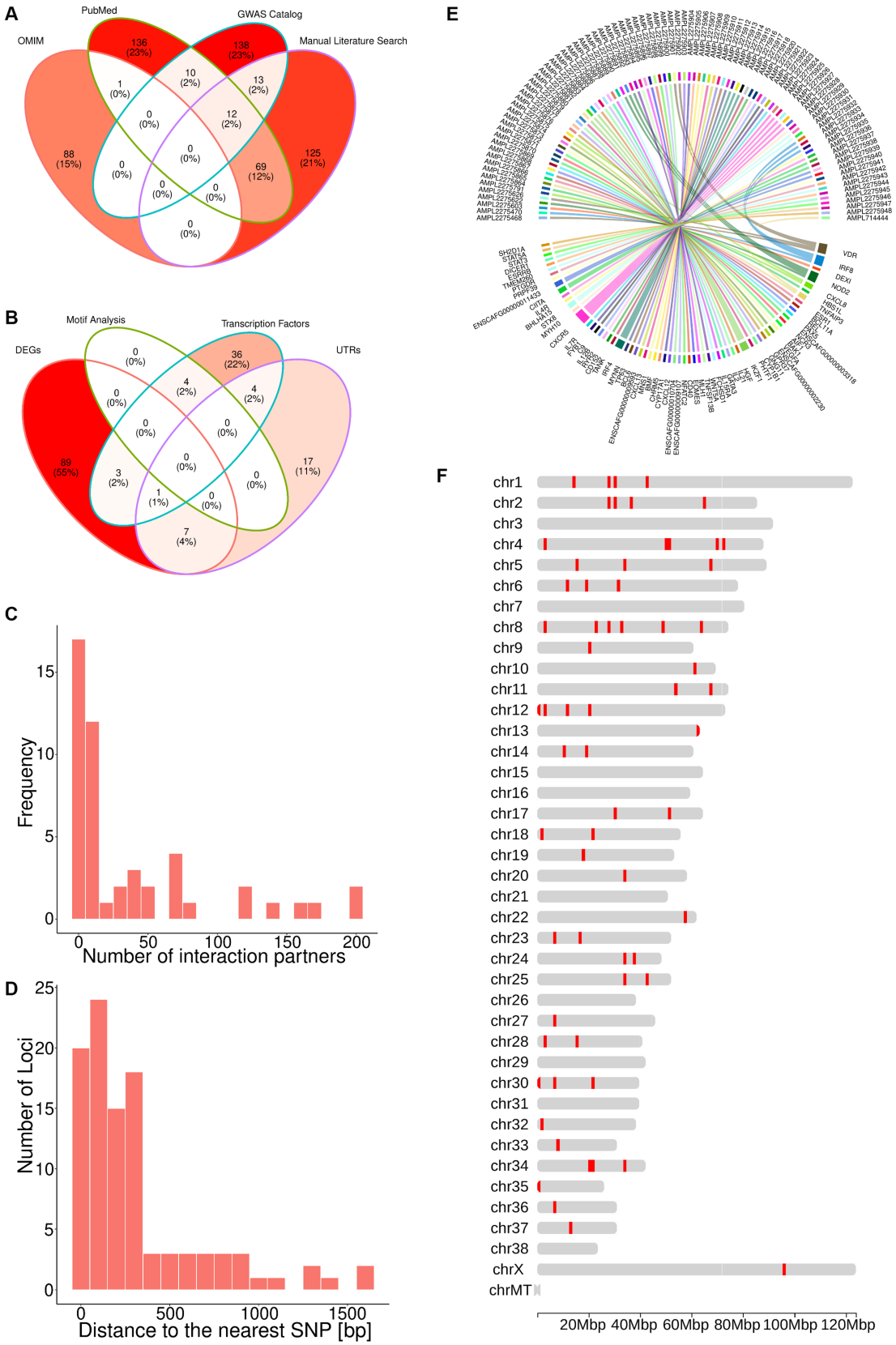

FIGURE 1
The TiHoCL targeted sequencing panel relies on SNPs associated with NHL to detect variants in CL. **(A)** Venn diagram showing the sources of the 592 human lymphoma-associated SNPs; 89 SNPs were retrieved from the OMIM, 173 from the GWAS Catalog, 228 from PubMed, and 219 through manual literature curation. **(B)** Venn diagram displaying how the SNPs from **(A)** were selected based on the different filtering strategies. The brightness of the filling color in **(A,B)** corresponds to the number of SNPs. **(C)** Number of interaction partners for the DEGs. **(D)** Distance between selected 98 potential lymphoma-associated loci and the nearest known SNPs in the canine genome, which was also a filtering criteria for the SNPs. **(E)** Circos plot showing the nearest gene for each target. **(F)** Distribution of the 93 targets across the dog genome.

3.2 Functional genomics and network approaches identified high-priority loci for CL patient management

Since the aim was to develop a fast and relatively inexpensive SNP genotyping panel for diagnosis and monitoring of CL patients, we applied a combination of functional genomics and network approaches to single out approximately 100 most promising putative lymphoma-associated canine loci out of the aforementioned 482.

First, we selected the 29 loci located within untranslated regions (UTRs) and 48 loci for which the nearest upstream or downstream TSS was that of a gene annotated as a TF (Methods). Variants in UTRs may alter transcription binding sites, splicing sites and polyadenylation of mRNAs (80–83). Similarly, variants within or in the neighborhood of TF genes may lead to aberrant TF expression and, in turn, gene dysregulation of almost all known cellular processes related to tumorigenesis (84), which could explain the widespread gene expression dysregulation observed in lymphoma (85, 86).

Next, we examined the loci in the neighborhood of genes found to be differentially expressed in lymphoma in several transcriptomic studies (Methods). We found four loci located in the Vitamin D Receptor gene, which encodes a putative key regulator of gene expression in lymphoma. Because genetic variation in this gene has been associated with lymphomagenesis (87–94), these four loci were also selected for the panel. Further, the nearest TSS to 100 of the loci corresponded to a DEG. Eleven of these loci were also in the neighborhood of a TF gene or within a UTR and, hence, had already been selected for the panel (Figure 1B). From the remaining loci, we selected 29 near protein-coding genes that possessed more than 10 interaction partners (Methods). Genes with a large number of interaction partners are referred to as network "hubs" (Figure 1C), and hubs are typically deemed important, because their perturbations can have major consequences for the regulatory networks to which they contribute (95).

In total, the aforementioned approaches yielded 101 loci in the canine genome representing the orthologous sites of human SNPs. Importantly, these loci are not necessarily polymorphic in the canine genome. In order to associate them with known canine SNPs, we constructed and analyzed a canine haplotype block map (Methods). We observed that the median block size over all individuals was 5,725 bp and that all loci of interest were located at a distance smaller than the median haplotype block size from a known SNP in the canine genome, with a median distance of 195 bp and a maximum of 1,616 bp (Figure 1D). This implies that the loci of interest and their nearest SNPs are very likely to be in linkage disequilibrium, and hence, we chose the latter to represent the former in our panel. Since some of the loci were located in the proximity of the same SNP, the total number of SNPs associated with the loci of interest was 100.

3.3 The TiHoCL sequencing panel targets 93 SNPs in the canine genome

The 100 canine SNPs derived from the multi-step genomic analyses presented above together with the three SNPs that had been reported in the literature to be associated with CL were used for designing the TiHoCL targeted sequencing panel. Using the Ion Ampliseq Designer (Methods) we were able to design primers for 93 of the 103 SNPs (Figures 1E,F). The resulting custom, single pool, multiplexed, PCR-based, NGS library panel comprised 93 target amplicons with an insert size between 220 and 335 bp in length (median = 324 bp), each covering one of the aforementioned 93 SNPs, and had a total size of ~30 kb (Supplementary Table S1). We further refer to the target amplicons as *targets*.

3.4 TiHoCL targeted sequencing panel identifies variants in CL samples

We technically validated the TiHoCL targeted sequencing panel using DNA extracted from a cohort of 29 dogs presenting B-cell multicentric lymphoma (Supplementary Table S2). The most encountered breeds were mixed-breed dogs (6/29, 21%), Bernese Mountain Dog (5/29, 17%), Golden Retriever (2/29, 7%), and Rottweiler (2/29, 7%), but other 14 additional breeds were found (14/29, 48%). There were 18 males and 11 female dogs; half of them were neutered, and half were intact. The age at diagnosis ranged from two to 11 years (mean [SD]: 6.45 [2.21] years). Weight was recorded for 25 dogs; they weighed between 6.8 and 51 kg. According to the WHO clinical stage classification, 2 dogs had stage III disease, 16 dogs stage IV disease, and 11 dogs stage V disease. Six dogs were treated with a 12-week CHOP protocol followed by three doses of CCNU (lomustine), while 23 dogs received the same protocol with the addition of L-asparaginase in the first week. A group of five patients relapsed before the induction phase was finished, and all 29 patients relapsed before the end of the study period (24 months). Univariable Cox regression revealed no association between WHO clinical stage classification, sex, neuter status, treatment protocol, and age at diagnosis and PFS or OS (Supplementary Table S3).

Sequencing run metrics showed good data quality for all samples (Supplementary Table S4). Uniformity of base coverage across samples ranged from 89 to 96%. After quality filtering, the average read length per sample ranged between 306 and 318 bp with an average of 312 bp (Figure 2A). Depending on the sample, the number of reads mapped to targets ranged from 188,712 to 582,628. This corresponds to a percentage of reads on target between 98.50 and 99.99%, confirming adequate target design, library preparation, and sequencing. The median target coverage exceeded 1,000X, with an average over all samples of 2,612X (Figure 2B). Similarly, the median sample coverage was greater than 500X, with only nine exceptions, with an average over all targets of 2,641X (Figure 2C). This is in line with the minimum coverage generally recommended for clinical oncology panels (96). In addition, 77 to 88% of the bases in the targets indicated no strand bias. Because of the satisfying run metrics we continued with functional validation.

To assess the level of polymorphism of the targets we performed variant calling (Methods). To obtain a reliable list of potential variants, we used three different variant callers: Freebayes, GATK Haplotypecaller, and BCFtools mpileup and call, and solely considered variants called by all three variant callers for downstream analysis. The three variant callers were chosen because they are partly based on different approaches and are broadly used in the field (97–100).

Compared to the reference genome, we detected a total of 188 "pooled" (heterozygous or homozygous) variants (Figure 3A, Supplementary Table S5), with each sample exhibiting between 56 and 96 variants (Methods). For 10 of the variants, all 29 samples were homozygous for the same allele (but polymorphic relative to the

10.3389/fvets.2023.1301536

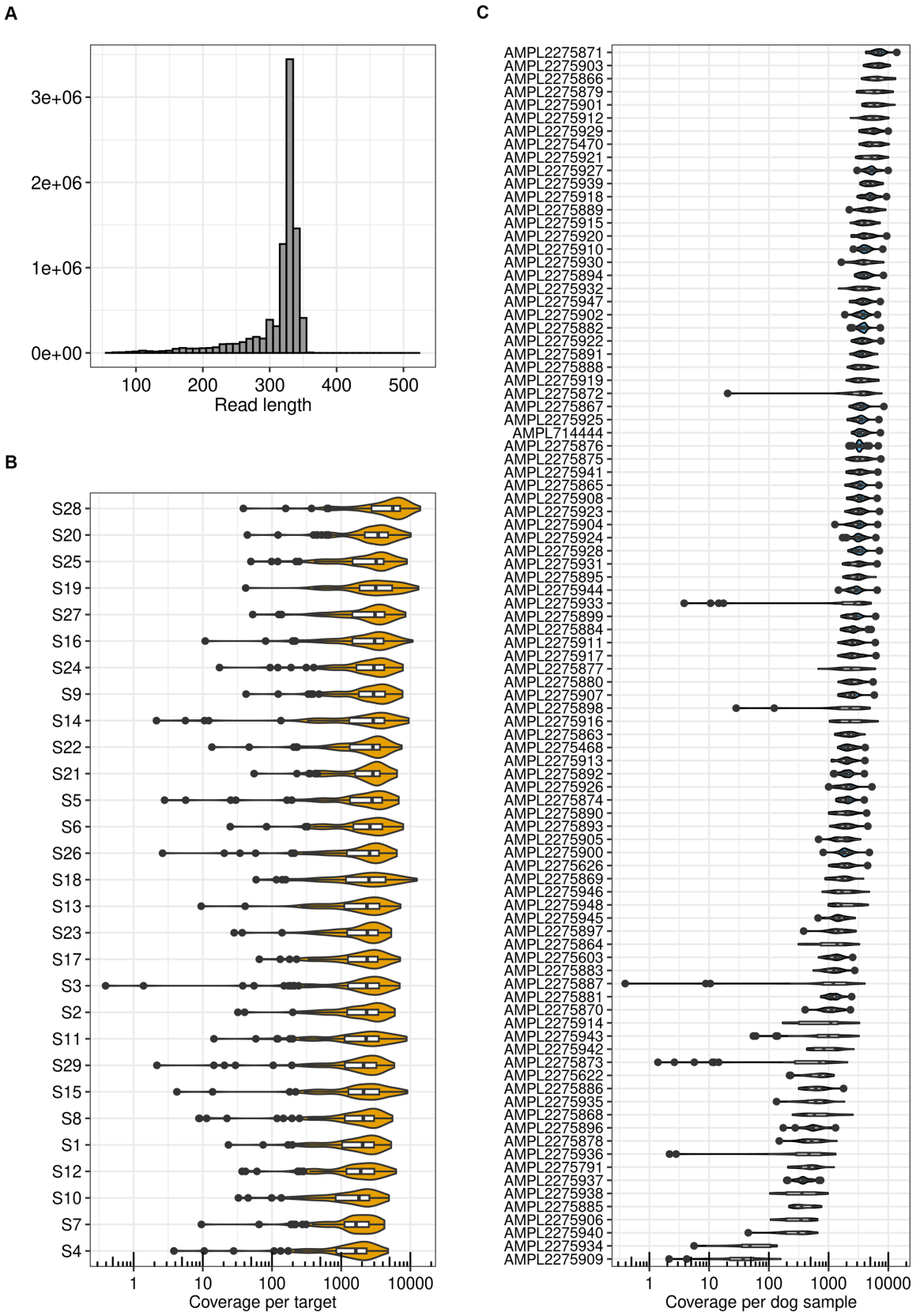

FIGURE 2
TiHoCL targeted sequencing panel achieved good run metrics. **(A)** Distribution of read lengths obtained after mapping quality (MAPQ) filtering with the panel on 29 dog samples. **(B)** Target coverage per sample. The Median coverage was greater than 500X for all samples. **(C)** Coverage of all samples per target. For seven targets the median coverage was smaller than 500X, two of them being outliers with a median coverage smaller than 100X.

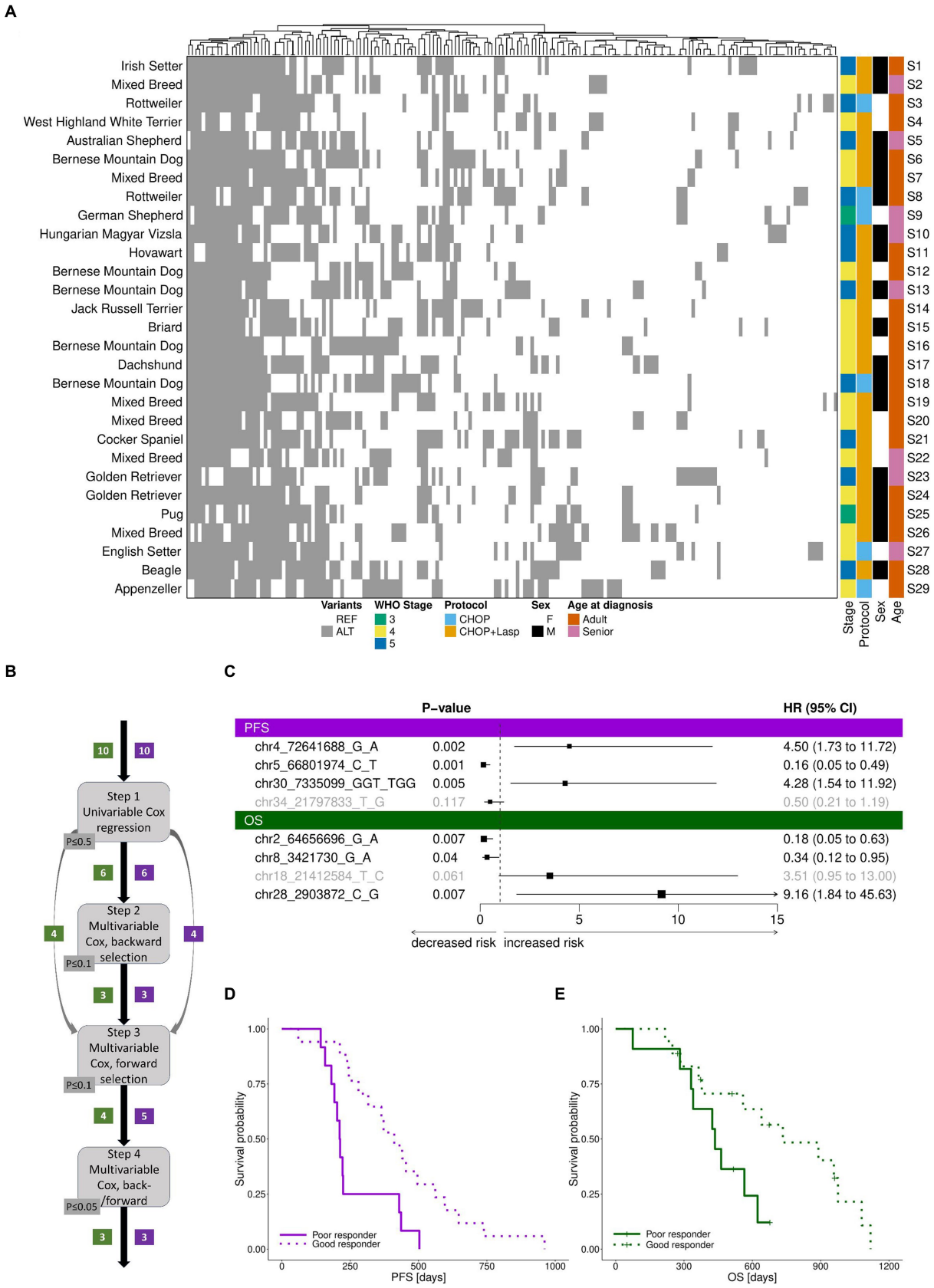

FIGURE 3
TiHoCL targeted sequencing panel enabled detection of natural genetic variation in the study cohort and of variants associated with CL relapse and survival. **(A)** Heatmap of polymorphic "pooled" variants across 29 dog samples. Variants are indicated with respect to the reference genome. REF:

(Continued)

FIGURE 3 (Continued)

reference allele; ALT: alternative allele. No association was observed between WHO clinical stage classification, sex, neuter status, treatment protocol, and age at diagnosis and PFS or OS using univariate Cox regression modeling. Heatmap columns were clustered hierarchically using complete linkage, based on their euclidean distances. Heatmap rows were sorted according to sample number. **(B)** Graphical workflow of the approach applied to identify genetic variants associated with PFS and OS. The numbers in boxes indicate the number of genetic variants selected in the corresponding step for PFS (violet) and OS (green). **(C)** Forest plot of cox regression hazard ratios for analysis of PFS and OS. A significant *p*-value and a hazard ratio smaller than 1 indicate a strong relationship between the variant and a decreased risk of death (OS)/relapse (PFS); a significant *p*-value and a hazard ratio greater than 1 indicate a strong relationship between the variant and an increased risk of death (OS)/relapse (PFS). Non-significant variants in the models are displayed in gray. The variant chr30:7335189G > C, which is placed on the same target and features the same pattern as chr30:7335099GGT > TGG, was removed prior to the analysis, but would also have a positive hazard ratio for PFS. Similarly, the variant chr2:64656755G > A, which is placed on the same target and features the same pattern as chr2:64656696G > A, was removed prior to the analysis, but would also have a negative hazard ratio for OS. **(D,E)** Survival based on samples separated by the median risk scores derived from the final cox models for PFS **(D)** and **(E)** OS.

reference genome sequence). Of the 188 pooled variants, the majority (81%) were SNPs, followed by indels (19%). Consistent with the panel design, the 87% were non-protein coding. From the original 93 SNPs used to design the panel, 70 were also polymorphic relative to the reference genome sequence in the samples. Each target exhibited an average of 0.7 variants per sample.

Of the pooled variants, 12 were seen in 11–19 dogs, and considered polymorphic in the cohort. We checked this list for variants showing the same ALT/REF pattern and removed the duplicated ones for the next step which left 10 variants. These variants were then subjected to multistep survival analysis using Cox proportional hazards regression (Figure 3B). The Cox (proportional hazards or PH) model describes the relation between the (cumulative) incidence of an event of interest (in our case, death for OS and relapse for PFS) and a set of covariates (in our case, genetic variants), and is a commonly used approach for analyzing survival time data in medical research. Using univariate Cox regression analysis, we first identified 6 variants weakly associated with overall survival (OS). Then, we applied multivariable Cox regression analysis to establish a prognostic model. The final model included three variants (Figure 3C). Among them, one was associated with increased risk of death and two were associated with decreased risk of death. For PFS, the same procedure resulted in a model including three variants (Figure 3C), of which two were associated with increased risk of relapse and one was associated with decreased risk of relapse. The final models clearly distinguished patients into poor (median OS: 436 days, median PFS: 212 days) and good responders (median OS: 600 days, median PFS: 411; Figures 3D,E).

To summarize, the TiHoCL targeted sequencing panel showed good run metrics and allowed us to characterize known and novel genetic variation in the cohort. Furthermore, we identified eight variants associated with a decreased and increased risk of relapse or death.

3.5 TiHoCL targeted sequencing panel is labor- and cost-saving

The total costs for sequencing on an Ion Torrent PGM platform, including primer pool, library preparation, emulsion PCR and massively parallel sequencing, are approximately 220 € per sample using the maximum capacity of a 318 v2 chip with 16 samples. Initially, the 318 v2 Chip allows 5×10^6 reads, thus considering the uniform target amplification kinetics of the TiHoCL Panel, 100 samples could be sequenced with coverage of 500X. However, as sequencing efficiency is strongly dependent on chip-loading, the sequencing of 16 to 29 samples per chip will be delivering easily 1,000X coverage of all analyzed bases for less than 250€ per sample in 2 to 5 h.

4 Discussion

The widespread use of targeted sequencing panels in human oncology (101) anticipates new directions for veterinary science, wherein similar panels have the potential to revolutionize our understanding and management of cancer in animals. Recent technological developments illustrate the significance and viability of this. For example, Sirivisoot and colleagues (102) used mass spectrometry to assess variation in 41 loci previously reported to drive lymphomagenesis and associated with genes producing targetable proteins, and found that their panel provides useful prognostic information when screening a cohort of 60 dogs with diffuse large B-cell lymphoma. To move the research to the next level, we demonstrate how functional genomics and network approaches can be combined to select SNPs mined from the literature with the aim of designing a targeted panel for CL. This panel was evaluated in a cohort of 29 CL patients, achieving satisfactory sequencing metrics, capturing natural polymorphisms in the canine population, and exhibiting a promising potential to stratify CL patients.

Although our knowledge about the molecular mechanisms underlying CL is limited, CL resembles the much better researched human disease NHL in many regards, and this can be used to design tools that can help guide treatment decisions in CL patients.

Our panel design primarily relied on knowledge from the literature and the OMIM and GWAS catalog databases. Automatic text mining resulted in 467 SNPs. Manual inspection of the full text of selected PubMed articles produced 125 additional SNPs. In this manner, we identified a total of 592 human and three canine SNPs. These SNPs were then filtered for the most promising candidates using a combination of functional genomics and network biology approaches to build a CL panel including approximately 100 loci. Including a relatively small number of loci in the panel design enabled us to subject samples to deep sequencing—which is considered superior over technologies such as whole-genome sequencing, whole-exome sequencing, and PCR when analyzing multiple mutational spots in parallel (103, 104)—at an affordable cost. On these grounds we specifically prioritized loci within UTRs, near TFs, or near genes that are differentially expressed in CL patients and code for proteins that act as "hubs" in relevant regulatory networks. The TiHoCL panel was technically and preliminary functionally assessed on a cohort of 29 CL patients. Most (90%) amplicons performed well, reaching a coverage of 500X. Furthermore, the panel detected 56 to 96 variants in each CL patient, successfully capturing some of the natural genetic variation within the cohort and paving the way for personalized CL therapy. Highly encouraging, a stringent multistep approach to variable selection and survival analysis on a set of 12 variants detected

in more than 10 patients identified four variants associated with decreased or increased risk of death, and another four, of relapse. These variants merit further investigation for validation as prognostic biomarkers.

Two main limitations should be acknowledged. First, our panel was based on a relatively small number of SNPs extracted from the literature and specialized databases, which only partially represent the scientific knowledge about CL. In particular, we restricted ourselves to two manually-curated, high-quality databases to increase our chances of including high-confident SNPs in the panel design, but those are not the only –or the most comprehensive– databases that can be used as source of disease-associated SNPs. For future panel designs it could be worth considering databases like ClinVar (105), which is focused on disease associated SNPs, COSMIC (105, 106), which is focused on SNPs for cancer research and diagnostics, or dbVar (107), a database for human structural variation to cover also larger rearrangements. In addition, our search did not distinguish between germline and somatic variation, and thus, the SNPs finally included in the panel were not optimized for patient stratification and management, which is the ultimate goal of the TiHoCL panel. Indeed, such restriction appeared excessive in light of the scarce genetic knowledge available for CL. Second, functional assessment of the panel was performed on a cohort of only 29 dogs, which may not represent the full spectrum of CL genetic subtypes and canine breeds. Although our results provide preliminary evidence about the functional capabilities of the TiHoCL panel, we acknowledge that the variants identified as being associated with risk of relapse or death warrant further examination. The decision on the cohort size and diversity was made considering the exploratory nature of our study and the constraints imposed by cost, time and case incidence. While focusing on specific, lymphoma-prone breeds would help reduce genetic background heterogeneity and population structure, leading to more reliable results, this approach could miss important genetic interactions, and would have limited utility for mixed-breed dogs. Breed diversity is also supported by a study of Elvers and colleagues (108) indicating that breeds predisposed to B-cell lymphoma have commonly mutated genes and pathways. A larger cohort would increase the statistical power of the study, and improve the reliability and robustness of our findings. In summary, knowledge transfer to clinical practice would entail leveraging the most current information for panel design and an extensive functional validation of the thereby enhanced TiHoCL panel on a larger and more diverse cohort.

Our design and assessment framework is a proof of principle, representing a foundation upon which other targeted sequencing panels could be built. The version of the TiHoCL targeted sequencing panel presented here can be seen as the first stage in an iterative development model. Our framework streamlines the establishment of refined and updated versions of the TiHoCL panel. As genomic data for lymphoma accumulates, new loci could be periodically incorporated into the panel, especially those arising from progressively more accessible whole-genome sequencing studies, while systematically removing loci with limited potential. With each iteration, the panel's performance is set to increase, enabling novel opportunities for enhancing CL patient management. Our frameworks flexibility ensures its enduring relevance in the constantly evolving landscape of cancer research and propels the field of precision veterinary medicine to new heights.

Because human diseases are generally more thoroughly researched and documented, most genetic databases, including OMIM and the GWAS catalog, are limited to human variants. Moreover, most of the SNPs obtained from the literature were human SNPs. Therefore, the TiHoCL targeted sequencing panel for CL was primarily built based on knowledge acquired for a different, but related disease, namely NHL. This concept is transferable to other cancer types or diseases that share features with diseases in other species, like sarcomas in dogs or urothelial neoplasms in sea lions (109). In contrast to the situation in human medicine, advanced molecular analysis tools for veterinary patients are scarce, limiting clinical options. The reasons for this are manyfold, but economic factors should not be underestimated. Thus, many more resources are invested in human than in dog cancer research. In addition, while many costs in human medicine are often covered by national health care systems, veterinarian costs are normally covered by the animal's owner. Of course, our design framework could also be beneficial for human medicine and have an impact on translational medicine. Clinical trials in dogs with spontaneous cancers must be conducted ethically and in compliance with relevant animal welfare regulations, but offer several advantages compared to studies in humans, including reduced liability and faster approval timelines. CL is a unique spontaneous model for NHL, and therefore, can be used to understand NHL progression and drug resistance processes, as well as to develop new treatments (9, 10, 14). Furthermore, while certain diseases might be rare in humans and hence, difficult to study, they could occur frequently in dogs, providing a unique perspective for research.

The broad application of panels similar to our TiHoCL targeted sequencing panel for CL not only has the potential of improving the health and welfare of all species suffering from cancer, but also contribute to our understanding of the underlying pathology.

Data availability statement

The datasets presented in this study can be found in online repositories. The names of the repository/repositories and accession number(s) can be found at: https://www.ncbi.nlm.nih.gov/, PRJNA1017182.

Ethics statement

The animal studies were approved by the Small Animal Clinic of the University of Veterinary Medicine Hannover, Foundation (Hanover, Germany) in accordance with the German Animal Welfare Guidelines, approved by the Ethics Committee of the State of Lower Saxony, Germany (No. 14/1700). None of the dogs were euthanized due to reasons of sample collection. The studies were conducted in accordance with the local legislation and institutional requirements. Written informed consent was obtained from the owners for the participation of their animals in this study.

Author contributions

SF-S: Writing – original draft, Data curation, Formal Analysis, Methodology, Software, Visualization, Writing – review & editing. CI: Data curation, Writing – original draft, Writing – review & editing. DS: Data curation, Formal Analysis, Software, Writing – review & editing.

NE: Data curation, Writing – review & editing. JG-S: Data curation, Writing – review & editing. WL: Data curation, Writing – review & editing. SK: Investigation, Writing – review & editing. CJ: Funding acquisition, Project administration, Writing – review & editing. IN: Funding acquisition, Methodology, Project administration, Writing – review & editing. LT: Conceptualization, Supervision, Writing – original draft, Writing – review & editing. HM: Conceptualization, Supervision, Writing – original draft, Writing – review & editing.

Funding

The author(s) declare financial support was received for the research, authorship, and/or publication of this article. This study was supported by TU Graz Open Access Publishing Fund.

Acknowledgments

We would like to express our gratitude to all the dog owners who graciously allowed their beloved companions to participate in this study.

Conflict of interest

The authors declare that the research was conducted in the absence of any commercial or financial relationships that could be construed as a potential conflict of interest.

Publisher's note

Supplementary material

The Supplementary material for this article can be found online at: https://www.frontiersin.org/articles/10.3389/fvets.2023.1301536/full#supplementary-material

References

1. Di Resta C, Ferrari M. Next generation sequencing: from research area to clinical practice. *EJIFCC*. (2018) 29:215–20.

2. Sikkema-Raddatz B, Johansson LF, de Boer EN, Almomani R, Boven LG, van den Berg MP, et al. Targeted next-generation sequencing can replace sanger sequencing in clinical diagnostics. *Hum Mutat*. (2013) 34:1035–42. doi: 10.1002/humu.22332

3. Gerstung M, Beisel C, Rechsteiner M, Wild P, Schraml P, Moch H, et al. Reliable detection of subclonal single-nucleotide variants in tumour cell populations. *Nat Commun*. (2012) 3:811. doi: 10.1038/ncomms1814

4. Garcia EP, Minkovsky A, Jia Y, Ducar MD, Shivdasani P, Gong X, et al. Validation of OncoPanel: a targeted next-generation sequencing assay for the detection of somatic variants in Cancer. *Arch Pathol Lab Med*. (2017) 141:751–8. doi: 10.5858/arpa.2016-0527-OA

5. Deshpande A, Lang W, McDowell T, Sivakumar S, Zhang J, Wang J, et al. Strategies for identification of somatic variants using the ion torrent deep targeted sequencing platform. *BMC Bioinformatics*. (2018) 19:5. doi: 10.1186/s12859-017-1991-3

6. Suminda GGD, Bhandari S, Won Y, Goutam U, Kanth Pulicherla K, Son YO, et al. High-throughput sequencing technologies in the detection of livestock pathogens, diagnosis, and zoonotic surveillance. *Comput Struct Biotechnol J*. (2022) 20:5378–92. doi: 10.1016/j.csbj.2022.09.028

7. Petersen JL, Coleman SJ. Next-generation sequencing in equine genomics. *Vet Clin North Am Equine Pract*. (2020) 36:195–209. doi: 10.1016/j.cveq.2020.03.002

8. Lustgarten JL, Zehnder A, Shipman W, Gancher E, Webb TL. Veterinary informatics: forging the future between veterinary medicine, human medicine, and one health initiatives-a joint paper by the Association for Veterinary Informatics (AVI) and the CTSA one health Alliance (COHA). *JAMIA Open*. (2020) 3:306–17. doi: 10.1093/jamiaopen/ooaa005

9. Richards KL, Suter SE. Man's best friend: what can pet dogs teach us about non-Hodgkin's lymphoma? *Immunol Rev*. (2015) 263:173–91. doi: 10.1111/imr.12238

10. Ito D, Frantz AM, Modiano JF. Canine lymphoma as a comparative model for human non-Hodgkin lymphoma: recent progress and applications. *Vet Immunol Immunopathol*. (2014) 159:192–201. doi: 10.1016/j.vetimm.2014.02.016

11. Linschoten M, Kamphuis JAM, van Rhenen A, Bosman LP, Cramer MJ, Doevendans PA, et al. Cardiovascular adverse events in patients with non-Hodgkin lymphoma treated with first-line cyclophosphamide, doxorubicin, vincristine, and prednisone (CHOP) or CHOP with rituximab (R-CHOP): a systematic review and meta-analysis. *Lancet Haematol*. (2020) 7:e295–308. doi: 10.1016/S2352-3026(20)30031-4

12. Mee MW, Faulkner S, Wood GA, Woods JP, Bienzle D, Coomber BL. RNA-Seq analysis of gene expression in 25 cases of canine lymphoma undergoing CHOP chemotherapy. *BMC Res Notes*. (2022) 15:111. doi: 10.1186/s13104-022-06003-5

13. Zandvliet M. Canine lymphoma: a review. *Vet Q*. (2016) 36:76–104. doi: 10.1080/01652176.2016.1152633

14. Marconato L, Gelain ME, Comazzi S. The dog as a possible animal model for human non-Hodgkin lymphoma: a review. *Hematol Oncol*. (2013) 31:1–9. doi: 10.1002/hon.2017

15. Marconato L. The staging and treatment of multicentric high-grade lymphoma in dogs: a review of recent developments and future prospects. *Vet J*. (2011) 188:34–8. doi: 10.1016/j.tvjl.2010.04.027

16. Ansell SM. Non-Hodgkin lymphoma: diagnosis and treatment. *Mayo Clin Proc*. (2015) 90:1152–63. doi: 10.1016/j.mayocp.2015.04.025

17. Zahid U, Akbar F, Amaraneni A, Husnain M, Chan O, Riaz IB, et al. A review of autologous stem cell transplantation in lymphoma. *Curr Hematol Malig Rep*. (2017) 12:217–26. doi: 10.1007/s11899-017-0382-1

18. Zandvliet M, Teske E, Schrickx JA. Multi-drug resistance in a canine lymphoid cell line due to increased P-glycoprotein expression, a potential model for drug-resistant canine lymphoma. *Toxicol In Vitro*. (2014) 28:1498–506. doi: 10.1016/j.tiv.2014.06.004

19. Hedström G, Thunberg U, Amini RM, Zainuddin N, Enblad G, Berglund M. The MDM2 polymorphism SNP309 is associated with clinical characteristics and outcome in diffuse large B-cell lymphoma. *Eur J Haematol*. (2014) 93:500–8. doi: 10.1111/ejh.12388

20. Cordano P, Lake A, Shield L, Taylor GM, Alexander FE, Taylor PRA, et al. Effect of IL-6 promoter polymorphism on incidence and outcome in Hodgkin's lymphoma. *Br J Haematol*. (2005) 128:493–5. doi: 10.1111/j.1365-2141.2004.05353.x

21. Park YH, Sohn SK, Kim JG, Lee MH, Song HS, Kim MK, et al. Interaction between BCL2 and interleukin-10 gene polymorphisms alter outcomes of diffuse large B-cell lymphoma following rituximab plus CHOP chemotherapy. *Clin Cancer Res*. (2009) 15:2107–15. doi: 10.1158/1078-0432.CCR-08-1588

22. Gustafson HL, Yao S, Goldman BH, Lee K, Spier CM, LeBlanc ML, et al. Genetic polymorphisms in oxidative stress-related genes are associated with outcomes following treatment for aggressive B-cell non-Hodgkin lymphoma. *Am J Hematol*. (2014) 89:639–45. doi: 10.1002/ajh.23709

23. Bassig BA, Cerhan JR, Au WY, Kim HN, Sangrajrang S, Hu W, et al. Genetic susceptibility to diffuse large B-cell lymphoma in a pooled study of three eastern Asian populations. *Eur J Haematol*. (2015) 95:442–8. doi: 10.1111/ejh.12513

24. Wang SS, Vajdic CM, Linet MS, Slager SL, Voutsinas J, Nieters A, et al. Associations of non-Hodgkin lymphoma (NHL) risk with autoimmune conditions according to putative NHL loci. *Am J Epidemiol*. (2015) 181:406–21. doi: 10.1093/aje/kwu290

25. Baecklund F, Foo JN, Bracci P, Darabi H, Karlsson R, Hjalgrim H, et al. A comprehensive evaluation of the role of genetic variation in follicular lymphoma survival. *BMC Med Genet*. (2014) 15:113. doi: 10.1186/s12881-014-0113-6

26. He J, Liao XY, Zhu JH, Xue WQ, Shen GP, Huang SY, et al. Association of MTHFR C677T and A1298C polymorphisms with non-Hodgkin lymphoma susceptibility: evidence from a meta-analysis. *Sci Rep*. (2014) 4:6159. doi: 10.1038/srep06159

27. Hernández-Verdin I, Labreche K, Benazra M, Mokhtari K, Hoang-Xuan K, Alentorn A. Tracking the genetic susceptibility background of B-cell non-Hodgkin's lymphomas from genome-wide association studies. *Int J Mol Sci [Internet]*. (2020) 22:122. doi: 10.3390/ijms22010122

28. Ghesquieres H, Slager SL, Jardin F, Veron AS, Asmann YW, Maurer MJ, et al. Genome-wide association study of event-free survival in diffuse large B-cell lymphoma treated with Immunochemotherapy. *J Clin Oncol*. (2015) 33:3930–7. doi: 10.1200/JCO.2014.60.2573

29. Cerhan JR, Wang S, Maurer MJ, Ansell SM, Geyer SM, Cozen W, et al. Prognostic significance of host immune gene polymorphisms in follicular lymphoma survival. *Blood*. (2007) 109:5439–46. doi: 10.1182/blood-2006-11-058040

30. Habermann TM, Wang SS, Maurer MJ, Morton LM, Lynch CF, Ansell SM, et al. Host immune gene polymorphisms in combination with clinical and demographic factors predict late survival in diffuse large B-cell lymphoma patients in the pre-rituximab era. *Blood*. (2008) 112:2694–702. doi: 10.1182/blood-2007-09-111658

31. Armitage JO, Gascoyne RD, Lunning MA, Cavalli F. Non-Hodgkin lymphoma. *Lancet*. (2017) 390:298–310. doi: 10.1016/S0140-6736(16)32407-2

32. Cerhan JR, Slager SL. Familial predisposition and genetic risk factors for lymphoma. *Blood*. (2015) 126:2265–73. doi: 10.1182/blood-2015-04-537498

33. Cerhan JR, Ansell SM, Fredericksen ZS, Kay NE, Liebow M, Call TG, et al. Genetic variation in 1253 immune and inflammation genes and risk of non-Hodgkin lymphoma. *Blood*. (2007) 110:4455–63. doi: 10.1182/blood-2007-05-088682

34. Giannuzzi D, Marconato L, Cascione L, Comazzi S, Elgendy R, Pegolo S, et al. Mutational landscape of canine B-cell lymphoma profiled at single nucleotide resolution by RNA-seq. *PLoS One*. (2019) 14:e0215154. doi: 10.1371/journal.pone.0215154

35. Online Mendelian Inheritance in Man, OMIM®. McKusick-Nathans Institute of Genetic Medicine, Johns Hopkins University (Baltimore, MD). World Wide Web. Available at: https://omim.org/ (Accessed December 5, 2016).

36. MacArthur J, Bowler E, Cerezo M, Gil L, Hall P, Hastings E, et al. The new NHGRI-EBI catalog of published genome-wide association studies (GWAS catalog). *Nucleic Acids Res*. (2017) 45:D896–901. doi: 10.1093/nar/gkw1133

37. NCBI Resource Coordinators. Database resources of the National Center for biotechnology information. *Nucleic Acids Res*. (2018) 46:D8–D13. doi: 10.1093/nar/gkx1095

38. Sherry ST, Ward M, Sirotkin K. dbSNP-database for single nucleotide polymorphisms and other classes of minor genetic variation. *Genome Res*. (1999) 9:677–9. doi: 10.1101/gr.9.8.677

39. Kuhn RM, Haussler D, Kent WJ. The UCSC genome browser and associated tools. *Brief Bioinform*. (2013) 14:144–61. doi: 10.1093/bib/bbs038

40. Notredame C, Higgins DG, Heringa J. T-coffee: a novel method for fast and accurate multiple sequence alignment. *J Mol Biol*. (2000) 302:205–17. doi: 10.1006/jmbi.2000.4042

41. Heinz S, Benner C, Spann N, Bertolino E, Lin YC, Laslo P, et al. Simple combinations of lineage-determining transcription factors prime cis-regulatory elements required for macrophage and B cell identities. *Mol Cell*. (2010) 38:576–89. doi: 10.1016/j.molcel.2010.05.004

42. Aken BL, Achuthan P, Akanni W, Amode MR, Bernsdorff F, Bhai J, et al. Ensembl 2017. *Nucleic Acids Res*. (2017) 45:D635–42. doi: 10.1093/nar/gkw1104

43. Quinlan AR, Hall IM. BEDTools: a flexible suite of utilities for comparing genomic features. *Bioinformatics*. (2010) 26:841–2. doi: 10.1093/bioinformatics/btq033

44. Thomas R, Smith KC, Ostrander EA, Galibert F, Breen M. Chromosome aberrations in canine multicentric lymphomas detected with comparative genomic hybridisation and a panel of single locus probes. *Br J Cancer*. (2003) 89:1530–7. doi: 10.1038/sj.bjc.6601275

45. Edgar R, Domrachev M, Lash AE. Gene expression omnibus: NCBI gene expression and hybridization array data repository. *Nucleic Acids Res*. (2002) 30:207–10. doi: 10.1093/nar/30.1.207

46. Taher L, Beck J, Liu W, Roolf C, Soller JT, Rütgen BC, et al. Comparative high-resolution transcriptome sequencing of lymphoma cell lines and de novo lymphomas reveals cell-line-specific pathway dysregulation. *Sci Rep*. (2018) 8:6279. doi: 10.1038/s41598-018-23207-7

47. Love MI, Huber W, Anders S. Moderated estimation of fold change and dispersion for RNA-seq data with DESeq2. *Genome Biol*. (2014) 15:550. doi: 10.1186/s13059-014-0550-8

48. Wilson CL, Miller CJ. Simpleaffy: a BioConductor package for Affymetrix quality control and data analysis. *Bioinformatics*. (2005) 21:3683–5. doi: 10.1093/bioinformatics/bti605

49. Gautier L, Cope L, Bolstad BM, Irizarry RA. Affy—analysis ofAffymetrix GeneChipdata at the probe level. *Bioinformatics*. (2004) 20:307–15. doi: 10.1093/bioinformatics/btg405

50. Ritchie ME, Phipson B, Wu D, Hu Y, Law CW, Shi W, et al. Limma powers differential expression analyses for RNA-sequencing and microarray studies. *Nucleic Acids Res*. (2015) 43:e47. doi: 10.1093/nar/gkv007

51. Bailey TL, Boden M, Buske FA, Frith M, Grant CE, Clementi L, et al. MEME SUITE: tools for motif discovery and searching. *Nucleic Acids Res*. (2009) 37:W202–8. doi: 10.1093/nar/gkp335

52. Mathelier A, Fornes O, Arenillas DJ, Chen CY, Denay G, Lee J, et al. JASPAR 2016: a major expansion and update of the open-access database of transcription factor binding profiles. *Nucleic Acids Res*. (2016) 44:D110–5. doi: 10.1093/nar/gkv1176

53. Gupta S, Stamatoyannopoulos JA, Bailey TL, Noble WS. Quantifying similarity between motifs. *Genome Biol*. (2007) 8:R24. doi: 10.1186/gb-2007-8-2-r24

54. Szklarczyk D, Franceschini A, Wyder S, Forslund K, Heller D, Huerta-Cepas J, et al. STRING v10: protein-protein interaction networks, integrated over the tree of life. *Nucleic Acids Res*. (2015) 43:D447–52. doi: 10.1093/nar/gku1003

55. Gray MM, Granka JM, Bustamante CD, Sutter NB, Boyko AR, Zhu L, et al. Linkage disequilibrium and demographic history of wild and domestic canids. *Genetics*. (2009) 181:1493–505. doi: 10.1534/genetics.108.098830

56. Boyko AR, Boyko RH, Boyko CM, Parker HG, Castelhano M, Corey L, et al. Complex population structure in African village dogs and its implications for inferring dog domestication history. *Proc Natl Acad Sci U S A*. (2009) 106:13903–8. doi: 10.1073/pnas.0902129106

57. Boyko AR. The domestic dog: man's best friend in the genomic era. *Genome Biol*. (2011) 12:216. doi: 10.1186/gb-2011-12-2-216

58. Boyko AR, Quignon P, Li L, Schoenebeck JJ, Degenhardt JD, Lohmueller KE, et al. A simple genetic architecture underlies morphological variation in dogs. *PLoS Biol*. (2010) 8:e1000451. doi: 10.1371/journal.pbio.1000451

59. vonHoldt BM, Pollinger JP, Earl DA, Knowles JC, Boyko AR, Parker H, et al. A genome-wide perspective on the evolutionary history of enigmatic wolf-like canids. *Genome Res*. (2011) 21:1294–305. doi: 10.1101/gr.116301.110

60. Vonholdt BM, Pollinger JP, Lohmueller KE, Han E, Parker HG, Quignon P, et al. Genome-wide SNP and haplotype analyses reveal a rich history underlying dog domestication. *Nature*. (2010) 464:898–902. doi: 10.1038/nature08837

61. Serres-Armero A, Povolotskaya IS, Quilez J, Ramirez O, Santpere G, Kuderna LFK, et al. Similar genomic proportions of copy number variation within gray wolves and modern dog breeds inferred from whole genome sequencing. *BMC Genomics*. (2017) 18:977. doi: 10.1186/s12864-017-4318-x

62. Hayward JJ, Castelhano MG, Oliveira KC, Corey E, Balkman C, Baxter TL, et al. Complex disease and phenotype mapping in the domestic dog. *Nat Commun*. (2016) 7:10460. doi: 10.1038/ncomms10460

63. Chang CC, Chow CC, Tellier LC, Vattikuti S, Purcell SM, Lee JJ. Second-generation PLINK: rising to the challenge of larger and richer datasets. *Gigascience*. (2015) 4:7. doi: 10.1186/s13742-015-0047-8

64. Owen LN. Classification of tumors in domestic animals [internet]. (1980). Available at: http://apps.who.int/iris/bitstream/handle/10665/68618/VPH_CMO_80.20_eng.pdf;jsessionid=A47651067E1EDA208CAE09C97BA3227B?sequence=1.

65. Simon D, Nolte I, Eberle N, Abbrederis N, Killich M, Hirschberger J. Treatment of dogs with lymphoma using a 12-week, maintenance-free combination chemotherapy protocol. *J Vet Intern Med*. (2006) 20:948–54. doi: 10.1892/0891-6640(2006)20[948:todwlu]2.0.co;2

66. Vail DM, Michels GM, Khanna C, Selting KA, London CA. Veterinary cooperative oncology group. Response evaluation criteria for peripheral nodal lymphoma in dogs (v1.0)--a veterinary cooperative oncology group (VCOG) consensus document. *Vet Comp Oncol*. (2010) 8:28–37. doi: 10.1111/j.1476-5829.2009.00200.x

67. Cunningham F, Allen JE, Allen J, Alvarez-Jarreta J, Amode MR, Armean IM, et al. Ensembl 2022. *Nucleic Acids Res*. (2022) 50:D988–95. doi: 10.1093/nar/gkab1049

68. Danecek P, Bonfield JK, Liddle J, Marshall J, Ohan V, Pollard MO, et al. Twelve years of SAMtools and BCFtools. *Gigascience [Internet]*. (2021) 10:giab008. doi: 10.1093/gigascience/giab008

69. Erik Garrison GM. Haplotype-based variant detection from short-read sequencing [internet]. (2012). Available at: https://arxiv.org/abs/1207.3907.

70. van der Auwera GA, O'Connor BD. *Genomics in the cloud: Using Docker, GATK, and WDL in Terra*. Sebastopol, CA: O'Reilly Media (2020).

71. Mose LE, Perou CM, Parker JS. Improved indel detection in DNA and RNA via realignment with ABRA2. *Bioinformatics*. (2019) 35:2966–73. doi: 10.1093/bioinformatics/btz033

72. Danecek P, Auton A, Abecasis G, Albers CA, Banks E, DePristo MA, et al. The variant call format and VCFtools. *Bioinformatics*. (2011) 27:2156–8. doi: 10.1093/bioinformatics/btr330

73. Picard [Internet]. Available at: http://broadinstitute.github.io/picard/ (Accessed July 20, 2023).

74. McLaren W, Gil L, Hunt SE, Riat HS, Ritchie GRS, Thormann A, et al. The Ensembl variant effect predictor. *Genome Biol*. (2016) 17:122. doi: 10.1186/s13059-016-0974-4

75. Survival [Internet]. Available at: https://cran.r-project.org/web/packages/survival/survival.pdf (Accessed July 20, 2023).

76. Survminer [Internet]. Available at: https://cran.r-project.org/web/packages/survminer/survminer.pdf (Accessed July 20, 2023).

77. MASS [Internet]. Available at: https://www.stats.ox.ac.uk/pub/MASS4/ (Accessed July 20, 2023).

78. Cox DR. Regression models and life-tables. *J R Stat Soc*. (1972) 34:187–202. doi: 10.1111/j.2517-6161.1972.tb00899.x

79. Collett D. *Modelling survival data in medical research*. New York: Chapman & Hall/CRC Press (2023). p. 556.

80. Oleson L, von Moltke LL, Greenblatt DJ, Court MH. Identification of polymorphisms in the 3′-untranslated region of the human pregnane X receptor (PXR) gene associated with variability in cytochrome P450 3A (CYP3A) metabolism. *Xenobiotica*. (2010) 40:146–62. doi: 10.3109/00498250903420243

81. Revathidevi S, Sudesh R, Vaishnavi V, Kaliyanasundaram M, MaryHelen KG, Sukanya G, et al. Screening for the 3'UTR polymorphism of the PXR gene in south Indian breast Cancer patients and its potential role in pharmacogenomics. *Asian Pac J Cancer Prev*. (2016) 17:3971–7.

82. Skeeles LE, Fleming JL, Mahler KL, Toland AE. The impact of 3'UTR variants on differential expression of candidate cancer susceptibility genes. *PLoS One*. (2013) 8:e58609. doi: 10.1371/journal.pone.0058609

83. Jiang Y, Chen J, Wu J, Hu Z, Qin Z, Liu X, et al. Evaluation of genetic variants in microRNA biosynthesis genes and risk of breast cancer in Chinese women. *Int J Cancer*. (2013) 133:2216–24. doi: 10.1002/ijc.28237

84. Jiang W, Mitra R, Lin CC, Wang Q, Cheng F, Zhao Z. Systematic dissection of dysregulated transcription factor-miRNA feed-forward loops across tumor types. *Brief Bioinform*. (2016) 17:996–1008. doi: 10.1093/bib/bbv107

85. Zhai K, Chang J, Hu J, Wu C, Lin D. Germline variation in the 3′-untranslated region of the POU2AF1 gene is associated with susceptibility to lymphoma. *Mol Carcinog*. (2017) 56:1945–52. doi: 10.1002/mc.22652

86. Yang B, Liu C, Diao L, Wang C, Guo Z. A polymorphism at the microRNA binding site in the 3′ untranslated region of C14orf101 is associated with non-Hodgkin lymphoma overall survival. *Cancer Genet*. (2014) 207:141–6. doi: 10.1016/j.cancergen.2014.03.007

87. Gascoyne DM, Lyne L, Spearman H, Buffa FM, Soilleux EJ, Banham AH. Vitamin D receptor expression in Plasmablastic lymphoma and myeloma cells confers susceptibility to vitamin D. *Endocrinology*. (2017) 158:503–15. doi: 10.1210/en.2016-1802

88. Kulling PM, Olson KC, Olson TL, Feith DJ, Loughran TP Jr. Vitamin D in hematological disorders and malignancies. *Eur J Haematol*. (2017) 98:187–97. doi: 10.1111/ejh.12818

89. Purdue MP, Hartge P, Davis S, Cerhan JR, Colt JS, Cozen W, et al. Sun exposure, vitamin D receptor gene polymorphisms and risk of non-Hodgkin lymphoma. *Cancer Causes Control*. (2007) 18:989–99. doi: 10.1007/s10552-007-9039-z

90. Smedby KE, Eloranta S, Duvefelt K, Melbye M, Humphreys K, Hjalgrim H, et al. Vitamin D receptor genotypes, ultraviolet radiation exposure, and risk of non-Hodgkin lymphoma. *Am J Epidemiol*. (2011) 173:48–54. doi: 10.1093/aje/kwq340

91. Kelly JL, Drake MT, Fredericksen ZS, Asmann YW, Liebow M, Shanafelt TD, et al. Early life sun exposure, vitamin D-related gene variants, and risk of non-Hodgkin lymphoma. *Cancer Causes Control*. (2012) 23:1017–29. doi: 10.1007/s10552-012-9967-0

92. Purdue MP, Lan Q, Kricker A, Vajdic CM, Rothman N, Armstrong BK. Vitamin D receptor gene polymorphisms and risk of non-Hodgkin's lymphoma. *Haematologica*. (2007) 92:1145–6. doi: 10.3324/haematol.11053

93. Pezeshki SMS, Asnafi AA, Khosravi A, Shahjahani M, Azizidoost S, Shahrabi S. Vitamin D and its receptor polymorphisms: new possible prognostic biomarkers in leukemias. *Oncol Rev*. (2018) 12:366. doi: 10.4081/oncol.2018.366

94. Gandini S, Gnagnarella P, Serrano D, Pasquali E, Raimondi S. Vitamin D receptor polymorphisms and cancer. *Adv Exp Med Biol*. (2014) 810:69–105. doi: 10.1007/978-1-4939-0437-2_5

95. Helsen J, Frickel J, Jelier R, Verstrepen KJ. Network hubs affect evolvability. *PLoS Biol*. (2019) 17:e3000111. doi: 10.1371/journal.pbio.3000111

96. Koboldt DC. Best practices for variant calling in clinical sequencing. *Genome Med*. (2020) 12:91. doi: 10.1186/s13073-020-00791-w

97. Hwang S, Kim E, Lee I, Marcotte EM. Systematic comparison of variant calling pipelines using gold standard personal exome variants. *Sci Rep*. (2015) 5:17875. doi: 10.1038/srep17875

98. Lefouili M, Nam K. The evaluation of Bcftools mpileup and GATK HaplotypeCaller for variant calling in non-human species. *Sci Rep*. (2022) 12:11331. doi: 10.1038/s41598-022-15563-2

99. Yao Z, You FM, N'Diaye A, Knox RE, McCartney C, Hiebert CW, et al. Evaluation of variant calling tools for large plant genome re-sequencing. *BMC Bioinformatics*. (2020) 21:360. doi: 10.1186/s12859-020-03704-1

100. Stegemiller MR, Redden RR, Notter DR, Taylor T, Taylor JB, Cockett NE, et al. Using whole genome sequence to compare variant callers and breed differences of US sheep. *Front Genet*. (2022) 13:1060882. doi: 10.3389/fgene.2022.1060882

101. Pei XM, Yeung MHY, Wong ANN, Tsang HF, Yu ACS, Yim AKY, et al. Targeted sequencing approach and its clinical applications for the molecular diagnosis of human diseases. *Cells [Internet]*. (2023) 12:493. doi: 10.3390/cells12030493

102. Sirivisoot S, Kasantikul T, Techangamsuwan S, Radtanakatikanon A, Chen K, Lin TY, et al. Evaluation of 41 single nucleotide polymorphisms in canine diffuse large B-cell lymphomas using MassARRAY. *Sci Rep*. (2022) 12:5120. doi: 10.1038/s41598-022-09112-0

103. Lim ECP, Brett M, Lai AHM, Lee SP, Tan ES, Jamuar SS, et al. Next-generation sequencing using a pre-designed gene panel for the molecular diagnosis of congenital disorders in pediatric patients. *Hum Genomics*. (2015) 9:33. doi: 10.1186/s40246-015-0055-x

104. Lih CJ, Sims DJ, Harrington RD, Polley EC, Zhao Y, Mehaffey MG, et al. Analytical validation and application of a targeted next-generation sequencing mutation-detection assay for use in treatment assignment in the NCI-MPACT trial. *J Mol Diagn*. (2016) 18:51–67. doi: 10.1016/j.jmoldx.2015.07.006

105. Landrum MJ, Lee JM, Benson M, Brown GR, Chao C, Chitipiralla S, et al. ClinVar: improving access to variant interpretations and supporting evidence. *Nucleic Acids Res*. (2018) 46:D1062–7. doi: 10.1093/nar/gkx1153

106. Tate JG, Bamford S, Jubb HC, Sondka Z, Beare DM, Bindal N, et al. COSMIC: the catalogue of somatic mutations in Cancer. *Nucleic Acids Res*. (2019) 47:D941–7. doi: 10.1093/nar/gky1015

107. Lappalainen I, Lopez J, Skipper L, Hefferon T, Spalding JD, Garner J, et al. DbVar and DGVa: public archives for genomic structural variation. *Nucleic Acids Res*. (2013) 41:D936–41. doi: 10.1093/nar/gks1213

108. Elvers I, Turner-Maier J, Swofford R, Koltookian M, Johnson J, Stewart C, et al. Exome sequencing of lymphomas from three dog breeds reveals somatic mutation patterns reflecting genetic background. *Genome Res*. (2015) 25:1634–45. doi: 10.1101/gr.194449.115

109. Schiffman JD, Breen M. Comparative oncology: what dogs and other species can teach us about humans with cancer. *Philos Trans R Soc Lond B Biol Sci [Internet]*. (2015) 370:20140231. doi: 10.1098/rstb.2014.0231

frontiers | Frontiers in Veterinary Science

TYPE Brief Research Report
PUBLISHED 12 January 2024
DOI 10.3389/fvets.2023.1309877

OPEN ACCESS

EDITED BY
Vittoria Castiglioni,
IDEXX Laboratories (Germany), Germany

REVIEWED BY
Jorge Del Pozo,
University of Edinburgh, United Kingdom
Diana Giannuzzi,
University of Padua, Italy

*CORRESPONDENCE
Lorenzo Ressel
✉ ressel@liverpool.ac.uk

RECEIVED 08 October 2023
ACCEPTED 04 December 2023
PUBLISHED 12 January 2024

CITATION
Hubbard-Perez M, Luchian A, Milford C and Ressel L (2024) Use of deep learning for the classification of hyperplastic lymph node and common subtypes of canine lymphomas: a preliminary study.
Front. Vet. Sci. 10:1309877.
doi: 10.3389/fvets.2023.1309877

Use of deep learning for the classification of hyperplastic lymph node and common subtypes of canine lymphomas: a preliminary study

Magdalena Hubbard-Perez, Andreea Luchian, Charles Milford and Lorenzo Ressel*

DiMoLab, Institute of Infection Veterinary and Ecological Sciences, Department of Veterinary Anatomy Physiology and Pathology, University of Liverpool, Liverpool, United Kingdom

Artificial Intelligence has observed significant growth in its ability to classify different types of tumors in humans due to advancements in digital pathology technology. Among these tumors, lymphomas are quite common in dogs, despite studies on the application of AI in domestic species are scarce. This research aims to employ deep learning (DL) through convolutional neural networks (CNNs) to distinguish between normal lymph nodes and 3 WHO common subtypes of canine lymphomas. To train and validate the CNN, 1,530 high-resolution microscopic images derived from whole slide scans (WSIs) were used, including those of background areas, hyperplastic lymph nodes ($n = 4$), and three different lymphoma subtypes: diffuse large B cell lymphoma (DLBCL; $n = 5$), lymphoblastic (LBL; $n = 5$), and marginal zone lymphoma (MZL; $n = 3$). The CNN was able to correctly identify 456 images of the possible 457 test sets, achieving a maximum accuracy of 99.34%. The results of this study have demonstrated the feasibility of using deep learning to differentiate between hyperplastic lymph nodes and lymphomas, as well as to classify common WHO subtypes. Further research is required to explore the implications of these findings and validate the ability of the network to classify a broader range of lymphomas.

KEYWORDS

lymphoma, canine, convolutional neural network, Artificial Intelligence, transfer learning

Introduction

Lymphomas are a common type of neoplasm found in canines (1). They typically derive from lymphoid tissues, including lymph nodes, bone marrow, and spleen, although they can develop within any tissue in the body (2). Lymphomas can arise from both B- and T-cell lymphocytes, and the origin of the lymphoma often determines its form (2). B-cell lymphomas are the most common in canines, with approximately 65–75% being B cell and 25–35% being T cell (3). There are multiple forms of lymphomas, the most common being multicentric, with a prevalence of 84% in dogs (2). Other forms include alimentary, mediastinal, and cutaneous, which are much more uncommon (2). Canine lymphomas share many characteristics with human

non-Hodgkin lymphomas (NHL) (4). Due to the similarity between human NHLs and canine lymphomas, the World Health Organization (WHO) system for human NHLs has been adapted to classify the types of canine lymphomas (4). Even though considered outdated by some authors, the updated Kiel classification is also an appropriate and commonly used classification for canine lymphomas (5). According to the WHO classification, three of the most diagnosed lymphomas are diffuse large B cell lymphoma (DLBCL), marginal zone lymphoma (MZL), and lymphoblastic lymphoma (LBL). Diffuse large B cell lymphoma (DLCBL) is the most common form of lymphoma found in dogs, with 79% of subjects being diagnosed with this subtype (3). Histologically, they are defined as having a diffuse pattern with uniformly large nuclei (6). These nuclei are generally round and infrequently cleaved or indented, with a variable mitotic rate (4). Dogs with this type of lymphoma commonly present with generalized lymphadenopathy, and they are typically classified at stages III to V using the WHO system (7). It is unclear if this type of lymphoma is more common in specific breeds. However, some studies indicate that Golden Retrievers, Labrador Retrievers, Bernese Mountain Dogs, and German Shepherds are more frequently affected (6). Marginal zone lymphomas (MZL) are the second most common lymphoma in dogs, with 17% of cases being classified as MZL (3). It is a B-cell lymphoma that is typically found in either the lymph nodes or the spleen (4). They are characterized as having a nodular pattern, with intermediate-sized cells with a central nucleolus and abundant lightly stained cytoplasm compared with other lymphomas (6). Mitoses are prominent only in advanced cases (4). This type of lymphoma is characterized morphologically by its "fading germinal centers," which makes it resemble the marginal zone of a typical lymph node follicle (3). In addition to this, late stage MZL keep their cellular characteristics, but they lose their distinctive nodular pattern (6). This makes it challenging for pathologists to differentiate between this subtype and DLBCL (6). Dogs with this type of lymphoma generally present to the clinic with an enlarged submandibular or cervical lymph node which remains mobile under the skin. Most often, MZLs are present in large-breed dogs (4). Lymphoblastic lymphomas can originate from either B or T cell, although T phenotype is much more frequently found for this type (8). It is a less common lymphoma type if compared with DLBCL or MZL (9). Histologically, they are characterized by having uniformly intermediate-sized nuclei with evenly distributed chromatin, which conceals nuclear detail and a high mitotic rate (4). It is the most aggressive subtype frequently found in practices with dogs presenting with one or more enlarged peripheral lymphnodes (4). The study by Comazzi and Riondato (9) also suggested that this type of lymphoma is more frequently found in boxers. Due to their different morphological characteristics, these three common types of lymphoma represent a good target to explore the ability of Artificial Intelligence to discriminate between them and distinguish a lymphoid neoplastic proliferation (for which they offer common examples) from hyperplastic lymphoid tissue. In fact, reactive lymph node hyperplasia represents the main differential diagnosis for an enlarged lymph node. The most used approach for image classification is deep learning (DL) implemented with convolutional neural networks (CNNs) (10). Deep Learning is a form of machine learning where a neural network's design is influenced by the human brain structure (11) and learns by example directly from the given data. Examples of types of data include images, sound, and text. This form of machine learning is known for achieving very high accuracies in image classification. These networks can achieve high accuracies if trained with a large amount of data and a deep network with multiple layers that allow learning millions of different features (11). Transfer learning is a common method used in DL. In this form of learning, a pre-trained network is selected and used as a starting point to train a network to learn a new task. Specific features are added or swapped out in order to alter the process before the training occurs. This allows the network to build from its previous knowledge and achieve the goal more successfully (12). This is one of the most used methods of training as it is easier to implement and is generally faster as it only involves fine-tuning (13). The use of machine learning and DL, in particular for processing and analyzing digital images in pathology, has become more popular in recent years. This is due to the rise in the use of whole digital slide scanners and an increased interest in digital pathology, allowing image analysis to be approached more freely (14). This project aims to investigate the feasibility of a CNN to distinguish hyperplastic lymph node from lymphoma and classify three common types of canine lymphoma. This is approached using a transfer learning strategy.

Materials and methods

Different cases of lymphoma and reactive hyperplastic lymph node slides were selected from the slides archive of the Department of Veterinary Anatomy Physiology and Pathology, Section of Veterinary Pathology at the University of Liverpool. In total, 4 cases of hyperplastic lymph node, 5 cases for each DLBCL and LBL, and 3 cases of MZL were selected as the classic examples of each category, following the criteria present in the WHO classification (4). All slides were previously stained with hematoxylin and eosin (HE) staining and diagnosed by board-certified pathologists with the use of immunohistochemistry for the determination of the phenotype. Slides were scanned by an Aperio CS2 (Leica Biosystems, Wetzlar, Germany) microscope slide scanner using native 40X magnification. In the preview of the slides, the region of interest (ROI) was cropped, and a final whole slide image (WSI) was generated. The image analysis software QuPath (15) was used to convert all the WSIs into the tiles that would later be selected for training the neural network. For each lymphoma slide, the area of lymphoma was manually annotated as "tumor," while for reactive lymph node, all the lymph node areas (cortex and medulla) were annotated as "lymph node." The automate tab, followed by the script editor, was selected, and a custom script was used, which allowed the creation of non-overlapping tiles and 512x512x3 pixels in size. This was repeated for each type of lymphoma, background areas of the slide, and hyperplastic lymph node slides. Examples of each classification were selected among the large number of tiles generated with this process (range: 2000–18,000 depending on the size of the sample). For each lymphoma, 75 tiles of the best examples of each DLBCL (Figure 1A), LBL (Figure 1B), MZL (Figure 1C), or hyperplastic lymph node (Figure 1D) were manually selected and cross-checked by a board-certified veterinary pathologist (LR), making sure that they would represent morphological criteria mentioned in the WHO classification. For the background, 15 tiles from each slide were also selected from areas without any tissue. These tiles from each slide were then grouped into their classes and put into

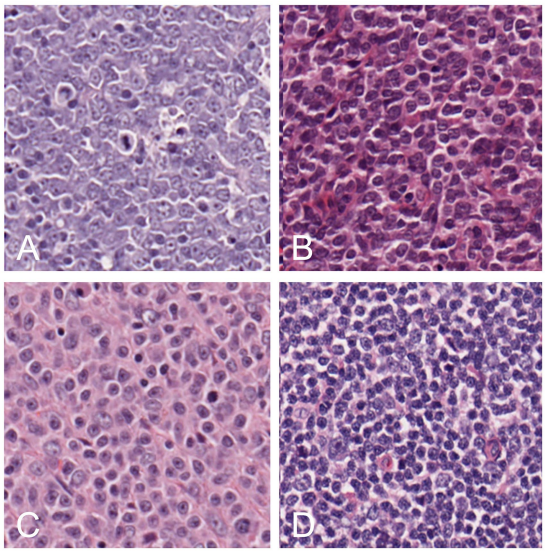

FIGURE 1
Examples of tiles of different classes: DLBCL **(A)**, LBL **(B)**, MZL **(C)**, and hyperplastic lymph node **(D)**.

folders, resulting in 5 folders of tiles, with a maximum of 375 tiles per class to be input into the neural network. The training was achieved in MATLAB (R2022a, Natick, Massachusetts: The MathWorks Inc.) with Deep Network Toolbox installed, and the learning method was transfer learning. GoogLeNet was chosen among possible CNNs as a fast network while retaining high depth and accuracy (19). The last fully connected layer was deleted and replaced by a new untrained fully connected layer, while the output size was changed to five classes (DLBCL, LBL, MZL, Hyperplastic, and Background). The WeightLearnRateFactor and BiasLearnRateFactor values were also increased to 2 to make the overall learning rate faster. All the classified tiles were imported into the network. Among 1,530 tiles, each class was split randomly between training set (70%) and testing set (30%), and a hold-out cross-validation strategy was applied, as the test set was considered a good statistical representation of the whole dataset. The network automatically resized the images to fit with the pre-trained network input layer-accepted format from 512x512x3 to an input size of 224x224x3 (downsampling). Tiles were randomized between training and test every time the network was run. In the training options tab, one of the three solvers (sgdm, adam, or rmsprop) was selected (a solver is the stochastic gradient descent algorithm, which evaluates the learning gradient and updates the network parameters using a portion of the training data during learning of a neural network to reduce loss) as well as an initial learning rate. Once the deep learning training process was completed, the results for the run were recorded. After reviewing and recording the results, the network was rerun with a combination of different solvers and/or initial learning rate values until a combination with high accuracy and low losses was achieved. Once this experiment was run multiple times and the best solver was identified, the data were run in a refining experiment using Bayesian optimization in order to find the best learning rate and get the highest accuracy. In this optimization phase, the solver sgdm was used, and since an initial learning rate of 0.0075 had high accuracy, the learning rate range was set between 0.00075 and 0.075. A maximum limit of 30 trials was selected beforehand. All 30 trials were run. After the optimization was completed, the final hyperparameters are shown in Supplementary Table S1. From this data, graphs showing the training and validation accuracies and losses were generated during the learning process. When the training was completed, the network produced a confusion matrix to show how well it learned the data and areas of errors (performance) on test images (30% of the tiles generated). Parameters such as False Positives, Sensitivity, False negatives, and Specificity for each class were calculated. All the experimental steps were run on a computationally efficient PC equipped with AMD Ryzen Threadripper PRO 3995WX CPU, 6x NVIDIA RTX 3090 GPUs, 1.00 TB of RAM, and Windows 10 Professional. A graphical summary of the workflow of the CNN for training and testing is presented in Figure 2.

Results

The network was run three times for each solver, each with a different learning rate, to work out a rough range of what learning rate would have higher validation accuracy. From these experiments, sgdm solver was able to run with a higher learning rate (0.005) while still having a high validation accuracy of 99.34%. The average accuracy of three different experiments, with a random split of training and testing tiles using sgdm solver with different learning rates, was 97.01% (Supplementary Table S2). Following Bayesian optimization, 18 out of 30 trials were identified as the best, which had a learning rate of 0.0057 (Supplementary Figure S1). The training plots showed that the network converged approximately 50 iterations, reaching accuracy close to 100% for training and test sets before the 250th iteration (Supplementary Figure S2). The results of the test set (examples of DLBCL, LBL, MZL, normal lymph node, and background) presented in a confusion matrix (Table 1) showed that the CNN was able to correctly identify 456 images of the possible 457 of the test set. All the LBL, MZL, hyperplastic, and background tiles were correctly predicted, while 90 examples of DLBCL out of 91 (98.9) were correctly identified, with one example of DLBCL wrongly classified as hyperplastic lymph node. Considering the performance of distinguishing hyperplastic lymph node from lymphoma (DLBCL+LBL + MZL), all the predictions for lymphoma were correct, while a single prediction for hyperplastic lymph node out of 90 was misclassified as lymphoma.

Discussion

The present preliminary work demonstrated that transfer learning applied to the problem of differentiation between hyperplastic and neoplastic lymph node and of classification of lymphoid neoplasms in dogs can be successful. We also demonstrated that our methodological strategy for network learning hyperparameter optimization is promising. Our approach used a hold-out cross-validation approach, as the test set was considered a good statistical representation of the whole dataset. Given the average accuracy of 97.01% in 3 different experiments with different learning rates and randomization of training and test tiles, the network seems to perform consistently. Despite the study being preliminary and focusing primarily on the proof of principle of technique application, at present, there are no studies published

10.3389/fvets.2023.1309877

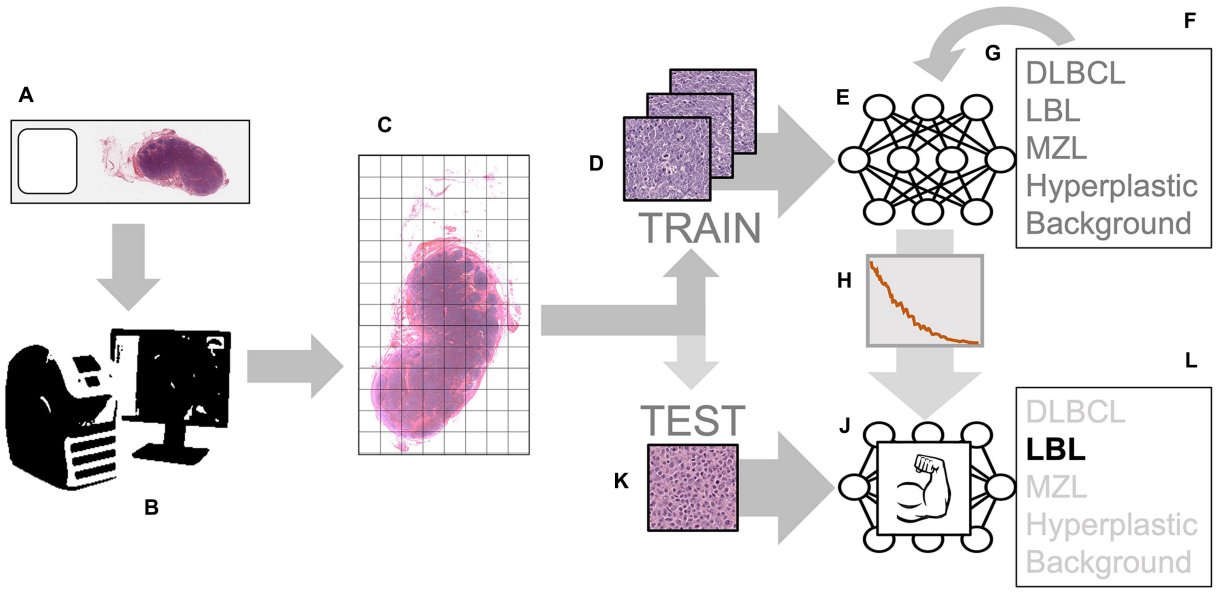

FIGURE 2
Workflow for training and testing the convolutional neural network (CNN): the process starts with histological slides representing various classes, such as DLBCL, LBL, MZL, and Hyperplastic lymph nodes **(A)**. These slides are scanned using a digital slide scanner, creating a Whole Slide Image (WSI) **(B)**. The WSI is divided into smaller tiles **(C)**. These tiles from different classes are used as examples to train the input layer of the CNN **(D)**. The CNN processes the input tiles **(E)** and predicts the probability of each class **(F)**. The error in these predictions is then used to adjust the neuron weights through back propagation **(G)**. This process continues until the error is minimized to an optimal value **(H)**. The result is a "trained" network **(J)**. This trained network can now be used to analyze never-before-seen tiles obtained through the same tiling process **(K)**. When fed with these new tiles, the network accurately predicts the class **(L)**.

TABLE 1 **Confusion matrix for the 5 different classes.**

							FN	SE
True class	Background	**76**					0.0	100.0
	DLBCL		**111**			1	0.9	99.1
	LBL			**112**			0.0	100.0
	MZL				**67**		0.0	100.0
	Hyperplastic					**90**	0.0	100.0
		Background	**DLBCL**	**LBL**	**MZL**	Hyperplastic		
		Predicted class						
	FP	0.0	0.0	0.0	0.0	1.1		
	SP	100.0	100.0	100.0	100.0	98.9		

DLBCL: Diffuse Large B cell Lymphoma; **LBL**: LymphoBlastic Lymphoma; **MZL**: Marginal Zone Lymphoma; **FN**: False negatives; **SE**: Sensitivity; **FP**=False Positives; **SP**=Specificity. FN,SE,FP,SP parameters are expressed as percentages.

applying CNNs to canine lymphomas, while machine learning has been applied only marginally to clinical data in canine lymphomas (16), with no exploration of the potential of CNNs. The accuracy of the network was very high. In the one image where the classification of the network was incorrect, it mistakenly categorized a DLBCL tile as a hyperplastic lymph node tile instead. This is encouraging, as the network was still able to correctly classify 99.1% of the DLBCL tiles presented to it, and it can be argued that a very high-power view of a germinal center in a hyperplastic node can overlap with a small area of DLBCL. Considered within a scenario where the outcome of multiple tiles should achieve the final diagnosis, this error can be considered almost irrelevant. It remains likely a challenge to establish, at tile level, what should be considered as normal lymph node, due to the heterogeneity of the lymph node structure, and likely a segmentation approach at lower magnification, similar to the one we recently approached on a similarly complex anatomical structure (kidney) (17) could prove an effective alternative strategy. However, it is interesting to observe that the network seems to capture features of different classes without the need for a sub-microscopic structure of the lymph node, likely relying on cytological features. One limitation of this preliminary study is, inherently, the low number of slides used in the experiments, which may not simulate fully the complexity of a wider scale experiment using a larger number of cases. However, the suggestion that features are learned at this accuracy rate using a reasonably low number of examples

(hundreds per class) in the context of a transfer learning approach is promising for future larger experiments, which should include a larger and more diverse set of training and test datasets. In an ideal scenario, the development of a comprehensive CNN for facilitating AI-assisted diagnosis on a large scale would also gain significant advantages through the incorporation of diverse slide scanners and staining protocols sourced from various laboratories. It is important to note that, at present, this aspect remains one of the foremost limitations in the context of histology CNN approaches (18). The results from this experiment have shown that the GoogLeNet network is a highly reliable network to use for deep learning when applied to lymphoma histological images using a transfer learning approach. This strongly suggests that the basic patterns learned in the early layers during the original training on 1.2 million images and 1,000 different classes, representative of common objects and living beings (19), represent a solid starting point to refine the features for histological images of canine lymphomas. A smaller number of tiles were used for one of the neoplasm categories (MZL). However, despite this, there was no effect on the performance, suggesting that lymphomas are, in the "eyes" of the CNN, a reasonably homogeneous type of tumors, where a relatively low number of examples can result in successful training. There are many studies that discuss the similarities between canine and human lymphomas and how canine models may contribute to lymphoma research. Due to the similarities and use of a derived classification system, this preliminary result appears likely translational to human medicine. DLBCL lymphomas in both humans and canines are especially similar, as they resemble each other in many features, including that they are the most common subtype of B cell lymphoma in both dogs and humans (6). The workflow proposed uses easily accessible software: MATLAB and QuPath are both open-source software or offer free versions, making them accessible to researchers with limited budgets. Moreover, this software is commonly used in academic settings and has a wide base of users, which promotes transparency, reproducibility, and collaboration within the scientific community. In conclusion, this study has successfully shown that a convolutional neural network can be used to differentiate between hyperplastic and neoplastic lymph nodes, as well as classify specific subtypes of canine lymphomas. The integration of AI-aided diagnosis in canine lymphoma histology, among other areas, promises to revolutionize veterinary diagnostics, but potential benefits and challenges we might encounter as this technology becomes more prevalent are still to be unraveled; therefore further studies are encouraged. These findings not only demonstrate the potential of deep learning in distinguishing canine lymphomas from normal lymph nodes but also lay the groundwork for larger scale studies encompassing different species and a broader range of lymphoma subtypes.

Data availability statement

The raw data supporting the conclusions of this article can be made available by the authors, without undue reservation upon request.

Ethics statement

The animal study was approved by the School of Veterinary Science, University of Liverpool, Ethics Committee. The study was conducted in accordance with the local legislation and institutional requirements (RETH000942).

Author contributions

MH-P: Conceptualization, Data curation, Investigation, Visualization, Writing – original draft, Writing – review & editing. AL: Conceptualization, Investigation, Methodology, Writing – review & editing. CM: Conceptualization, Investigation, Writing – review & editing. LR: Conceptualization, Project administration, Resources, Supervision, Visualization, Writing – review & editing.

Funding

The author(s) declare that no financial support was received for the research, authorship, and/or publication of this article.

Acknowledgments

The authors thank NVIDIA® for the support of GPUs and the Histology Laboratory of the University of Liverpool for the sectioning and staining of the histological slides.

Conflict of interest

The authors declare that the research was conducted in the absence of any commercial or financial relationships that could be construed as a potential conflict of interest.

Publisher's note

Supplementary material

The Supplementary material for this article can be found online at: https://www.frontiersin.org/articles/10.3389/fvets.2023.1309877/full#supplementary-material

SUPPLEMENTARY FIGURE S1
Screenshot of the outcome of the Bayesan optimization, with the chosen experiment 18 highlighted.

SUPPLEMENTARY FIGURE S2
Accuracy (blue) and Loss (red) curves for run 18: the network reached an optimal training due to high accuracy and very low loss.

SUPPLEMENTARY TABLE S1
Hyperparameters after optimization.

SUPPLEMENTARY TABLE S2
Validation accuracy running 3 experiments using 3 different solvers.

References

1. Greenlee PG, Filippa DA, Quimby FW, Patnaik AK, Calvano SE, Matus RE, et al. Lymphomas in dogs a morphologic, immunologic, and clinical study. *Cancer*. (1990) 66:480–90. doi: 10.1002/1097-0142(19900801)66:3<480::aid-cncr2820660314>3.0.co;2-x

2. Vail DM, Pinkerton ME, Young KM. Hematopoietic Tumours In: SJ Withrow, R Page and DM Vail, editors. *Withrow and MacEwen's small animal clinical oncology*. *5th* ed. Saint Louis: Elsevier (2013). 608–78.

3. Richards KL, Suter SE. Man's best friend: what can pet dogs teach us about non-Hodgkin's lymphoma?'. *Immunol Rev*. (2014) 263:173–91. doi: 10.1111/imr.12238

4. Valli VE, San Myint M, Barthel A, Bienzle D, Caswell J, Colbatzky F, et al. Classification of canine malignant lymphomas according to the World Health Organization criteria. *Vet Pathol*. (2010) 48:198–211. doi: 10.1177/0300985810379428

5. Sayag D, Fournel-Fleury C, Ponce F. Prognostic significance of morphotypes in canine lymphomas: a systematic review of literature. *Vet Comp Oncol*. (2017) 19:12–9. doi: 10.1111/vco.12320

6. Avery AC. The genetic and molecular basis for canine models of human Leukaemia and lymphoma. *Front Oncol*. (2020) 10:32. doi: 10.3389/fonc.2020.00023

7. Assumpção ALFV, Jark PC, Hong CC, Lu Z, Ruetten HM, Heaton CM, et al. STAT3 expression and activity are up-regenerated in large B cell lymphoma of dogs. *J Vet Intern Med*. (2017) 32:361–9. doi: 10.1111/jvim.14860

8. Holm F, Hardon T, Clasen-Linde E, Hjorth Mikkelsen L, Heegaard S. B-cell lymphoblastic lymphoma of the nictitating membrane as the first presenting sign in a 2-year-old springer spaniel. *Clin Case Rep*. (2018) 6:2246–51. doi: 10.1002/ccr3.1862

9. Comazzi S, Riondato F. Flow cytometry in the diagnosis of canine T-cell lymphoma. *Front Vet Sci*. (2021) 8:600963. doi: 10.3389/fvets.2021.600963

10. Krizhevsky A, Sutskever I, Hinton GE. Image net classification with deep convolutional neural networks. *Commun ACM*. (2012) 60:84–90. doi: 10.1145/3065386

11. LeCun Y, Bengio Y, Hinton G. Deep learning. *Nature*. (2015) 521:436–44. doi: 10.1038/nature14539

12. Janowczyk A, Madabhushi A. Deep learning for digital pathology image analysis: a comprehensive tutorial with selected use cases. *J Pathol Inform*. (2016) 7:29. doi: 10.4103/2153-3539.186902

13. Pan SJ, Yang Q. A survey of transfer learning. *IEEE Trans Knowl Data Eng*. (2010) 22:1345–59. doi: 10.1109/TKDE.2009.191

14. Madabhushi A, Lee G. Image analysis and machine learning in digital pathology: challenges and opportunities. *Med Image Anal*. (2016) 33:170–5. doi: 10.1016/j.media.2016.06.037

15. Bankhead P, Loughrey MB, Fernández JA, Dombrowski Y, McArt DG, Dunne PG, et al. QuPath: open source software for digital pathology image analysis. *Sci Rep*. (2017) 7:16878. doi: 10.1038/s41598-017-17204-5

16. Koo J, Choi K, Lee P, Polley A, Pudupakam RS, Tsang J, et al. Predicting dynamic clinical outcomes of the chemotherapy for canine lymphoma patients using a machine learning model. *Vet Sci*. (2021) 8:301. doi: 10.3390/vetsci8120301

17. Luchian A, Cepeda KT, Harwood R, Murray P, Wilm B, Kenny S, et al. Quantifying acute kidney injury in an Ischaemia-reperfusion injury mouse model using deep-learning-based semantic segmentation in histology. *Biol Open*. (2023) 12:bio059988. doi: 10.1242/bio.059988

18. Litjens G, Kooi T, Bejnordi BE, Setio AAA, Ciompi F, Ghafoorian M, et al. A survey on deep learning in medical image analysis. *Med Image Anal*. (2017) 42:60–88. doi: 10.1016/j.media.2017.07.005

19. Szegedy C, Liu W, Jia Y, Sermanet P, Reed S, Anguelov D, et al. Going deeper with convolutions. *Proc IEEE Conf Comput Vis Pattern Recognit*. (2015) 1:1–9. doi: 10.1109/CVPR.2015.7298594

frontiers | Frontiers in Veterinary Science

TYPE Original Research
PUBLISHED 07 February 2024
DOI 10.3389/fvets.2024.1328058

OPEN ACCESS

EDITED BY
Monica Sforna,
University of Perugia, Italy

REVIEWED BY
Tim Williams,
University of Cambridge, United Kingdom
Vittoria Castiglioni,
IDEXX Laboratories, Germany

*CORRESPONDENCE
John L. Robertson
✉ drbob@vt.edu;
✉ robersonj@rametrixtech.com
Ryan S. Senger
✉ senger@vt.edu

RECEIVED 26 October 2023
ACCEPTED 18 January 2024
PUBLISHED 07 February 2024

CITATION
Robertson JL, Dervisis N, Rossmeisl J, Nightengale M, Fields D, Dedrick C, Ngo L, Issa AS, Guruli G, Orlando G and Senger RS (2024) Cancer detection in dogs using rapid Raman molecular urinalysis. *Front. Vet. Sci.* 11:1328058. doi: 10.3389/fvets.2024.1328058

Cancer detection in dogs using rapid Raman molecular urinalysis

John L. Robertson[1,2]*, Nikolas Dervisis[3], John Rossmeisl[3], Marlie Nightengale[3], Daniel Fields[3], Cameron Dedrick[3], Lacey Ngo[1], Amr Sayed Issa[2], Georgi Guruli[4], Giuseppe Orlando[5] and Ryan S. Senger[2,6]*

[1]Department of Biomedical Engineering and Mechanics, College of Engineering, Virginia Tech, Blacksburg, VA, United States, [2]Rametrix Technologies Inc., Blacksburg, VA, United States, [3]Virginia Maryland College of Veterinary Medicine, Virginia Tech, Blacksburg, VA, United States, [4]Department of Surgery, VCU Health, Richmond, VA, United States, [5]Department of General Surgery, Wake Forest University School of Medicine, Winston-Salem, NC, United States, [6]Department of Biological Systems Engineering, College of Agriculture & Life Sciences and College of Engineering, Virginia Tech, Blacksburg, VA, United States

Introduction: The presence of cancer in dogs was detected by Raman spectroscopy of urine samples and chemometric analysis of spectroscopic data. The procedure created a multimolecular spectral fingerprint with hundreds of features related directly to the chemical composition of the urine specimen. These were then used to detect the broad presence of cancer in dog urine as well as the specific presence of lymphoma, urothelial carcinoma, osteosarcoma, and mast cell tumor.

Methods: Urine samples were collected via voiding, cystocentesis, or catheterization from 89 dogs with no history or evidence of neoplastic disease, 100 dogs diagnosed with cancer, and 16 dogs diagnosed with non-neoplastic urinary tract or renal disease. Raman spectra were obtained of the unprocessed bulk liquid urine samples and were analyzed by ISREA, principal component analysis (PCA), and discriminant analysis of principal components (DAPC) were applied using the Rametrix®Toolbox software.

Results and discussion: The procedure identified a spectral fingerprint for cancer in canine urine, resulting in a urine screening test with 92.7% overall accuracy for a cancer vs. cancer-free designation. The urine screen performed with 94.0% sensitivity, 90.5% specificity, 94.5% positive predictive value (PPV), 89.6% negative predictive value (NPV), 9.9 positive likelihood ratio (LR+), and 0.067 negative likelihood ratio (LR-). Raman bands responsible for discerning cancer were extracted from the analysis and biomolecular associations were obtained. The urine screen was more effective in distinguishing urothelial carcinoma from the other cancers mentioned above. Detection and classification of cancer in dogs using a simple, non-invasive, rapid urine screen (as compared to liquid biopsies using peripheral blood samples) is a critical advancement in case management and treatment, especially in breeds predisposed to specific types of cancer.

KEYWORDS

Raman spectroscopy, cancer, lymphoma, urine, chemometric, osteosarcoma, mast cell tumor, urothelial carcinoma (UC)

1 Introduction

Cancer is common in dogs. According to the American Veterinary Medical Association "Approximately 1 in 4 dogs will, at some stage in their life, develop neoplasia. Almost half of dogs over the age of 10 will develop cancer" (1). Dogs, their owners, and veterinarians, alike, would benefit from tests that differentiate cancer from other disease processes in sick dogs. Likewise, early detection of cancer, when treatment and care might produce better outcomes, would be especially useful in breeds predisposed to a high incidence of specific cancers (e.g., Boxers, Golden Retrievers, Scottish Terriers, German Shepherd Dogs, many others) (2–4).

Recently, several blood sample-based methods for canine cancer detection were described in the literature. One test relies on next-generation genomic sequencing for detection of cancer-associated cell-free DNA fragments in plasma (5, 6). The reported relative observed sensitivity of the blood-based test was 61.5%, with a specificity of 97.5%, and a positive predictive value of 75% for screening patients. A urine-based assay, based on reactive olfactory chemotaxis to volatile organic molecules and other urine molecule by the nematode *Caenorhabditis elegans*, indicated that this nematode could detect cancer in dogs with 90% specificity in a comparison of 48 samples from dogs with cancer and 30 samples from "non-cancer" dogs (7). Other tests and technologies, specifically for detection of canine lymphoma, (plasma microRNA, circulating small extracellular vesicles) have been described in research literature, but are not in general use or commercially-available for cancer detection/management (8, 9).

Urine is a continuously produced "liquid biopsy" of the urinary tract, as well as the entire body. The production and composition of urine is meticulously regulated in health and can be significantly dysregulated in systemic and renal disease (10). Cancer and cancer treatment is known to dysregulate renal structure and function and affect urine composition. This has been recognized in humans for over a century (11) and in dogs since the mid-1960s (12). Cancers localized in the kidney, such as lymphoma and renal cell carcinoma, physically disrupt renal structure and alter renal function as they grow. In humans, malignancies in other organs (lung, colon, prostate)—that may be releasing tumor neoantigens and soluble products—are associated with inflammatory and reactive changes in renal structure and function (13–16); these have been described as malignancy-associated renal paraneoplastic syndromes (17–21). Potentially nephrotoxic chemotherapies clearly can alter renal structure and function during treatment (22–24).

We developed a novel technology—based on precision Raman spectroscopy of urine—that rapidly (within 15 s) distinguishes among molecular vibrations, caused by non-destructive laser irradiation, in hundreds of discrete molecules in urine samples (25–28). The resulting molecular vibration profile is displayed as a spectral image and can be computationally and statistically analyzed, allowing comparison of spectra from healthy individuals and patients with disease, such as cancer.

We have previously reported on this use of a Raman spectroscopy-based technology (Rametrix®) (29, 30) for detection of chronic kidney disease (31), diabetic nephropathy (32), renal effects of COVID19 disease (33), microhematuria (34), bladder cancer (35), and chronic Lyme disease (36), validated by comparing Raman spectral patterns in more than 3,000 human patient-derived urine samples and more than 200 healthy human individuals with no clinical or laboratory evidence of renal disease.

We hypothesized in this study that Rametrix® technology would detect metabolic, inflammatory, immune, physiologic (i.e., paraneoplastic) effects of cancer—that alter urine composition. This would create unique "spectral fingerprints" composed of signals from hundreds of molecules present in the urine of dogs with cancer.

Here, we report the results of Raman analysis of urine specimens from 100 dogs with one of four common types of cancer (lymphoma, urothelial carcinoma, osteosarcoma, and mast cell tumor), compared with Raman analysis of 89 clinically healthy dogs and 16 dogs with non-neoplastic urinary tract disease. We demonstrate the detection of cancer-associated multimolecular Raman spectral fingerprints, reflecting local and systemic effects of disease. These results indicate this simple, rapid, noninvasive/minimally invasive method could be used as an aid to the detection and management of cancer in dogs.

2 Methods

2.1 Study population

Informed written consent for the collection and analysis of urine specimens was obtained from dog owners, following approved Virginia Tech IACUC protocols 15-217, 17-011, and 19-240. A total of 292 dogs were enrolled and urine specimens were collected at the Veterinary Teaching Hospital [VTH] (Blacksburg, VA), Animal Cancer Care and Research Center [ACCRC] (Roanoke, VA), or from study-affiliated referring veterinarians. Referring veterinarians were asked to provide information on whether samples were from generally healthy dogs (based on physical and current laboratory evaluations) or dogs with a confirmed neoplastic disease (cancer) diagnosis. All dogs enrolled from VTH or ACCRC were referred to these hospitals based on prior physical and laboratory evaluations. Of the samples included in this analysis, 100 were from dogs with a cancer diagnosis [Neoplastic (Cancer) group], 89 were from clinically healthy dogs (Healthy group), and 16 from dogs with non-neoplastic urinary tract (UT) disease (UT Disease group) (see Table 1).

Histologic confirmation of all tumors was done by board-certified/highly experienced veterinary pathologists associated with veterinary diagnostic laboratories. The expertise in histologic (light microscopic) classification and subtyping of subtle variations in canine lymphoma morphology varied among members of the pathologist cohort. Supplementary immunohistochemical (IHC) staining and flow cytometric (FC) analysis was used to provide additional diagnostic information for some dogs with lymphoma (based on owner participation).

As shown in Table 2, of the 100 dogs with neoplastic cancer included in this study, 53 were diagnosed with canine lymphoma (cL). Histologic/IHC/FC classification of cL subtypes was available for 43/53 patients; 33/43 dogs were classified as having B cell lymphoma, 7 dogs as having T cell lymphoma, and 3 dogs were classified as "mixed histotype". Thirty-five (35) dogs with cL were enrolled in multiagent chemotherapy protocols; although, none underwent treatment immediately prior to sample collection. Eighteen (18) other dogs with a diagnosis of cL were not undergoing chemotherapy at the time of sample collection. We did not assess whether or how individual drugs or combinations of them may have affected the results of the

10.3389/fvets.2024.1328058

TABLE 1 Study population demographics.

Study group	# of patients	Age (years) Range Median	% Male/female	% Male/male neutered	% Female/female neutered
Cancer	100	2–14.67 9.04	51.8/48.2	14.0/86.0	4.0/96.0
Healthy	89	0.2–15 6.67	46.8/50.6	56.4/43.6	50.0/50.0
UT Disease	16	0.3–15 7.34	43.8/56.2	71.4/28.6	44.4/55.6

TABLE 2 Urine sample dataset diagnostic classifications.

Urine specimen group (with abbreviation)	Group abbreviation	Number of cases
Neoplastic diseases (cancer)	**Cancer**	100
Canine lymphoma	cL	53
[Lymphoma treated with multiagent chemotherapy]	cL Chemo	[35]
[Lymphoma treated with other/no therapies]	cL No Chemo	[18]
Urothelial carcinoma	UC	18
Mast cell tumor	MCT	17
Osteosarcoma	OS	12
Non-neoplastic urinary tract diseases	**UT Disease**	**16**
Clinically-healthy dogs	**Healthy**	**89**

test. Our study was designed as a first-in-dog pilot of this technology as a screening tool, and assessing the effect of different chemotherapeutics on the performance of the test was not in the scope of this pilot study.

Eighteen (18) patients were diagnosed with urothelial carcinoma (UC), 17 were diagnosed with mast cell tumor (MCT), and 12 were diagnosed with osteosarcoma (OS). Of those with MCT, these included cutaneous/visceral tumors that were not distinguished in this study. Likewise, the OS group included appendicular/axial/extraskeletal tumors. Sixteen (16) patients with non-neoplastic urinary tract disease were also included in the study. These included 8 patients with non-tumor bladder disease (cystitis), 5 with kidney stones, and 3 with developmental anomalies, urethral or prostate-associated stricture/retention. Multiple urine samples were obtained from some patients during therapy, but the number of dogs sampled in this manner was insufficient to correlate with efficacy of treatment (i.e., remission or stable disease). This is now being studied with additional cases.

2.2 Sample collection and preparation

Urine specimens were collected as midstream "free-catch" voided samples in sterile urine specimen cups or with cystocentesis, as needed. The urine collection methods used represent the standard of care in a veterinary medicine. The goal of our study was to test a novel screening tool for use in real world scenario. We believe that using both urine collection methodologies based purely on clinical need (dogs that would not provide urine via free catch would provide it via cystocentesis) reflects common practice and clinical reality. Urine specimens were stored frozen (−30°C) in sterile vials for no longer than 4 weeks.

To prepare for Raman scanning, samples were thawed in an incubator to 27°C and then approximately 1 mL was pipetted into 1.5 mL screw-top silica glass vials (Thermo Fisher Scientific, Waltham, MA) and sealed. Samples were mixed to suspend any dissolved solids and cellular debris and then Raman spectroscopy was performed on the bulk liquid. The Raman signal was acquired through the side of the glass vial.

2.3 Raman spectroscopy

Urine specimens were analyzed by Raman spectroscopy in bulk liquid phase using a PeakSeeker PRO-785 (Agiltron, Woburn, MA) spectrometer equipped with liquid vial holder and fiber optic cable. A 785 nm laser was used with 30s excitation and 30 mW power. The laser spot size was 0.2 mm, and the spectral resolution was 8 cm^{-1}. Spectra were collected over the 200–2,000 cm^{-1} wavenumber range, and 10 replicate spectral scans were obtained per sample. RSIQ software (Agiltron) was used to collect spectra and perform initial processing. Surine™ Urine Negative Control (Dyna-Tek Industries, Lenexa, KS) was used to align Raman spectra and ensure calibration of the Raman spectrometer.

2.4 Chemometric and statistical analysis

Raman spectra were analyzed using the Rametrix® Toolbox v2.0 with MATLAB (R2018a) and the Statistics and Machine Learning Toolbox. The Rametrix® Toolbox v2.0 is available through GitHub and combines elements of the previously published Rametrix® LITE (29) and PRO (30) Toolboxes. The Rametrix® Toolbox was used to read spectral files, average replicates, and truncate spectra to 400–1,800 cm^{-1}. It was also used to apply baselining, wavenumber calibration using Surine™, vector normalization, principal component analysis (PCA), discriminant analysis of principal components (DAPC), multivariate analysis of variance (MANOVA), and cross-validation with leave-one-out analysis. Two different baselining methods were applied with the Rametrix® Toolbox. The first was Savitzky–Golay (hereafter abbreviated SG) using a 3rd order polynomial and frame length of 301. The second was ISREA (37), which inserts a cubic spline along defined nodes (knots) of a spectrum. The locations of the nodes were adjusted to improve baseline fit and

predictive capabilities. We have applied similar methods in several of our previous studies with human urine (32–34, 36).

2.5 Molecular contributions

PCA and MANOVA loading values were used to identify Raman shifts responsible for the clustering separations observed between groups. These loading values were obtained from the PCA and MANOVA procedures performed in MATLAB (using the *pca* and *manova1* functions, respectively). To identify a significant Raman band, a cutoff of 0.3% was used in PCA loadings and 0.2% in MANOVA loadings. These bands were considered significantly different between the groups analyzed, and available Raman libraries (38, 39) were used to determine the biological molecules associated with these bands. We have also applied this approach in other human urine studies and found correlations with available mass spectrometry-based metabolomics data (35, 36).

2.6 Cross-validation and screening method development

To validate the modeling described above, a leave-one-out cross-validation method was used. Here, one sample was left-out from the model-building process with PCA, MANOVA, and DAPC. The completed model was then used to predict the group (e.g., cL, Healthy, UC, etc.) of the left-out sample. The prediction was recorded, and the procedure was repeated until every sample in the dataset had been left-out of model-building once. Given the actual and predicted groups of each sample, the overall performance metrics of: prediction accuracy, sensitivity, specificity, positive-predictive value (PPV), and negative-predictive value (NPV) were calculated according to the definitions and formulas published in Trevethan (40). In addition, the resulting urine screen positive and negative likelihood ratios (LR+ and LR−, respectively) were calculated (41) and included as performance metrics.

2.7 Study targets for hypothesis testing

This study sought to answer the following questions:

A Can Raman spectroscopy detect differences in the urine metabolomes of dogs with cancer from healthy dogs or those with other non-neoplastic urinary tract disease?
B Can Raman spectroscopy of canine urine be used to distinguish between canine lymphoma (cL), urothelial carcinoma (UC), osteosarcoma (OS), and mast cell tumors (MCT)?
C Does the presence of chemotherapeutic agents impair or influence the urine screen?
D Can Raman spectroscopy of canine urine be used to identify the presence of non-neoplastic urinary tract disease?

These questions were used to compile the overall screening test flow diagram for canine cancer and non-neoplastic urinary tract diseases shown in Figure 1. It is important to note that the urine screening test described here is intended to supplement established gold-standard testing methods, physical exams, and treatment methods.

3 Results

3.1 Procedural and computational approach

Scanning of individual urine specimens was accomplished in less than five (5) minutes per sample (multiple laser scans), with no sample preparation required. Urine specimens were aliquoted into 1.5 mL borosilicate glass vials and then scanned. The overall procedure from Raman scanning to obtaining medical information about a urine sample is shown in Figure 2. Once implemented in practice, the spectral processing, baselining, and chemometric calculations associated with Rametrix® were near-instantaneous.

Following the acquisition of a urine Raman spectrum, it was transformed by baselining (Figure 2). This allowed removal of background fluorescence and normalization of the Raman signal. In this study, we used two methods for this: (i) Savitzky–Golay (SG) and (ii) ISREA. SG is a widely known algorithm throughout analytical chemistry, and ISREA is a relatively new development (37). Where SG preserves the entire Raman spectrum, ISREA can amplify regions of spectra containing disease-related information, while minimizing conserved regions. This has served to improve prediction accuracy for spectra of unknown samples in previous studies (32, 33, 36). Results obtained when using ISREA are presented here, and results obtained when using SG are given in the Supplementary material.

Following baselining, chemometric models were produced using PCA, MANOVA, and DAPC. The goal of chemometric modeling was to associate entire spectra (composed of signals from hundreds/thousands of molecules) with a disease condition (e.g., cancer, cL, UC, etc.). In doing this, a spectral "fingerprint" was identified for a specific disease. This has been shown to identify a disease in urine without quantifying all molecules of the underlying metabolome (25, 36, 42–45).

In PCA and DAPC models (Figure 2), each baselined spectrum was reduced to a single data point. Clustering revealed the similarities or differences among the spectra of groups of samples, as with Raman spectroscopy, the spectrum of a sample is representative of its metabolome. Following the building of PCA and DAPC models, the models were cross-validated with leave-one-out analysis, as described previously. Its identity (e.g., a member of the cL group, Healthy group, etc.) was determined and compared to its actual classification. From these calculations, the performance metrics (accuracy, sensitivity, specificity, PPV, NPV, LR+, and LR−) (40, 41) of the Rametrix® urine screening procedure were derived and reported.

3.2 Raman spectra

Raman spectra for the cL, UC, OS, MCT, UT Disease, and Healthy groups are shown in Figure 3. The spectra for all Surine™ samples analyzed throughout the study are also shown here. In all spectra, color lines represent the average spectrum of the group. The shaded grey region represents the total deviation observed at each Raman

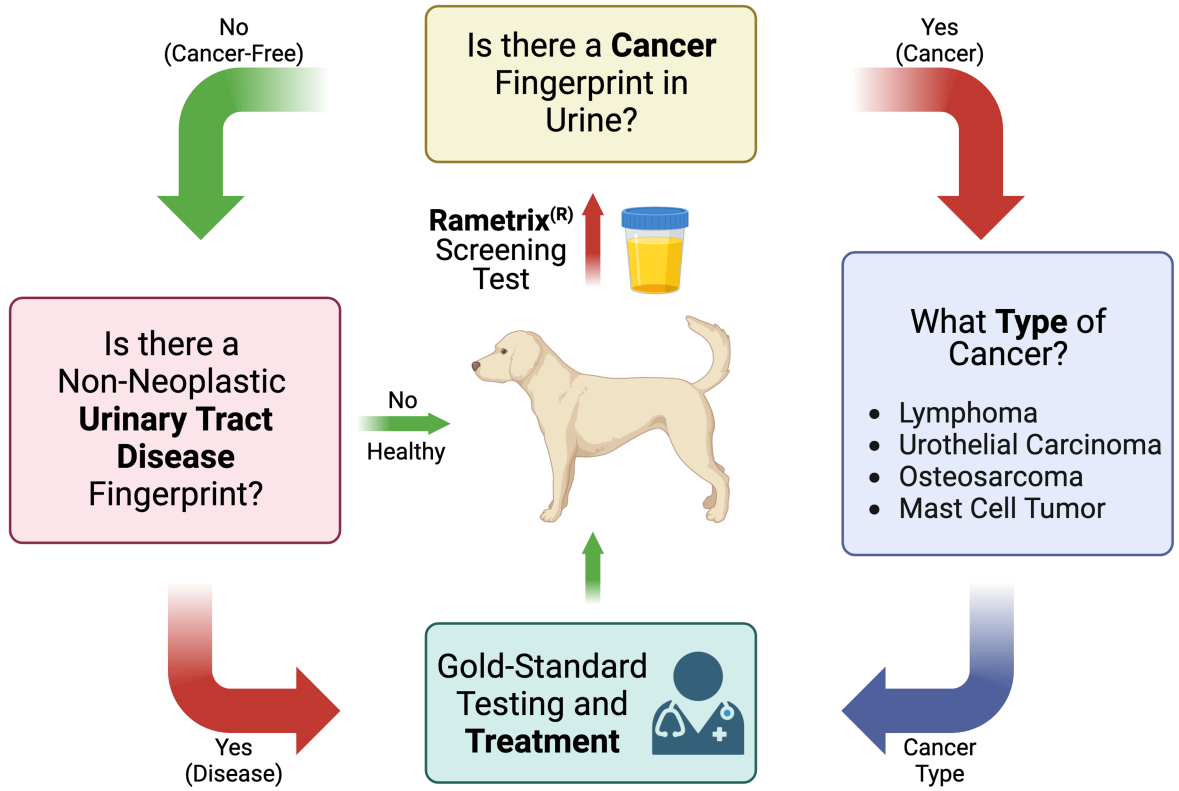

FIGURE 1
Flow diagram of the Raman spectroscopy-based canine urine screen for cancer, cancer type, and other non-neoplastic urinary tract diseases.

shift (or wavenumber). This helps infer a total amount of variability observed among samples. For example, relatively little variability was observed among the 18 samples and scans of Surine™ (Figure 3) acquired. These results affirmed the good working order and calibration of the Raman spectrometer throughout the study.

For samples of the neoplastic (Cancer) disease group (cL, UC, OS, and MCT), a region of relatively high variability was observed in the Raman shift region 1,200–1,400 cm^{-1}. This region is routinely dominated by amide Raman bands associated with β-sheet structures and collagen (among others) (38). Upon visual inspection of spectra, many similarities and differences were noted. The chemometric analysis with the Rametrix® Toolbox was used to determine which of these gave rise to unique spectral fingerprints that could be used to determine the identity of an unknown urine specimen. This was done by addressing the four study questions identified earlier.

3.3 Can Raman spectroscopy detect differences in the urine metabolomes of dogs with cancer from healthy dogs or those with other non-neoplastic urinary tract disease?

This addresses the first question in Figure 1 (Is there a cancer fingerprint in [canine] urine?). Urine Raman spectra of the Cancer group were compared against the Healthy and UT Disease groups (both cancer-free) using the Rametrix® Toolbox. Chemometric models were built, as shown in Figure 2, to extract a unique spectral fingerprint (s) associated with cancer in dogs. The model was cross-validated with leave-one-out analysis, as described previously, to produce a urine screening model for cancer. The performance metrics (accuracy, sensitivity, specificity, PPV, NPV, LR+, and LR−) are given in Table 3. All percentage-based metrics exceeded 90% (except NPV at 89.6%). The LR+ was 9.9, and the LR− was 0.067. It is noted that an LR+ > 10 and LR− < 0.1 have been identified as "very useful in establishing or excluding a diagnosis" (41). The ISREA nodes used are given in Supplementary Table S1, and performance metrics when using SG are given in Supplementary Table S2. ISREA baselining provided an advantage over SG in extracting a unique spectral fingerprint for cancer from canine urine. For example, the overall accuracy with ISREA was 92.7% (Table 3) and 85.1% with SG (Supplementary Table S2). The plots for ISREA baselined spectra, PCA, and MANOVA testing are shown below in Figure 4. In Figure 4C, the results shown are the predictions when each sample was treated as an unknown, and the remainder of the samples were used to build the predictive model.

The PCA and MANOVA loadings were also investigated to determine which Raman bands were responsible for comprising the cancer fingerprint in canine urine. Here, the top 27 loadings were investigated. Of these, 11 were associated with Raman bands present in both PCA and MANOVA loadings. One was assigned, according to Talari et al. (38) and Movasaghi et al. (39), to phosphatidylinositol (576 cm^{-1}) and six were associated with protein (notably collagen) (621, 1,011, 1,160, 1,260, 1,313, 1,344 cm^{-1}). In addition, two bands

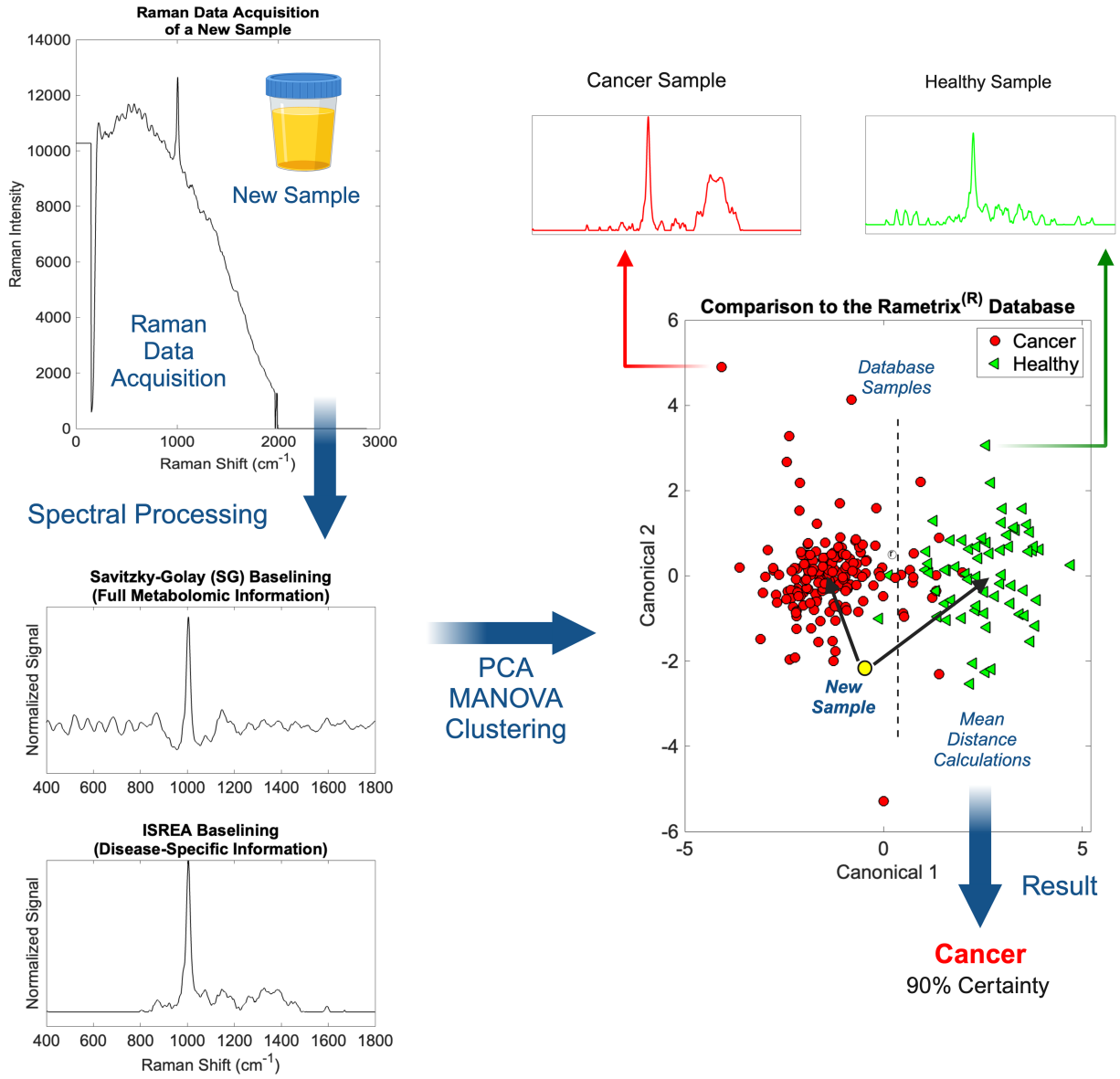

FIGURE 2
An overview of Raman spectral processing and Rametrix® computations with ISREA and SG baselining.

were associated with fatty acids and lipids (1,300 and 1,313 cm^{-1}), one with glucose (1,344 cm^{-1}), and three bands were undefined (685, 983, 1,644 cm^{-1}). Notable among the MANOVA loadings included assignments for red blood cells (991 cm^{-1}) (46) and malignant tissues (1,450 cm^{-1}) (47, 48).

3.4 Can Raman spectroscopy of canine urine be used to distinguish between canine lymphoma (cL), urothelial carcinoma (UC), osteosarcoma (OS), and mast cell tumors (MCT)?

Next, we sought to determine if Rametrix® could distinguish between the different cancer types. This is shown in Figure 1, where cancer type would be determined should a sample screen positive for cancer (see the previous section). To do this, a particular cancer group (e.g., cL) was analyzed against the combination of the other cancer groups (e.g., UC + OS + MCT) do determine if a unique spectral fingerprint existed for that particular cancer. Results are shown in Table 3 (and in Supplementary Table S2 for SG baselining). UC was the most recognizable cancer, with all prediction metrics exceeding 83%. As outlined in Trevethan (40) and Ranganathan and Aggarwal (41), the suitability of a screening method is determined by all of its percentage-based performance metrics (accuracy, sensitivity, specificity, PPV, and NPV) as well as LR+ and LR−. Thus, when considering a Rametrix® urine screen for UC, we do so by the minimum percentage-based metric (sensitivity and PPV of 83.3%) even though other metrics (specificity and NPV) achieved 96.3%. This helps evaluate cases, such as OS, which had a similar overall accuracy to UC (92.0% vs. 94.0%) but had a minimal metric of 58.3% (sensitivity). This is also apparent in LR+ and LR− values, but these

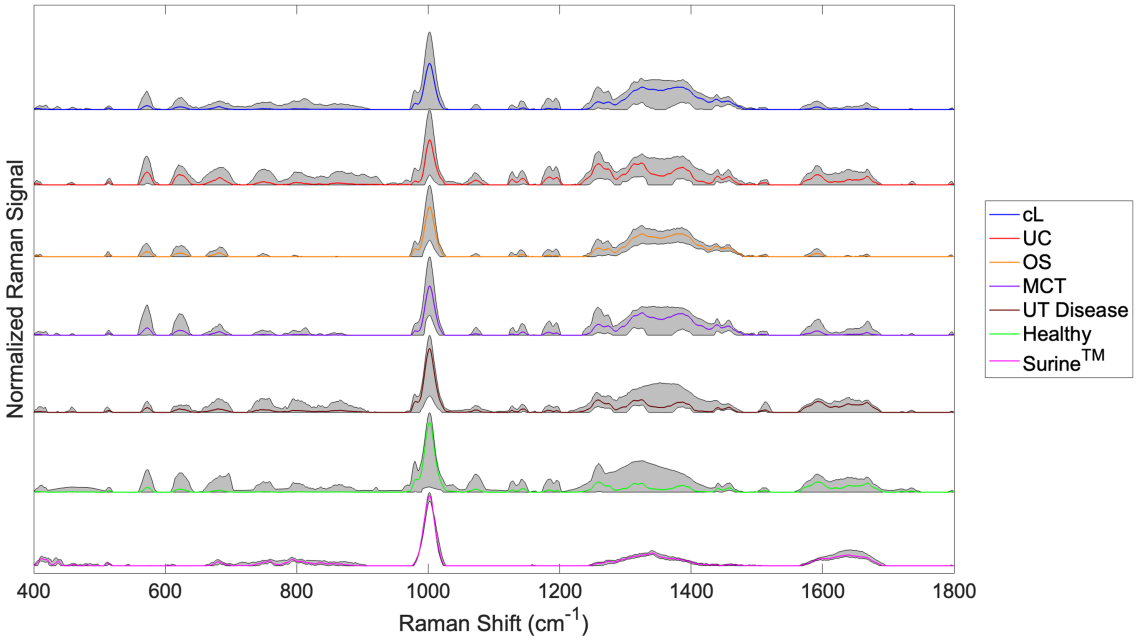

FIGURE 3
Urine Raman spectra for the canine lymphoma (cL), urothelial carcinoma (UC), osteosarcoma (OS), mast cell tumor (MCT), non-neoplastic urinary tract disease (UT Disease), healthy dogs, and Surine™ groups defined in Table 2. Color lines represent the average group spectrum, and shaded regions show the range of the Raman signal for the group. All spectra were truncated to 400–1,800 cm^{-1}, baselined with SG and vector normalized.

TABLE 3 Prediction metrics for urine screens distinguishing Group 1 from Group 2.

Group 1	Group 2	Accuracy (%)	Sensitivity (%)	Specificity (%)	PPV (%)	NPV (%)	LR+ (Group 1)	LR− (Group 2)
Cancer	UT Disease + Healthy	92.7	94.0	90.5	94.5	89.6	9.9	0.067
cL	UC + OS + MCT	71.0	69.8	72.3	74.0	68.0	2.5	0.42
UC	cL + OS + MCT	94.0	83.3	96.3	83.3	96.3	22.5	0.17
OS	cL + UC + MCT	92.0	58.3	96.6	70.0	94.4	17.1	0.43
MCT	cL + UC + OS	81.0	52.9	86.8	45.0	90.0	4.0	0.54
cL	Healthy	100	100	100	100	100	Inf*	0
UC	Healthy	95.3	88.9	96.6	84.2	97.7	26.1	0.11
OS	Healthy	100	100	100	100	100	Inf	0
MCT	Healthy	98.1	88.2	100	100	97.8	Inf	0.12
cL (No Chemo)	cL (Chemo)	73.6	82.8	55.6	78.4	62.5	1.86	0.31
UT Disease	Healthy	93.3	68.8	97.8	84.6	94.6	31.2	0.32

*Inf, infinite due to division by zero.

calculated values incorporate sensitivity and specificity only. Thus, the screening test for UC was considered superior to that of OS. This is likely a reflection of the direct interaction of urothelial carcinoma and cancer associated pathology (local inflammatory reaction and bleeding) with urine sampled. The screen for cL had a minimal metric of 68.0%, and that for MCT had a minimal metric of 52.9%.

The individual cancers were also tested against the Healthy group. These results are also given in Table 3 and Supplementary Table S2. Here, the minimal metrics for cL, UC, OS, and MCT were 100%, 84.2%, 100%, and 88.2%, respectively. This suggests that when screening for one particular type of cancer, in the absence of any non-neoplastic UT diseases, more effective urine screens exist.

3.5 Does the presence of chemotherapeutic agents impair or influence the urine screen?

It was necessary to show that chemotherapeutic agents in the urine of cancer patients were not responsible for the cancer spectral fingerprint detected earlier. To verify our result, we compared the cL Chemo group (cL patients receiving chemotherapeutics) to the cL No Chemo group (cL patients receiving treatment not involving chemotherapeutics). Again, the prediction metrics of Rametrix® urine screen are given in Table 3 and Supplementary Table S2. As shown previously, the minimal metric for cancer detection was 89.6% (NPV).

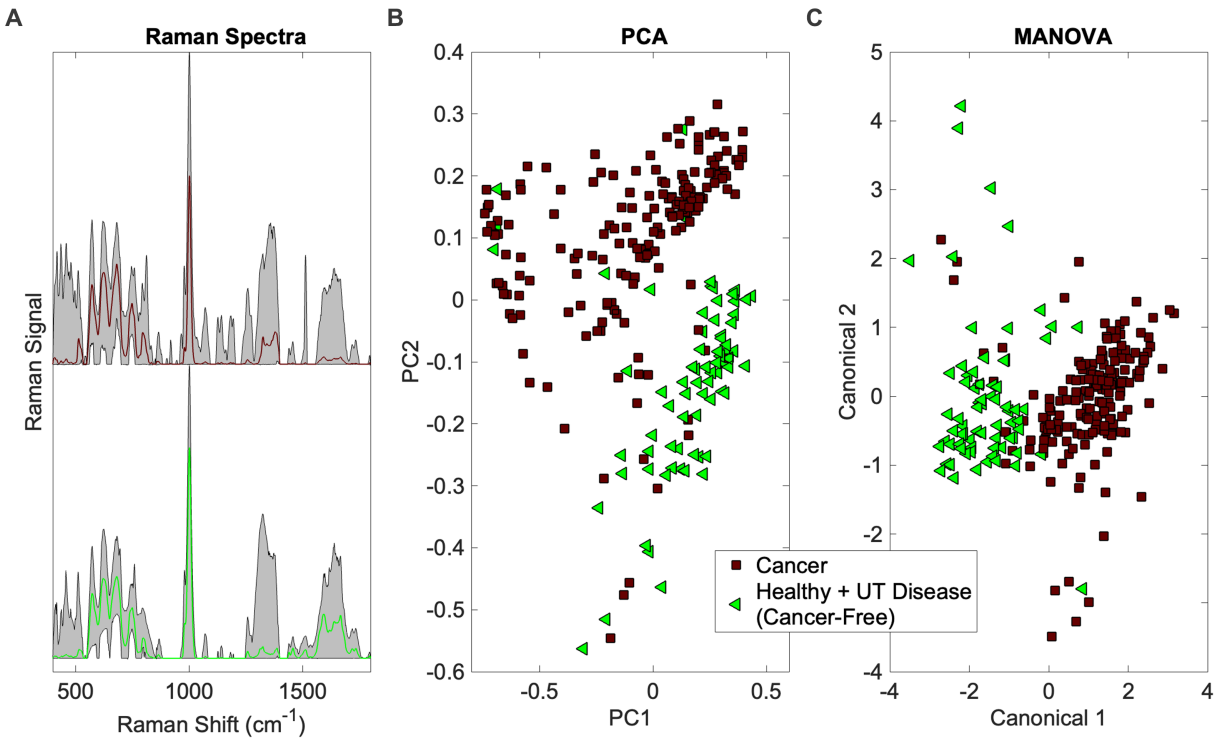

FIGURE 4
Identification of the cancer spectral signature in canine urine. **(A)** Raman spectra (averaged spectrum in color with total range shaded), **(B)** PCA, and **(C)** MANOVA clustering.

In distinguishing the groups cL Chemo from cL No Chemo, the minimal metric was 55.6% (specificity). In addition, the overall accuracies of the screens were 92.7% and 73.6% for cancer and chemotherapeutic detection, respectively. Furthermore, spectral plots (see Supplementary Figure S1) appear nearly identical for the cL Chemo and cL No Chemo groups. Because of this, we conclude cL (and likely other cancers) has/have a spectral fingerprint that is independent of chemotherapeutics (or their break-down products) that might reside in the urine. This clearly will require further study with a larger number of dogs undergoing sequential urine collection during chemotherapy.

The PCA and MANOVA loadings were also investigated to learn which Raman bands are significant in separating the cL No Chemo and Healthy groups. Unique Raman bands were sought that did not appear in the previous cancer fingerprint. There were 10 unique loadings investigated. Of these, four were related to nucleic acids (particularly cytosine) (1,287, 1,293, 1,325, 1,423 cm^{-1}). Three were related to protein (700, 1,602, 1,660 cm^{-1}), and one was related to porphyrin (1,620 cm^{-1}) (49). The malignant tissue band (1,450 cm^{-1}) was recognized in this analysis. In addition, numerous bands were recognized in the cL spectral signature that coincided with the general cancer signature discussed earlier.

3.6 Can Raman spectroscopy of canine urine be used to identify the presence of non-neoplastic urinary tract disease?

As shown in Figure 1, if a urine specimen screened negative for cancer, it would be screened further for the presence of non-neoplastic urinary tract disease. Thus, the UT Disease group was analyzed against the Healthy group to determine if a UT Disease fingerprint was present. We note that the Cancer group is not included here, as cancer is screened first and given top priority in our screening model. Results are given in Table 3 and Supplementary Table S2. The overall accuracy for detecting UT disease, such as uroliths and inflammatory/infectious cystitis was 93.3%, with a minimal metric of 68.8% (sensitivity), LR+ of 31.2, and an LR− of 0.32. Thus, the screen for a cancer fingerprint produced better overall metrics than that for a non-neoplastic urinary tract disease given the dataset analyzed.

4 Discussion

A simple, rapid, and inexpensive urine screening test, comparable in cost ($75–$150) to routine hematology/chemistry/urinalysis testing (individually), to identify the presence of cancer, using dog urine, should be of significant interest to dog owners, breeders, and veterinarians. Individual pet owners clearly want to enjoy the many benefits of their pets and have a sincere, well-founded interest in maintaining their dog's health. Many/most are aware that neoplastic disease is common in middle-aged and older dogs, and owners of some "high risk breeds" (Golden Retrievers, Boxers, for example) are acutely aware of the ever-present reality of cancer with the advancing age of their pets. Most dog owners and their veterinarians understand that, in many cases, early detection of cancer is potentially correlated with better outcomes in terms of tumor control and quality of life. By the same token, when presented with dogs that have cancer, owners and their veterinarians face difficult choices, including whether to treat and how they can evaluate if treatment is working. Our current

tools (clinical observation, imaging, and laboratory studies) are, at best, imprecise (and expensive) for determining treatment efficacy. The method described here is designed to inform veterinarians using a rapid and inexpensive urine screen that could be applied broadly. Veterinarians will likely choose to supplement these results with further testing, including imaging, biopsy, and other laboratory tests. We are not proposing to replace any gold-standard methods or accepted practices.

Here, we have shown that our approach with Raman spectroscopy and Rametrix® chemometric modeling may be able to fill gaps and to provide a readily-accessible, simple, and accurate method for cancer detection. In this "first-in-dog" pilot study, when testing with a Cancer group consisting of 100 samples representing four common cancers in canines, the broad spectral fingerprint of cancer was detected with better than 92% accuracy (with 94% sensitivity, 90% specificity, LR+ of 9.9, and LR− of 0.067).

The resulting canine urine screens could be implemented in practice as follows. Each screen (e.g., Cancer vs. UT Disease + Healthy in Table 3) consists of a set of ISREA nodes, a PCA coefficient matrix, a PCA vector of mean values, a MANOVA eigenvector matrix, and a logic gate to separate clusters by canonical scores (Figure 4C). These numerical values comprise the Rametrix® screening model, and they can be delivered to remote Raman scanners. Thus, large datasets of Raman spectra of canine urine only need to be compiled in one centralized location. Once installed, the resulting Rametrix® screening model will enable screening of a locally obtained urine sample against our large database of samples. As our database continues to grow, the Rametrix® screening model will be updated and distributed to Raman scanners (either at a commercial veterinary pathology laboratory service or at veterinary practices) easily. We also have developed methods to calibrate and synchronize remotely deployed scanners and have even developed custom Raman devices to automate scanning multiple urine samples and provide Rametrix® screening model results. Implementation of this long-term vision is a future endeavor beyond the scope of the study described in this paper though.

From a data modeling perspective, we observed in this study an advantage from ISREA baselining over an industry-standard SG method. We highlighted the comparison of these two methods because ISREA remains relatively new and has appeared in a limited number of our recent publications of results analyzing human patient urine specimens. SG, on the other hand, has been well established in signal processing and analytical chemistry for many years. We would question results if discernible differences and cancer fingerprints were detected with ISREA but absent with SG baselining. Here, we observed the identification of fingerprints with both methods but saw seemingly significant advantages from ISREA, making it a necessary inclusion in the Rametrix® screening model. In addition, this method enabled us to identify numerous Raman bands (and associated biomolecules) that differ in the urine of dogs with cancer and healthy dogs. Thus, the identification of cancer in urine was done here by the recognition of spectral signatures from several molecules, instead of a singular cancer biomarker. In addition, the signature for cL shared many similarities to the general cancer signature; however, unique characteristics were noted for cL.

There are limitations of this study that affect interpretation and broad generalizations of the results:

i The Cancer group of this study consisted of samples from dogs with cL, UC, MCT, and OS. These were included because they were most commonly referred to us for evaluation and treatment; thus, they were most represented in our larger dataset. In future studies, the Cancer group will contain samples from dogs with several other neoplastic diseases.

ii Although more than adequate for a proof-of-concept of the Raman spectral fingerprinting methodology, samples were obtained from a relatively small and heterogenous group of cancer cases. For example, differences among appendicular/axial/extraskeletal tumors were not sought among the OS group due to small sample numbers in the dataset. This will be remedied by ongoing case accrual and analysis in coming years. Another example is the UT Disease group in this study. This group was under-represented in patient numbers relative to the Cancer and Healthy groups. We hypothesize that with a larger and more well-defined population, the detection of non-neoplastic urinary tract disease with our screen will improve. We readily acknowledge that we need to do additional research on spectral fingerprints associated with chronic renal disease, a very common morbidity in middle-aged and older dogs (50–57).

iii It is possible that some dogs that were clinically healthy may have had undiagnosed neoplastic disease or other evolving co-morbidities. Future studies will include provisions for continuing contact with dog owners and their veterinarians to define the context of "healthy" at the time of sampling. In fact, one realistic and desirable use of this Raman spectroscopy-based technology may be periodic screening of healthy dogs for undiagnosed neoplastic disease (i.e., early detection through screening). Based on the results presented here, however, we cannot determine if our methods are sensitive enough to detect incipient neoplastic disease. We are committed, in planned studies, to see if early detection is indeed possible.

iv We acknowledge that approximately 95% of urine samples were collected by voided "free-catch," while the others were collected from catheters or cystocentesis. Again, the sample numbers were too small in this proof-of-concept study to probe the collection method in detail. No significant differences were noted in spectra by collection method by visual inspection. In addition, no significant differences were observed for voided vs. catheter urine collections from human patients in prior studies (33, 58).

v We did not document, with serial sampling, the effects of antineoplastic treatments for dogs on this study. A few dogs, under treatment, did provide multiple samples both during and at the conclusion of treatment (due to remission, withdrawal from study, or disease progression). However, the number of dogs for which we had serial sampling data was insufficient to draw meaningful conclusions. Serial sampling during treatment will be written into future sampling protocols and studies, especially studies we intend to conduct on lymphoma, where we hypothesize that there would be changes in the Raman urine molecular fingerprint correlated to disease remission, stabilization, or conversely, to progression and treatment failure.

vi We readily acknowledge that the results of our Raman spectroscopy-based molecular urinalysis must be kept and used in a clinical context of history, physical examination, concurrent laboratory and imaging studies, and patient observation. It would be inappropriate and ill-advised to have a positive (cancer positive) Raman urine spectral fingerprint trigger expensive and perhaps needless testing—or to be used to be a definitive, single metric for deciding whether or not to euthanize a dog.

We hope the novel technology described here can be made available—for the benefit of dogs, their owners, breeders, and veterinarians, alike through distributed urine Raman scanning devices and Rametrix® screening model. To be of real value in managing cancer in dogs, much future work needs to be done.

5 Conclusion

An accurate and rapid urine screening test for detecting cancer in dogs is presented here. The assay uses Raman spectroscopy to discern spectral fingerprints—composed of hundreds of molecules (*not* single biomarkers)—in urine. It could be used as part of regular wellness evaluations—as an aid in early/earlier detection of cancer, especially in breeds highly predisposed to development of certain types of cancer. It may also be useful in assessing responses to therapy and potentially in evaluating recurrence or progression of tumors. Although in this study, we focused on lymphoma, the most common hematologic cancer in dogs, and on other common and serious malignancies (urothelial carcinoma, mast cell tumor, and osteosarcoma), we intend to expand our studies to dogs of all ages and breeds, including those suffering from other malignancies. Major advantages of the approach presented here are that it is inexpensive, rapid, and requires minimal sample preparation. The numerous molecules of the cancer spectral fingerprint can be measured in a single assay.

Data availability statement

The raw data supporting the conclusions of this article will be made available by the authors, without undue reservation.

Ethics statement

The animal studies were approved by Virginia Tech IACUC protocols 15-217, 17-011, and 19-240. The studies were conducted in accordance with the local legislation and institutional requirements. Written informed consent was obtained from the owners for the participation of their animals in this study.

Author contributions

JLR: Conceptualization, Funding acquisition, Investigation, Methodology, Project administration, Resources, Supervision, Validation, Visualization, Writing – original draft, Writing – review & editing. ND: Conceptualization, Investigation, Methodology, Resources, Supervision, Validation, Writing – review & editing. JR: Investigation, Methodology, Resources, Supervision, Validation, Writing – review & editing, Data curation. MN: Investigation, Methodology, Resources, Writing – review & editing. DF: Investigation, Data curation, Writing – review & editing. CD: Data curation, Investigation, Writing – review & editing. LN: Data curation, Investigation, Writing – review & editing. AI: Data curation, Investigation, Formal analysis, Methodology, Software, Supervision, Writing – review & editing. GG: Conceptualization, Validation, Writing – review & editing. GO: Conceptualization, Validation, Writing – review & editing. RS: Conceptualization, Validation, Data curation, Formal analysis, Funding acquisition, Investigation, Methodology, Project administration, Resources, Software, Supervision, Visualization, Writing – original draft, Writing – review & editing.

Funding

The author(s) declare financial support was received for the research, authorship, and/or publication of this article. The financial and research support (urine specimens) of the Westie Foundation of America and the American Shetland Sheepdog Association are gratefully acknowledged.

Acknowledgments

The meticulous collection of urine specimens from dogs undergoing treatment for cancer by personnel of the Animal Cancer Care and Research Center, Roanoke, VA, and Oncology Service of the Virginia-Maryland College of Medicine, Blacksburg, VA, is also gratefully acknowledged. The participation of David Grant in case accrual, sample collection, and manuscript review is also gratefully acknowledged. Figures 1 and 2 was created using biorender.com.

Conflict of interest

JLR and RS co-founded Rametrix Technologies, Inc. to commercialize some/all findings described in this paper. AI was employed by Rametrix Technologies, Inc.

The remaining authors declare that the research was conducted in the absence of any commercial or financial relationships that could be construed as a potential conflict of interest.

The author(s) declared that they were an editorial board member of Frontiers, at the time of submission. This had no impact on the peer review process and the final decision.

Publisher's note

Supplementary material

The Supplementary material for this article can be found online at: https://www.frontiersin.org/articles/10.3389/fvets.2024.1328058/full#supplementary-material

References

1. Cancer in Pets | American Veterinary Medical Association. Available at: https://www.avma.org/resources/pet-owners/petcare/cancer-pets (Accessed January 16, 2024).

2. Grüntzig K, Graf R, Boo G, Guscetti F, Hässig M, Axhausen KW, et al. Swiss canine cancer registry 1955-2008: occurrence of the most common tumour diagnoses and influence of age, breed, body size, sex and neutering status on tumour development. *J Comp Pathol*. (2016) 155:156–70. doi: 10.1016/j.jcpa.2016.05.011

3. Comazzi S, Marelli S, Cozzi M, Rizzi R, Finotello R, Henriques J, et al. Breed-associated risks for developing canine lymphoma differ among countries: an European canine lymphoma network study. *BMC Vet Res*. (2018) 14:232. doi: 10.1186/s12917-018-1557-2

4. Schwartz SM, Urfer SR, White M, Megquier K, Shrager S, Dog Aging Project Consortium et al. Lifetime prevalence of malignant and benign tumours in companion dogs: cross-sectional analysis of dog aging project baseline survey. *Vet Comp Oncol*. (2022) 20:797–804. doi: 10.1111/vco.12839

5. Kruglyak KM, Chibuk J, McLennan L, Nakashe P, Hernandez GE, Motalli-Pepio R, et al. Blood-based liquid biopsy for comprehensive cancer genomic profiling using next-generation sequencing: an emerging paradigm for non-invasive cancer detection and management in dogs. *Front Vet Sci*. (2021) 8:704835. doi: 10.3389/fvets.2021.704835

6. Rafalko JM, Kruglyak KM, McCleary-Wheeler AL, Goyal V, Phelps-Dunn A, Wong LK, et al. Age at cancer diagnosis by breed, weight, sex, and cancer type in a cohort of more than 3,000 dogs: determining the optimal age to initiate cancer screening in canine patients. *PLoS One*. (2023) 18:e0280795. doi: 10.1371/journal.pone.0280795

7. Namgong C, Kim JH, Lee MH, Midkiff D. Non-invasive cancer detection in canine urine through *Caenorhabditis elegans* chemotaxis. *Front Vet Sci*. (2022) 9:932474. doi: 10.3389/fvets.2022.932474

8. Craig KKL, Wood GA, Keller SM, Mutsaers AJ, Wood RD. MicroRNA profiling in canine multicentric lymphoma. *PLoS One*. (2019) 14:e0226357. doi: 10.1371/journal.pone.0226357

9. Garnica TK, Lesbon JCC, Ávila ACFCM, Rochetti AL, Matiz ORS, Ribeiro RCS, et al. Liquid biopsy based on small extracellular vesicles predicts chemotherapy response of canine multicentric lymphomas. *Sci Rep*. (2020) 10:20371. doi: 10.1038/s41598-020-77366-7

10. Bouatra S, Aziat F, Mandal R, Guo AC, Wilson MR, Knox C, et al. The human urine metabolome. *PLoS One*. (2013) 8:e73076. doi: 10.1371/journal.pone.0073076

11. Galloway J. Remarks on Hodgkin's disease. *Br Med J*. (1922) 2:1201–8. doi: 10.1136/bmj.2.3234.1201

12. Hottendorf GH, Nielsen SW. Collagen necrosis in canine mastocytomas. *Am J Pathol*. (1966) 49:501–13.

13. Cambier J-F, Ronco P. Onco-nephrology: glomerular diseases with cancer. *Clin J Am Soc Nephrol*. (2012) 7:1701–12. doi: 10.2215/CJN.03770412

14. Berns JS, Rosner MH. Onco-nephrology: what the nephrologist needs to know about cancer and the kidney. *Clin J Am Soc Nephrol*. (2012) 7:1691. doi: 10.2215/CJN.03240312

15. Chan S, Oliver KA, Gray NA. An association between membranoproliferative glomerulonephritis and metastatic colorectal carcinoma: a case report. *J Med Case Rep*. (2016) 10:199. doi: 10.1186/s13256-016-0979-3

16. Pani A, Porta C, Cosmai L, Melis P, Floris M, Piras D, et al. Glomerular diseases and cancer: evaluation of underlying malignancy. *J Nephrol*. (2016) 29:143–52. doi: 10.1007/s40620-015-0234-9

17. Bacchetta J, Juillard L, Cochat P, Droz J-P. Paraneoplastic glomerular diseases and malignancies. *Crit Rev Oncol Hematol*. (2009) 70:39–58. doi: 10.1016/j.critrevonc.2008.08.003

18. Ahmed M, Solangi K, Abbi R, Adler S. Nephrotic syndrome, renal failure, and renal malignancy: an unusual tumor-associated glomerulonephritis. *J Am Soc Nephrol*. (1997) 8:848–52. doi: 10.1681/ASN.V85848

19. Lee JC, Yamauchi H, Hopper J. The association of cancer and the nephrotic syndrome. *Ann Intern Med*. (1966) 64:41–51. doi: 10.7326/0003-4819-64-1-41

20. Pai P, Bone JM, McDicken I, Bell GM. Solid tumour and glomerulopathy. *QJM Int J Med*. (1996) 89:361–8. doi: 10.1093/qjmed/89.5.361

21. Usalan C, Emri S. Membranoproliferative glomerulonephritis associated with small cell lung carcinoma. *Int Urol Nephrol*. (1998) 30:209–13. doi: 10.1007/BF02550579

22. Porta C, Bamias A, Danesh FR, Dębska-Ślizień A, Gallieni M, Gertz MA, et al. KDIGO controversies conference on onco-nephrology: understanding kidney impairment and solid-organ malignancies, and managing kidney cancer. *Kidney Int*. (2020) 98:1108–19. doi: 10.1016/j.kint.2020.06.046

23. Soomro Z, Youssef M, Yust-Katz S, Jalali A, Patel AJ, Mandel J. Paraneoplastic syndromes in small cell lung cancer. *J Thorac Dis*. (2020) 12:6253–63. doi: 10.21037/jtd.2020.03.88

24. Higashihara T, Okada A, Nakamura Y, Saigusa H, Homma S, Matsumura M, et al. Proliferative glomerulonephritis with monoclonal immunoglobulin deposits without conspicuous mesangial proliferation, complicated with squamous cell lung carcinoma. *Intern Med*. (2020) 59:557–62. doi: 10.2169/internalmedicine.2993-19

25. Senger RS, Scherr D. Resolving complex phenotypes with Raman spectroscopy and chemometrics. *Curr Opin Biotechnol*. (2020) 66:277–82. doi: 10.1016/j.copbio.2020.09.007

26. Butler HJ, Ashton L, Bird B, Cinque G, Curtis K, Dorney J, et al. Using Raman spectroscopy to characterize biological materials. *Nat Protoc*. (2016) 11:664–87. doi: 10.1038/nprot.2016.036

27. Cialla-May D, Schmitt M, Popp J. Theoretical principles of Raman spectroscopy. *Phys Sci Rev*. (2019):4. doi: 10.1515/psr-2017-0040

28. Shen Y, Hu F, Min W. Raman imaging of small biomolecules. *Annu Rev Biophys*. (2019) 48:347–69. doi: 10.1146/annurev-biophys-052118-115500

29. Fisher AK, Carswell WF, Athamneh AIM, Sullivan MC, Robertson JL, Bevan DR, et al. The Rametrix™ LITE toolbox v1.0 for MATLAB®. *J Raman Spectrosc*. (2018) 49:885–96. doi: 10.1002/jrs.5348

30. Senger RS, Robertson JL. The Rametrix™ PRO toolbox v1.0 for MATLAB®. *PeerJ*. (2020) 8:e8179. doi: 10.7717/peerj.8179

31. Senger RS, Sullivan M, Gouldin A, Lundgren S, Merrifield K, Steen C, et al. Spectral characteristics of urine from patients with end-stage kidney disease analyzed using Raman Chemometric urinalysis (Rametrix). *PLoS One*. (2020) 15:e0227281. doi: 10.1371/journal.pone.0227281

32. Kavuru V, Senger RS, Robertson JL, Choudhury D. Analysis of urine Raman spectra differences from patients with diabetes mellitus and renal pathologies. *PeerJ*. (2023) 11:e14879. doi: 10.7717/peerj.14879

33. Robertson JL, Senger RS, Talty J, Du P, Sayed-Issa A, Avellar ML, et al. Alterations in the molecular composition of COVID-19 patient urine, detected using Raman spectroscopic/computational analysis. *PLoS One*. (2022) 17:e0270914. doi: 10.1371/journal.pone.0270914

34. Carswell W, Robertson J, Senger R. Raman spectroscopic detection and quantification of macro- and microhematuria in human urine. *Appl Spectrosc*. (2022) 76:273–83. doi: 10.1177/00037028211060853

35. Huttanus HM, Vu T, Guruli G, Tracey A, Carswell W, Said N, et al. Raman chemometric urinalysis (Rametrix) as a screen for bladder cancer. *PLoS One*. (2020) 15:e0237070. doi: 10.1371/journal.pone.0237070

36. Senger RS, Sayed Issa A, Agnor B, Talty J, Hollis A, Robertson JL. Disease-associated multimolecular signature in the urine of patients with Lyme disease detected using Raman spectroscopy and chemometrics. *Appl Spectrosc*. (2022) 76:284–99. doi: 10.1177/00037028211061769

37. Xu Y, Du P, Senger R, Robertson J, Pirkle JL. ISREA: an efficient peak-preserving baseline correction algorithm for Raman spectra. *Appl Spectrosc*. (2021) 75:34–45. doi: 10.1177/0003702820955245

38. Talari ACS, Movasaghi Z, Rehman S, Rehman IU. Raman spectroscopy of biological tissues. *Appl Spectrosc Rev*. (2015) 50:46–111. doi: 10.1080/05704928.2014.923902

39. Movasaghi Z, Rehman S, Rehman DIU. Raman spectroscopy of biological tissues. *Appl Spectrosc Rev*. (2007) 42:493–541. doi: 10.1080/05704920701551530

40. Trevethan R. Sensitivity, specificity, and predictive values: foundations, pliabilities, and pitfalls in research and practice. *Front Public Health*. (2017) 5:5. doi: 10.3389/fpubh.2017.00307

41. Ranganathan P, Aggarwal R. Understanding the properties of diagnostic tests – part 2: likelihood ratios. *Perspect Clin Res*. (2018) 9:99–102. doi: 10.4103/picr.PICR_41_18

42. Guo S, Popp J, Bocklitz T. Chemometric analysis in Raman spectroscopy from experimental design to machine learning–based modeling. *Nat Protoc*. (2021) 16:5426–59. doi: 10.1038/s41596-021-00620-3

43. Guo S, Rösch P, Popp J, Bocklitz T. Modified PCA and PLS: towards a better classification in Raman spectroscopy–based biological applications. *J Chemom*. (2020) 34:e3202. doi: 10.1002/cem.3202

44. Krafft C, Popp J. The many facets of Raman spectroscopy for biomedical analysis. *Anal Bioanal Chem*. (2015) 407:699–717. doi: 10.1007/s00216-014-8311-9

45. Ralbovsky NM, Lednev IK. Raman spectroscopy and chemometrics: a potential universal method for diagnosing cancer. *Spectrochim Acta A Mol Biomol Spectrosc*. (2019) 219:463–87. doi: 10.1016/j.saa.2019.04.067

46. Nawaz H, Bonnier F, Meade AD, Lyng FM, Byrne HJ. Comparison of subcellular responses for the evaluation and prediction of the chemotherapeutic response to cisplatin in lung adenocarcinoma using Raman spectroscopy. *Analyst*. (2011) 136:2450–63. doi: 10.1039/C1AN15104E

47. Gazi E, Dwyer J, Gardner P, Ghanbari-Siahkali A, Wade AP, Miyan J, et al. Applications of Fourier transform infrared microspectroscopy in studies of benign prostate and prostate cancer. A pilot study. *J Pathol*. (2003) 201:99–108. doi: 10.1002/path.1421

48. Bonnier F, Byrne HJ. Understanding the molecular information contained in principal component analysis of vibrational spectra of biological systems. *Analyst*. (2011) 137:322–32. doi: 10.1039/C1AN15821J

49. Bhattacharjee T, Kumar P, Maru G, Ingle A, Krishna CM. Swiss bare mice: a suitable model for transcutaneous in vivo Raman spectroscopic studies of breast cancer. *Lasers Med Sci*. (2014) 29:325–33. doi: 10.1007/s10103-013-1347-9

50. Robertson JL. Chemically induced glomerular injury: a review of basic mechanisms and specific xenobiotics. *Toxicol Pathol*. (1998) 26:64–72. doi: 10.1177/019262339802600109

51. Robertson JL. Diseases of the tubules and interstitium In: KC Bovee, editor. *Canine nephrology*. Media, PA: Harwal Publishing (1983).

52. Robertson JL. Immunologic injury and the renal response In: KC Bovee, editor. *Canine nephrology*. Media, PA: Harwal Publishing (1983).

53. Robertson JL. The kidney in the aging dog In: *Pathobiology of the aging dog*. Eds. U. Mohr, W. W. Carlton, D. L. Dungworth, S. A. Benjamin, C. C. Capen, F. F. Hahn, Aimes, IA: Iowa State University Press (2001).

54. Robertson JL. Spontaneous renal disease in dogs. *Toxicol Pathol*. (1986) 14:101–8. doi: 10.1177/019262338601400112

55. Stone EA, Littman MP, Robertson JL, Bovée KC. Renal dysfunction in dogs with pyometra. *J Am Vet Med Assoc*. (1988) 193:457–64.

56. Pomeroy MJ, Robertson JL. The relationship of age, sex, and glomerular location to the development of spontaneous lesions in the canine kidney: analysis of a life-span study. *Toxicol Pathol*. (2004) 32:237–42. doi: 10.1080/01926230490274407

57. Littman MP, Robertson JL, Bovée KC. Spontaneous systemic hypertension in dogs: five cases (1981-1983). *J Am Vet Med Assoc*. (1988) 193:486–94.

58. Robertson J, Issa AS, Gomez M, Sullivan K, Senger R. Profiling renal dysfunction using Raman chemometric urinalysis, with special reference to COVID19, lupus nephritis, and diabetic nephropathy. *Med Res Arch*. (2023) 11. doi: 10.18103/mra.v11i9.4384

frontiers | Frontiers in Veterinary Science

TYPE Original Research
PUBLISHED 17 May 2024
DOI 10.3389/fvets.2024.1379146

OPEN ACCESS

EDITED BY
Vittoria Castiglioni,
IDEXX Laboratories, Germany

REVIEWED BY
Seungmee Lee,
University of Edinburgh, United Kingdom
Hugo Murua Escobar,
University of Rostock, Germany

*CORRESPONDENCE
Sabine E. Hammer
✉ sabine.hammer@vetmeduni.ac.at

†These authors have contributed equally to this work

RECEIVED 30 January 2024
ACCEPTED 25 April 2024
PUBLISHED 17 May 2024

CITATION
Hammer SE, Sprung J, Škor O, Burger S, Hofer M, Schwendenwein I and Rütgen BC (2024) Exploratory screening for micro-RNA biomarkers in canine multicentric lymphoma.
Front. Vet. Sci. 11:1379146.
doi: 10.3389/fvets.2024.1379146

Exploratory screening for micro-RNA biomarkers in canine multicentric lymphoma

Sabine E. Hammer[1]*, Julia Sprung[1†], Ondřej Škor[2], Stefanie Burger[3], Martin Hofer[4], Ilse Schwendenwein[5] and Barbara C. Rütgen[5]

[1]Immunology, Department of Biological Sciences and Pathobiology, University of Veterinary Medicine Vienna, Vienna, Austria, [2]Laboklin GMBH & CO.KG, Bad Kissingen, Germany, [3]VetBioBank, VetCore, University of Veterinary Medicine Vienna, Vienna, Austria, [4]Genomics Core Facility, VetCore, University of Veterinary Medicine Vienna, Vienna, Austria, [5]Clinical Pathology, Department of Biological Sciences and Pathobiology, University of Veterinary Medicine Vienna, Vienna, Austria

Lymphoma is one of the most frequent hematopoietic tumors in dogs and shares similar features with human counterparts. MicroRNAs (miRNA, small non-coding RNAs) are pivotal in gene regulation fine tuning and cancer hallmarks are influenced by their aberrant expression. Consequently, miRNA biomarkers may assist predicting therapeutic response and clinical outcome by providing less-invasive novel diagnostics tools. The aim of this study was to detect dysregulated miRNAs in lymphomatous lymph node tissues in comparison to lymph node material or PBMCs from healthy control dogs. Potential significant differences in miRNA expression profiles between four lymphoma entities were evaluated. A customized PCR array was utilized to profile 89 canine target miRNAs. Quantification was performed using qPCR, relative expression was determined by the delta–delta Ct method, and *p*-values were calculated with student's *t*-test. In the 14 diffuse large B-cell lymphoma (DLBCL) patients, 28 and 24 different miRNAs were significantly dysregulated compared to lymph node material or PBMCs. Sixteen miRNAs occurred in both control groups, with 12 miRNAs being down- and four miRNAs being upregulated. The six peripheral T-cell lymphoma (PTCL) samples showed 24 and 25 dysregulated miRNAs when compared to the healthy controls. A combined analysis of DLBCL and PTCL samples revealed seven shared and 19 differently expressed miRNAs. Potential biomarkers in T- and B-cell lymphoma could be the miRNA-17/92 cluster and miRNA-181-family together with miRNA-34a and miRNA-150. Diagnostic utility of potential biomarkers must be validated in larger, prospective cohorts of canine lymphoma cases and in higher numbers of physiological patient material.

KEYWORDS

***Canis lupus familiaris*, diffuse large B-cell lymphoma (DLBCL), peripheral T-cell lymphoma (PTCL), microRNA expression analysis, potential biomarker candidates, animal model, biomedical research and development**

1 Introduction

Lymphoma is one of the most common occurring tumors in dogs (1–4). The disease shows a prevalence of around 100 cases per 100.000 dogs and 83–85% of all canine hematopoietic neoplasias are represented by lymphoma (2, 4). This tumor initiates from lymphoid cells which are B- and T-cells (4–7). The proportions of lymphomas resulting from those cells are

approximately 70% of B-cell and 30% of T-cell lymphoma (8, 9). Since all pure and mixed breeds are affected by lymphoma, this proportion can vary. However, some breeds are prone to develop a certain type of canine lymphoma, for instance, Boxers tend to develop T-cell lymphoma, whereas Golden Retrievers have an equal likelihood of developing B-cell as well as T-cell lymphoma (8–10). Canine lymphoma is a heterogeneous disease which primarily occurs in lymphatic organs, such as lymph nodes or spleen (6). The most prominent clinical presentation of lymphoma is multicentric lymphoma, which is characterized by generalized lymphadenopathy (2, 3, 9–11). The most dominant multicentric lymphoma which is also the most common subtype found in dogs is the diffuse large B-cell lymphoma (DLBCL) which will be characterized in more detail below (7, 8). It represents about 50–60% of all canine entities (8, 12). Beside the multicentric form, also extranodal anatomic forms exist. Most common are the alimentary, mediastinal, and cutaneous lymphoma. All three types originate either exclusively or typically from T-cells (9, 10).

In this retrospective study, four types of canine lymphoma will be analyzed. The DLBCL is as mentioned before the most common lymphoma entity in dogs also being the case for the studied cohort (13–16). The second subtype of interest represents the entity marginal zone lymphoma (MZL). This indolent B-cell lymphoma mainly occurs in the spleen and shares CD79a and CD20 expression with DLBCL in immunohistochemistry (IHC) but lacks CD3 expression (13, 14, 17, 18). In contrast, T-cell lymphoma (PTCL) shows expression of CD3 by lacking CD79a and CD20, characterizing them as T-cell type in IHC (13, 14, 19, 20). Finally, the subtype T-zone lymphoma (TZL), is an indolent low-grade T-cell lymphoma, in which frequent CD25 and CD3 expression is accompanied by missing CD45, CD79a and CD20. In flow cytometry this entity shows a unique phenotype being $CD45^{-}$, $CD5^{+}$ and $CD21^{-}$ (13, 14, 18, 20, 21).

Canine lymphoma shares many similarities with the human non-Hodgkin lymphoma (NHL) in terms of their immunophenotypic composition, diagnosis, clinical presentation, treatment methods and molecular biology (3–5, 8, 9, 22). Furthermore, humans and dogs are both exposed to the same environmental and therefore the same risk factors that promote the development of cancers (3, 9, 22). Those environmental exposure include, for instance, household chemicals and polluted sites (9). Due to those similarities between the dog and their human counterpart, canine lymphoma is seen as a potential animal model for humans. Thus, new findings would be beneficial for both veterinary and human medicine especially concerning new diagnostic methods (1, 4, 5, 11).

MicroRNAs (miRNA, miR) are physiological occurring small non-coding RNA molecules which amount to approximately 18–25 nucleotides per miRNA. MicroRNAs are transcribed from individual genes which are located between introns and exons. They are widely expressed in all tissues, organs, and cells of a multicellular organism (1–4, 11, 22–25). However, some few miRNAs are restricted to certain cell types (22). Although miRNAs are unable to code for proteins, they regulate gene expressions in the post-transcription process through binding in 3'UTR of target mRNA (4, 22, 24). Each miRNA has the ability to control hundreds of targets for almost all pathways (1, 3, 11, 24). They are part of modification processes including cell differentiation, stress resistance, metabolism, cell cycle progression and apoptosis in normal cells (1, 7, 22). However, in neoplastic cells miRNAs are dysregulated and therefore, they have an effect on the functional roles in cancer cells, such as the initiation, progression and metastasis (2, 3, 25). MicroRNAs in cancer cells are either upregulated or downregulated in comparison to healthy cells, depending on if those miRNAs act as an oncogene or tumor suppressor (1, 3, 4, 7, 22). As a matter of fact, some even have a dual-function depending on the cell type (3). Those dysregulated miRNAs have the potential to be used as biomarkers for detection, classification or even prediction of tumors (1).

The diagnosis of canine lymphoma is challenging to achieve rapid and accurate results (7). The standard procedures nowadays focus on a morphological evaluation of biopsies as well as a cytologic examination of clinically suspect lymph nodes or other mostly lymphoid organs (3, 4, 7). To differentiate between the lymphoma entities, immunophenotyping, grading and clinical staging are necessary for tailored treatment decisions and prognostic information (3). For some common entities, as the large B-cell lymphoma (LBCL), peripheral T-cell lymphoma (PTCL) or peripheral T-zone lymphoma (PTZL), this currently can be provided by diagnostic flow cytometry (4, 7, 26–28). However, histopathological evaluation including World Health Organization (WHO) classification of a biopsy sample is still the diagnostic gold standard (13). As a matter of fact, the gold standard methods for diagnosis of canine lymphoma are rather time-consuming (7). The general presence, high stability and the minimally invasive material extraction of miRNAs might offer promising biomarkers as a new diagnostic approach for canine lymphomas (1–4, 7, 29). Furthermore, this reliable characterized material harboring miRNAs has the potential for getting deeper insight into genetic background, origin and cause for neoplastic development and differences in all different entities (3).

Compared to healthy dogs, the miRNA profile of the canine lymphoma-affected dogs is not thoroughly studied. To discover differentially expressed miRNAs in canine lymphoma, we utilized 24 archival cryopreserved lymph nodes, representing four canine lymphoma entities and material from eight normal healthy dogs. The identification and quantification of dysregulated miRNAs were assessed by applying the "qPCR-based miRCURY custom assay/panel system" (Qiagen) targeting a custom-made panel which consisted of 89 miRNAs that were selected from various literature sources. This retrospective study should deepen the understanding of entity-specific miRNAs expression profiles, which could be further developed into valuable diagnostic tools in dogs. By means of this study we could also improve our understanding of disease mechanisms, molecular pathways, biomarkers discovery, dysregulated miRNAs, and personalized medicine.

2 Materials and methods

2.1 Lymphoma patients and non-neoplastic control material

In this retrospective pilot study, all samples used here have already been analyzed regarding clinics, cytology, histopathology, immunophenotyping using flow cytometry and PCR for clonality testing (16). The examination material concerning the lymphoma patients consisted of 24 archival cryopreserved lymph nodes, representing four canine lymphoma entities: 14 samples of diffuse large B-cell lymphoma (DLBCL), six samples of Peripheral T-cell lymphoma (PTCL) including one enteric T-cell lymphoma (ent. TCL), as well as two samples each of Marginal zone lymphoma (MZL) and

T-zone lymphoma (TZL) (16). The samples were provided by the archive of the VetBiobank (Vetmeduni), which have been already diagnosed as already mentioned by flow cytometry, clonality testing, histopathology including WHO classification and immunohistochemistry (16, 30). Lymph node sample material was available in sample duplicates. The solid lymph node pieces were on average approximately 2.5 × 2.5 × 2.5 mm in size and were stored in RNA-Later (Qiagen GmbH, Hilden, Germany). One sample per duplicate was processed and the second was stored as a backup in case of need for repetition. The detailed list of patients can be found in Supplementary Table 1. The non-neoplastic and non-inflammatory control material consisted of eight samples: four samples not-lymphoma bearing canine lymph node material and four samples canine peripheral blood mononuclear cells (PBMCs; Supplementary Table 2). The material consisted of archive material being characterized and immunophenotyped in course of a previous study (31). The lymph node material was provided in single cell suspension vials of about 1×10^7 cells in freezing medium 50% RPMI 1640 medium (PAA, Pasching, Austria), 40% FCS (PAA, Pasching, Austria), 10% DMSO (Sigma-Aldrich, Austria). The PBMC were stored in freezing medium with a cell count between 5×10^6–1×10^7 cells. Since the pilot project was a retrospective study and all samples and controls have already been used in previous studies, no additional ethics approval was necessary (16, 31).

2.2 MicroRNA expression analysis

Prior to miRNA extraction and cDNA synthesis, control spike-ins were pre-prepared by using the "RNA Spike-in Kit for RT" (Qiagen) following the manufacturer's instructions (32). It was used as a control to ensure a qualitative RNA isolation, cDNA synthesis as well as qPCR amplification. Next, miRNA was extracted from all examination materials by using the "miRNeasy Tissue/cells Advanced Micro Kit" (Qiagen) according to the manual supplied with the kit (33). After extraction, miRNA concentrations (ng/μL) and purity of miRNA (ratios: 260/280 and 260/230) were measured by using the Nanodrop 2000c (Thermo Fisher Scientific, Waltham, MA, United States). Afterwards, 20 ng of the extracted miRNAs were transformed into cDNA by using the "miCURY LNA RT Kit" (Qiagen) according to protocol (34). The identification and quantification of dysregulated miRNAs were assessed by applying the "qPCR-based miRCURY custom assay/panel system" (Qiagen) targeting a custom-made panel which consisted of 89 miRNAs that were selected from various literature sources (Supplementary Table 3) (1–3, 5, 7, 11, 22, 24, 25). Alongside with the patient samples and control groups, validated primer sets were used for normalization of miRNA expression levels in qPCR analyses (Qiagen). The detection was performed on "miRCURY LNA miRNA Custom PCR Panels" (Qiagen) consisting of 384-well plates. Each plate had the capacity for the assessment of four samples. The probes were analyzed in a 384er Cycler ViiA™ 7 qPCR System (Thermo Fisher Scientific).

2.3 Evaluation of data

The web-based "miRCURY LNA miRNA Expression Analysis" platform (Qiagen) was used for the data analysis of the raw data from this project. The Ct-values were transferred to an appropriate input file, excluding four miRNAs based on their percentage of which their Ct value was greater than 45 in the studied samples: miR-122 (69.44%), miR-127 (36.11%), miR-206 (41.67%), and miR-8908a-3p (80.56%). The first step of data analysis included grouping the samples according to their entities while the PBMCs and lymph nodes were selected as "control group" for comparing pathological samples to PBMCs and lymph nodes samples separately. Prior to statistical data evaluation, normalization of miRNAs was conducted by using the geNorm method (Supplementary Table 4). GeNorm is a normalization method based on a same expression ratio of the predefined reference miRNAs by using standard deviation of log-transformed reference miRNA ratios which should be identical in all samples. The stability factor which should be below 1.5 shows an average pairwise variation between one miRNA compared to all other reference miRNAs (35, 36). MiR-16, miR-21, miR-22, miR-146a, and miR-350 were the most stable expressed miRNAs across all samples and were used as endogenous controls to normalize differences in the patient samples (35). After normalization, the parameter Fold change, Fold regulation and *p*-value were calculated based on the ΔΔCt method (Fold change: $2^{(-\Delta\Delta Ct)}$) (36). Fold regulation and Fold change are identical in terms of their information. However, data is presented differently in terms of a downregulation of the miRNA. While in Fold changes a decimal number between 0 and 1 is shown, it is presented as a negative inverse fraction in Fold regulation (37). *p*-values were calculated by using the student's t-test to the linearized normalized miRNA expression levels for each miRNA in each group (control group as well as test group) by assuming an equal variance. As for the significance of the *p*-value, the threshold was set to 0.05 (37). For data visualization, bar charts were used to show dysregulations of the lymphoma entities in comparison to each control group. Furthermore, scatter plots were used to compare the normalized expression levels of each miRNA between two defined groups (37).

3 Results

3.1 DNA concentration and quality of studied samples

After miRNA extraction of the samples, their concentration and quality were assessed with the NanoDrop 2000c spectrophotometer (Thermo Fisher Scientific). The results of miRNA concentration ranged from 6.95 to 4251.15 ng/μl, with the average value of 1220.45 ng/μl. The 260/280 ratios of the examined animals varied between 1.61 and 3.60, with the average value of 2.08. The 260/230 ratios ranged from 0.04 to 2.21 with a mean value of 1.33 (Supplementary Table 5).

3.2 MicroRNA expression profiles of canine lymphoma entities compared to control group 'PBMC'

3.2.1 DLBCL and PTCL (incl. Enteric TCL)

The predefined miRNAs (miR-16, miR-21, miR-22, miR-146a, and miR-350) had a stability factor below 1.5 and were used for normalization (Supplementary material "miRNA Expression Analysis

Report 1," page 10). In the 14 DLBCL patients, numerous miRNAs were dysregulated but only 24 miRNAs were significantly differentially expressed (Supplementary Figure 1; Supplementary Table 6). Out of these, 17 miRNAs were downregulated while seven miRNAs were upregulated (Figure 1A; Supplementary material "miRNA Expression Analysis Report 1" - Group 3). Five miRNAs showed Fold regulation (Fr) thresholds greater than ±20. The highest overexpression was found in miR-143 (Fr: 393.10, *p*-value: 0.012269), followed by miR-34a (Fr: 50.61, p-value: 0.006348), and miR-30a (Fr: 47.83, *p*-value: 0.001155). In contrast, downregulation was highest only in miR-223 (Fr: −138.82, *p*-value: 0.00) and miR-150 (Fr: −24.41, *p*-value: 0.000012; Table 1). The Fold regulation of miRNAs in PTCL and enteric TCL resulted in 25 significantly dysregulated miRNAs. Sixteen of those miRNAs were downregulated, while nine miRNAs were upregulated (Figure 1B; Supplementary material "miRNA Expression Analysis Report 1" - Group 4). Six of those miRNAs showed a higher Fold regulation threshold than ±20. Upregulations greater than 20 were found in four miRNAs which were the following: miR-143 (Fr: 432.19, *p*-value: 0.004948), miR-145 (Fr: 398.57, *p*-value: 0.01012), miR-214 (Fr: 34.58, *p*-value: 0.008617), and miR-30a (Fr: 32.97, *p*-value: 0.018914). Downregulations greater than −20 were found in two miRNAs which were miR-223 (Fr: −181.72, *p*-value: 0.000133) and miR-150 (Fr: −29.51, *p*-value: 0.000045; Table 1).

When comparing DLBCL and PTCL (incl. Enteric TCL), 24 out of 37 miRNAs were excluded from the analyzation due to lack of significance because of the analysis program (Figures 2A,B). Therefore, 13 miRNAs were excluded in DLBCL and 11 in PTCL. The remaining 13 miRNAs were significantly dysregulated in both entities (Table 1). As a matter of fact, one miRNA (miR-181a) was upregulated in PTCL and downregulation in DLBCL. Upregulations in both lymphoma entities were found in four miRNAs which were the following: miR-18a, miR-30a, miR-34a, and miR-143 (Table 1). Downregulations in both entities were detected in eight miRNAs (miR-23a, miR-24, miR-27a, miR-150, miR-197, miR-222, miR-223, and miR-423a; Table 1). In comparison, DLBCL and PTCL (incl. Enteric TCL) share 13 differentially expression miRNAs including four miRNAs that show potential specific expression profiles in these two entities (Fold regulations are given in parenthesis): miR-34a (DLBCL: 4.50 vs. PTCL: 50.61), miR-197 (DLBCL: −7.12 vs. PTCL: −2.80), miR-223

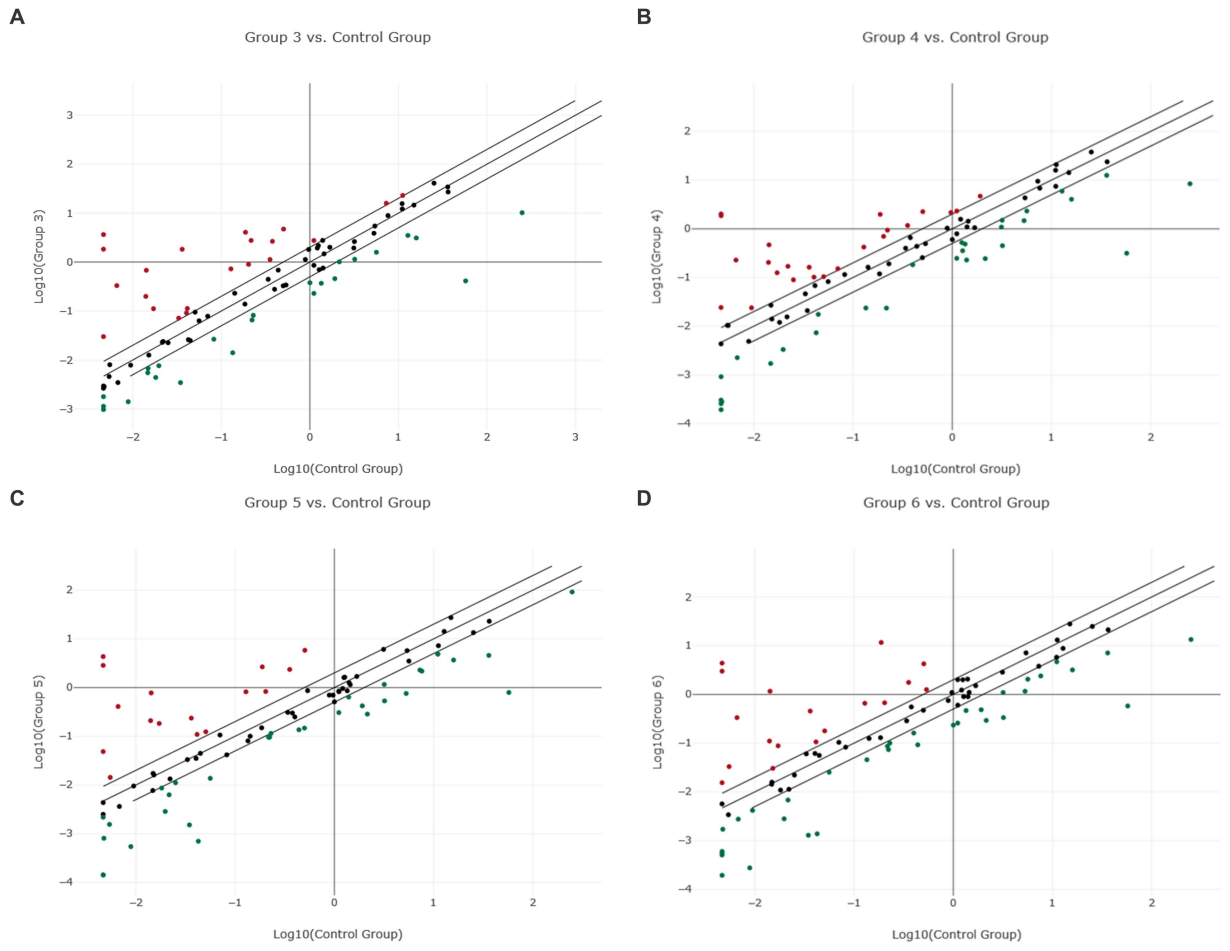

FIGURE 1
Scatter plot of normalized miRNA expression in four canine lymphoma entities compared to PBMC as control group. The center diagonal line indicates unchanged miRNA expression, while the outer diagonal lines indicate the Fold regulation threshold >2.0. MicroRNAs with data points beyond the outer lines in the upper left and lower right corners are up-regulated (red dots) or down-regulated (green dots), by more than the Fold regulation threshold in the y-axis Group relative to the x-axis Group. **(A)** Group 3 = DLBCL vs. Control Group = PBMC; **(B)** Group 4 = PTCL (incl. Enteric TCL) vs. Control Group = PBMC; **(C)** Group 5 = TZL vs. Control Group = PBMC; **(D)** Group 6 = MZL vs. Control Group = PBMC.

10.3389/fvets.2024.1379146

TABLE 1 Fold regulation of significantly dysregulated miRNAs in four canine lymphoma entities by using PBMC as control group.

miRNA ID	DLBCL	PTCL	TZL*	MZL*	miRNA ID	DLBCL	PTCL	TZL*	MZL*
cfa-let-7c	n.s.	n.s.	2.64	2.57	cfa-miR-136	n.s.	n.s.	n.s.	−2.27
cfa-let-7f	−2.80	n.s.	−2.01	−2.29	cfa-miR-143	393.10	432.19	612.46	643.49
cfa-miR-10a	n.s.	n.s.	2.60	6.01	cfa-miR-145	n.s.	398.57	928.49	940.67
cfa-miR-10b	n.s.	n.s.	10.38	3.31	cfa-miR-148a	n.s.	n.s.	n.s.	2.34
cfa-miR-15b	−4.83	n.s.	−3.61	−4.29	cfa-miR-149	n.s.	n.s.	n.s.	−2.47
cfa-miR-18a	2.49	2.09	n.s.	n.s.	cfa-miR-150	−24.41	−29.51	−2.70	−18.53
cfa-miR-20a	n.s.	n.s.	−2.24	n.s.	cfa-miR-151	−2.20	n.s.	n.s.	n.s.
cfa-miR-23a	−9.55	−5.68	n.s.	−2.94	cfa-miR-155	n.s.	n.s.	−6.90	−7.04
cfa-miR-24	−3.54	−2.43	n.s.	−2.75	cfa-miR-181a	−4.17	2.45	−4.53	−3.93
cfa-miR-25	n.s.	−2.12	−2.74	−2.90	cfa-miR-181b	n.s.	n.s.	−2.33	−3.01
cfa-miR-26b	−5.11	n.s.	−4.32	−4.99	cfa-miR-181c	−3.09	n.s.	n.s.	n.s.
cfa-miR-27a	−3.64	−2.15	n.s.	n.s.	cfa-miR-181d	n.s.	n.s.	−2.10	n.s.
cfa-miR-29a	n.s.	−3.58	n.s.	n.s.	cfa-miR-182	n.s.	n.s.	−2.25	n.s.
cfa-miR-29b	n.s.	−2.88	n.s.	n.s.	cfa-miR-183	n.s.	n.s.	−3.49	n.s.
cfa-miR-29c	n.s.	−2.38	n.s.	n.s.	cfa-miR-197	−2.80	−7.12	−6.01	−9.55
cfa-miR-30a	47.83	32.97	54.55	81.80	cfa-miR-199	n.s.	7.30	10.70	5.15
cfa-miR-30d	n.s.	−3.59	−6.98	−4.55	cfa-miR-200b	n.s.	n.s.	−5.90	−2.78
cfa-miR-31	n.s.	−9.21	−2.27	−2.51	cfa-miR-210	n.s.	n.s.	−3.39	n.s.
cfa-miR-34a	50.61	4.50	6.53	12.61	cfa-miR-214	n.s.	34.58	62.01	50.56
cfa-miR-92a	n.s.	−2.87	−7.86	−5.06	cfa-miR-218	n.s.	n.s.	n.s.	2.00
cfa-miR-93	n.s.	n.s.	−3.50	−3.18	cfa-miR-221	−2.64	n.s.	n.s.	−4.27
cfa-miR-99a	5.66	n.s.	6.39	5.14	cfa-miR-222	−3.65	−2.76	n.s.	−2.88
bta-miR-99b	n.s.	n.s.	14.90	7.87	cfa-miR-223	−138.82	−181.72	−72.21	−98.71
cfa-miR-101	n.s.	n.s.	2.45	3.54	cfa-miR-363	7.03	n.s.	n.s.	n.s.
cfa-miR-103	n.s.	n.s.	−2.27	−2.36	cfa-miR-378	n.s.	n.s.	−3.23	−4.73
cfa-miR-106a	2.19	n.s.	−3.17	n.s.	cfa-miR-423a	−2.12	−8.77	−7.52	−7.33
cfa-miR-107	n.s.	−2.18	n.s.	−2.47	cfa-miR-450a	−10.01	n.s.	−22.87	−26.89
cfa-miR-125a	n.s.	3.45	4.09	3.32	cfa-miR-450b	−6.30	n.s.	−16.36	−32.19
cfa-miR-125b	n.s.	4.47	11.58	8.43	cfa-miR-451	n.s.	n.s.	14.19	62.15
cfa-miR-126	n.s.	n.s.	6.66	4.98	cfa-miR-486	n.s.	n.s.	−2.19	n.s.
cfa-miR-128	n.s.	n.s.	−3.43	−3.17	cfa-miR-8865	n.s.	n.s.	−60.75	−30.77
cfa-miR-130b	n.s.	n.s.	−4.09	−2.22					

Fold regulation threshold > 2.0; *p*-value threshold < 0.05; *no calculated *p*-value; ID, identifier; DLBCL (Group 3), Diffuse Large B-cell lymphoma; PTCL (incl. Enteric T-cell lymphoma) (Group 4), Peripheral T-cell lymphoma; TZL (Group 5), T-zone lymphoma; MZL (Group 6), Marginal zone lymphoma; PBMC (Control Group), Peripheral blood mononuclear cells; cfa, Canis lupus familiaris; bta, Bos taurus; miR, microRNA; n.s., not significant.

(DLBCL: −181.72 vs. PTCL: −138.82), and miR-423a (DLBCL: −8.77 vs. PTCL: −2.12; Table 1).

3.2.2 TZL and MZL

As already mentioned, TZL and MZL samples only included two samples each and therefore no *p*-value calculation was possible. As precise statements are not justified due to the small sample size, the results must be taken into consideration cautiously. For TZL, data evaluation via the Qiagen Analysis platform revealed a total of 46 of the analyzed 89 miRNAs exhibiting a Fold regulation threshold >2.0 (Figure 1C; Supplementary material "miRNA Expression Analysis Report 1" - Group 5). Seven out of those 46 miRNAs exhibited Fold regulations greater than ±20, with four miRNAs being upregulated (miR-145, Fr: 928.49; miR-143, Fr: 612.46; miR-214, Fr: 62.01; miR-30a, Fr: 54.55). In contrast, three miRNAs were downregulated, including miR-223 (Fr: −72.21), miR-8865 (Fr: −60-75), and miR-450a (Fr: −22.87; Table 1). Analysis of the two MZL patients showed that in total 48 of the assessed miRNAs had a higher Fold regulation threshold than 2.0 (Figure 1D; Supplementary material "miRNA Expression Analysis Report 1" - Group 6). Eighteen miRNAs out of those 48 were upregulated, whereas 30 were downregulated. Nine miRNAs showed a Fold regulation threshold greater/lower than ±20. While miR-145 (Fr: 940.67), miR-143 (Fr: 643.49), miR-30a (Fr: 81.80), miR-451 (Fr: 62.15), and miR-214 (Fr: 50.56) were upregulated.

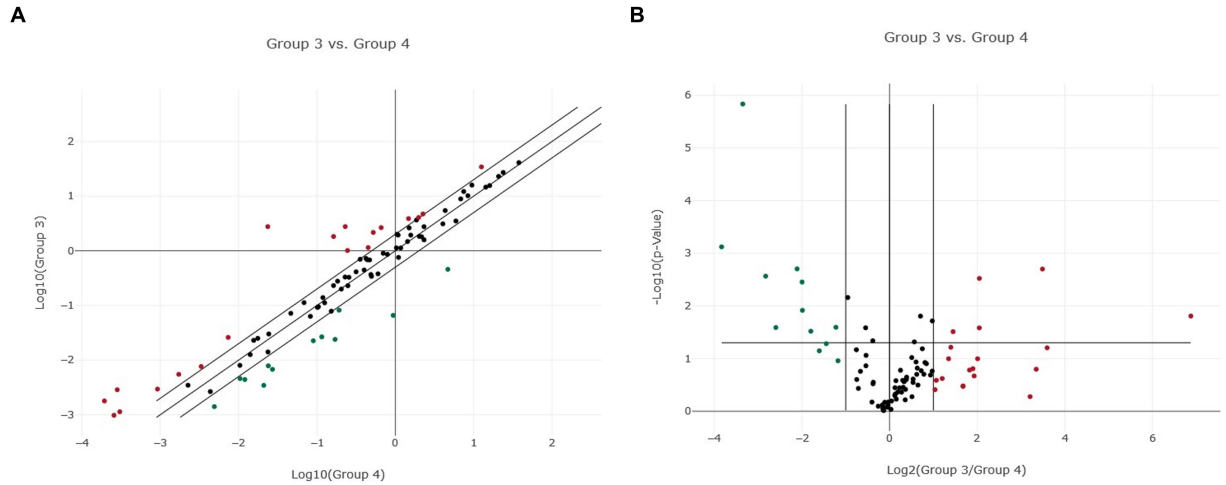

FIGURE 2
Normalized miRNA expression in two canine lymphoma entities. **(A)** Scatter plot of normalized miRNA expression comparing Group 3 (DLBCL) with Group 4 (PTCL, incl. Enteric TCL). The center diagonal line indicates unchanged miRNA expression, while the outer diagonal lines indicate the Fold regulation threshold >2.0. MicroRNAs with data points beyond the outer lines in the upper left and lower right corners are up-regulated (red dots) or down-regulated (green dots), by more than the Fold regulation threshold in the y-axis Group relative to the x-axis Group. **(B)** Volcano Plot illustrating significant miRNA expression changes when comparing Group 3 (DLBCL) with Group 4 (PTCL, incl. Enteric TCL). The center vertical line indicates unchanged miRNA expression, while the two outer vertical lines indicate the selected Fold regulation threshold. The horizontal line indicates the selected *p*-value threshold <0.05. MicroRNAs with data points in the far upper left and far upper right sections are down-regulated (green dots) or up-regulated (red dots) and meet the selected Fold regulation and p-value thresholds.

In contrast, downregulations were found in miR-223 (Fr: −98.71), miR-450b (Fr: −32.19), miR-8865 (Fr: −30.77) and miR-450a (Fr: −26.89; Table 1). In comparison, TZL and MZL share 38 differentially expression miRNAs including nine miRNAs that show potential characteristic expression profiles in these two entities: miR-10b (TZL: 10.38 vs. MZL: 3.31), miR-30a (TZL: 54.55 vs. MZL: 81.8), miR-34a (TZL: 6.53 vs. MZL: 12.61), miR-99b (TZL: 14.90 vs. MZL: 7.87), miR-150 (TZL: −2.70 vs. MZL: −18.53), miR-199 (TZL: 10.70 vs. MZL: 5.15), miR-450b (TZL: −16.36 vs. MZL: −32.19), miR-451 (TZL: 14.19 vs. MZL: 62.15), and miR-8865 (TZL: −60.75 vs. MZL: −30.77; Table 1).

3.3 MicroRNA expression profiles of canine lymphoma entities compared to control group 'lymph node'

3.3.1 DLBCL and PTCL (incl. Enteric TCL)

Fold regulation of miRNAs in DLBCL showed numerous dysregulations, but only 28 miRNAs showed significant differences (Supplementary Figure 2; Table 7). Nineteen of those miRNAs were downregulated while 9 miRNAs were upregulated (Figure 3A; Supplementary material "miRNA Expression Analysis Report 2" - Group 3). Six miRNAs showed a Fold regulation threshold greater than ±10. The highest overexpression in fold regulations were found in miR-34a (Fr: 14.68, *p*-value: 0.008108) and miR-363 (Fr: 14.63, *p*-value: 0.008807). Downregulations greater than −10 were found in four miRNAs which were miR-8865 (Fr: −11.94, *p*-value: 0.003054), miR-23a (fold regulation: −11.43, *p*-value: 0.000000), miR-150 (Fr: −10.98, *p*-value: 0.018023) and miR-155 (Fr: −10.92, *p*-value: 0.000028; Table 2). Fold regulation of miRNAs in PTCL and enteric TCL resulted in 24 significant miRNA dysregulations. Fifteen of those miRNAs were downregulated while 9 miRNAs were overexpressed (Figure 3B; Supplementary material "miRNA Expression Analysis Report 2" - Group 4). Six of those miRNAs showed a Fold regulation below −10 (Table 2). Those downregulations were found in the following miRNAs: miR-8865 (Fr: −42.31, *p*-value: 0.048379), miR-155 (Fr: −25.11, *p*-value: 0.000169), miR-200b (Fr: −16.27, *p*-value: 0.031405), miR-150 (Fr: −13.28, *p*-value: 0.000105), miRNA-31 (Fr: −11.61, *p*-value: 0.00227), and miR-423a (Fr: - 11.00, *p*-value: 0.000563; Table 2).

When comparing DLBCL and PTCL (incl. Enteric TCL), 22 out of 37 miRNAs were excluded from the analyzation due to lack of significance because of the analysis program (Figures 2A,B). Consequently, nine miRNAs were excluded in DLBCL and 13 in PTCL. However, these entities share significantly dysregulated miRNAs which were either up-or downregulated in both groups (Table 2). Upregulations in both lymphoma entities were found in seven miRNAs: miR-18a, miR-19a, miR-19b, miR-20a, miR-93, miR-106a, and miR-350. Downregulations in both entities were shown in eight miRNAs including miR-23a, miR-26b, miR-146a, miR-150, miR-155, miR-222, miR-423a, and miR-8865 (Table 2). In comparison, DLBCL and PTCL (incl. Enteric TCL) share 15 differentially expression miRNAs including four miRNAs that show potential specific expression profiles in these two entities (Fold regulations are given in parenthesis): miR-23a (DLBCL: −11.43 vs. PTCL: 6.80), miR-155 (DLBCL: −10.92 vs. PTCL: −25.11), miR-423a (DLBCL: −2.66 vs. PTCL: −11.00), and miR-8865 (DLBCL: −11.94 vs. PTCL: −42.31; Table 2).

3.3.2 TZL and MZL

As already mentioned, TZL and MZL samples included only two samples, therefore, no *p*-value calculation was possible. As precise statements are not justified due to the small sample size, the

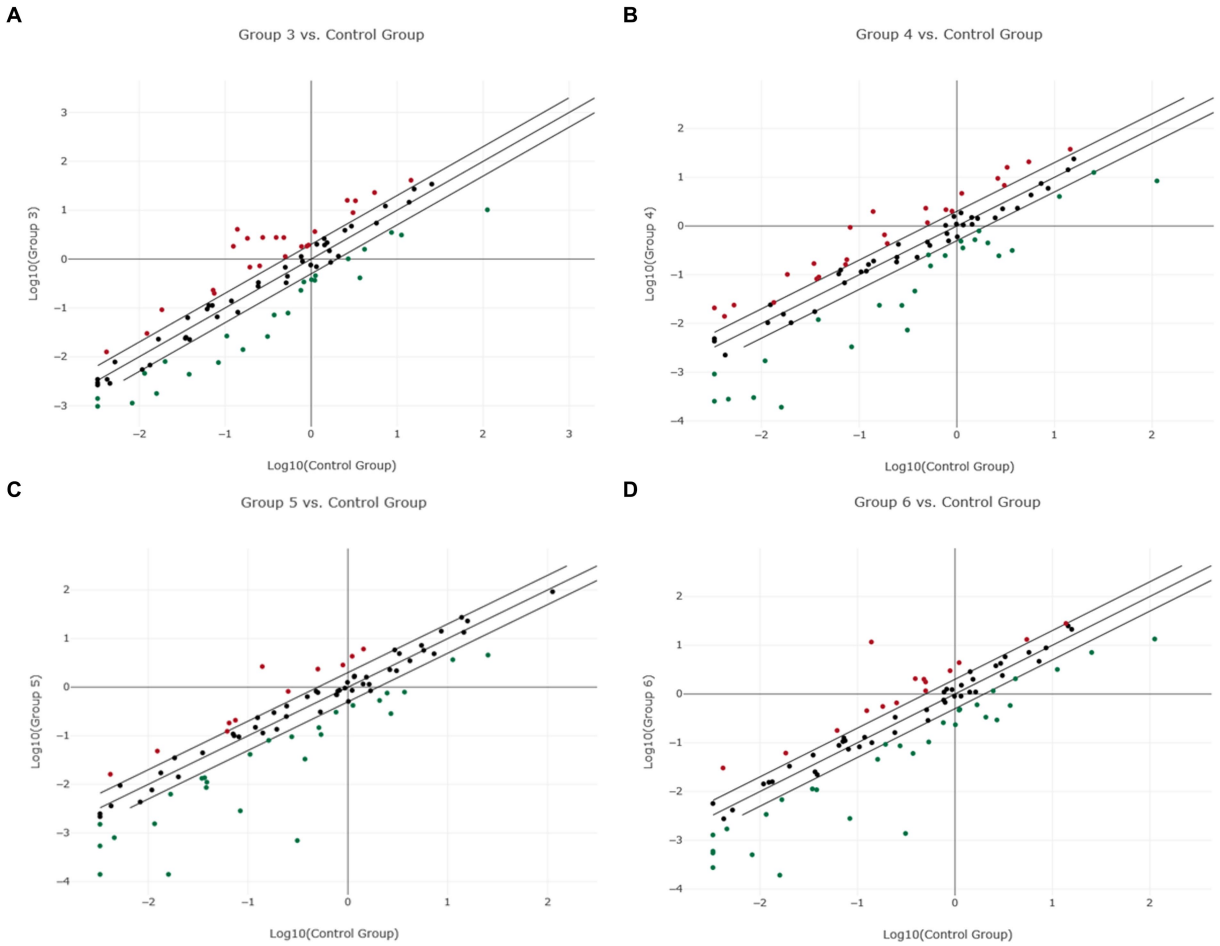

FIGURE 3
Scatter plot of normalized miRNA expression in four canine lymphoma entities compared to Lymph node (LN) as control group. The center diagonal line indicates unchanged miRNA expression, while the outer diagonal lines indicate the Fold regulation threshold >2.0. MicroRNAs with data points beyond the outer lines in the upper left and lower right corners are up-regulated (red dots) or down-regulated (green dots), by more than the Fold regulation threshold in the y-axis Group relative to the x-axis Group. **(A)** Group 3 = DLBCL vs. Control Group = LN; **(B)** Group 4 = PTCL (incl. Enteric TCL) vs. Control Group = LN; **(C)** Group 5 = TZL vs. Control Group = LN; **(D)** Group 6 = MZL vs. Control Group = LN.

presented results must be taken into consideration cautiously. For TZL, data evaluation via the Qiagen Analysis platform revealed a total of 36 of the analyzed miRNAs exceeding the Fold regulation threshold of 2.0 including 11 upregulated and 25 downregulated miRNAs (Figure 3C; Supplementary material "miRNA Expression Analysis Report 2" - Group 5). Among these 36, four miRNAs showed Fold regulation values greater/lower than ±10; whereas upregulation was found in one miRNA, namely miR-451 (Fr: 19.20) On the other hand, three miRNAs were downregulated, including miR-155 (Fr: −29.22), miR-671 (Fr: −11.19), and miR-8865 (Fr: −444.91; Table 2). Analysis of the two MZL patients showed that in total 42 of the assessed miRNAs had a higher Fold regulation threshold than 2.0 (Figure 3D; Supplementary material "miRNA Expression Analysis Report 2" - Group 6). Fifteen miRNAs out of those 42 were upregulated, whereas 27 were downregulated. Four miRNAs showed a Fold regulation threshold greater/lower than ±10. While miR-451 (Fr: 84.07) was upregulated, downregulations were found in miR-155 (Fr: −29.79), miR-450b (Fr: −11.91) and miR-8865 (Fr: −225.39; Table 2).

3.4 Influence of selected control group on microRNA expression data analysis

In this section, the lymphoma entities DLBCL and PTCL (incl. Enteric TCL) will be compared to the two control groups to evaluate data consistency and to describe potential differences (Table 3; Supplementary Table 8). In DLBCL, 16 miRNAs showed Fold regulations >2.0 when compared to both control groups, albeit 12 and 8 not significantly dysregulated miRNAs had to be excluded in comparison to PBMC or lymph node (LN), respectively (Table 3). Out of these 16 dysregulated miRNAs, miR-18a, miR-34a, miR-106a, and miR-363 were upregulated in both groups (PBMC and LN; Supplementary Figure 3). Downregulations were observed in 12 miRNAs: miR-15b, miR-23a, miR-24, miR-26b, miR-27a, miR-150, miR-181c, miR-221, miR-222, miR-223, miR-423a, and miR-450b (Table 3). For most miRNAs, Fold regulations were higher in PBMCs than in lymph node. Interestingly, all seven significantly dysregulated miRNAs exhibited higher Fold regulations in physiological lymph nodes compared to PBMCs: miR-18a, miR-23a, miR-106a, miR-181c,

10.3389/fvets.2024.1379146

TABLE 2 Fold regulation of significantly dysregulated miRNAs in four canine lymphoma entities by using Lymph node as control group.

miRNA ID	DLBCL	PTCL	TZL*	MZL*	miRNA ID	DLBCL	PTCL	TZL*	MZL*
cfa-miR-10a	−2.50	n.s.	n.s.	n.s.	cfa-miR-132	n.s.	n.s.	−2.58	−3.04
cfa-miR-10b	n.s.	n.s.	3.93	n.s.	cfa-miR-143	n.s.	n.s.	3.21	3.37
cfa-miR-15b	−3.31	n.s.	−2.47	−2.94	cfa-miR-145	n.s.	n.s.	3.93	3.99
cfa-miR-17	n.s.	n.s.	n.s.	3.35	cfa-miR-146a	−6.85	−3.53	−5.07	−5.18
cfa-miR-18a	5.74	4.83	n.s.	4.18	cfa-miR-148a	−2.41	n.s.	n.s.	n.s.
cfa-miR-19a	4.21	3.81	n.s.	2.41	cfa-miR-150	−10.98	−13.28	n.s.	−8.34
cfa-miR-19b	2.83	2.60	n.s.	n.s.	cfa-miR-155	−10.92	−25.11	−29.22	−29.79
cfa-miR-20a	4.77	4.89	n.s.	n.s.	cfa-miR-181a	n.s.	4.17	−2.66	−2.31
cfa-miR-21	n.s.	n.s.	n.s.	2.03	cfa-miR-181c	−3.93	n.s.	−2.52	n.s.
cfa-miR-23a	−11.43	−6.80	−2.00	−3.52	cfa-miR-181d	−8.66	n.s.	−4.41	−3.50
cfa-miR-24	−2.62	n.s.	n.s.	−2.03	cfa-miR-182	n.s.	n.s.	−3.47	n.s.
cfa-miR-26b	−3.61	−2.78	−3.05	−3.52	cfa-miR-183	n.s.	n.s.	−7.46	−3.41
cfa-miR-27a	−2.45	n.s.	n.s.	n.s.	cfa-miR-186	n.s.	−2.13	n.s.	−2.80
cfa-miR-29a	n.s.	−3.24	n.s.	n.s.	cfa-miR-197	n.s.	−4.61	−3.89	−6.19
cfa-miR-29b	n.s.	n.s.	4.25	n.s.	cfa-miR-199	n.s.	n.s.	2.84	n.s.
cfa-miR-29c	n.s.	−2.92	n.s.	n.s.	cfa-miR-200b	n.s.	−16.27	−5.70	−2.67
cfa-miR-30a	n.s.	n.s.	n.s.	2.33	cfa-miR-210	n.s.	n.s.	−3.47	n.s.
cfa-miR-30b	n.s.	n.s.	n.s.	n.s.	cfa-miR-218	n.s.	n.s.	3.87	7.28
cfa-miR-30d	n.s.	n.s.	−3.26	−2.12	cfa-miR-221	−2.66	n.s.	n.s.	−4.31
cfa-miR-31	n.s.	−11.61	−2.86	−3.16	cfa-miR-222	−2.98	−2.26	n.s.	−2.36
cfa-miR-34a	14.68	n.s.	n.s.	3.66	cfa-miR-223	−8.93	n.s.	−4.64	−6.35
cfa-miR-92a	n.s.	−2.01	−5.51	−3.55	cfa-miR-350	3.19	2.25	n.s.	n.s.
cfa-miR-93	2.91	2.23	n.s.	n.s.	cfa-miR-363	14.63	n.s.	n.s.	3.06
cfa-miR-99a	n.s.	n.s.	3.25	2.62	cfa-miR-378	n.s.	n.s.	n.s.	−2.09
bta-miR-99b	n.s.	n.s.	2.80	n.s.	cfa-miR-423a	−2.66	−11.00	−9.42	−9.18
cfa-miR-101	n.s.	n.s.	2.00	2.90	cfa-miR-450a	n.s.	n.s.	−2.17	−2.55
cfa-miR-106a	6.07	3.61	n.s.	n.s.	cfa-miR-450b	−2.34	n.s.	−6.05	−11.91
cfa-miR-106b	n.s.	2.80	n.s.	n.s.	cfa-miR-451	n.s.	n.s.	19.20	84.07
cfa-miR-126	n.s.	n.s.	4.73	3.53	cfa-miR-486	n.s.	n.s.	n.s.	5.27
cfa-miR-128	n.s.	n.s.	−2.66	−2.46	cfa-miR-671	−5.17	n.s.	−11.18	−6.14
cfa-miR-130b	n.s.	n.s.	−2.68	n.s.	cfa-miR-8865	−11.94	−42.31	−444.91	−225.39

Fold regulation threshold > 2.0; *p*-value threshold < 0.05; *no calculated *p*-value; ID = identifier; DLBCL (Group 3) = Diffuse Large B-cell lymphoma; PTCL (incl. Enteric T-cell lymphoma) (Group 4) = Peripheral T-cell lymphoma; TZL (Group 5) = T-zone lymphoma; MZL (Group 6) = Marginal zone lymphoma; PBMC (Control Group), Peripheral blood mononuclear cells; cfa, Canis lupus familiaris; bta, Bos taurus; miR, microRNA; n.s., not significant.

miR-221, miR-363, and miR-423a. MiRNA-18a, miRNA-106a, and miRNA-363 were upregulated, whereas miRNA-23a, miRNA-181c, miRNA-221, and miRNA-423a were downregulated (Table 3). In PTCL, for 11 miRNAs Fold regulations >2.0 were found when compared to both control groups, although 13 and 15 not significantly dysregulated miRNAs had to be excluded in comparison to PBMC or LN, respectively (Table 3). Out of these 11 dysregulated miRNAs, miR-18a and miR-181a were upregulated in both groups (PBMC and LN; Supplementary Figure 4). Downregulations were found for nine miRNAs: miR-23a, miR-29a, miR-29c, miR-31, miR-92a, miR-150, miR-197, miR-222, and miR-423a. As in DLBCL, six out of these miRNAs revealed higher Fold regulations with LN than in comparison to PBMC, including miR-18a, miR-181a, miR-23a, miR-29c, miR-31, and miR-423a (Table 3). Finally, three significantly dysregulated miRNAs were shared between by both entities in comparisons with PBMC and LN as control groups (Fold regulations are given in parenthesis): miR-18a (DLBCL/PBMC: 2.49; DLBCL/LN: 5.74; PTCL/PBMC: 2.09; PTCL/LN: 4.83), miR-23a (DLBCL/PBMC: -9.55; DLBCL/LN: -11.43; PTCL/PBMC: -5.68; PTCL/LN: −6.80), and miR-423a (DLBCL/PBMC: -2.12; DLBCL/LN: -2.66; PTCL/PBMC: -8.77; PTCL/LN: −11.00; Table 3).

4 Discussion

4.1 Differentially expressed microRNAs in canine lymphoma entities

In this exploratory study, canine lymphoma sample material was compared to two different control groups, PBMC and

10.3389/fvets.2024.1379146

TABLE 3 DLBCL and PTCL (incl. Enteric TCL) miRNA fold regulations compared between the two control groups.

	DLBCL		PTCL	
miRNA ID	PBMC	LN	PBMC	LN
cfa-miR-15b	−4.83	−3.31	n.m.	n.m.
cfa-miR-18a	**2.49**	**5.74**	**2.09**	**4.83**
cfa-miR-23a	**−9.55**	**−11.43**	**−5.68**	**−6.80**
cfa-miR-24	−3.54	−2.62	n.m.	n.m.
cfa-miR-26b	−5.11	−3.61	n.m.	n.m.
cfa-miR-27a	−3.64	−2.45	n.m.	n.m.
cfa-miR-29a	n.m.	n.m.	−3.58	−3.24
cfa-miR-29c	n.m.	n.m.	**−2.38**	**−2.92**
cfa-miR-31	n.m.	n.m.	**−9.21**	**−11.61**
cfa-miR-34a	50.61	14.68	n.m.	n.m.
cfa-miR-92a	n.m.	n.m.	−2.87	−2.01
cfa-miR-106a	**2.19**	**6.07**	n.m.	n.m.
cfa-miR-150	−24.41	−10.98	−29.51	−13.28
cfa-miR-181a	n.m.	n.m.	**2.45**	**4.17**
cfa-miR-181c	**−3.09**	**−3.93**	n.m.	n.m.
cfa-miR-197	n.m.	n.m.	−7.12	−4.61
cfa-miR-221	**−2.64**	**−2.66**	n.m.	n.m.
cfa-miR-222	−3.65	−2.98	−2.76	−2.26
cfa-miR-223	−138.82	−8.93	n.m.	n.m.
cfa-miR-363	**7.03**	**14.63**	n.m.	n.m.
cfa-miR-423a	**−2.12**	**−2.66**	**−8.77**	**−11.00**
cfa-miR-450b	−6.30	−2.34	n.m.	n.m.

MicroRNAs marked in bold exhibited higher fold regulations when using 'control group' LN for data analysis compared to 'control group' PBMC. Fold regulation threshold > 2.0; *p*-value threshold < 0.05; ID, identifier; DLBCL, Diffuse Large B-cell lymphoma; PTCL (incl. Enteric T-cell lymphoma), Peripheral T-cell lymphoma; PBMC, Peripheral blood mononuclear cells; LN, lymph node; cfa, Canis lupus familiaris; miR, microRNA; n.m., no match.

physiological lymph node material. When comparing the different lymphoma entities to the control groups, there were bigger differences in dysregulations using PBMC as control group than to physiological lymph nodes. Not many miRNAs showed significant differences between PBMC and DLBCL. In contrast, in the six PTCL (incl. Enteric TCL) patient samples, a higher number of miRNAs were significantly differentially expressed when using the same control group. In a comparable study, malignant samples were also compared to the two different control groups PBMC and lymph nodes, which also showed that the use of more than one control group is important for the analysis of dysregulated miRNAs in canine lymphomas (1).

MicroRNA-350 showed upregulation in DLBCL in comparison to lymph node material, being consistent with findings in previous studies (5). By downregulating Phosphoinositide-3-Kinase Regulatory Subunit 3 (PIK3R3), miRNA-350 promotes apoptosis. However, upregulations could be explained through its properties of inactivation of immune cells around tumors (5). In agreement with current canine literature, miRNA-155 was downregulated in both lymphoma entities when using physiological lymph nodes as control group. Since miRNA-155 activates the AKT serine/threonine kinase signaling pathway, downregulation leads to a higher proliferation as well as a higher risk for developing a more aggressive tumor (4, 7, 38). Downregulation of miRNA-23a and miRNA-26b in DLBCL and PTCL is supported by previous canine lymphoma studies (3, 39, 40). MicroRNA-23a was downregulated in both lymphoma entities when comparing them to both control groups, while for miRNA-26b this was only the case by using physiological lymph nodes as control group. To current knowledge, miRNA-23a targets two and miRNAs-26b five tumor suppressor genes, respectively. Here, the detected downregulation of these miRNAs promotes cell proliferation (3, 39, 40). Likewise in the current study, miRNA-106a was upregulated in canine DLBCL, when compared to both control groups, thus promoting uncontrolled lymphoid proliferation, cellular growth, and apoptosis inhibition (41). This axis is also regulated by miRNA-31 which was found to be downregulated in PTCL in comparison to both control groups. This finding contrasts with data being obtained during a recently conducted miRNome expression analysis in six canine DLBCL patient samples (41).

The oncogenic polycistronic cluster miRNA-17/92 was represented by five miRNAs: miRNA-18a, miRNA-19a, miRNA-19b, miRNA-20a, miRNA-92a. Except the latter one, miRNAs were upregulated in the lymphoma entities, DLBCL and PTCL when compared to lymph nodes as control group. Only miRNA-18a was also significantly expressed in comparison to PBMC, as already being described in previous studies (1, 3, 4). Upregulation of the miRNA-17/92 cluster seems to reflect the functional roles of its miRNA members as potential oncogenes in proliferation, tumor initiation and metastasis while also working as an inhibitor for apoptosis (4, 7, 41). The miRNA-181 family or to be more precise miRNA-181a (compared to PBMC), miRNA-181c (compared to both control groups), and miRNA181d (compared to physiological lymph nodes) were all downregulated in DLBCL as already been shown previously (1, 3). Those miRNAs play an important role in B- and T-cell development as they are part of the thymic differentiation, positive as well as negative selection (3). However, miRNA-181 seems to be differentially expressed in B- and T-cell lymphoma as miRNA-181a was downregulated in DLBCL while upregulated in PTCL when compared to both control groups. The overexpression of miRNA-181a has already been shown in other studies focusing on canine lymphoma (3, 7, 22). In human, miRNA-181a affects γδ T cell differentiation and depending on the cellular context it can act as a tumor suppressor (B-cell lymphoma) but can also play a role in oncogenesis (T-cell lymphoma) (22, 42, 43).

4.2 Comparative microRNA expression in human and canine lymphoma

MicroRNA-25 which was significantly downregulated in PTCL using PBMC as control group, reflecting same trends found in literature by playing an important role in regulating large tumor suppressor kinase 2 (LATS2) (2, 4, 44). In human, miRNA-25 also regulates other tumor-related genes, such as p53 and E-cadherin (2). Downregulation of miRNA-25 leads to proliferation, tumor initiation,

metastasis, cell migration, invasion, and apoptosis by different pathways (4, 44). As found in this study, miRNA-150 was downregulated in DLBCL and PTCL (incl. Enteric TCL) compared to PBMC and physiological lymph node samples. It has been shown that miRNA-150 is expressed in murine mature resting B- and T-cells, leading to the assumption that its downregulation mirrors the reduction of lymphocytes in neoplastic lymph nodes (3, 41). In human, shorter survival time and negative therapeutic response might by evidenced by miRNA-150 downregulation (3, 7). Downregulation of miRNA-151 in DLBCL when using PBMC as control group was also found in human lymphoma in the regulation of target genes being associated with tumor cells such as the neurotrophic tyrosine receptor kinase 2 (NTRK2) gene (5). When comparing PTCL (incl. Enteric TCL) to PBMC and lymph nodes, three canine miRNAs showed differences in dysregulation between the current study and published data (4, 45). These miRNAs were miRNA-29a (both control groups), miRNA-29b (PBMC as control group), and miRNA-29c (both control groups). Here, all three miRNAs were downregulated, while they usually tend to be upregulated in human study material, pointing towards different regulatory functions of these miRNAs in dogs, needing further investigations (4, 41, 45). In this study, miRNA-34a showed upregulation in both canine lymphoma entities (DLBCL and PTCL) when using both control groups, while in human, it has been shown that miRNA-34a works as tumor suppressor and is therefore downregulated (3, 7, 11). In canine lymphoma, previous studies confirmed upregulation of miRNA-34a of which it is known to target four genes being involved in cell migration thus acting as oncogene (3, 4, 7). The results for miRNA-143 being obtained in DLBCL and PTCL showed major discrepancies to previous studies. In mice, miRNA-143 was found to be downregulated in radiation induced thymic lymphoma (46). Two genes are influenced by miRNA-143, namely programmed death-ligand 1 (B7H1) and the B-cell lymphoma apoptosis regulator (Bcl-2), hence downregulation of miRNA-143 influences tumor B-cell proliferation (4, 46). Since the role of miRNA-143 in dogs has not yet been described, upregulation of miRNA-143 in canine DLBCL and PTCL could point towards an alternative role of miRNA-143 in dogs by acting as an oncogene in T- and B-cell lymphoma.

4.3 Novel described dysregulated microRNAs in canine lymphoma

At time of data analyses for the presented study, no literature evidence was available for some of the differentially expressed miRNAs under investigation. As an example, miRNA-15b, miRNA-24, miRNA-27a, miRNA-221, miRNA-223, and miRNA-450b were found to be downregulated in DLBCL in comparison to both control groups. Notably, upregulation of miRNA-363 was detected in DLBCL when compared to both control groups, PBMC and healthy lymph nodes. Together with miRNA-106a, miRNA-363 builds the oncogenic cluster miRNA-106a/363 (miRNA-106a and miRNA-92a), the paralogue to the miRNA-17/92 cluster. Additionally, miRNA-222 and miRNA-423a showed downregulations in both canine lymphoma entities, whereas miRNA-197 was downregulated only in PTCL when compared to both control groups. However, future studies will require a higher number of patients and sample number in each control group to better interpret these miRNA results.

5 Conclusion

In summary, numerous miRNAs were amplified in this exploratory project and exhibited similar results compared to other studies. Some miRNAs could be potential biomarkers in different lymphoma entities, such as the differentially expressed miRNA-181a in the investigated canine T- and B-cell lymphoma patients. Furthermore, miRNA-34a as well as miRNA-150 were significantly dysregulated in comparison to the control groups. The following miRNAs were suggested by the miRNA PCR Data Analysis Software (Qiagen) for further validation as potential biomarkers for canine DLBCL: miR-15b, miR-18a, miR-26b, miR-34a, miR-150, miR-181c, miR-223, miR-363, miR-423a, and miR-450b. However, to validate the diagnostic utility of these potential biomarkers, further studies are needed to confirm the miRNAs identified in this study as well as those, for which no data were available in the current literature. Hence, it would be advisable to work with a larger, prospective cohort of patients in all lymphoma entities and to continue the use of multiple control groups with a higher number of physiological patient material. It is of utmost importance to conduct more studies with larger sample sizes to assign differential biomarkers to canine lymphoma entities to primarily distinguish DLBCL from other lymphoma subtypes and reactive lymph nodes.

Data availability statement

The original contributions presented in the study are included in the article/Supplementary material, further inquiries can be directed to the corresponding author/s.

Ethics statement

Ethical approval was not required for the studies involving animals in accordance with the local legislation and institutional requirements because remnants of biopsy material of canine lymphoma cases served as study material together with lymph node material from eight dogs, being euthanized for reasons other than hematopoietic neoplasia. Their remains were left by the owners for disposal. Written informed consent was obtained from the owners for the participation of their animals in this study.

Author contributions

SH: Conceptualization, Investigation, Project administration, Visualization, Writing – original draft. JS: Formal analysis, Methodology, Writing – original draft. OŠ: Methodology, Resources, Writing – review & editing. SB: Methodology, Resources, Writing – review & editing. MH: Resources, Writing – review & editing, Methodology. IS: Project administration, Resources, Supervision, Writing – review & editing. BR: Resources, Writing – review & editing, Project administration, Supervision.

Funding

The author(s) declare financial support was received for the research, authorship, and/or publication of this article. Publication fees were covered by the Open Access Fonds of the University of Veterinary Medicine Vienna, Austria.

Acknowledgments

We are thankful for the excellent technical assistance to Sandra Groiss (Immunology, Department of Biological Sciences and Pathobiology, University of Veterinary Medicine Vienna, Vienna, Austria). This research was conducted using the VetBioBank resource of the VetCore Facility operated by the University of Veterinary Medicine, Vienna.

Conflict of interest

OŠ is employed by Laboklin GmbH & Co. KG.

The remaining authors declare that the research was conducted in the absence of any commercial or financial relationships that could be construed as a potential conflict of interest.

Publisher's note

Supplementary material

The Supplementary material for this article can be found online at: https://www.frontiersin.org/articles/10.3389/fvets.2024.1379146/full#supplementary-material

References

1. Uhl E, Krimer P, Schliekelman P, Tompkins SM, Suter S. Identification of altered MicroRNA expression in canine lymphoid cell lines and cases of B- and T-cell lymphomas. *Genes Chromosom Cancer*. (2011) 50:950–67. doi: 10.1002/gcc.20917

2. Fujiwara-Igarashi A, Igarashi H, Mizutani N, Goto-Koshino Y, Takahashi M, Ohno K, et al. Expression profile of circulating serum microRNAs in dogs with lymphoma. *Vet J*. (2015) 205:317–21. doi: 10.1016/j.tvjl.2015.04.029

3. Craig KKL, Wood GA, Keller SM, Mutsaers AJ, Wood RD. MicroRNA profiling in canine multicentric lymphoma. *PLoS One*. (2019) 14:e0226357. doi: 10.1371/journal.pone.0226357

4. Montaner-Angoiti E, Marín-García PJ, Llobat L. Epigenetic alterations in canine malignant lymphoma: future and clinical outcomes. *Animals (Basel)*. (2023) 13:468. doi: 10.3390/ani13030468

5. Asada H, Tomiyasu H, Uchikai T, Ishihara G, Goto-Koshino Y, Ohno K, et al. Comprehensive analysis of miRNA and protein profiles within exosomes derived from canine lymphoid tumour cell lines. *PLoS One*. (2019) 14:e0208567. doi: 10.1371/journal.pone.0208567

6. Sparks A, Woods JP, Bienzle D, Wood GA, Coomber BL. Whole genome sequencing analysis of high confidence variants of B-cell lymphoma in *Canis familiaris*. *PLoS One*. (2020) 15:e0238183. doi: 10.1371/journal.pone.0238183

7. Elshafie NO, Nascimento NC, Lichti NI, Kasinski AL, Childress MO, Santos AP. MicroRNA biomarkers in canine diffuse large B-cell lymphoma. *Vet Pathol*. (2021) 58:34–41. doi: 10.1177/0300985820967902

8. Ito D, Frantz AM, Modiano JF. Canine lymphoma as a comparative model for human non-Hodgkin lymphoma: recent progress and applications. *Vet Immunol Immunopathol*. (2014) 159:192–201. doi: 10.1016/j.vetimm.2014.02.016

9. Zandvliet M. Canine lymphoma: a review. *Vet Q*. (2016) 36:76–104. doi: 10.1080/01652176.2016.1152633

10. Ettinger SN. Principles of treatment for canine lymphoma. *Clin Tech Small Anim Pract*. (2003) 18:92–7. doi: 10.1053/svms.2003.36622

11. Garnica TK, Lesbon JCC, Ávila ACFCM, Rochetti AL, Matiz ORS, Ribeiro RCS, et al. Liquid biopsy based on small extracellular vesicles predicts chemotherapy response of canine multicentric lymphomas. *Sci Rep*. (2020) 10:20371. doi: 10.1038/s41598-020-77366-7

12. Giannuzzi D, Marconato L, Fanelli A, Licenziato L, de Maria R, Rinaldi A, et al. The genomic landscape of canine diffuse large B-cell lymphoma identifies distinct subtypes with clinical and therapeutic implications. *Lab Anim (NY)*. (2022) 51:191–202. doi: 10.1038/s41684-022-00998-x

13. Valli VE, Myint MS, Barthel A, Bienzle D, Caswell J, Colbatzky F, et al. Classification of canine malignant lymphomas according to the World Health Organization criteria. *Vet Pathol*. (2011) 48:198–211. doi: 10.1177/0300985810379428

14. Marconato L, Gelain ME, Comazzi S. The dog as a possible animal model for human non-Hodgkin lymphoma: a review. *Hematol Oncol*. (2013) 31:1–9. doi: 10.1002/hon.2017

15. Riondato F, Comazzi S. Flow cytometry in the diagnosis of canine B-cell lymphoma. *Front Vet Sci*. (2021) 8:600986. doi: 10.3389/fvets.2021.600986

16. Rigillo A, Fuchs-Baumgartinger A, Sabattini S, Škor O, Agnoli C, Schwendenwein I, et al. Ki-67 assessment-agreeability between immunohistochemistry and flow cytometry in canine lymphoma. *Vet Comp Oncol*. (2021) 19:551–66. doi: 10.1111/vco.12694

17. Stefanello D, Valenti P, Zini E, Comazzi S, Gelain ME, Roccabianca P, et al. Splenic marginal zone lymphoma in 5 dogs (2001-2008). *J Vet Intern Med*. (2011) 25:90–3. doi: 10.1111/j.1939-1676.2010.0639.x

18. Valli VE, Vernau W, Lorimier L-P, Graham PS, Moore PF. Canine indolent nodular lymphoma. *Vet Pathol*. (2006) 43:241–56. doi: 10.1354/vp.43-3-241

19. Harris LJ, Hughes KL, Ehrhart EJ, Labadie JD, Yoshimoto J, Avery AC. Canine CD4+ T-cell lymphoma identified by flow cytometry exhibits a consistent histomorphology and gene expression profile. *Vet Comp Oncol*. (2019) 17:253–64. doi: 10.1111/vco.12460

20. Fournel-Fleury C, Ponce F, Felman P, Blavier A, Bonnefont C, Chabanne L, et al. Canine T-cell lymphomas: a morphological, immunological, and clinical study of 46 new cases. *Vet Pathol*. (2002) 39:92–109. doi: 10.1354/vp.39-1-92

21. Comazzi S, Riondato F. Flow cytometry in the diagnosis of canine T-cell lymphoma. *Front Vet Sci*. (2021) 8. doi: 10.3389/fvets.2021.600963

22. Mortarino M, Gioia G, Gelain ME, Albonico F, Roccabianca P, Ferri E, et al. Identification of suitable endogenous controls and differentially expressed microRNAs in canine fresh-frozen and FFPE lymphoma samples. *Leuk Res*. (2010) 34:1070–7. doi: 10.1016/j.leukres.2009.10.023

23. Joos D, Leipig-Rudolph M, Weber K. Tumour-specific microRNA expression pattern in canine intestinal T-cell-lymphomas. *Vet Comp Oncol*. (2020) 18:502–8. doi: 10.1111/vco.12570

24. Lawrie CH, Gal S, Dunlop HM, Pushkaran B, Liggins AP, Pulford K, et al. Detection of elevated levels of tumour-associated microRNAs in serum of patients with diffuse large B-cell lymphoma. *Br J Haematol*. (2008) 141:672–5. doi: 10.1111/j.1365-2141.2008.07077.x

25. Ohyashiki K, Umezu T, Yoshizawa SI, Ito Y, Ohyashiki M, Kawashima H, et al. Clinical impact of down-regulated plasma miR-92a levels in non-Hodgkin's lymphoma. *PLoS One*. (2011) 6:e16408. doi: 10.1371/journal.pone.0016408

26. Seelig DM, Avery P, Webb T, Yoshimoto J, Bromberek J, Ehrhart EJ, et al. Canine T-zone lymphoma: unique Immunophenotypic features, outcome, and population characteristics. *J Vet Intern Med*. (2014) 28:878–86. doi: 10.1111/jvim.12343

27. Rao S, Lana S, Eickhoff J, Marcus E, Avery PR, Morley PS, et al. Class II major histocompatibility complex expression and cell size independently predict survival in canine B-cell lymphoma. *J Vet Intern Med*. (2011) 25:1097–105. doi: 10.1111/j.1939-1676.2011.0767.x

28. Avery PR, Burton J, Bromberek JL, Seelig DM, Elmslie R, Correa S, et al. Flow cytometric characterization and clinical outcome of CD4+ T-cell lymphoma in dogs: 67 cases. *J Vet Intern Med*. (2014) 28:538–46. doi: 10.1111/jvim.12304

29. Gourbault O, Llobat L. MicroRNAs as biomarkers in canine osteosarcoma: a new future? *Vet Sci*. (2020) 7:146–158. doi: 10.3390/vetsci7040146

30. Walter I, Burger S, Stargardt M, Kummer S, Wieser M. VetBiobank, Vetmeduni Vienna: a bioresource for clinical animal biospecimens. *Open J Bioresources*. (2020) 7:9. doi: 10.5334/ojb.60

31. Rütgen BC, König R, Hammer SE, Groiss S, Saalmüller A, Schwendenwein I. Composition of lymphocyte subpopulations in normal canine lymph nodes. *Vet Clin Pathol*. (2015) 44:58–69. doi: 10.1111/vcp.12221

32. Qiagen. *RNA spike-in kit, for RT, handbook. For controlling the quality of RNA isoliation, cDNA synthesis and PCR amplification for miRCURY® LNA® miRNA PCR and miRCURY LNA miRNA probe PCR experiments*, 9–13 (2020).

33. Qiagen. *miRNeasy tissue/cells advanced Micro kit handbook. For purification of total RNA, including miRNA from tissue and cells*, 7–32 (2021).

34. Qiagen. *miRCURY® LNA® miRNA SYBR® green PCR handbook. For highly sensitive, real-time RT-PCR detection of miRNAs using SYBR® green*, 16–42 (2019).

35. Vandesompele J, de Preter K, Pattyn F, Poppe B, van Roy N, de Paepe A, et al. Accurate normalization of real-time quantitative RT-PCR data by geometric averaging of multiple internal control genes. *Genome Biol*. (2002) 3:RESEARCH0034.

36. Livak KJ, Schmittgen TD. Analysis of relative gene expression data using real-time quantitative PCR and the 2(-Delta Delta C(T)) method. *Methods*. (2001) 25:402–8. doi: 10.1006/meth.2001.1262

37. Qiagen. *miRCURY LNA miRNA PCR Panels & Assays Data Analysis Handbook. For analyzing miRNA expression data from miRCURY LNA miRNA focus and custom PCR panels and miRCURY LNA miRNA PCR assays*, 6–48 (2019).

38. Albonico F, Mortarino M, Avallone G, Gioia G, Comazzi S, Roccabianca P. The expression ratio of miR-17-5p and miR-155 correlates with grading in canine splenic lymphoma. *Vet Immunol Immunopathol*. (2013) 155:117–23. doi: 10.1016/j.vetimm.2013.06.018

39. Gao P, Tchernyshyov I, Chang TC, Lee YS, Kita K, Ochi T, et al. C-Myc suppression of miR-23a/b enhances mitochondrial glutaminase expression and glutamine metabolism. *Nature*. (2009) 458:762–5. doi: 10.1038/nature07823

40. Niu F, Kazimierska M, Nolte IM, Terpstra MM, de Jong D, Koerts J, et al. The miR-26b-5p/KPNA2 Axis is an important regulator of Burkitt lymphoma cell growth. *Cancers (Basel)*. (2020) 12:1464–1484. doi: 10.3390/cancers12061464

41. Elshafie NO, Gribskov M, Lichti NI, Sayedahmed EE, Childress MO, Dos Santos AP. miRNome expression analysis in canine diffuse large B-cell lymphoma. *Front Oncol*. (2023) 13:1238613. doi: 10.3389/fonc.2023.1238613

42. Gordino G, Costa-Pereira S, Corredeira P, Alves P, Costa L, Gomes AQ, et al. MicroRNA-181a restricts human γδ T cell differentiation by targeting Map3k2 and Notch2. *EMBO Rep*. (2022) 23:e52234. doi: 10.15252/embr.202052234

43. Schönefeldt S, Wais T, Herling M, Mustjoki S, Bekiaris V, Moriggl R, et al. The diverse roles of γδ T cells in Cancer: from rapid immunity to aggressive lymphoma. *Cancers (Basel)*. (2021) 13:6212–6243. doi: 10.3390/cancers13246212

44. Wu T, Hu H, Zhang T, Jiang L, Li X, Liu S, et al. miR-25 promotes cell proliferation, migration, and invasion of non-small-cell lung Cancer by targeting the LATS2/YAP signaling pathway. *Oxidative Med Cell Longev*. (2019) 2019:1–14. doi: 10.1155/2019/9719723

45. Mazzoccoli L, Robaina MC, Bacchi CE, Soares Lima SC, Klumb CE. miR-29 promoter and enhancer methylation identified by pyrosequencing in Burkitt lymhoma cells: interplay between MYC and miR-29 regulation. *Oncol Rep*. (2019) 42:775–84. doi: 10.3892/or.2019.7183

46. Zhao H, Cheng Y, Dong S, du J, Gao F, Sun D, et al. Down regulation of miR-143 promotes radiation - induced thymic lymphoma by targeting B7H1. *Toxicol Lett*. (2017) 280:116–24. doi: 10.1016/j.toxlet.2017.07.891

frontiers | Frontiers in Veterinary Science

TYPE Original Research
PUBLISHED 23 May 2024
DOI 10.3389/fvets.2024.1373180

OPEN ACCESS

EDITED BY
Vittoria Castiglioni,
IDEXX Laboratories, Germany

REVIEWED BY
Elisabetta Treggiari,
Croce Blu Veterinaria SRL, Italy
Paola Valenti,
Clinica Veterinaria Malpensa, Italy

*CORRESPONDENCE
Antonio Giuliano
✉ agiulian@cityu.edu.hk

RECEIVED 19 January 2024
ACCEPTED 30 April 2024
PUBLISHED 23 May 2024

CITATION
Lai YY, Horta RdS, Almendros A, Ha PWY and Giuliano A (2024) L-LOP/LOPP for the treatment of canine gastrointestinal/hepatosplenic lymphoma.
Front. Vet. Sci. 11:1373180.
doi: 10.3389/fvets.2024.1373180

L-LOP/LOPP for the treatment of canine gastrointestinal/hepatosplenic lymphoma

Yu Ying Lai[1], Rodrigo dos Santos Horta[2], Angel Almendros[1,3], Patrick W. Y. Ha[3] and Antonio Giuliano[1,3]*

[1]Department of Veterinary Clinical Sciences, Jockey Club College of Veterinary Medicine, City University of Hong Kong, Kowloon, Hong Kong SAR, China, [2]Department of Veterinary Medicine and Surgery, Veterinary School, Universidade Federal de Minas Gerais, Belo Horizonte, Brazil, [3]CityU Veterinary Medical Centre, City University of Hong Kong, Kowloon, Hong Kong SAR, China

Canine gastrointestinal (GI) and hepatosplenic (HS) high-grade (large cell) lymphomas are uncommon forms of canine lymphomas, with a very poor response to chemotherapy and a very poor prognosis. Currently, there are no established effective chemotherapy protocols for canine GI/HS lymphomas. This case series aimed to retrospectively evaluate the efficacy of lomustine-based protocols L-LOP (L-asparaginase, lomustine, vincristine, and prednisolone) and L-LOPP (with the addition of procarbazine) for treatment of canine GI/HS lymphomas. Medical records of dogs with cytologically or histologically diagnosed lymphoma at CityU Veterinary Medical Centre from 2019 to 2022 were retrospectively reviewed. The L-LOP/LOPP treatment protocol was well tolerated with rare severe adverse events. Median progression-free survival for GI and HS lymphoma was 56 days (range, 10–274 days) and 57 days (range 8–135 days) respectively; while median survival time for GI and HS lymphoma was 93 days (range 10–325 days) and 210 days (range 8–240 days) respectively.

KEYWORDS

canine, lymphoma, gastrointestinal, hepatosplenic, chemotherapy, LOP, LOPP

1 Introduction

Lymphoma is one of the most common canine malignancies contributing to 85% of canine hematopoietic cancers (1). The classification of lymphoma is mainly based on the anatomical locations, grade, and immunophenotype. The most common form of high-grade lymphoma is the multicentric form that affects mainly the peripheral lymph nodes. Lymphoma of the gastrointestinal (GI) tract affects the GI tract and mesenteric lymph nodes, and hepatosplenic (HS) lymphoma is characterized by infiltration within the hepatic and splenic sinusoids (2–4). Lymphoma is categorized histologically into intermediate to high- or low-grade, as well as B- or T-cell immunophenotype, based on the Revised European American Lymphoma/World Health Organization (REAL/WHO) system for lymphoid neoplasms (5). This system also includes a cytological classification of lymphoma into large-, intermediate- or small-cells. Grading can only be established by histopathology, however, in the clinical setting, tru-cut biopsies are rarely collected in dogs with internal organ abnormalities and fine needle aspirates (FNAs) are preferred as a minimally invasive procedure carrying a low risk of complications. In the most common type of lymphoma, cell size and appearance obtained by cytology are often associated with clinical behavior, with large cells and small cells often associated with clinically aggressive and indolent progression of the lymphoma, respectively (6).

Gastrointestinal and hepatosplenic lymphomas are rare in dogs. Gastrointestinal lymphoma comprises 5–7% of all canine lymphomas, while there were only a few cases of HS lymphoma previously reported (2–4, 7–10). Upon presentation, dogs with either GI or HS large cell lymphoma show aspecific clinical signs, including inappetence, vomiting, diarrhea, lethargy, and weight loss (2, 4, 11). Both forms of lymphoma share similar biological behavior: both exhibit aggressive clinical progression, respond poorly to chemotherapy, and have a poor prognosis despite treatment (median survival time post-diagnosis ranging from 13 days to only a few months) (3, 4, 8, 9, 11–15).

The recommended treatment modality for canine lymphoma is chemotherapy (1). However, there are currently no effective and established treatment protocols for canine GI/HS lymphomas. COP[1]/CHOP[2]-based multiagent chemotherapy protocols, which are the gold standard treatment for canine multicentric lymphoma, have been administered as the first-line treatment for canine GI/HS lymphomas with very limited efficacy (4, 13, 14).

LOP[3]/LOPP[4]-based multiagent chemotherapy protocols have been used commonly as rescue protocols for relapsed canine lymphoma, with an overall response rate and complete remission of 52–61% and 27–36% reported for LOPP protocol (16, 17). Recent studies assessing the use of LOP/LOPP-based protocols as first-line treatment for multicentric high-grade canine T-cell lymphomas have shown a longer median survival time than other retrospective studies using CHOP-based protocols (18, 19). Another study assessing the efficacy of continuous L-asparaginase as first-line treatment for large cell GI lymphoma in dogs has shown promising results, suggesting L-asparaginase as a reasonable option to be used in combination with other chemotherapeutic agents as first-line therapy (15). Owing to these findings, the use of L-LOP[5]/LOPP[6]-based multiagent chemotherapy protocols for the treatment of canine GI/HS lymphomas warrant further investigation.

This retrospective study aimed to evaluate the efficacy and safety of L-LOP/LOPP-based chemotherapy protocols as first-, second-, and third-line treatment for canine GI/HS lymphomas. An additional objective was to describe signalment and clinicopathologic features for dogs with GI/HS lymphomas.

2 Materials and methods

2.1 Case selection

Electronic medical records were retrospectively reviewed to identify dogs presented with high-grade (large cell) GI and HS lymphoma to a single referral center in Hong Kong (CityU Veterinary Medical Centre), from 2019 to 2022. Dogs that at presentation had predominantly involvement of the gastrointestinal tract and mesenteric lymph nodes without significant peripheral lymphadenomegaly were considered primary GI lymphoma, while dogs with predominantly affected liver and spleen without significant involvement of the peripheral lymph nodes or other organs were classified as HS lymphoma. Case selection was limited to dogs with cytologically or histologically confirmed large cell/ high-grade lymphoma treated with (L-)LOP/LOPP-based chemotherapy protocols (either LPP, LOP or LOPP, which includes lomustine, prednisolone, procarbazine, vincristine, plus/minus L-asparaginase).

2.2 Medical records review

Data collected from the medical histories included signalment (age, sex, neuter status, and breed), clinical signs at initial presentation, date of diagnosis, body weight at diagnosis, hematology and serum biochemistry including total serum calcium results, three views thoracic radiographs and abdominal ultrasonography, methods used for confirmation of diagnosis, methods and results of immunophenotyping, anatomic locations of the lymphoma, and the date and cause of death.

Details of the treatment protocols used (surgery, chemotherapy, or their combinations) were retrieved, including the type and dosage of each chemotherapeutic drug used as first-, second- and third-line treatment. First-line treatment was defined as the planned chemotherapy protocol for each patient at the beginning of the treatment course while second- or third-line treatment involved a change to another chemotherapy protocol or agent based on the attending veterinarian's decision (after deeming the patient non-responsive to the previous treatment, following lymphoma relapse, or due to severe adverse events (AEs) related to the previously used protocol).

Response to treatment, including clinical response and objective response, were retrospectively analyzed according to the RECIST (Response Evaluation Criteria for Solid Tumors) criteria for canine lymphoma (20). Adverse events after chemotherapy were categorized and graded according to the Veterinary Cooperative Oncology Group–Common Terminology Criteria for Adverse Events version 2 guidelines (21). Staging was performed for all patients with three views thoracic radiographs and abdominal ultrasound. Assessment of response was achieved by repeated abdominal ultrasound examination and measurement of the mass/lesions when present. Clinical improvement was judged by physical examination and owner interview at each revisit. All dogs were managed and followed up at the same institution from the diagnosis to the euthanasia or death of the patient. Details of the chemotherapy protocol can be found in Table 1.

2.3 Statistical analysis

Median survival time (MST) and progression-free survival (PFS) were calculated separately for dogs with gastrointestinal lymphoma and hepatosplenic lymphoma, using the Kaplan–Meier analysis method. Survival time was defined as the time from initial diagnosis to death from any cause. Dogs alive at the end of the study or lost to follow-up were censored. Progression free survival was defined as the time from confirmed diagnosis until disease progression, disease relapse, or death. For all analyses, a p-value of ≤ 0.05 was considered statistically significant. Statistical analyses were performed using

1 COP: cyclophosphamide, vincristine, prednisolone.
2 CHOP: cyclophosphamide, doxorubicin, vincristine, prednisolone.
3 LOP: lomustine, vincristine, prednisolone.
4 LOPP: lomustine, vincristine, procarbazine, prednisolone.
5 L-LOP: LOP with the addition of l-asparaginase.
6 L-LOPP: LOPP with the addition of l-asparaginase.

10.3389/fvets.2024.1373180

TABLE 1 Median and range of doses of chemotherapeutic drugs administered as part of the L-LOP/LOPP protocol 21-day cycle.

Abbreviation	Drug	Median dose (range)
L-	L-asparaginase	10,000 IU/m2 (5000–13,000) Day 1
L	Lomustine	50 mg/m2 (30–60)- Day 7 every 3 weeks
O	Vincristine	0.5 mg/m2 (0.35–0.75) Day 2 (weekly)
P	Procarbazine	50 mg/m2 (35–65) day 1 for 10/15 days
P	Prednisolone	0.83 mg/kg daily (0.18–1.79)

standard softwares SPSS, v. 29, IBM Corp, and GrphPadPrism v. 6.02.

3 Results

3.1 Signalment

Fourteen dogs were retrieved from the clinic database, seven with GI lymphoma and seven with HS lymphoma. All dogs received treatment at CityU Veterinary Medical Centre. Data of dogs with GI/HS lymphoma were presented in Tables 2, 3, respectively.

The median age at the time of diagnosis was 13 years (range 4–14 years). There were 5 males (5/7 [71%]), 3 castrated and 2 sexually intact; and 2 females (2/7 [29%]), both spayed. The median weight at initial presentation was 7.1 kg (range 5.4–29.4 kg).

Dogs with HS lymphoma consisted of 6 breeds, namely Poodle (1/7 [14%]), French Bulldog (1 [14%]), Corgi (1 [14%]), Shiba Inu (1 [14%]) and Japanese Spitz (1 [14%]). There were also two mixed-breed dogs (29%). The median age at the time of diagnosis was 11 years (range 6–13 years). There were 6 males (6/7 [86%]), all castrated; and one spayed female (1/7 [14%]). The median weight at initial presentation was 13.4 kg (range 7.18–19.2 kg).

3.2 Clinical and ultrasound imaging findings

All dogs were classified into the substage b and showed different clinical signs at presentation. The most common clinical sign for dogs with GI lymphoma included diarrhea (7/7 [100%]), anorexia (7 [100%]), lethargy (5 [71%]), vomiting (5 [71%]), and weight loss (4 [57%]). On physical examination, 2 dogs (29%) were presented with painful abdomen while 2 other dogs had subjectively distended abdomen, but no significant ascites. Common findings on abdominal ultrasound were small intestinal wall thickening with loss of layering and/or small intestinal mass (7/7 [100%]), mesenteric lymph node(s) enlargement (6 [86%]), peritonitis (4 [57%]), mild splenomegaly (3 [43%]), mild hepatomegaly (2 [29%]) and stomach wall thickening (2 [29%]). Most dogs (5/7 [71%]) were presented with focal disease on abdominal ultrasound, including focal wall thickening with loss of wall layering of a small intestinal segment or stomach, or a hypoechoic irregularly vascularized small intestinal/mesenteric mass. Often coupled with the focal lesion was regional peritonitis (hyperechoic peritoneum or mesentery plus/minus a small amount of anechoic abdominal effusion in the area of the affected intestine) and enlarged hypoechoic mesenteric lymph nodes. Dogs with diffuse disease on abdominal ultrasound (2/7 [29%]) were presented with generalized wall thickening of the small intestines or stomach plus/minus layering loss and marked abdominal lymphadenopathy (multiple mesenteric lymph nodes enlarged with hypoechoic texture).

For dogs with HS lymphoma, the most common clinical signs were anorexia (6/7 [86%]), lethargy (6 [86%]), weight loss (4 [57%]), diarrhea (4 [57%]), and vomiting (4 [57%]). On physical examination, most dogs were presented with distended abdomen due to organomegaly (4/7 [57%]), while 2 other dogs (29%) had painful abdomen. Common findings on abdominal ultrasound included hepatomegaly (7/7 [100%]), splenomegaly (6 [86%]), and mesenteric lymph node(s) enlargement (5 [71%]). One dog (14%) showed tracheobronchial lymph node(s) enlargement on thoracic radiography. In dogs with hepatomegaly on abdominal ultrasound, the most common presentation was generalized increased echogenicity and coarse architecture of the liver (4 out of 7 cases [57%]), while others presented as normal echogenicity, hypoechoic, or diffused infiltration by mixed echogenic multi-nodular masses within the hepatic parenchyma. The enlarged spleen mostly appeared diffusely heterogeneous on ultrasound, either with mottled echotexture and multiple miliary to coalescing hypoechoic nodules, or diffusely effaced by mixed echogenic multi-nodular mass lesions.

3.3 Laboratory abnormalities

Both hematology and serum biochemistry including total calcium tests were conducted in all cases at the time of initial diagnosis and during every weekly recheck, but serum ionized calcium and bone marrow evaluation were not performed in any of the patients. Dogs with GI lymphoma were commonly presented with mild to moderate anemia (5/7 [71%]), mild to moderate hypoalbuminemia (5 [71%]), mildly increased liver parameters (2 [29%] – median value of increased ALT of 302.5 U/L and ALP of 1106.5 U/L), mild thrombocytopenia (2 [29%]), mild neutrophilia (2 [29%]), and mild hypoglycemia (2 [29%]). For dogs with HS lymphoma, mildly increased liver parameters (6/7 [86%] – median value of increased ALT of 354.5 U/L and ALP of 1403.6 U/L), mild thrombocytopenia (5 [71%]), mild anemia (4 [57%]), and mild hypoalbuminemia (3 [43%]) were the most commonly reported findings.

3.4 Diagnosis and immunophenotype

Diagnosis of GI lymphoma was achieved mainly via cytology (6/7 [86%]) through ultrasound-guided FNAs of the small intestinal lesion and/or mesenteric lymph node(s). No FNAs of liver and spleen were obtained in those patients without significant abnormalities of the liver and spleen on ultrasound. One remaining dog was diagnosed by histology (Table 2, case 4) through exploratory laparotomy with resection and anastomosis of a grossly abnormal section of the small intestine. Immunophenotyping was performed for 2 dogs by immunocytochemistry ($n = 1$) and immunohistochemistry ($n = 1$), with both cases testing positive for T-cell CD3.

TABLE 2 Data on 7 dogs with gastrointestinal lymphoma.

Case no.	Signalment			Diagnostic method	Immuno-phenotype	Affected locations	Treatments	Chemotherapy protocol			Clinical Response**	Objective Response‡	PFS^ (d)	Survival time (d)
	Age (year)	Breed	Sex*					First-line	Second-line	Third-line				
1	13	Shih tzu	M	Cytology	NA†	Small intestine, mesenteric lymph nodes	Chemotherapy only	L-LPP	Doxorubicin/ epirubicin, cytarabine, l-asparaginase	None	+	CR	274	325
2	13	Jack russell terrier	MN	Cytology	NA	Small intestine	Chemotherapy only	L-LOPP	None	None	+	SD	18	18
3	13	Husky	MN	Cytology	NA	Small intestine, mesenteric and peripheral lymph nodes, liver, spleen, CNS#	Chemotherapy only	L-LOP	None	None	+	PR	37	37
4	7	Husky	FN	Histology	T-cell	Small intestine, mesenteric lymph nodes	Surgery and chemotherapy	LOPP	Doxorubicin	None	+	SD	94	124
5	4	English bulldog	M	Cytology	NA	Small intestine, stomach, mesenteric and peripheral lymph nodes, CNS	Chemotherapy only	L-LOP	None	None	–	PD	10	10
6	7	Shih tzu	MN	Cytology	T-cell	Small intestine, liver, spleen, mesenteric and peripheral lymph nodes	Chemotherapy only	L-LOP	None	None	+	PR	56	93
7	14	Shih tzu	FN	Cytology	NA	Small intestine, mesenteric lymph nodes	Chemotherapy only	L-LOPP	Modified L-CHOP	Cytarabine, chlorambucil, l-asparaginase	+	CR	78	113

*M = Male; MN = Male neutered; F=Female; FN=Female neutered.

**Clinical response was reported for the chemotherapy protocol(s) of interest (i.e., L-LPP or L-LOP or (L-)LOPP). + = improvement; – = no improvement.

‡Objective response was reported for the chemotherapy protocol(s) of interest (i.e., L-LPP or L-LOP or (L-)LOPP). CR = Complete response; PR = Partial response; SD=Stable disease, PD=Progressive disease.

^PFS was reported for the chemotherapy protocol(s) of interest (i.e., L-LPP or L-LOP or (L-) LOPP).

†NA = not available.

#CNS=Central nervous system.

10.3389/fvets.2024.1373180

TABLE 3 Data on 7 dogs with hepatosplenic lymphoma.

Case no.	Signalment			Diagnostic method	Immuno-phenotype	Affected locations	Treatments	Chemotherapy protocol			Clinical response##	Objective response‡	PFS^ (d)	Survival time (d)
	Age (year)	Breed	Sex*					First-line	Second-line	Third-line				
8	11	Cross breed	MN	Cytology	T-cell	Liver, spleen, mesenteric and peripheral lymph nodes	Chemotherapy only	L-COP	Doxorubicin	L-LPP, cytarabine	+	SD	59	110^^
9	13	Poodle	MN	Cytology	NA†	Liver, spleen, peripheral lymph nodes, eyes	Chemotherapy only	L-COP	LOP	None	+	SD	133	197^^
10	6	French bulldog	MN	Cytology	B-cell	Liver, spleen, small intestine, mesenteric and peripheral lymph nodes, central nervous system	Chemotherapy only	L-CHOP	LPP	Modified CHOP, cytarabine	+	PD	24	210
11	13	Corgi	MN	Cytology	NA	Liver, spleen	Chemotherapy only	Lomustine, l-asp#	None	None	–	PD	8	8
12	8	Shiba inu	MN	Cytology	T-cell	Liver, spleen, mesenteric lymph nodes	Chemotherapy only	L-LOP, leflunomide	Doxorubicin, leflunomide, l-asp	None	+	PD	57	Lost to follow-up
13	6	Cross breed	FN	Cytology	T-cell	Liver, spleen, mesenteric and peripheral lymph nodes, bone marrow, kidneys	Chemotherapy only	L-LOP	L-CHOP, cytarabine, chlorambucil	None	+	SD	135	240
14	12	Japanese spitz	MN	Cytology	NA	Liver, spleen, peripheral lymph nodes, skin	Chemotherapy only	LOP	Doxorubicin, l-asp	None	+	CR	57	64

*M = Male; MN = Male neutered; F=Female; FN=Female neutered.

##Clinical response was reported for the chemotherapy protocol(s) of interest (i.e., lomustine, (L-)LPP or (L-)LOP). + = improvement; – = no improvement.

‡Objective response was reported for the chemotherapy protocol(s) of interest (i.e., lomustine, (L-)LPP or (L-)LOP). CR = Complete response; PR = Partial response; SD=Stable disease, PD=Progressive disease.

^PFS was reported for the chemotherapy protocol(s) of interest (i.e., lomustine, (L-)LPP or (L-)LOP).

^^Non-lymphoma-related death.

#l-asp = L-asparaginase.

10.3389/fvets.2024.1373180

Diagnosis of all 7 cases of HS lymphoma was confirmed by cytology, through ultrasound-guided fine needle aspiration of the liver and spleen. Immunophenotyping was performed for 4 dogs by immunocytochemistry: 3/4 (75%) tested positive for T-cell CD3, while 1/4 (25%) tested positive for B-cell Pax-5.

3.5 Treatment

The majority of dogs with GI lymphoma (6/7 [86%]) received chemotherapy as the sole treatment, while 1 dog (Table 2, case 4) underwent surgical resection of the affected small intestinal segment followed by chemotherapy. All the chemotherapy protocols used as first-line treatment in GI lymphoma were LOP/LOPP based (either LPP, LOP or LOPP plus/minus L-asparaginase, as reported in Table 2). Rescue treatments were administered in 2 dogs (Table 2, case 1 and 4), whereas 1 dog received up to three rescue treatments (Table 2, case 7).

All dogs diagnosed with HS lymphoma were treated with chemotherapy only. Four out of 7 dogs (57%) were administered LOP/LOPP-based protocols as first-line treatment (either lomustine as a single agent or LOP plus/minus L-asparaginase, as reported in Table 3). LOP/LOPP-based protocols were used as second-line treatment in 2 cases (Table 3, case 9 and 10) and as third-line treatment in 1 case (Table 3, case 8). The median values and ranges of doses of each drug included in the L-LOP/LOPP protocol for the treatment of both gastrointestinal and hepatosplenic lymphoma (i.e., l-asparaginase, lomustine, vincristine, procarbazine, and prednisolone) are reported in Table 1.

3.6 Outcomes

3.6.1 Survival time and progression-free survival (PFS)

The MST and PFS for all the 14 cases treated with the (L-)LOP/LOPP were 103 days and 57 days, respectively (Figure 1).

All seven dogs with GI lymphoma and 4 out of 7 dogs (57%) with HS lymphoma had died or were euthanized due to the lymphoma by the end of the study. Among the three remaining dogs with HS lymphoma, one was lost to follow-up, one died of pneumonia and sepsis, and one died of renal failure.

The MST and PFS for dogs with GI treated with (L-)LOP/LOPP-based chemotherapy protocols were 93 days (range 10–325 days); whereas the MST for dogs with HS lymphoma was 210 days (range 8–240 days).

The PFS for dogs with GI and HS lymphoma were 56 days (range 10–274 days) and 57 days (range 8–135 days) respectively.

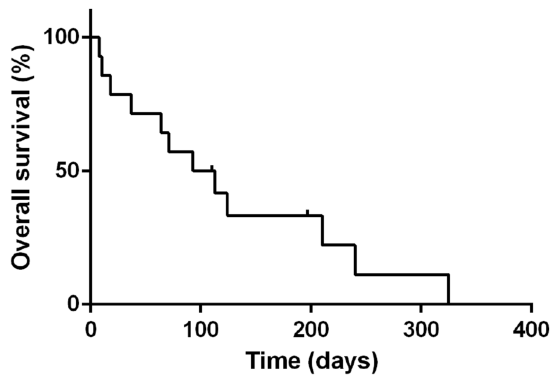

FIGURE 1
Median survival time of all 14 dogs treated with L-LOP/P. Dots represent censored patients.

3.6.2 Response to treatment and adverse events

Of all the dogs with GI lymphoma that received chemotherapy as the sole treatment and were treated with LOP/LOPP as a first-line treatment, 5/6 dogs (83%) showed clinical improvement after starting the treatment, such as improved appetite, increased activity and weight gain. The dog that was surgically treated followed by first-line chemotherapy with LOPP (Table 2, case 4) also showed clinical improvement. As assessed by the RECIST criteria for lymphoma in dogs, 2/7 dogs (29%) showed complete response, 2/7 dogs (29%) showed partial response, 2/7 dogs (29%) showed stable disease, and 1/7 dog (14%) showed progressive disease after initial chemotherapy treatment (Table 2) (20).

For dogs with HS lymphoma that received LOP/LOPP-based chemotherapy treatments as first-, second-, or third-line treatment, 6/7 (86%) showed clinical improvement. Responses to LOP/LOPP chemotherapy were: 1/7 (14%) showed complete response, 3/7 (43%) showed stable disease, and 3/7 (43%) showed progressive disease (Table 3). The MST of patients who received L-LOP/LOPP-based first-line treatment was 64 days, (ranging from 8 to 240 days) while patients who received non-L-LOP/LOPP-based first-line treatment was 210 days (ranging from 110 to 210 days).

The main AE observed in 14 dogs after receiving L-LOP/LOPP-based chemotherapy, either as first-line treatments or rescue protocols, were reported in Table 4. Gastrointestinal adverse events (AEs) were reported in 79% of cases (11/14), which included hyporexia, vomiting and diarrhea. Both neutropenia and anemia in 71% of cases (10/14). Most adverse events observed were mild (Grade I or Grade II), and no Grade V adverse events were recorded.

4 Discussion

A high-grade GI lymphoma is an aggressive form of lymphoma that carries a poor response to chemotherapy and a very poor prognosis. Similar to other studies, the findings of the present study showed a poor survival time with a median PFS of 56 days (range 10–274 days) and an MST of 93 days (range 10–325 days). Literature reports with CHOP-based protocols had MSTs of 60 days and 77 days, comparable with the MST of patients receiving L-LOP/LOPP-based chemotherapy in the present study (13, 14). In the other two studies, single-agent lomustine treatment (MST 144 days) and continuous L-asparaginase treatment (MST 147 days) had longer survival times than the current study (13, 15). From our and other previous small studies, it is unclear if lomustine-based protocols are superior or similarly effective to CHOP protocol. Larger prospective studies are necessary to have a definitive answer on what is the best chemotherapy treatment protocol, if any, for GI lymphoma in dogs.

TABLE 4 Incidence of adverse events of different severity after L-LOP/LOPP chemotherapy.

Category	Grade I	Grade II	Grade III	Grade IV	Total incidence
Gastrointestinal tract	5	6	0	0	79% (11/14)
Hematologic					
Neutropenia	2	2	3	3	71% (10/14)
Thrombocytopenia	3	2	0	3	57% (8/14)
Anemia	1	4	3	2	71% (10/14)
Hepatotoxicity	2	6	1	0	64% (9/14)

In our study, the median PFS (57 days, range 8–135 days) and MST (210 days, range 8–240 days) for dogs with HS lymphoma were numerically much longer than in previous literature, which reported survival times ranging from 1 to 24 days with a single case exception surviving up to 196 days (4, 8, 9). A possible explanation is that in previously reported cases of HS lymphomas, only 2 out of 9 cases received chemotherapy, whereas the others showed rapid clinical deterioration and hence did not receive any treatment. However, in another study of dogs treated with CHOP-based protocol for presumed primary hepatic lymphoma an MST of 64 days was achieved (22).

The commonly reported clinical signs of GI and HS lymphomas in the present study (anorexia, lethargy, weight loss, diarrhea, and vomiting) coincide with previous studies (2, 4, 11, 13). these non-specific clinical signs with insidious onset may delay the confirmation of diagnosis, causing the patients to be presented with an advanced disease state resulting in a poorer prognosis.

The majority of GI and HS lymphomas are of T-cell origin (4, 8–13, 23). The present study was unable to exhibit a trend of immunophenotype for GI lymphoma, as most cases (5/7 cases) did not undergo immunophenotyping. In dogs with HS lymphoma, T-cell lymphoma appeared to be the predominant immunophenotype (3 cases of T-cell origin, 1 case of B-cell origin). Although there are only scarce reports of HS lymphoma in dogs it is likely to arise from splenic cytotoxic γδ-T-cells, which represents a specific syndrome in people known as hepatosplenic gamma-delta T-cell lymphoma (4, 8, 9). Nevertheless, primary or secondary HS large B-cell lymphomas are also reported in humans and may also occur in dogs (24, 25). Lack of immunolabeling for both T- and B-cell markers may also occur as a result of loss of T/B-cell antigen receptor complex expression (4). T-cell high-grade canine multicentric lymphomas have been associated with more aggressive biological behavior and poorer response to chemotherapy compared to the B-cell phenotype (26–28). However, there is no known prognostic significance for T and B immunophenotypes in GI or HS lymphoma.

L-LOP/LOPP-based chemotherapy exhibited an acceptable level of toxicity in the present study as most adverse events recorded were mild, and were all transient (i.e., patients recovered after reducing the dose or increasing the dosing intervals of chemotherapeutic drugs). In addition, the adverse events observed (e.g., diarrhea, vomiting) may not be entirely attributable to the drugs but may be due to the presence of the lymphoma or a combination of the above, which often represents a confounding factor, especially in retrospective studies. Lomustine-based treatment carries a risk of drug-induced hepatotoxicity (29) and the choice of administering a lomustine-based protocol in HS lymphoma could increase the risk of hepatotoxicity. Vincristine is also metabolized mainly in the liver and liver impairment could decrease the clearance of the drug and increase AEs (30). However, all the dogs were started on L-asparaginase and prednisolone followed by vincristine injection before the liver parameters improved and were considered acceptable. Only then, lomustine was administered. Both the doses of lomustine and vincristine were also reduced if some degree of liver impairment was suspected. The degree of dose reduction was established at the discretion of the clinician based on clinical assessment and the result of liver parameters.

There are a few limitations to this study. The retrospective nature of the study and the small number of cases for both groups is one of the most important limitations. The chemotherapeutic drugs used, dosages, and dosing intervals were not standardized. Histopathology confirmation and immunohistochemistry were performed in only one case; however, this is standard procedure in clinical practice where most large-cell/high-grade lymphomas are diagnosed by cytology, especially if involving internal organs. The lack of histopathology confirmation may result in the accidental inclusion of cases of other round-cell neoplasms with comparable survival, although this is quite unlikely. With canine GI/HS lymphomas being rare diseases, the sample size ($n = 14$) of the present study was small, resulting in low statistical power.

In the current study, the use of L-LOP/LOPP-based chemotherapy protocols for the treatment of canine GI/HS lymphomas has shown clinical improvement in most cases, comparable survival times with other chemotherapy protocols including CHOP, and well-tolerated AEs in patients, thus making it a viable treatment option which warrants further investigations. Future prospective studies are needed to better assess the efficacy of L-LOP/LOPP in GI and HS lymphoma in dogs.

Data availability statement

The original contributions presented in the study are included in the article/supplementary material, further inquiries can be directed to the corresponding author.

Ethics statement

The study has been approved by the animal research ethics committee of CityU, application n. ASTA-00000016.

Author contributions

YL: Data curation, Formal analysis, Writing – original draft. RH: Writing – review & editing. AA: Writing – review & editing. PH: Data curation, Writing – review & editing. AG: Conceptualization, Data curation, Investigation, Methodology, Supervision, Writing – review & editing.

Funding

The author(s) declare that no financial support was received for the research, authorship, and/or publication of this article.

Conflict of interest

The authors declare that the research was conducted in the absence of any commercial or financial relationships that could be construed as a potential conflict of interest.

The author(s) declared that they were an editorial board member of Frontiers, at the time of submission. This had no impact on the peer review process and the final decision.

Publisher's note

References

1. Ettinger SN. Principles of treatment for canine lymphoma. *Clin Tech Small Anim Pract*. (2003) 18:92–7. doi: 10.1053/svms.2003.36622

2. Valls SM, Purzycka K. Canine alimentary lymphoma: clinical presentation and treatment options. *Vet Ireland J*. (2022) 12:152–4.

3. Couto CG, Rutgers HC, Sherding RG, Rojko J. Gastrointestinal lymphoma in 20 dogs. A retrospective study. *J Vet Intern Med*. (1989) 3:73–8. doi: 10.1111/j.1939-1676.1989.tb03082.x

4. Keller SM, Vernau W, Hodges J, Kass PH, Vilches-Moure JG, McElliot V, et al. Hepatosplenic and hepatocytotropic T-cell lymphoma: two distinct types of T-cell lymphoma in dogs. *Vet Pathol*. (2013) 50:281–90. doi: 10.1177/0300985812451625

5. Valli VE, San Myint M, Barthel A, Bienzle D, Caswell J, Colbatzky F, et al. Classification of canine malignant lymphomas according to the World Health Organization criteria. *Vet Pathol*. (2011) 48:198–211. doi: 10.1177/0300985810379428

6. Valli VE, Kass PH, San Myint M, Scott F. Canine lymphomas: association of classification type, disease stage, tumor subtype, mitotic rate, and treatment with survival. *Vet Pathol*. (2013) 50:738–48. doi: 10.1177/0300985813478210

7. Coyle KA, Steinberg H. Characterization of lymphocytes in canine gastrointestinal lymphoma. *Vet Pathol*. (2004) 41:141–6. doi: 10.1354/vp.41-2-141

8. Fry MM, Vernau W, Pesavento PA, Bromel C, Moore PF. Hepatosplenic lymphoma in a dog. *Vet Pathol*. (2003) 40:556–62. doi: 10.1354/vp.40-5-556

9. Cienava EA, Barnhart KF, Brown R, Mansell J, Dunstan R, Credille K. Morphologic, immunohistochemical, and molecular characterization of hepatosplenic T-cell lymphoma in a dog. *Vet Clin Pathol*. (2004) 33:105–10. doi: 10.1111/j.1939-165X.2004.tb00357.x

10. Akiyoshi M, Hisasue M, Asakawa MG, Neo S, Akiyoshi M. Hepatosplenic lymphoma and visceral mast cell tumor in the liver of a dog with synchronous and multiple primary tumors. *Vet Clin Pathol*. (2022) 51:414–21. doi: 10.1111/vcp.13086

11. Frank JD, Reimer SB, Kass PH, Kiupel M. Clinical outcomes of 30 cases (1997-2004) of canine gastrointestinal lymphoma. *J Am Anim Hosp Assoc*. (2007) 43:313–21. doi: 10.5326/0430313

12. Ozaki K, Yamagami T, Nomura K, Narama I. T-cell lymphoma with eosinophilic infiltration involving the intestinal tract in 11 dogs. *Vet Pathol*. (2006) 43:339–44. doi: 10.1354/vp.43-3-339

13. Sogame N, Risbon R, Burgess KE. Intestinal lymphoma in dogs: 84 cases (1997-2012). *J Am Vet Med Assoc*. (2018) 252:440–7. doi: 10.2460/javma.252.4.440

14. Rassnick KM, Moore AS, Collister KE, Northrup NC, Kristal O, Chretin JD, et al. Efficacy of combination chemotherapy for treatment of gastrointestinal lymphoma in dogs. *J Vet Intern Med*. (2009) 23:317–22. doi: 10.1111/j.1939-1676.2008.0270.x

15. Nakagawa T, Kojima M, Ohno K, Chambers JK, Uchida K, Ohmi A, et al. Efficacy and adverse events of continuous l-asparaginase administration for canine large cell lymphoma of presumed gastrointestinal origin. *Vet Comp Oncol*. (2022) 20:102–8. doi: 10.1111/vco.12749

16. LeBlanc AK, Mauldin GE, Milner RJ, LaDue TA, Mauldin GN, Bartges JW. Efficacy and toxicity of BOPP and LOPP chemotherapy for the treatment of relapsed canine lymphoma. *Vet Comp Oncol*. (2006) 4:21–32. doi: 10.1111/j.1476-5810.2006.00088.x

17. Fahey CE, Milner RJ, Barabas K, Lurie D, Kow K, Parfitt S, et al. Evaluation of the University of Florida lomustine, vincristine, procarbazine, and prednisone chemotherapy protocol for the treatment of relapsed lymphoma in dogs: 33 cases (2003-2009). *J Am Vet Med Assoc*. (2011) 239:209–15. doi: 10.2460/javma.239.2.209

18. Brown PM, Tzannes S, Nguyen S, White J, Langova V. LOPP chemotherapy as a first-line treatment for dogs with T-cell lymphoma. *Vet Comp Oncol*. (2018) 16:108–13. doi: 10.1111/vco.12318

19. Morgan E, O'Connell K, Thomson M, Griffin A. Canine T cell lymphoma treated with lomustine, vincristine, procarbazine, and prednisolone chemotherapy in 35 dogs. *Vet Comp Oncol*. (2018) 16:622–9. doi: 10.1111/vco.12430

20. Vail DM, Michels GM, Khanna C, Selting KA, London CA, Veterinary Cooperative Oncology Groupet al. Response evaluation criteria for peripheral nodal lymphoma in dogs (v1.0)-a veterinary cooperative oncology group (VCOG) consensus document. *Vet Comp Oncol*. (2010) 8:28–37. doi: 10.1111/j.1476-5829.2009.00200.x

21. LeBlanc AK, Atherton M, Bentley RT, Boudreau CE, Burton JH, Curran KM, et al. Veterinary cooperative oncology group-common terminology criteria for adverse events (VCOG-CTCAE v2) following investigational therapy in dogs and cats. *Vet Comp Oncol*. (2021) 19:311–52. doi: 10.1111/vco.12677

22. Dank G, Rassnick KM, Kristal O, Rodriguez CO, Clifford CA, Ward R, et al. Clinical characteristics, treatment, and outcome of dogs with presumed primary hepatic lymphoma: 18 cases (1992-2008). *J Am Vet Med Assoc*. (2011) 239:966–71. doi: 10.2460/javma.239.7.966

23. Miura T, Maruyama H, Sakai M, Takahashi T, Koie H, Yamaya Y, et al. Endoscopic findings on alimentary lymphoma in 7 dogs. *J Vet Med Sci*. (2004) 66:577–80. doi: 10.1292/jvms.66.577

24. Zhang X, Sun M, Zhang L, Shao H. Primary hepatosplenic CD5-positive diffuse large B-cell lymphoma: a case report with literature review. *Int J Clin Exp Pathol*. (2013) 6:985–9.

25. Ibrahim U, Garcia G, Saqib A, Hussein S, Dai Q. T cell Histiocyte rich large B cell lymphoma presenting as Hemophagocytic Lymphohistiocytosis: an uncommon presentation of a rare disease. *Case Rep Oncol Med*. (2017) 2017:1–5. doi: 10.1155/2017/6428461

26. Carter RF, Valli VE, Lumsden JH. The cytology, histology and prevalence of cell types in canine lymphoma classified according to the National Cancer Institute working formulation. *Can J Vet Res*. (1986) 50:154–64.

27. Simon D, Moreno SN, Hirschberger J, Moritz A, Kohn B, Neumann S, et al. Efficacy of a continuous, multiagent chemotherapeutic protocol versus a short-term single-agent protocol in dogs with lymphoma. *J Am Vet Med Assoc*. (2008) 232:879–85. doi: 10.2460/javma.232.6.879

28. Simon D, Nolte I, Eberle N, Abbrederis N, Killich M, Hirschberger J. Treatment of dogs with lymphoma using a 12-week, maintenance-free combination chemotherapy protocol. *J Vet Intern Med*. (2006) 20:948–54. doi: 10.1892/0891-6640(2006)20[948:todwlu]2.0.co;2

29. Chakkath T, Lavergne S, Fan T, Bunick D, Dirikolu L. Preliminary metabolism of Lomustine in dogs and comparative cytotoxicity of Lomustine and its major metabolites in canine cells. *Vet Sci*. (2014) 1:159–73. doi: 10.3390/vetsci1030159

30. Hantrakul S, Klangkaew N, Kunakornsawat S, Tansatit T, Poapolathep A, Kumagai S, et al. Clinical pharmacokinetics and effects of vincristine sulfate in dogs with transmissible venereal tumor (TVT). *J Vet Med Sci*. (2014) 76:1549–53. doi: 10.1292/jvms.14-0180

Frontiers in Veterinary Science

Transforms how we investigate and improve animal health

The third most-cited veterinary science journal, bridging animal and human health with a comparative approach to medical challenges. It explores innovative biotechnology and therapy for improved health outcomes.

Discover the latest Research Topics

See more →

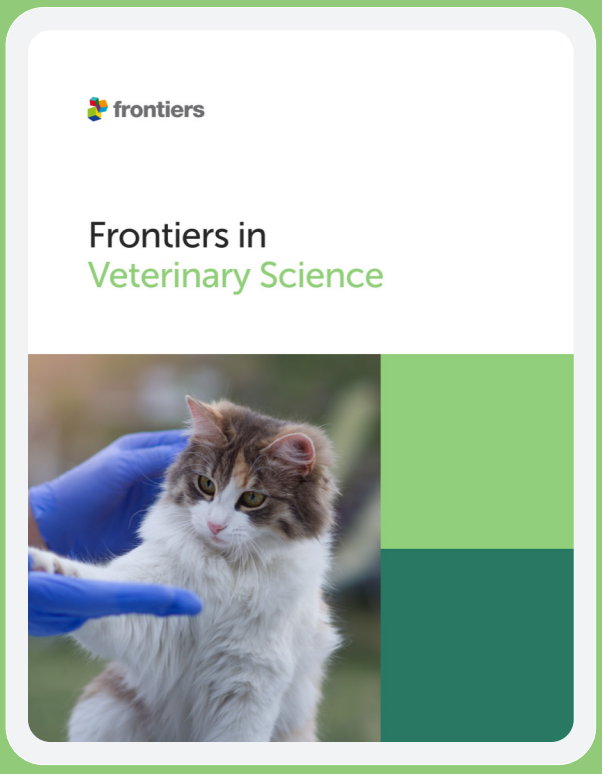

Frontiers

Avenue du Tribunal-Fédéral 34
1005 Lausanne, Switzerland
frontiersin.org

Contact us

+41 (0)21 510 17 00
frontiersin.org/about/contact